1988

OPTICAL ATTENUATION COEFFICIENTS IN OCEANIC AND ESTUARINE WATERS

Pilgrim, Derek Arthur

OPTICAL ATTENUATION COEFFICIENTS IN OCEANIC AND ESTUARINE WATERS

D. A. PILGRIM

Ph. D. 1988

For my part I had set up various optical accessories, hoping that they would prove useful to me.

Secchi, 1865.

DECLARATIONS

At no time during the registration for the degree of Doctor of Philosophy has the author been registered for any other C.N.A.A. or University award. This study was financed with the aid of the Plymouth Polytechnic Fellowship Scheme. The study was undertaken in collaboration with Plymouth Marine Laboratories.

A programme of advanced study was undertaken which included, at the Polytechnic, the development of microcomputing skills for the automatic logging and subsequent statistical analysis of large data bases. Also, an Open University course in photochemistry was successfully completed. Experience of shipboard techniques was gained during three deep sea scientific cruises.

During the period of registration four relevant scientific meetings were attended, three conference papers were presented and seven papers were published or are in press.

Publications

Pilgrim DA.
The Secchi disc in principle and in use
Hydrographic J., 33:25-30, 1984.

Uncles RJ, Elliot RCA, Weston SA, Pilgrim DA, Ackroyd DR, McMillan DJ and Lynn NM.
Synoptic observations of salinity, suspended sediment and vertical current structure in a partially mixed estuary
In: Physics of Shallow Estuaries and Bays (van de Kreeke C, ed.)
Springer-Verlag, Berlin Heidelberg, 58-70, 1986.

Pilgrim DA.
Measurement and estimation of the extinction coefficient in turbid estuarine waters
Proceedings of the 16th EBSA Symposium: Dynamics of Turbid Coastal Environments.
Continental Shelf Research, 7(11/12):1425–1428, 1987.

Pilgrim DA.
Light and Sound
In: Oceanography, vol 2: Seawater (Wright J, ed.), OU Oceanography Course (S330), The Open University, in press.

Pilgrim DA, Redfern TA, MacLachlan GS and Marsh RI.
Estimation of optical coefficients from diver observations of visibility
Progress in Underwater Science, 13, in press.

Pilgrim DA and Millward GE.
Variations in the diffuse optical depth of the bed of a tidal estuary
Proceedings of the 17th EBSA Symposium: Estuarine and Marine Methodologies, in press.

Pilgrim DA and Aiken J.
Measurement of the optical diffuse attenuation coefficient
Hydrographic J., in press.

also

External assessor to: Oceanography, vol 2: Seawater (Wright J, ed), The Open University, in press.

Technical editor (with J Aiken) to the English translation of: Introduction to ocean optics (Shifrin KS, 1983; in Russian), Kogan Page, London, in press.

Conferences attended

EBSA local meeting: The Humber Estuary, University of Hull, April 1984.

16th EBSA Symposium: Dynamics of Turbid Coastal Environments, Plymouth Polytechnic, September 1986.
Presented paper: Measurement and estimation of the extinction coefficient in turbid estuarine waters

17th EBSA Symposium: Estuarine and Marine Methodologies, University of Dundee, September 1987.
Presented paper: Variations in the diffuse optical depth of the bed of a tidal estuary

Underwater Association Annual Symposium, Zoological Society, London, March 1988.
Presented paper: Estimation of optical coefficients from diver observations of visibility

OPTICAL ATTENUATION COEFFICIENTS IN OCEANIC AND ESTUARINE WATERS

by

DEREK ARTHUR PILGRIM, B.Sc., M.Sc., Master Mariner.

A thesis submitted to the Council for National Academic Awards in partial fulfilment of the requirements for admittance to the degree of:

DOCTOR OF PHILOSOPHY

Undertaken at:

Plymouth Polytechnic Institute of Marine Studies
Department of Marine Science and Technology
Drakes Circus
Plymouth
Devon
UK

In collaboration with:

Plymouth Marine Laboratories
Prospect Place
The Hoe
Plymouth
Devon
UK

Submitted August 1988

ACKNOWLEDGEMENTS

I am glad of this opportunity to express my gratitude to a number of colleagues for their help and support during this study; without them, much of this work could not have been attempted.

Particularly, I thank my supervisors Dr GE Millward (Plymouth Polytechnic) and Drs J Aiken and PH Burkill (Plymouth Marine Laboratories) for their advice, guidance, patience and constant encouragement throughout. I am also grateful to Dr Aiken for organising my three week research cruise to the Norwegian and Greenland Seas on USNS Lynch, and for the loan and gift of optical instrumentation.

I am also indebted to Dr RD Pingree (IOS/PML) for the two research cruises in the NE Atlantic on RRS Frederick Russell, and for the valuable advice that he gave me in the early days of this study.

To the Masters and Crews of RRS Frederick Russell and USNS Lynch I express my gratitude for their willing assistance and my survival.

My thanks also to American colleagues. Firstly to Dr Jerome Williams (Oceanography Dept., US Naval Academy, Annapolis) for his encouragement in work which is, I know, dear to his heart. Also to Dr R Howarth (NOSC, San Diego), and Dr C Trees and Messrs G Edwards and G Nolten (Visibility Lab., Scripps Inst. of Oceanography, La Jolla), fellow scientists during the Lynch cruise, for their scintillating discussions on matters hydro-optical.

I am grateful to Dr NK Højerslev (University of Copenhagen) for notes on Secchi disc theory and measurement; I trust that he will not take it amiss that I am not entirely in agreement with them.

I acknowledge, with gratitude, the technical support and advice that has been freely given by Messrs RD Jones, BA Davis, TG Parrott and S Johnston (Plymouth Polytechnic) and Messrs I Bellan, GT Mardell and G Siley (PML). For advice on microcomputing, I am greatly indebted to Mr JR Douglas (Plymouth Polytechnic), and for advice on the use of

main-frame graphics facilities I thank Mr G Bouch (Polytechnic Computer Centre).

My thanks to Miss JE Potter, BSc Nautical Science student, for her assistance in logging beam transmissometer readings in the Tamar Estuary. It is with great sadness that I recall the help that I received - in measuring estuarine reflectances - from Stuart Vance, BSc Fishery Science student, during the last brave year of his life.

For underwater visibility observations, I have depended upon the cooperation of many fellow divers at Plymouth Polytechnic. I acknowledge, with gratitude, the assistance and interest of Messrs JD Vaudin, HF Knott and RD Jones, and the many BSc Fishery Science students involved, particularly Messrs RI Marsh, GS MacLachlan and TA Redfern who have shared my interest in the problems of diver visibility. Some of the underwater visibility observations were made by Mr MacLachlan during a visit to Singapore and SE Malaysia.

I would also like to thank Capt LW Fifield, my HoD at the time, for his support of my application for a Polytechnic fellowship and registration for a higher degree, Dr GE Millward for his conviction that I was capable of such a thing, and Professors RH Motte and KR Dyer for their continued support of my research.

Special thanks are due to my dear wife Jenny for the typing of this thesis, and more, for her patience and unwavering support and encouragement during many periods of frustration and disappointment. Truly, without her this work would not have been completed.

ABSTRACT

OPTICAL ATTENUATION COEFFICIENTS IN OCEANIC AND ESTUARINE WATERS

by

DEREK ARTHUR PILGRIM, B.Sc., M.Sc., Master Mariner.

Published hydro-optical theory pertinent to this study is critically reviewed; the optical quality of the instrumentation used is assessed and a method is proposed for judging the angular response of a diffuse collector. Consideration is given to the possibility of self shading, by an Undulating Oceanographic Recorder (UOR), of upwelling irradiance measurements; this would adversely affect the calculation of reflectance, an important optical parameter in remote sensor calibration work.

A selection of optical measurements made at estuarine, coastal and deep sea locations are analysed and empirical relationships between optical coefficients are presented. A sample set of data obtained by means of a UOR during a tow across the Arctic Front is considered in detail, and a simple analysis of the contributing components of the diffuse attenuation coefficient is carried out.

Since underwater visibility is limited by the beam and diffuse attenuation coefficients, diver observations of targets of known optical quality should provide a simple means of estimating these. Two methods suggested in the literature are considered but rejected on both theoretical and practical grounds; new methods are proposed, tested, found satisfactory and recommended for diver use.

Relationships are established between the turbidity and the penetration of light in an estuarine environment. The proportion of light reaching the bed of an estuary depends upon the depth and turbidity, and this may be represented by the diffuse optical depth of the bed, Jh. Theoretical considerations show that Jh(t) varies at twice the tidal frequency and this is confirmed by field observations. Calculations indicate that the same phenomenon must occur in coastal waters where tidal ranges and tidal variations in turbidity are significant.

Certain aspects of hydro-optical research that require further work are identified, and viable programmes of investigation are proposed.

CONTENTS

Chapter 1

I N T R O D U C T I O N

It was recommended by Dominique Argo, the nineteenth century astronomer and optical physicist, that 'sailors should study the transparency of the sea and its colour'. This idea was taken up by Commander Alessandro Cialdi who, in 1865, was head of the Papal Navy. It was Cialdi who prepared a number of 'discs of different colour and sizes' (Cialdi, 1866), and engaged Professor PA Secchi to organize and conduct a programme of observations from on board the papal barge L'Immacolata Concezione, (Collier et al, 1968). Thus began a century of ship-board observations of hydro-optical phenomenon and improved measurement techniques, the most significant of which was the development by HH Poole and WRG Atkins at Plymouth in the 1920s, of an electrical irradiance meter (Poole, 1925, 1928; Poole and Atkins, 1926, 1928, 1929).

The status of hydro-optical research was much enhanced in 1978 with the launch of the Coastal Zone Colour Scanner, which was designed specifically for the remote sensing of the aquatic environment. The scope of remote sensing is global; the single observations which Secchi made off the coast of Civitavecchi in the Mediterranean may now be imitated synoptically over whole oceans. However, this quantum advance in observational technique has not rendered ship-board measurement redundant. The availability of satellite data has created an urgent need for appropriate and properly observed ground truth data, particularly those which relate upwelling fluxes of light to the oceanographic conditions - biological, biochemical, physical and/or geophysical - of the waters concerned.

Current interest in optical oceanography is not restricted to the calibration of remote sensing data, however. There remains great

scope for fundamental research in such diverse areas as: primary productivity, in situ measurement of suspended sediment concentration, flux and particle size distribution, the underwater visibility problems of man, fish and photographer, and submarine-satellite communication by laser.

In any optical experiment or investigation it is important that specific and appropriate optical properties of the water or light field be identified for study. Only then can the correct instrumentation be selected or modified. Usually it is appropriate to specify the required characteristics of the light sensor to be used - in terms of the spectral and angular response of its collector and the units of measurement. For example, the (apparent) property which best identifies the potential of a column of water to attenuate light capable of supporting photosynthesis is the total diffuse attenuation coefficient of quantum scalar irradiance in the 350-700 nm wave-band, (UNESCO, 1965). It follows that the correct sensor to be used in the study of aquatic photosynthesis is a 4π scalar (spherical) collector with an output proportional to the quantum flux. Another apt example is the use of the Secchi disc in estimating optical properties of the water column; it is not always recognised that as the Secchi depth is an observed value then, strictly, only optical coefficients specific to the spectral response of human vision can be estimated. In practice, it may be viable to use optical coefficients which are not strictly appropriate; however, in the design of any programme of optical observation it is imperative that theoretical constraints are not totally ignored for the sake of practicality.

Basic optical theory has been presented in several books, eg Jerlov

(1965, 1968, 1976), Preisendorfer (1976) and Kirk (1983), and numerous papers, including Hulbert (1945), Tyler and Preisendorfer (1962), Smith and Tyler (1967, 1975), Tyler et al (1972), Timofeeva (1974), Morel (1974), Tyler (1977) and Gordon et al (1979, 1984). Chapter 2 of this thesis comprises of a selection of those optical theory topics which are pertinent to the several facets of the study undertaken, starting with a detailed review of the terms and quantities which describe and define radiometric flux.

Two processes fundamental to any optical phenomenon are absorption and scattering. The present study is primarily physical in approach, whilst the absorption of light is a photochemical process. The first atomic and/or molecular events which follow the absorption of a photon (a quantum of light energy) are therefore described and some important hydro-optical examples - water, Chl.a and the major accessory pigments - are considered.

An important concept in the study of hydro-optics is the distinction between an inherent property, the operational value of which is independent of the radiation field, and an apparent optical property which is not independent of the radiation field. This distinction - essential to the definition of optical properties and to the design, use and calibration of optical instrumentation - is explored, as is the difference between radiance (collimated flux) and irradiance (diffuse flux).

There then follows a theoretical review of the measurement of the diffuse attenuation coefficient. The measurement of optical coefficients is fundamental to the aims of the present study, and the

two most important of these are the beam attenuation coefficient (of collimated light), $c(\lambda)$, and the diffuse attenuation coefficient (of diffuse light), $K(\lambda)$. The beam attenuation coefficient is an inherent property and its measurement is, in theory, straight forward. For example, it is quite in order to remove a water sample for measurement of $c(\lambda)$ by a beam transmissometer, providing that this removal does not cause a physical change in the water, such as the flocculation or breakdown of particulates. The diffuse attenuation coefficient, however, is an apparent property so must be measured in situ. This involves some form of vertical profiling of the water column. Also considered is the range of irradiance collectors available for measuring different aspects (vector/scalar, upwelling/downwelling/total) of the irradiance field.

A significant part of this study was devoted to the analysis of diver observations of visibility. The use of divers in the study of underwater visibility problems, such as the selection of optimum fishing net colour (Hemmings and Lythgoe, 1965; Tsudo and Inoue, 1973), is not new. In recent years, considerable attention has been given to the limitations of underwater visibility in diver operations. Most of the fundamental problems of diver vision and image transmisson have been described in the work of Hemmings (1965), Hemmings and Lythgoe (1965), Gazey (1970), Lythgoe (1971, 1979), and Cocking (1976). Other specific studies include size and distance judgement by divers (Ross, 1965), divers' stereoscopic acuity (Ross, 1967), polarized light and vision (Lythgoe and Hemmings, 1967), colour vision underwater (Fay, 1976), perception of colour change with distance (Emmerson, 1984), field dependency (Leach, 1985), the effects of nitrogen narcosis upon divers' visual abilities (Ross and

Rejman, 1976), and the effects of target-diver movement upon threshhold detection (Emmerson, 1987). These studies are, in the main, concerned with the ways in which optical physiology and the propagation of underwater light affect a diver's visual capabilities. In the visibility work carried out in the course of the present study, the problem was approached and exploited from the opposite direction. Since underwater visibility is limited by the beam and diffuse attenuation coefficients, diver observations of targets of known optical quality should provide a means of estimating these coefficients and other closely related parameters. The last part of Chapter 2 therefore concentrates on those aspects of underwater visibility that are directly related to this work. As optical coefficients are to be estimated from visual ranges, it is important that the performance of the eye be assessed in the same way as any other optical sensor, ie in terms of it's angular and spectral response, and units of flux measurement. This is followed by an explanation of the two basic concepts used in the study of underwater visibility: contrast transmittance and threshold contrast. Finally, this theory is applied to the visible ranging of two of the optical targets employed in subsequent experimental work, namely the Secchi disc, and the pair of grey and white discs proposed by Duntley (1952), and described by Preisendorfer (1976, 1986).

Most of the high turbidity observations were made in the estuary of the River Tamar and Plymouth Sound. This area has received considerable attention recently in the study of estuarine geochemistry (eg Morris et al, 1981, 1982a, 1982b, 1982c; Ackroyd et al, 1982; Glegg et al, 1985), hydrodynamics (eg Uncles et al, 1983, 1985, 1986), sediment transport (eg Bale et al, 1985; Bale and Morris,

1985) and primary production (eg Joint, 1978; Joint and Pomroy, 1981; Uncles and Joint, 1982). It was also the location of very early hydro-optical work (eg Poole, 1925, 1928; Poole and Atkins, 1926, 1928, 1929; Cooper and Milne, 1938). Coastal water observations were obtained off Plymouth, in the SW Approaches (Frederick Russell cruises, 1985 and 1987), and in the English Channel and Irish Sea (Lynch cruise, 1987). Oceanic data were collected in the NE Atlantic (Frederick Russell cruises), and Norwegian and Greenland Seas (Lynch cruise). For safety reasons, diving operations were conducted only in estuarine and coastal waters, mostly in Plymouth Sound, a local fresh-water reservoir and the turbid inshore waters of Singapore and SE Malaysia.

The objectives of this programme of research were:

(i) To critically review existing optical theory related to the work to be undertaken.

(ii) To establish relationships between the turbidity and the penetration of light in an estuarine environment.

(iii) To critically review existing empirical methods of estimating optical coefficients, and to formulate new ones.

(iv) To obtain irradiance measurements in coastal and oceanic waters in order to assess the contribution made by phytoplankton, and covarying pigmented detrital products, to the diffuse attenuation coefficent.

(v) To conduct underwater visibility experiments, and thereby estimate photometric attenuation coefficients.

(vi) To assess the performance and suitability of available optical instrumentation.

Chapter 2

OPTICAL THEORY

2.1 THE BEHAVIOUR OF LIGHT

Light is a form of electromagnetic radiation. James Clerk Maxwell (1831–1879) unified the laws of electricity and magnetism into a single theory of electromagnetism which incorporates all that is known about the macroscopic effects of electricity, magnetism and electromagnetic waves. Fundamental to this theory is the existence of electromagnetic waves: gamma radiation, visible light, radio waves and so on. These different types of radiation differ only in wave length and are, essentially, all of the same structure, namely a time varying combination of electric and magnetic fields, in phase and perpendendicular to the direction of propagation i.e. they are transverse waves. The bandwidth of visible light is a very small portion of the total electromagnetic spectrum, and extends from about 400 nm (deep violet) to 700 nm (dark red). The absorption of light for photosynthesis is also limited to this narrow but important band.

2.1.1 Properties of the radiation field

The radiometric quantities are those which describe the substance of the radiant field and include the two very important field quantities: radiance and irradiance. In the definitions following, ξ is the zenith angle (0 to π) and η is the azimuth (0 to 2π).

Radiant flux, $F(\lambda,z)$ $[qs^{-1},W]$, is the fundamental concept which

describes light propagation and is the time rate flow of radiant energy:

$$F(\lambda,z) = dQ(\lambda,z)/dt \ [qs^{-1} \text{ (or W)}] \qquad (2.1)$$

Radiant intensity, $I(\lambda,z,\xi,\eta)$ $[qs^{-1},W]$, is the measure of the radiant flux per unit solid angle in a specified direction:

$$I(\lambda,z,\xi,\eta) = dF(\lambda,z,\xi,\eta)/d\omega = d^2Q(\lambda,z,\xi,\eta)/d\omega.dt \qquad (2.2)$$

Radiance, $L(\lambda,z,\xi,\eta)$ $[qs^{-1}m^{-2},Wm^{-2}]$, (also termed radiant phase density by Preisendorfer, 1976) combines the concepts of radiant intensity and flux density. It is the energy per unit time per unit area per unit solid angle incident upon a point from the direction ξ,η (Smith and Tyler, 1975): $L(\lambda,z,\xi,\eta) = d^3Q(\lambda,z,\xi,\eta)/dt.dA.d\omega$, and incorporating Eqns.2.1 and 2.2:

$$L(\lambda,z,\xi,\eta) = d^2F(\lambda,z,\xi,\eta)/dA.d\omega = dI(\lambda,z,\xi,\eta)/dA \qquad (2.3)$$

Irradiance, $E(\lambda,z)$ $[qs^{-1}m^{-2},Wm^{-2}]$, is the radiant flux incident on an element of surface divided by the area of that element (Smith and Tyler, 1975).

Downwelling vector irradiance, $Ed(\lambda,z)$, is therefore the flux incident per unit area measured on a horizontal, upward facing cosine collector (see Fig.2.8):

$$Ed(\lambda,z) = \int_{2\pi} L(\lambda,z,\xi,\eta).\cos\xi.d\omega \qquad (2.4)$$

$$\text{where } \int_{2\pi} d\omega = \int_{\xi=0}^{\pi/2} \int_{\eta=0}^{2\pi} d\eta.d\xi$$

and for upwelling irradiance $Eu(\lambda,z)$:

$$Eu(\lambda,z) = \int_{-2\pi} L(\lambda,z,\xi,\eta).|\cos\xi|.d\omega \qquad (2.5)$$

$$\text{where } \int_{-2\pi} d\omega = -\int_{\xi=\pi/2}^{\pi} \int_{\eta=0}^{2\pi} d\eta.d\xi$$

Net downwelling irradiance, $Ee(\lambda,z)$, is therefore given by:

$$Ee(\lambda,z) = Ed(\lambda,z)-Eu(\lambda,z) = \int_{4\pi} L(\lambda,z,\xi,\eta).\cos\xi.d\omega \qquad (2.6)$$

$$\text{where } \int_{4\pi} d\omega = \int_{\xi=0}^{\pi} \int_{\eta=0}^{2\pi} d\eta.d\xi$$

The scalar irradiance, $Eo(\lambda,z)$, is the integral of a radiance distribution at a point at depth z over all directions about the point and is equivalent to the total energy flux, $dF(\lambda,z)/dt$:

$$Eo(\lambda,z) = \int_{4\pi} L(\lambda,z,\xi,\eta).d\omega \qquad (2.7)$$

We may also have downwelling scalar irradiance, $Eod(\lambda,z)$:

$$Eod(\lambda,z) = \int_{2\pi} L(\lambda,z,\xi,\eta).d\omega \qquad (2.8)$$

and upwelling scalar irradiance, $Eou(\lambda,z)$:

$$Eou(\lambda,z) = \int_{-2\pi} L(\lambda,z,\xi,\eta).d\omega \qquad (2.9)$$

The following summation is valid (Højerslev, 1984):

$$Eo(\lambda,z) = Eod(\lambda,z) + Eou(\lambda,z) \qquad (2.10)$$

Some authors (eg Shifrin, 1983; Højerslev, 1984) define a spherical irradiance, Es, as the ratio of radiant flux onto a spherical surface to the total area of the surface:

$$Es(\lambda,z) = dF/4\pi r^2 = Eo/4 \qquad (2.11)$$

The radiometric quantities of particular interest in this work are the quantum irradiances (especially 2π and 4π scalar) in the 400-700 nm photosynthetic band. Measurement in quanta over the 400-700 nm bandwidth will be indicated by the superscript '°' so that, for example:

$$^{\circ}Eo(z) = \int_{4\pi}\int_{\lambda=400}^{700} Lq(\lambda,\gamma,\eta,z).d\lambda.d\omega \qquad (2.12)$$

This will be referred to, simply, as PAR irradiance. We may also use °Eod(z) and °Eou(z) for the 2π downwelling and upwelling quantum scalar irradiances, and °Ed(z), °Eu(z), °Ee(z) for the downwelling, upwelling and net downwelling quantum vector irradiances, all in the 400-700nm band.

In this subsection the full suffix notation (λ,z,γ,η) has been used in defining the radiometric terms. From here on, for ease of reading, suffix terms will be included only where necessary; usually, the simpler suffix (λ,z) will suffice.

2.1.2 The absorption of light

If light is to induce photochemical change then it must first be absorbed (Grotthus-Draper law). Chemical change need not follow

absorption but if it does then only 1 photon per absorbing molecule (N_A photons per mol) is normally required (Stark-Einstein law). It is significant that absorption of light is quantisized; this is due to the fact that an atom or molecule is limited to a discrete series of energy levels.

The simplest form of atomic absorption causes an electron to move to a higher energy level at an increased distance from the nucleus. The electron can have only certain energy levels because, according to the quantum theory, only certain orbitals (wave functions or standing probability waves) are possible. In hydrogen, for example, a single photon could lead to a transition from the ground state, $1s^1$, to the lowest excited state, $2s^1$; there is, therefore, a series of energy levels corresponding exactly to the orbital energies. For other atoms the situation is complicated by electron-electron repulsion so that energy/orbital levels do not correspond exactly. Energy levels may also be split because spin-orbit coupling, an interaction between an electron's spin and orbital motion, causes the two components of the doublet ^2P state to have slightly different energies.

Of course, a molecule has electronic energy levels associated with the electrons of its component atoms; it also has quantisized vibrational and rotational energy levels. Vibrational energy levels are associated with oscillations in atom-atom bond distances, and rotational energy levels arise from the rotation of molecules in space. The energies associated with transitions between different rotational energy levels are much smaller than those for vibrations which are, in turn, less than those involved in changes in electronic energy levels. Consequently, each electronic level has associated

with it several vibrational levels and each of these have a large number of rotational levels. The ground electronic configuration of H_2O is shown on the right. There are eight valence electrons (H:1x2, O:6), and since six atomic orbitals are involved in bonding (H:1s, O:2s+2p), there are six molecular orbitals of which the lowest four are occupied. The lowest energy transition should be $n \rightarrow \sigma_4^*$ and is thought to be responsible for an absorption band with a maximum near 165 nm. A higher energy band in the UV is associated with excitation of an electron from σ_3 to an orbital involving the 3s atomic orbital of oxygen (a Rydberg transition). Absorption in the visible region involves not electronic excitation but molecular vibration. Patel and Tam (1979) have made accurate absorption measurements of pure water at 21°C in the 450-700 nm band using a specially developed opto-acoustic technique. They found a minimum absorption (1.7×10^{-4} cm^{-1}) at 475 nm and distinct shoulders at 514 nm and 604 nm associated with the sixth and fifth harmonics of O-H vibration. Smith and Baker (1981) have published a table of the optical properties of pure water and clearest ocean waters. Part of this tabulation (400-700 nm) is reproduced in Table 2.1, and the absorption coefficient of pure water in the visible band is graphed in Fig.2.2.

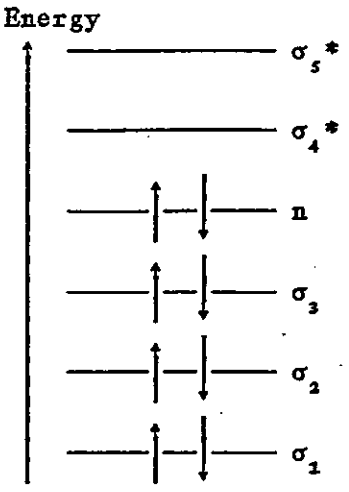

Fig.2.1
Ground state of H_2O

Chlorophyll-a is responsible for the conversion of light energy into the chemical energy of photosynthesis. The chlorophyll molecule belongs to a group of important naturally occuring tetrapyrrol pigments termed metalloporphins. The structure of the Chl-a molecule

Table 2.1: Absorption coefficient of pure water and the scattering and extinction coefficients for clearest ocean waters in the 400–700nm PAR band (from Smith and Baker, 1981)

λ(nm)	$a^W(m^{-1})$	$b^W(m^{-1})$	$K^W(m^{-1})$	λ(nm)	$a^W(m^{-1})$	$b^W(m^{-1})$	$K^W(m^{-1})$
400	0.0171	0.0076	0.0209	550	0.0638	0.0019	0.0648
410	0.0162	0.0068	0.0196	560	0.0708	0.0018	0.0717
420	0.0153	0.0061	0.0184	570	0.0799	0.0017	0.0807
430	0.0144	0.0055	0.0172	580	0.108	0.0016	0.109
440	0.0145	0.0049	0.0170	590	0.157	0.0015	0.158
450	0.0145	0.0045	0.0168	600	0.244	0.0014	0.245
460	0.0156	0.0041	0.0176	610	0.289	0.0013	0.290
470	0.0156	0.0037	0.0175	620	0.309	0.0012	0.310
480	0.0176	0.0034	0.0194	630	0.319	0.0011	0.320
490	0.0196	0.0031	0.0212	640	0.329	0.0010	0.330
500	0.0257	0.0029	0.0271	650	0.349	0.0010	0.350
510	0.0357	0.0026	0.0370	660	0.400	0.0008	0.400
520	0.0477	0.0024	0.0489	670	0.430	0.0008	0.430
530	0.0507	0.0022	0.0519	680	0.450	0.0007	0.450
540	0.0558	0.0021	0.0568	690	0.500	0.0007	0.500
				700	0.650	0.0007	0.650

is based upon a ring of four conjugated pyrroles with a single magnesium at its centre and a long chain phytol tail. It has one hydrogenated outer double bond and is therefore a chlorin; hence its name. Different chlorophylls have different side chains; the most important is Chl-a, the principle pigment. The strong absorption by Chl-a is primarily due to its extended conjugated system. When two carbons unite they form a double bond (C=C) which requires one π orbital; the other 10 electrons go into 5 σ orbitals. The ground configuration of ethene is, therefore: $(\sigma_1)^2(\sigma_2)^2(\sigma_3)^2(\sigma_4)^2(\sigma_5)^2(\pi_1)^2$. The energy diagram, (Fig.2.3), shows the effect of

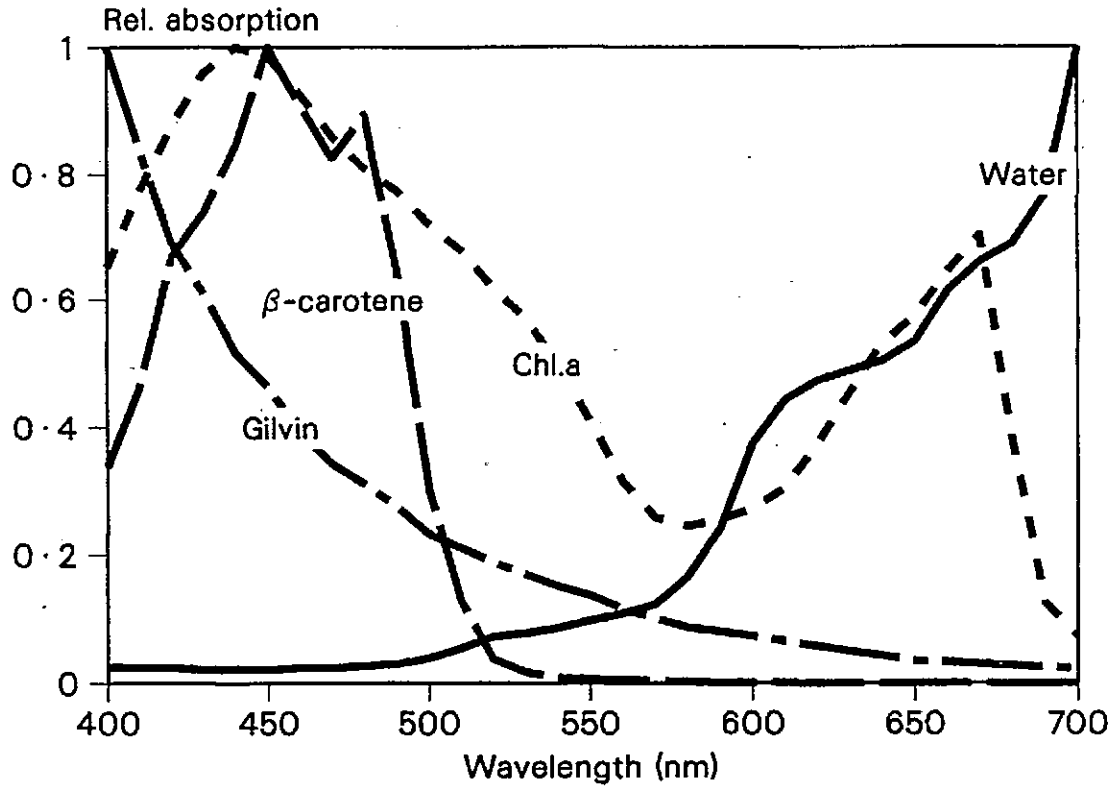

Fig.2.2: Relative absorption spectra of pure water, chloropyll-a, β-carotene and gilvin, using data from: Smith and Baker (1981) for pure water, Morel and Prieur (1977) for chlorophyll-a, Kirk (1983) for β-carotene, and Kirk (1976) for typical gilvin (Burrinjuck Dam)

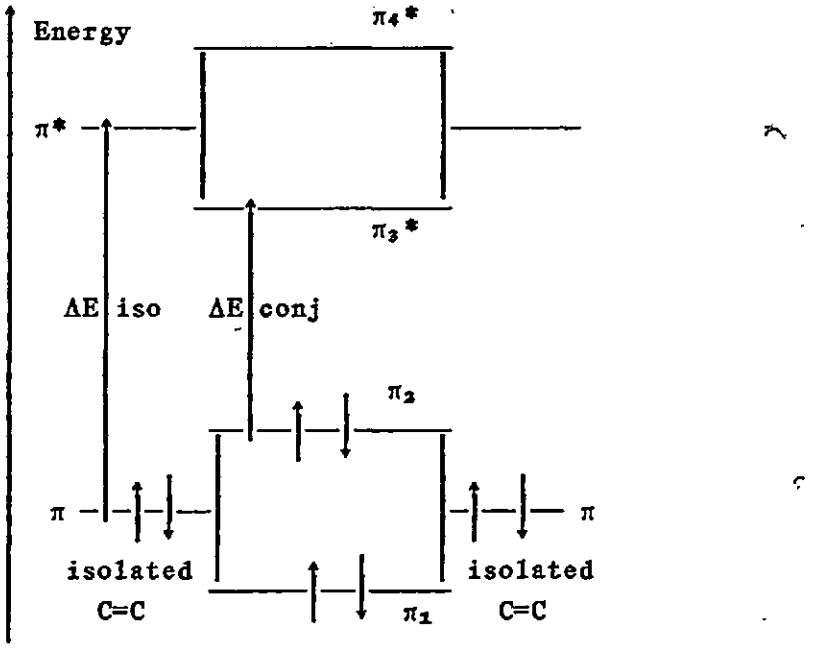

Fig.2.3: Delocalised π orbitals in the conjugation of two ethenes

conjugating two ethenes as in buta,1-3 diene (=-=). The π molecular orbitals combine to give delocalised orbitals: π_1 and π_2. In the same way, the two π^* orbitals give rise to delocalised orbitals: π_3^* and π_4^*. Thus the lowest energy transition, $\pi_2 \rightarrow \pi_3^*$, occurs at a lower energy than for the isolated C=C bonds in, for example, hexa-1,5 diene (=---=). The effect of further conjugation such as that in the extended system of Chl-a is to lower still further the energy transition from the highest occupied π orbital to the lowest unoccupied π^* orbital (OU.S341, 1982). The absorption spectrum of Chl-a is illustrated in Fig.2.2 and it is apparent that there are two important absorption bands (B and Q) centred at about 440 and 660 nm near each end of the PAR range; the Q band is actually a series of overlapping bands. The unutilized energy centred at 550 nm is reflected as the characteristic green colour of chlorophyll. In marine algae, the absorption band may be extended into the green by the action of accessory pigments, principally: chlorophyll-b, c_1, c_2, and the many carotenoids and biliproteins. For example, the absorption spectrum of β-carotene is illustrated in Fig.2.2; absorption is maximum at about 450 nm and zero at $\lambda > 550$, hence its 'carrot-red' colour. As in the case of Chl-a, the strong absorption by accessory pigments is due to $\pi \rightarrow \pi^*$ transitions associated with extended systems of conjugated carbon double-bonds.

Natural waters contain 'yellow substance', sometimes known as 'yellow organic acids', 'dissolved humic acid', 'humolimnic acid', 'fulvic acid' or by its German name 'Gelbstoff'; Kirk (1976) has coined the term 'gilvin'. Gilvin is produced during the decomposition of organic matter by bacteria. Studies indicate that these substances are polymers of phenolic and benzenecarboxylic acid (Kirk, 1983).

Some of the gilvin of estuarine and coastal waters is generated within the water body by the decomposition of plant material; it may also originate as water-soluble humic substances in soil which becomes leeched out by rainwater. Again, it is $\pi \rightarrow \pi^*$ transitions which lead to the strong absorption in the blue. A typical gilvin absorption spectrum is illustrated in Fig.2.3. The concentration of gilvin in natural waters varies enormously. Kirk (1976, 1983) suggests that the concentration of gilvin be indicated by g_{440}, the absorption coefficient at 440 nm. Bricaud et al (1981) say that throughout the 350-700 nm domain, absorption by gilvin approximately follows the law: $a(\lambda) = a(\lambda o).\exp[-S(\lambda-\lambda o)]$, where $0.01 \leq S \leq 0.02$. This is consistent with other published results, eg S=0.015 (Jerlov,1968), and $0.011 \leq S \leq 0.017$ (Lundgren, 1976).

Suppose a radiance, $L(\lambda)$ is propagated through an infinitesimally thin layer of absorbing but non-scattering medium, dz. There will be absorption loss, $dLa(\lambda)$, so transmittance: $T(\lambda) = (L(\lambda)-dLa(\lambda))/L(\lambda) = 1-dLa(\lambda)/L(\lambda)$, where $dLa(\lambda)/L(\lambda)$ is the absorbance, $A(\lambda)$. A specific expression of the absorption rate is provided by the absorption coefficient, $a(\lambda,z)$:

$$a(\lambda,z) = \frac{A(\lambda,z)}{dz} = \frac{dLa(\lambda,z)/L(\lambda,z)}{dz} = \frac{-d}{dz} \mathrm{Ln}[L(\lambda,z)] \qquad (2.13)$$

and by integration over the range $0 \geq z \geq z$:

$$\frac{L(\lambda,z)}{L(\lambda,0)} = T(\lambda,z) = \exp[-a(\lambda,z).\Delta z] \qquad (2.14)$$

This is Beer-Lambert's law for radiance absorption.

2.1.3. The scattering of light

When a photon interacts with a molecule or particle it may not be absorbed; it may simply undergo a change in direction. There are two basic forms of scattering; density fluctuation scattering and particle scattering.

Density fluctuation scattering

According to the Rayleigh theory, when a particle such as an air molecule is placed in a light field, a dipole is induced by the electric vector of the field. As the dipole oscillates at the frequency of the exciting radiation then it emits radiation of the same frequency in all directions. This reradiation is the scattered light; its intensity, $I(\sigma)$, in direction σ, is given (Morel, 1974) by:

$$I(\sigma) = \frac{1}{2d^2} \cdot \left[\frac{2p}{\lambda}\right]^4 \cdot p^2 \cdot (1 - \cos^2\sigma) \qquad (2.15)$$

where I is the incident intensity and d is the particle diameter. Three important results are apparent from this equation; density fluctuation scattering is:

- proportional to λ^{-4}, ie greater at smaller wavelengths
- proportional to d^{-2}, ie greater for particles small compared to the wavelength of light
- symmetrical about the direction of propagation.

In fact, Rayleigh scattering is applicable only to gases, (the atmosphere, for example), and not to dense fluids such as liquids; however, λ^{-4} type scattering does occur in very clear sea water and is often referred to loosely as 'Rayleigh scattering'. It is, in

fact, a type of molecular scattering caused by the water itself and its dissolved salts, which can be determined theoretically by the fluctuation theory of Smoluchowski and Einstein (Kullenberg, 1974). This theory attributes the scatterance to density or concentration fluctuations by molecular movements. This type of scattering is proportional to λ^{-4} and has, as regards intensity distribution, the same properties as Rayleigh scattering.

Particle scattering

The density fluctuation type of scattering applies only when the scattering centres are small relative to the wavelength of light. The particles of natural waters have a continuous, approximately hyperbolic distribution in which the number of particles, n, with diameter greater than d, is expressed (Kirk, 1983):

$$n = 1/d^m;\ 0.7 \leq m \leq 6 \qquad (2.16)$$

This distribution implies more small than large particles; however, Jerlov (1968) summarizes measurements by several workers who have shown that most of the scattering of light in natural waters is from particles of $d > 2\mu m$, ie particles large compared to the wavelength of light. Scattering by these 'large' particles comprises of three phenomena: diffraction, refraction and reflection. The diffraction is determined by the size and shape of the particle, whereas refraction and reflection depend upon its composition (refractive index), (Kullenberg, 1974).

The basis for predicting the light scattering behaviour of spherical particles of any size is the Mie theory, developed by Mie in 1908.

This theory is similar to that of Rayleigh in that it considers the oscillations set up within a polarizable body by the incident light field and the light reradiated (scattered) from the body as a result of these oscillations. Instead of equating the particle to a single dipole, the Mie theory considers the additive contributions of a series of electrical and magnetic multipoles located within the particle (Kirk, 1983). The advantage of the Mie theory is that it is all-embracing; for very small particles, for example, it leads to the same predictions as the Rayleigh theory. All workers are agreed on one point: the analytical expressions of the Mie theory are complex and do not lend themselves to easy numerical calculation. The magnitude of Mie scattering for any particle size at any wavelength is generally expressed in terms of the light scattering efficiency, ε, (effective scattering area over actual area), the particle size parameter $\alpha=\pi d/\lambda$ and the relative refractive index, $|(\mu-\mu_w)/\mu_w|$. This type of particle scattering is illustrated in Fig.2.4 and it is apparent that when the particle size parameter is small, (particle diameter small compared to wavelength), then the amount of energy scattered is quite small but rises to a maximum as particle size increases. With a further increase in α, the value of ε decreases and then oscillates, and eventually settles about a value of $\varepsilon=2$. According to Beardsley et al (1970), in a typical marine suspension the index of refraction difference is of the order of 0.1. This is aparently correct; eg taking $\mu_w = 4/3$ and $\mu = 1.15$ for clays/silts (Williams, 1970), then $|(\mu-\mu_w)/\mu_w| = 0.138$. The particle size parameter α will therefore be of the order: $\pi d/\lambda = 2\pi/0.5 = 12.6$, so that $\alpha.|(\mu-\mu_w)/\mu_w| < 1.3$. It follows, from Fig.2.4, that $1\leq\varepsilon\leq3$ for marine particulates; in fact Jerlov (1968) has measured values in the range: $1.4\leq\varepsilon\leq3.2$. We also see from Fig.2.4 that in very clear water

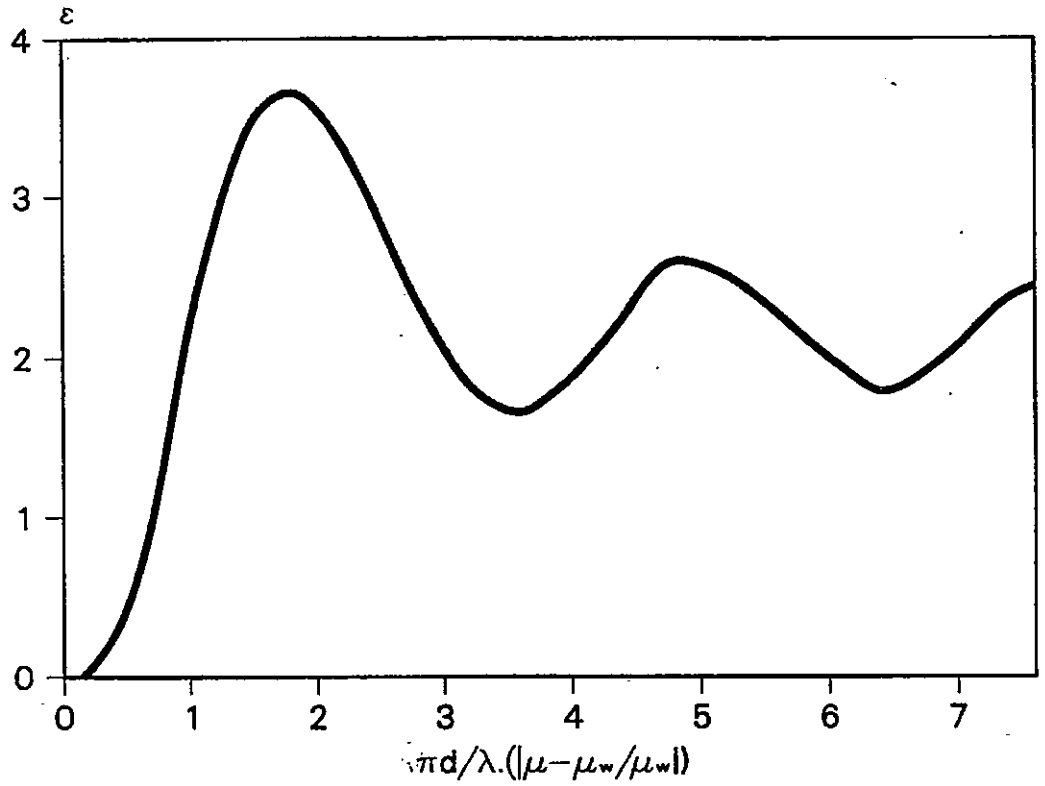

Fig.2.4: Mie scattering curve (Williams, 1970)

(small α) then for any particle size: $\varepsilon \propto (1/\lambda)$; ie scattering will be greater for shorter (blue) wavelengths.

The extent to which a flux of photons is scattered by a scattering medium may be expressed in terms of the volume scattering function and coefficients. These are widely derived and explained in the literature [eg. Tyler and Preisendorfer (1962), Duntley (1963), Jerlov and Nielsen (1974), Smith and Tyler (1975), Preisendorfer (1976), Morel (1974), Kirk (1983) etc.]. Fig.2.5 illustrates radiant intensity, I, being scattered by a small volume of scattering medium, $\delta V = \delta A.\delta r$. The volume scattering function $\beta(\lambda,z,\sigma)$, is the radiant intensity scattered in a given direction, σ, from volume element, δV,

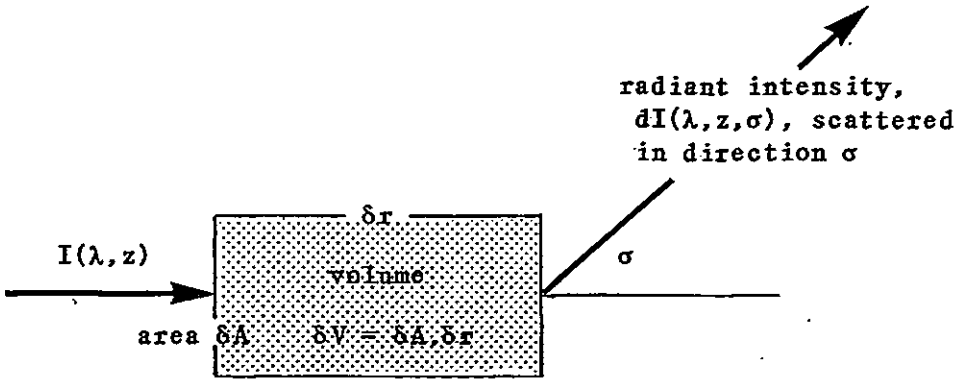

Fig.2.5 Scattering of irradiance.

illuminated by a parallel beam of light, per unit of incident irradiance onto the cross-section of the volume, and per unit volume (Kirk, 1983). It is given by:

$$\beta(\lambda,z,\sigma) = dI(\lambda,z,\sigma)/I(\lambda,z).\delta V \qquad (2.17)$$

The total volume scattering coefficient, $b(\lambda,z)$, is the proportion of incident intensity scattered in all directions:

$$b(\lambda,z) = \int_{4\pi} \beta(\lambda,z,\sigma).d\omega \qquad (2.18)$$

Simply, b is the integral of $\beta(\sigma)$ over all directions. It is sometimes useful to consider the total scattering coefficient, b, as comprising of forward-scattering, b_f, and backscattering, b_b coefficients:

$$b = b_f(\lambda,z) + b_b(\lambda,z)$$

$$= 2\pi\int_0^{2\pi} \beta(\lambda,z\ \sigma).\sin\sigma.d\sigma + 2\pi\int_{\pi/2}^{\pi} \beta(\lambda,z,\sigma).\sin\sigma.d\sigma \qquad (2.19)$$

To compare the shape of the angular distribution of scattering in different media, it is convenient to use the normalized volume scattering coefficients $\tilde{\beta}(\sigma)$, $\tilde{b}_f$ and $\tilde{b}_b$ (Kirk, 1983):

$$\tilde{\beta}(\lambda,z,\sigma) = \beta(\lambda,z,\sigma)/b(\lambda,z)$$

$$\tilde{b}_f(\lambda,z) = b_f(\lambda,z)/b(\lambda,z)$$

$$\tilde{b}_b(\lambda,z) = b_b(\lambda,z)/b(\lambda,z) \qquad (2.20)$$

Kalle's hypothesis states that the particle scattering coefficient is proportional to the total cross section of the particle. This yields a simple equation (Beardsley et al, 1970) for the scattering coefficient of a distribution of n spherical particles having different diameters and indices of refraction:

$$b_p = \sum_{i=1}^{n} \varepsilon_i(\lambda_i,d_i,n_i).(\pi/4).d_i^2$$

As $\varepsilon_i \geq 2$, (Fig.2.4), then for most expected marine particles this equation may be simplified to:

$$b_p = \sum_{i=1}^{n} 2(\pi/4).d_i^2 = (\pi/2).\sum_{i=1}^{n} d^2 \qquad (2.21)$$

2.2 OPTICAL PROPERTIES OF AQUATIC MEDIA

Optical properties are generally grouped into two main classifications: inherent and apparent, plus a hybrid classification.

2.2.1. Inherent optical properties

A property is defined as inherent if its operational value at a given point in a given medium is invariant under all changes of the radiation distribution at that point (Preisendorfer, 1960). The inherent optical properties are now considered.

The **volume absorption coefficient, $a(\lambda,z)$,** the **volume scattering function, $\beta(\lambda,z,\sigma)$,** and the **total volume scattering coefficient, $b(\lambda,z)$.** These were dealt with in detail in subsections 2.1.2 and 2.1.3, where they were defined by Eqns.2.13, 2.17 and 2.18.

The **volume (beam) attenuation coefficient, $c(\lambda,z)$.** We may now write for a medium in which there is both absorption and scattering, equivalent to Eqn.2.13 for an absorption-only medium:

$$c(\lambda,z) = \frac{C(\lambda,z)}{dz} = \frac{dL(\lambda,z)/L(\lambda,z)}{dz} = \frac{-d}{dz}\,\mathrm{Ln}[L(\lambda,z)] \qquad (2.22)$$

where $dL=dL_a+dL_b$, and in which is introduced the **attenuance, $C(\lambda,z)$,** and **attenuation coefficient, $c(\lambda,z)$,** defined by Gordon (1984) as the fraction of energy in a beam removed by both absorption and scattering per unit distance. By integration of Eqn.2.22 over the

[illegible]

depth range $0 \geq z \geq z$ we have, equivalent to Eqn.2.14, Beer Lambert's law for radiance attenuation:

$$\frac{L(\lambda,z_2)}{L(\lambda,z_1)} = T(\lambda,z) = \exp[-c(\lambda,z).\Delta z] = \exp[-j(\lambda,z)] \qquad (2.23)$$

$j(\lambda,z)$ is the optical length/depth/thickness:

$$j(\lambda,z) = c(\lambda,z).\Delta z = (a(\lambda,z)+b(\lambda,z)).\Delta z \qquad (2.24)$$

A term sometimes preferred to c, (eg Williams, 1970), is the characteristic attenuation length, $\frac{1}{c}(\lambda,z)$, the distance at which the transmission, T, is equal to 1/e. Substituting into Eqn.2.23: $\exp[-1] = \exp[-c.\frac{1}{c}]$, ie $\frac{1}{c} = 1/c$.

2.2.2 Apparent optical properties

Apparent optical properties are defined as those which are not invariant with changes in the radiation distribution; however, not all authors agree on which these are. Some (eg Preisendorfer, 1960; Gordon *et al*, 1984), include radiance, L, and irradiance, E, whilst others (eg Kirk, 1983), consider these to be properties of the radiation field. They have been treated as field properties in this work (subsection 2.1.1). Preisendorfer (1960) also includes the distribution function, D, and reflectance, R. Kirk (1983) points out that many workers now consider dimensionless D and R to be properties of the radiation field. This is so; however, in this study it will be convenient to treat them as apparent properties of the water in which they are measured. The apparent optical properties are now considered.

The **K-coefficients, K(λ,z)** describe the loss of photons during the propagation of irradiance, so are sometimes referred to as **diffuse attenuation coefficients.** They are considered apparent because they change, for example, with solar elevation, cloud cover and sea state (Højerslev, 1978). Field observations have indicated that these changes are normally very small (Preisendorfer, 1960), so that the K-coefficients have become widely used in the study of marine optics. They are of fundamental importance to this study where they will be granted much the same status as the inherent properties; there is considerable justification for this in turbid water where the radiation distribution rapidly approaches isotropic with depth.

The **extinction coefficient for downwelling irradiance, Kd,** may be expressed (Kirk, 1983):

$$Kd(\lambda,z) = a_d(\lambda,z) + b_{bd}(\lambda,z) - \underline{b_{bu}(\lambda,z).R(\lambda,z)} \qquad (2.25)$$

where the negative term describes the reinforcement of downwelling irradiance by the downward scattering of upwelling irradiance. Also, we may write for K, equivalent to Eqn.2.22 and Eqn.2.23 for c:

$$K(\lambda,z) = \frac{-dE(\lambda)/E(\lambda,z)}{dz} = \frac{-1}{E(\lambda,z)}.\frac{dE(\lambda)}{dz} = \frac{-d}{dz}\,\mathrm{Ln}[E(\lambda,z)] \qquad (2.26)$$

$$\frac{E(\lambda,z_2)}{E(\lambda,z_1)} = \exp[-K(\lambda,z).\Delta z] = \exp[-J(\lambda)] \qquad (2.27)$$

where $K(\lambda,z).\Delta z = J(\lambda,z)$ is equivalent to $c(\lambda,z).\Delta z = \gamma(\lambda,z)$, the optical length for radiance (Eqn.2.23). Kirk (1983) referred to K.z simply as an 'optical depth'; Preisendorfer (1986) used the term **diffuse optical depth,** which is preferred for this work; 'optical

length/depth' will refer only to: $j = c.\Delta z$. The coefficients which may be expressed in the form of Eqns.2.26 and 2.27 are for downwelling vector irradiance:

$$Kd(\lambda,z) = -d/dz(Ln[Ed(\lambda,z)]) \qquad (2.28)$$

for upwelling vector irradiance:

$$Ku(\lambda,z) = -d/dz(Ln[Eu(\lambda,z)]) \qquad (2.29)$$

and for net downward irradiance:

$$K(\lambda,z) = -d/dz(Ln[Ed(\lambda,z) - Eu(\lambda,z)]) \qquad (2.30)$$

Equivalent expressions may be written for downwelling , upwelling and total (rather than net) scalar irradiance and PAR irradiance, eg:

$$^{o}Ko(z) = -d/dz(Ln[^{o}Eo(z)]) \qquad (2.31)$$

$$^{o}Jo(z) = {}^{o}Ko(z).\Delta z \qquad (2.32)$$

Equivalent to the characteristic attenuation length, ℓ_c, for radiance there is a characteristic extinction length: $\ell_k=1/K$, $^{o}\ell_k=1/{}^{o}Ko$ etc.

Inherent optical properties are additive so that we may write, for example, for the (total) absorption coefficient: $a^{tot} = a^{w} + a^{g} + a^{t} + a^{ph}$, where the superscripts indicate: total, water, gilvin, tripton and phytoplankton respectively. The terms on the right-hand side of this equation are the partial coefficients. Kirk (1983) has pointed out that there is no obvious reason for supposing that an apparent property, such as K, can be partitioned in this way. However, by

further subdivision of the w, g, t, ph- components of K into the terms given in Eqn.2.25, Kirk argues that: $K = a^{w}_{d} + a^{g}_{d} + \ldots + b^{w}_{bu}.R + b^{g}_{bu}.R$, so that partial apparent optical properties can be unambiguously defined in the same way as partial inherent properties. It must therefore be legitimate to write:

$$K(\lambda) = K^{w}(\lambda) + K^{g}(\lambda) + K^{t}(\lambda) + K^{ph}(\lambda), \text{ where } K = K, {}^{o}Ko \text{ etc} \qquad (2.33)$$

Højerslev (1975) also defines K1 and K2 which will be used in association with the irradiance collectors described in subsection 2.4.3. In terms of PAR irradiance:

$${}^{o}K1(z) = {}^{o}K(z)\,\frac{{}^{o}Ko(z) + {}^{o}a(z)}{{}^{o}K(z) + {}^{o}a(z)} = -d/dz(Ln[{}^{o}Eo(z) + {}^{o}E(z)]) \qquad (2.34)$$

$${}^{o}K2(z) = {}^{o}K(z)\,\frac{{}^{o}Ko(z) - {}^{o}a(z)}{{}^{o}K(z) - {}^{o}a(z)} = -d/dz(Ln[{}^{o}Eo(z) - {}^{o}E(z)]) \qquad (2.35)$$

The distribution function, $D(\lambda,z)$, or its reciprocal, the average cosine, $\overline{\cos\gamma}(\lambda,z)$, describes the angular structure of the radiation field at any point. D is equal to the mean path-lengths travelled by photons propagating through a layer of unit thickness. For downwelling light:

$$Dd(\lambda,z) = \frac{\int_{2\pi} L(\lambda,z,\gamma,\eta).d\omega}{\int_{2\pi} L(\lambda,z,\gamma,\eta).\cos\gamma.d\omega} = \frac{Eod(\lambda,z)}{Ed(\lambda,z)} \qquad (2.36)$$

for upwelling light:

$$Du(\lambda,z) = Eou(\lambda,z)/Eu(\lambda,z) \qquad (2.37)$$

and for the total light field:

$$D(\lambda,z) = \frac{Eo(\lambda,z)}{E(\lambda,z)} = \frac{Eo(\lambda,z)}{Ed(\lambda,z) - Eu(\lambda,z)} = \frac{E(\lambda,z)}{Ed(\lambda,z) + |Eu(\lambda,z)|} \qquad (2.38)$$

Some workers prefer to use the average cosine, $\overline{\cos\gamma}(\lambda,z)$, the reciprocal of the distribution function:

$$\overline{\cos\gamma_d}(\lambda,z) = \frac{Ed(\lambda,z)}{Eod(\lambda,z)} \; ; \quad \overline{\cos\gamma_u}(\lambda,z) = \frac{Eu(\lambda,z)}{Eou(\lambda,z)}$$

$$\overline{\cos\gamma}(\lambda,z) = \frac{E(\lambda,z)}{Eo(\lambda,z)} \qquad (2.39)$$

Besides being a simple conceptual indicator of the structure of the radiance field, the distribution functions are indispensable links between the various optical properties (Preisendorfer, 1960).

The irradiance reflectance, $R(\lambda,z)$, is the ratio of upwelling to downwelling irradiance at a given point in the radiation field:

$$R(\lambda,z) = Eu(\lambda,z)/Ed(\lambda,z); \quad {}^{o}Ro(\lambda,z) = {}^{o}Eou(\lambda,z)/{}^{o}Eod(\lambda,z) \text{ etc} \qquad (2.40)$$

Although not directly used in this work, mention is made of the 'reflectance' of remote sensing methods (Gordon et al, 1984):

$$R_{RS}(\lambda,z) = Lu(\lambda,z)/Ed(\lambda,z).$$

2.2.3 Hybrid optical properties

Hybrid optical properties are measured with reference to upwelling or downwelling streams; they are produced by combining inherent and

apparent optical properties and so escape simple operational definition.

The forward scattering, $bf(\lambda,z)$, and back scattering, $bb(\lambda,z)$, coefficients. These were described in subsection 2.1.3

The diffuse absorption, $a^*(\lambda,z)$, diffuse scattering, $b^*(\lambda,z)$, and diffuse attenuation, $c^*(\lambda,z)$, coefficients. In subsection 2.1.2, 2.1.3 and 2.2.1, $a(\lambda)$, $b(\lambda)$ and $c(\lambda)$ were defined in terms of collimated radiance. Analagous coefficients may be defined for the loss of photons from upwelling and downwelling streams of diffuse light. $a^*(\lambda) > a(\lambda)$ because of the increased pathlengths, represented by the distribution function, $D(\lambda)$ (Eqns.2.36-2.38), and so:

$$a^*_d(\lambda,z) = Dd(\lambda,z).a(\lambda); \quad a^*_u(\lambda,z) = Du(\lambda,z).a(\lambda) \tag{2.41}$$

Similarly, the following relationships hold:

$$b^*_d(\lambda,z) = b^*_{fd}(\lambda,z) + b^*_{bd}(\lambda,z) = Dd(\lambda,z).b(\lambda) \tag{2.42}$$

$$b^*_u(\lambda,z) = b^*_{fu}(\lambda,z) + b^*_{bu}(\lambda,z) = Du(\lambda,z).b(\lambda) \tag{2.43}$$

$$c^*_d(\lambda,z) = a^*_d(\lambda,z) + b^*_d(\lambda,z) \tag{2.44}$$

$$c^*_u(\lambda,z) = a^*_u(\lambda\ ,z) + b^*_u(\lambda,z) \tag{2.45}$$

According to Kirk (1983), the relationship between b^*_b and b_b is not so simple but may be calculated; in natural water bodies b^*_{bd} is commonly 2-5 times as big as b_b.

2.3 SIMPLE MODELS FOR RADIANCE AND IRRADIANCE

The structure of the light field is infinitely complex so that precise description is impossible. Theoretic models simplify the problem by concentrating on just one facet of the complexity. The two simple models for radiance and irradiance which follow describe the light fields generated by sunlight and skylight.

2.3.1 The radiance model

The radiance model relates the radiances at the beginning and end of an arbitrary path as illustrated in Fig.2.6. It is expressed by the equation of radiative transfer. The derivation of the equation of radiative transfer, given below, is distilled from a number of papers such as Preisendorfer (1960,1961,1976), Tyler et al (1974), Tyler and Preisendorfer (1962), Gordon (1975,1980), Smith et al (1974) and Fry (1974).

Snell's classical law of refraction must apply to flux across an air-water interface: $v_1/v_2 = \sin\xi_1/\sin\xi_2 = \mu$, the refractive index. As light passes through the air-sea interface there will be a general narrowing of a bundle of refracted light rays. The increase is by a factor of $\mu^2 = (4/3)^2 = 1.78$; an increase of 78%. This is the μ^2-law of radiance which states that along an arbitrary path through a medium which exhibits neither absorption, scattering nor secondary source of radiant flux, then L/μ^2 is invariant. In such a case, the equation of radiative transfer is: $(1/v).D/Dt(L/\mu^2) = 0$. If the path

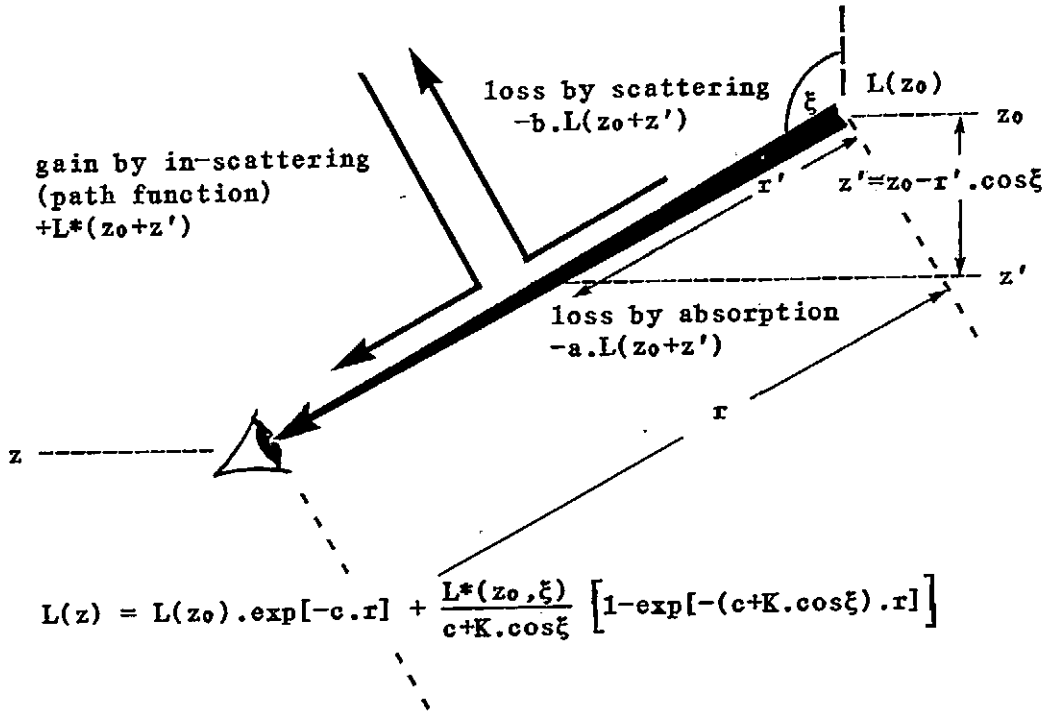

Fig.2.6: The radiance model

is now directed through a region in which there is absorption but no scattering, then: $(1/v).D/Dt(L/\mu^2) = -a.L/\mu^2$. In a real medium there must be scattering: $(1/v).D/Dt(L/\mu^2) = -(a+b).L/\mu^2 = -c.L/\mu^2$. The scattering medium will also scatter light into the path. It is this incoming radiance, termed the path function, L*, which gives rise to the veiling light of visibility problems. Taking this in-scattered radiance into account we have the Equation of Radiative Transfer:

$$(1/v).D/Dt[L(\lambda,z,\xi,\eta)/\mu^2(\lambda,z)]$$
$$= -c(\lambda,z).L(\lambda,z,\xi,\eta)/\mu^2(\lambda,z) + L^*(\lambda,z,\xi,\eta)/\mu^2(\lambda,z) \qquad (2.46)$$

where $L^*(\lambda,z,\xi,\eta) = \int_{4\pi} L(\lambda,z,\xi,\eta).\beta(\lambda,z,\xi,\eta).d\omega$

Light fields in the sea are in the steady state (D/Dt=0) and the index of refraction is essentially constant within the body of the sea ($d\mu/dt=0$) (Preisendorfer, 1960). It follows that the radiative transfer equation can be simplified to the more useful:

$$dL(\lambda)/dz = -c(\lambda,z).L(\lambda,z) + L^*(\lambda,z) \qquad (2.47)$$

Some optical instruments, such as the beam transmissometer, are shielded from in-scattered ambient light so that $dL/dr = -c(z).L(r)$:

$$c(\lambda,z) = \left[\frac{-1}{L(\lambda,r)}.\frac{dL(\lambda)}{dr}\right]_{L^*(\lambda)=0} = \left[\frac{1}{r}.Ln\left[\frac{L(\lambda,r)}{L(\lambda,0)}\right]\right]_{L^*(\lambda)=0} \qquad (2.48)$$

The differential equation, Eqn.2.46, is readily integrated if it is assumed that c is constant along the path, and that L* varies in the manner: $L^*(\lambda,z_2) = L^*(\lambda,z_1).\exp[-K.\Delta z]$ with depth only (Preisendorfer, 1976):

$$L(\lambda,z) = L(\lambda,z_0).\exp[-c(\lambda).r] + \int_0^r L^*(\lambda,z').\exp[-c(r-r')]\,dr' \qquad (2.49)$$

where $z' = z_0 - r'.\cos\xi$, therefore:

$$L(\lambda,z) = L(\lambda,z_0).\exp[-c(\lambda,r)] + \frac{L^*(\lambda,z)}{c(\lambda,z) + K(\lambda,z).\cos\xi}\left[1 - \exp[-(c(\lambda,z)+K(\lambda,z).\cos\xi).r]\right] \qquad (2.50)$$

Preisendorfer (1960) presents an interesting form of Eqn.2.50 based on the fact that in the sea, the radiance along a horizontal path is invariant with distance r, ie dL/dr=0, in which case: $c=L^*/L$. This

equation states that the spatial rate of loss of radiance by attenuation, $c.L = dL/dr$, is exactly replaced by the spatial rate of light scattered in, L^*. Kirk (1983) uses Eqn.2.47 to derive the well known optical divergence equation originally presented by Gershun (1936). He argues that since $dr = dz.\cos\xi$ then this equation may be rewritten: $\cos\xi.dL/dr = -c.L + L^*$. Integrating each term over all angles:

$$\int_{4\pi} \cos\xi.\frac{dL}{dz}.d\omega = -\int_{4\pi} c.L.d\omega + \int_{4\pi} L^*.d\omega \qquad (2.51)$$

whence it may be deduced that:

$$dE(\lambda,z)/dz = -c(\lambda,z).Eo(\lambda,z)+b(\lambda,z).Eo(\lambda,z) = -a(\lambda,z).Eo(\lambda,z) \qquad (2.52)$$

Gershun (1936) expressed this equation: $\text{div}\,E = -a.Eo$, but since $\text{div}_H E = 0$ in the sea then Eqn.2.52 must follow. It may be assumed that the hydro-optical environment is horizontally stratified; this is so even in frontal zones because the slope of β-isosurfaces and c-isosurfaces is so small (Højerslev, 1986).

Højerslev (1972) combines Eqn.2.52 with $K = -(1/E).(dE/dz)$, (Eqn.2.26), to derive the expression by which the absorption coefficient can be measured by means of the $2x2\pi$ irradiance sensor discussed in Chapters 3 and 4:

$$a(\lambda,z) = K(\lambda,z).E(\lambda,z)/Eo(\lambda,z) = K(\lambda,z).\overline{\cos\xi}(\lambda,z) \qquad (2.53)$$

2.3.2 The two-flow model for irradiance

The two-flow model supposes that in a natural hydrosol, the field is divided into two fluxes, namely the downwelling and upwelling irradiances, Ed and Eu (Preisendorfer, 1976). The purpose of the model is to predict Ed and Eu at any z, given values at any other depth. It is assumed that the propagation medium is plane-parallel and that: Dd = Du = D = Eod/Ed = Eou/Eu. If a is the absorption coefficient for irradiance, then from subsection 2.2.3: $a^* = D.a$ and $b_b^* = D.b_b$. Scattered photons are not lost from the diffuse flux but only redirected; it follows that the back-scattering coefficient, $b^* \neq D.b$ but $b^* = b$. So, the flux lost from Ed in propagating Δz is: $D.a.Ed.\Delta z + b.Ed.\Delta z$. Added to this flux will be the photons back-scattered (upwards) from Eu, so that:

$$\Delta Ed = -(a.D+b).Ed.\Delta z + b.Eu.\Delta z \qquad (2.54)$$

and for the upwelling flux:

$$\Delta Eu = -(a.D+b).Eu.(-\Delta z) + b.Eu.(-\Delta z) \qquad (2.55)$$

Dividing these eqnations by Δz and $-\Delta z$ respectively, and letting $\Delta z \to 0$:

$$\frac{d}{dz} Ed(\lambda,z) = -[a(\lambda,z).D(\lambda,z)+b(\lambda,z).Ed(\lambda,z)+b(\lambda,z).Eu(\lambda,z) \qquad (2.56)$$

$$\frac{d}{dz} Eu(\lambda,z) = -[a(\lambda,z).D(\lambda,z)+b(\lambda,z).Eu(\lambda,z)+b(\lambda,z).Ed(\lambda,z) \qquad (2.57)$$

These two equations constitute the two-flow model for irradiance, for

which the solutions (Preisendorfer, 1976) are:

$$Ed(\lambda,z) = Mu.(1-a(\lambda,z).D(\lambda,z)/K(\lambda,z)).\exp[K(\lambda,z).z] + Md.(1+a(\lambda,z).D(\lambda,z)/K(\lambda,z)).\exp[-K(\lambda,z).z] \quad (2.58)$$

$$Eu(\lambda,z) = Mu.(1+a(\lambda,z).D(\lambda,z)/K(\lambda,z)).\exp[K(\lambda,z).z] + Md.(1-a(\lambda,z).D(\lambda,z)/K(\lambda,z)).\exp[-K(\lambda,z).z] \quad (2.59)$$

where Mu, Md are arbitrary constants fixed by specifying Ed or Eu at two depths, and:

$$K(\lambda,z) = (a(\lambda,z).D(\lambda,z).(a(\lambda,z).D(\lambda,z)+2.b(\lambda,z)))^{0.5} \quad (2.60)$$

in which case we may write for PAR irradiance:

$$^{o}Ko = (^{o}a.^{o}D.(^{o}a.^{o}D + 2.^{o}b))^{0.5} \quad (2.61)$$

2.4 THE EXTINCTION OF IRRADIANCE

2.4.1 The irradiance profile

In a column of homogeneous water, quantum scalar irradiance, °Eo at any depth, z, is given from Eqn.2.27: $^{\circ}Eo(z) = {}^{\circ}Eo(0).\exp[-{}^{\circ}Ko.z]$. Generally, the column will not be totally homogeneous so we introduce $\langle{}^{\circ}Ko\rangle$, the depth-mean value of °Ko between the surface and depth z:

$$^{\circ}Eo(z) = {}^{\circ}Eo(0).\exp[-\langle{}^{\circ}Ko\rangle.z];\ \langle{}^{\circ}Ko\rangle = -d/dz(\mathrm{Ln}[{}^{\circ}Eo(z)]) \qquad (2.62)$$

It is usually preferred to express the exponential profile as a straight line of gradient $-\langle{}^{\circ}Ko\rangle$, ie $\mathrm{Ln}[{}^{\circ}Eo(z)] = \mathrm{Ln}[{}^{\circ}Eo(0)]-\langle{}^{\circ}Ko\rangle.z$. It is seldom the absolute value of $\mathrm{Ln}[{}^{\circ}Eo(z)]$ that is of interest as this is a function of °Eo(0), and so subject to large and rapid variations in skylight. More useful is the PAR diffuse optical depth, from Eqn.2.27: $^{\circ}Jo(z) = \langle{}^{\circ}Ko\rangle.z = \mathrm{Ln}[{}^{\circ}Eo(0)/{}^{\circ}Eo(z)]$.

Frequent reference is made in biological text (eg Kirk, 1983) to the euphotic zone, which extends from the surface to the euphotic depth, Ze, the depth at which the light level is 1% of the surface value. From Eqn.2.27:

$$^{\circ}Je = \mathrm{Ln}[{}^{\circ}Eo(0)/{}^{\circ}Eo(Ze)] = \mathrm{Ln}[100] = 4.605 \qquad (2.63)$$

and for the mid-depth of the euphotic zone, Zm, at which the PAR

level must be 10% of the surface value:

$$^{\circ}Jm = Ln[^{\circ}Eo(0)/^{\circ}Eo(Zm)] = Ln[10] = 2.303 \qquad (2.64)$$

Eqns.2.62, 2.63 and 2.64 are illustrated in Fig.2.7.

Biological texts also refer to the compensation depth, Zc, at which the rate of photosynthesis is equal to the rate of respiration and suggest that Zc lies, approximately, at the 1% level. It is to be noted, however, that Zc represents a biological concept whilst Ze is an apparent optical property of the water.

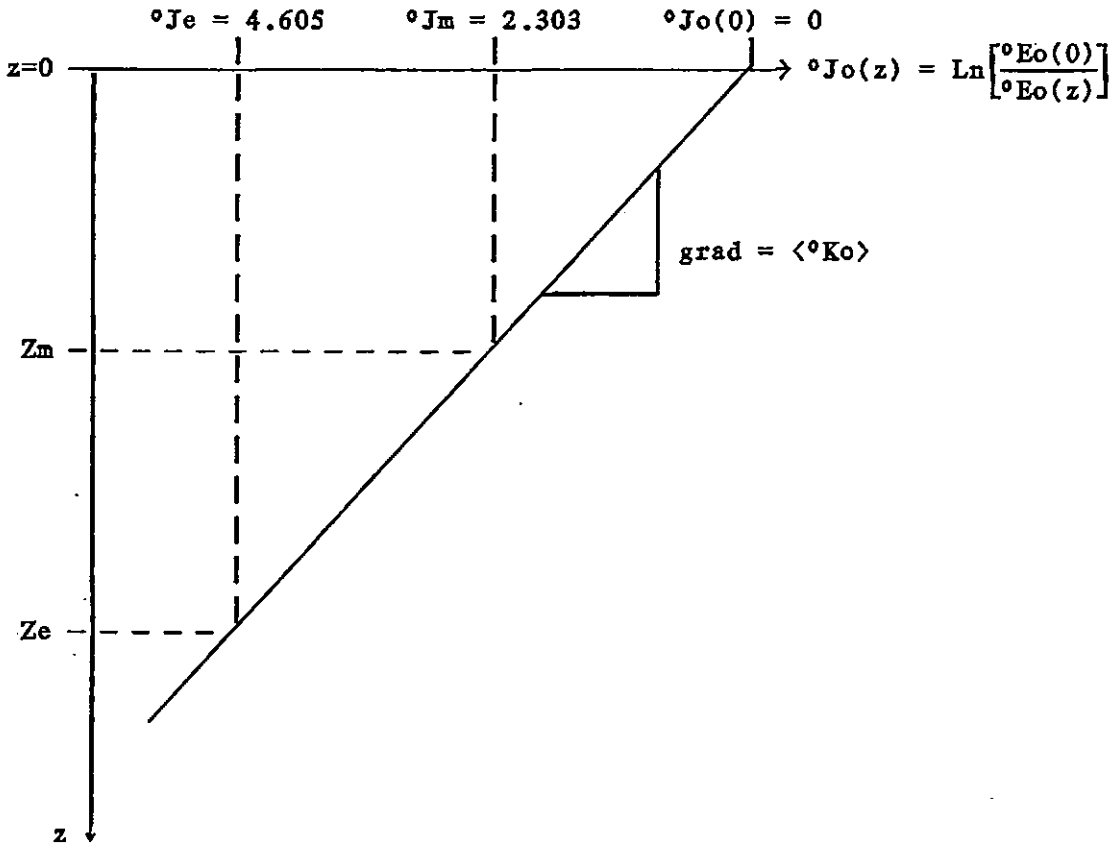

Fig.2.7: The °Jo(z) profile

2.4.2. Irradiance collectors

The form of irradiance measured by a system depends upon the shape and configuration of its collector. A range of irradiance collectors has been reviewed by Højerslev (1975) and are illustrated in Fig.2.8 on the next page. They are:

Ed-collector. This is the classical cosine collector in which the collected flux, F, is given by:

$$F = \int_{2\pi} L(\xi,\eta).\cos\xi.d\omega = Ed \qquad (2.65)$$

Inverted, it becomes an **Eu-collector.** An **E-collector**, or Janus collector comprises of two such collectors back-to-back.

Eo-collector. The flat senor dS is placed horizontally at the base of an opal sphere. The flux from ξ,η is: $dF(\xi,\eta) = \pi r^2.L(\xi,\eta).d\omega$, so the total flux is:

$$F = \int_{4\pi} dF(\xi,\eta).d\omega = \pi r^2 \int_{4\pi} L(\xi,\eta).d\omega = \pi r^2.Eo \qquad (2.66)$$

Eod-collector. The collector is sited on an infinite, absolutely black, horizontal plane at the same level as dS. Clearly, integration is now possible only for $0 \leq \xi \leq \pi$:

$$F = \int_{2\pi} dF(\xi,\eta).d\omega = \pi r^2 \int_{2\pi} L(\xi,\eta).d\omega = \pi r^2.Eod \qquad (2.67)$$

Inverted, it becomes a **Eou-collector.**

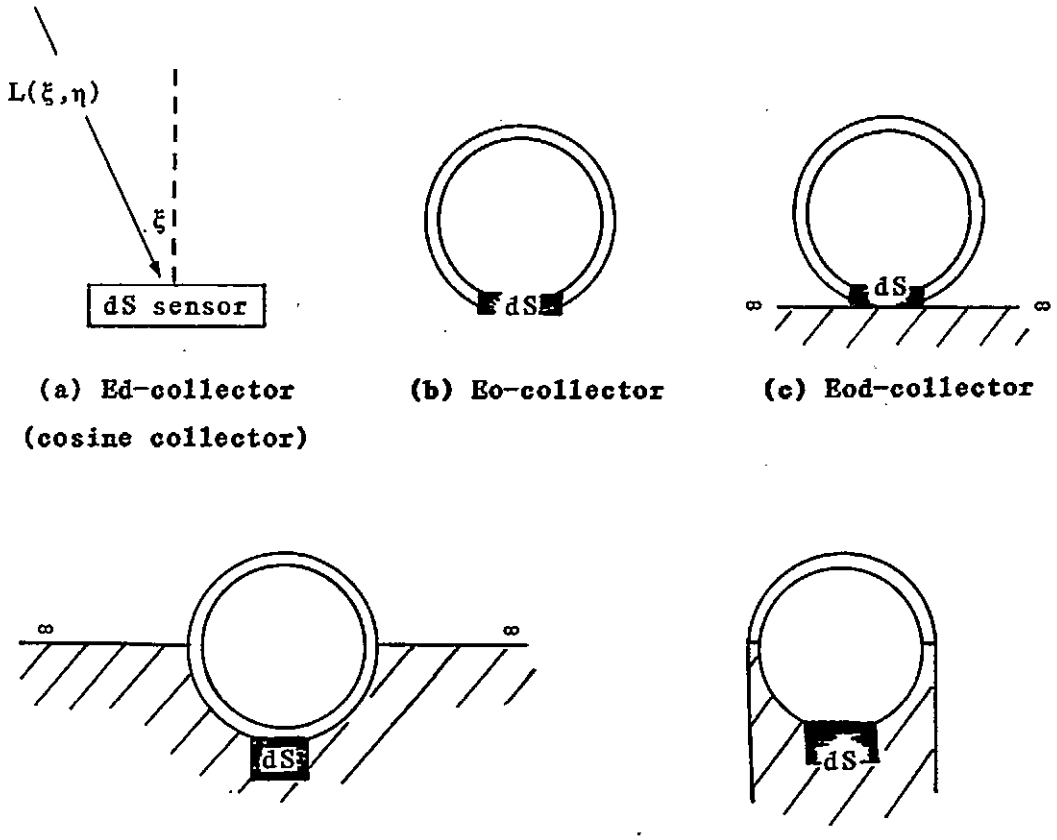

(a) Ed-collector (cosine collector)

(b) Eo-collector

(c) Eod-collector

(d) ½(Eod+Ed)-collector

(e) ½(Eo+E)-collector

Fig.2.8: Irradiance collectors

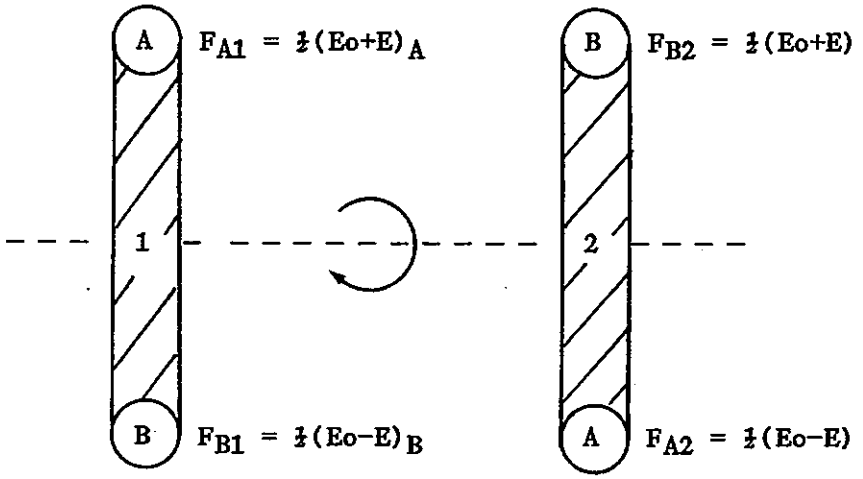

Fig.2.9: Højerslev's ½(Eo-E)+½(Eo-E) system

½(Eod+Ed)-collector. The horizontal black plane extends from the equator of the sphere to infinity, and the lower hemisphere is absolutely black.

$$dF(\gamma,\eta) = \tfrac{1}{2}\pi r^2.L(\gamma,\eta).d\omega + \tfrac{1}{2}\pi r^2.L(\gamma,\eta).\cos\gamma.d\omega$$

$$\text{so, } F = \tfrac{1}{2}\pi r^2\int_{2\pi} L(\gamma,\eta).d\omega + \tfrac{1}{2}\pi r^2\int_{2\pi} L(\gamma,\eta).\cos\gamma.d\omega$$

$$= \tfrac{1}{2}\pi r^2(Eod+Ed) \qquad (2.68)$$

Inverted, it becomes a½(Eou+Eu)-collector.

½(Eo+E)-collector. Again, only the upper hemisphere is exposed but the infinite horizontal plane is removed. Limits of integration are now $0 \leq \gamma \leq 2\pi$:

$$\text{so, } F = \tfrac{1}{2}\pi r^2\int_{4\pi} L(\gamma,\eta).d\omega + \tfrac{1}{2}\pi r^2\int_{4\pi} L(\gamma,\eta).\cos\gamma.d\omega$$

$$= \tfrac{1}{2}\pi r^2(Eo + Ed - Eu) = \tfrac{1}{2}\pi r^2(Eo + E) \qquad (2.69)$$

Inverted, it becomes a ½(Eo-E)-collector.

Højerslev's ½(Eo+E) + ½(Eo-E) system. Højerslev (1975) describes a meter which measures ½(Eo+E) and ½(Eo-E). From vertical profiles of these parameters it is possible to calculate Kd(z), Ko(z) and a(z). Moreover, by making the instrument invertible, it does not require the difficult calibration procedures generally associated with absorption meters. Consider the meter as illustrated in Fig.2.9 and suppose that sensors A and B have unknown calibration factors: f_A and f_B.

The four outputs (A and B, upwelling and downwelling) will be:

$$Ad = f_A.\tfrac{1}{2}(Eo + E)_A$$

$$Au = f_A.\tfrac{1}{2}(Eo - E)_A$$

$$Bd = f_B.\tfrac{1}{2}(Eo + E)_B$$

$$Bu = f_B.\tfrac{1}{2}(Eo - E)_B$$

whence:

$$Ad + Au = f_A.Eo$$

$$Bd + Bu = f_B.Eo$$

$$Ad - Au = f_A.E$$

$$Bd - Bu = f_B.E$$

We may therefore write:

$$\langle Ko\rangle_A = (-d/dz.Ln[Eo])_A = \frac{-d}{dz}.Ln\left[\frac{Ad + Au}{f_A}\right]$$

$$= \frac{-d}{dz}.Ln[Ad + Au], \text{ for } f_A = \text{const} \qquad (2.70)$$

and by similar argument:

$$\langle Ko\rangle_B = \frac{-d}{dz}.Ln[Bd + Bu], \text{ for } f_B = \text{const} \qquad (2.71)$$

Of course Eqns.2.70 and 2.71 should be the same; in practice a mean value may be used. By exactly similar reasoning we may find, for the extinction of vector irradiance:

$$\langle K\rangle_A = \frac{-d}{dz}.Ln[Ad - Au], \text{ and } \langle K\rangle_B = \frac{-d}{dz}.Ln[Bd - Bu] \qquad (2.72)$$

Because $dE/dz = -a.Eo$ (Gershun, 1936), and $K = (-1/E).dE/dz$, then the absorption coefficient, a(z) may be obtained from:

$$a(z)_A = \frac{-d}{dz}.Ln[Ad-Au].\left[\frac{Ad-Au}{Ad+Au}\right] \; ; \quad a(z)_B = \frac{-d}{dz}.Ln\left[\frac{Bd-Bu}{Bd-Bu}\right] \qquad (2.73)$$

The average cosine for the total light field, $\overline{\cos\xi}(z) = E(z)/Eo(z)$, is given by:

$$\overline{\cos\xi}(z)_A = \left[\frac{Ad-Au}{Ad+Au}\right] \; ; \; \overline{\cos\xi}(z)_B = \left[\frac{Bd-Bu}{Bd+Bu}\right] \qquad (2.74)$$

The vector reflectance coefficient, $R(z) = Eu(z)/Ed(z)$, can not be calculated as Eu and Ed are not separately obtained.

2.4.3 Kirk's Monte Carlo model for scalar irradiance

The inherent optical properties specify the probability of certain events occurring, eg $c(\lambda)$ governs the probability of a photon travelling a certain distance before interacting with some component of the medium (Kirk, 1981a). The inherent properties therefore provide a means of modelling light propagation by the Monte Carlo method; the fates of large numbers of photons are individually followed in the computer and the average behaviour of the total flux calculated. This technique has been used by several workers, including Plass and Kattawar (1969, 1972), Kattawar and Plass (1972), Gordon and Brown (1973, 1974, 1975), Gordon et al (1975). However, this work has concentrated on marine or clear freshwater systems; Kirk (1981a) conducted a Monte Carlo simulation of light propagation in turbid water. Kirk's model is described in some detail in Kirk (1981a, 1981c), and a Fortran programme is presented in Kirk (1981c).

To simplify the computation, Kirk assumes that all input light is direct sunlight and that surface reflection is zero. Once within a water body, the probability of a photon following a pathlength, r, before interacting with a component of the medium is governed by the attenuation coefficient, c. Thus the probability of attenuation within distance r is given by: $1 - \exp[-c.r]$. A random number, $0 \leq n \leq 1$, is generated by the programme and the pathlength calculated: $r = -(1/c).\mathrm{Ln}[1-n]$. Another random number, $0 \leq n \leq 1$, is selected and if $r \leq a/(a+b)$ then absorption is assumed and a new photon is introduced. If $r > a/(a+b)$ then the photon is considered to be scattered at randomly generated angle, σ, and a new trajectory is followed. It is assumed that photons reaching the surface at an angle $\geq 41.4°$ pass through; other photons are reflected down again. Every photon is thus followed until it is absorbed, reaches the totally absorbing bottom or is lost through the surface. By means of this model, Kirk (1981a) has shown that the averge cosine, $\overline{\cos}\xi(\lambda,z)$, and irradiance reflectance, $R(\lambda,z)$, may be deduced from a knowledge of the irradiance depth, $J(\lambda,z)$, scattering-absorption ratio, $b(\lambda)/a(\lambda)$, and solar altitude. Conversely, $a(\lambda)$, $b(\lambda)$ and $\overline{\cos}\xi(\lambda,z)$ may be found from measurements of $J(\lambda,z)$ and $R(\lambda,z)$. Of greater significance to the present research programme is the work of Kirk (1986) in which he shows that $\overline{\cos}\xi(z)$ and the ratio of the diffuse coefficients, b_o/a_o, may be found from scalar properties $J_o(z)$ and $R_o(z)$. For convenience, he uses $R_o(Zm)$ and $J_o(Zm)$ at the 10% level, Zm, and proceeds in the following manner. $R_o(Zm)$ is found from E_{ou}/E_{od} at Zm, and used in Fig.2.10 to obtain $b_o/a_o(Zm)$ and $\overline{\cos}\xi(Zm)$ for a particular solar altitude. Using $a = \overline{\cos}\xi.Ke$ and assuming that $Ke = Ko$, (found from the $E_o(z)$ profile), then $a_o(Zm) = \overline{\cos}\xi(Zm).K_o(Zm)$. Since $b_o/a_o(Zm)$ is known then $b_o(Zm)$ may also be deduced.

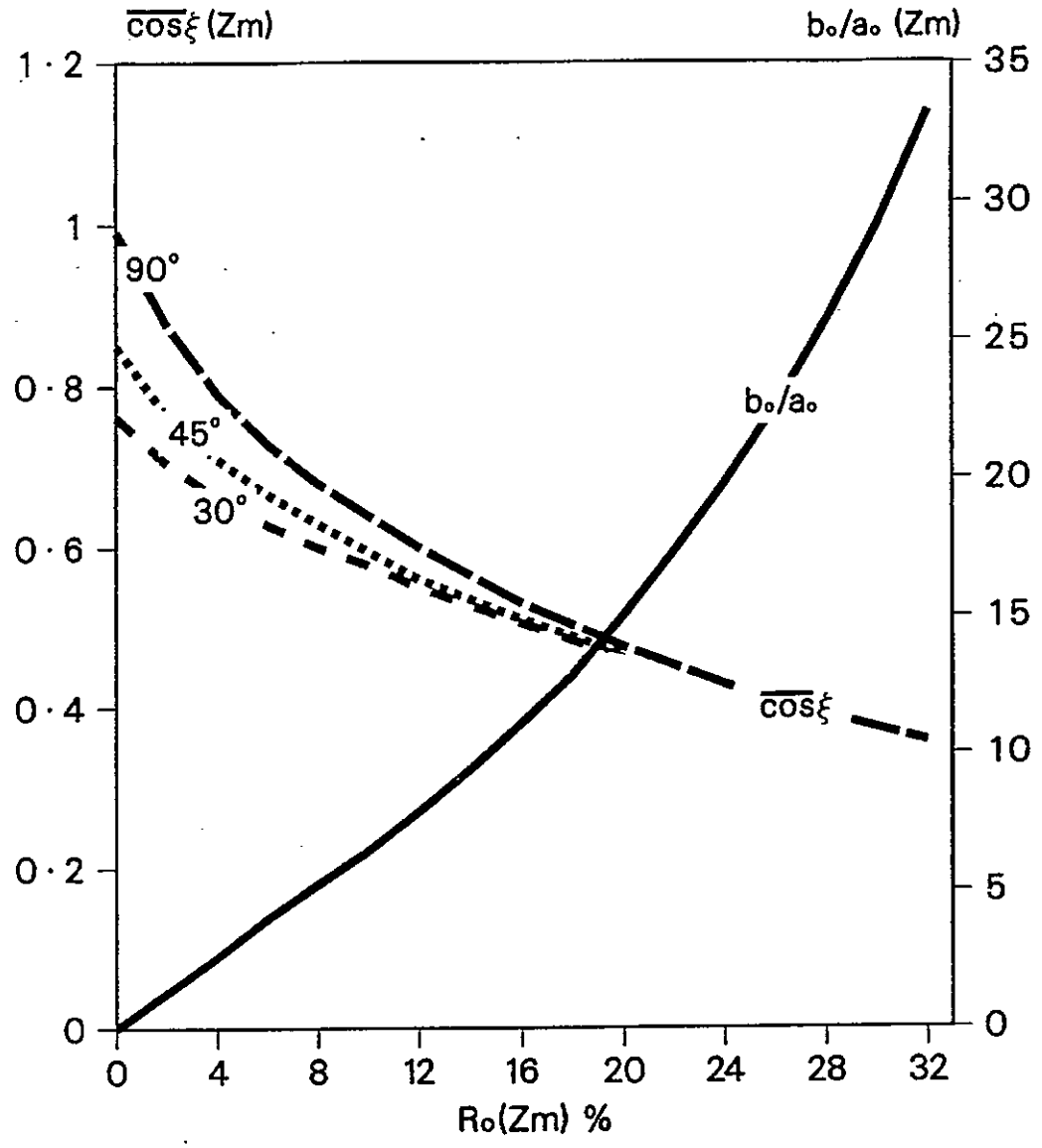

Fig.2.10: Graphs of the average cosine, $\overline{\cos}\xi$(Zm), for sun's altitude 30°, 45° and 90°, and the ratio b_o/a_o(Zm) as functions of water reflectivity Ro(Zm). Zm is the depth at which Eod(z)/Eod(0) = 10%, and corresponds approximately to the mid-depth of the euphotic zone, (Kirk, 1986).

2.5 UNDERWATER VISIBILITY

2.5.1 Photometric measurement

Photometry refers to light flux visually perceived by the human eye. The fundamental quantity used in the radiometric definitions considered in subsection 2.1.1 was radiant energy, given by Eqn.2.1: $F(\lambda) = dQ(\lambda)/dt$. This flux is an absolute quantity independent of the sensitivity of the detecting device. The flux units used in photometry depend upon the spectral sensitivity of the human eye which rises from zero at 400nm to a peak at 555nm (yellow-green), decreasing to zero at 700nm. For example, it would take about 2 watts of blue-green (510nm) or orange (610nm) light to produce the same sensation of brightness as 1 watt of yellow-green (555nm) light.

The unit of luminous (photometric) flux is the lumen, defined as the luminous flux emitted in all directions by a black body of surface area 1/60 cm^2 at a temperature of 2042 K (Preisendorfer,1976). Equivalent radiometric/photometric units are given in Table 2.2. Preisendorfer (1976) gives the following equation to convert a radiometric concept, X(rad), to its photometric counterpart X(photo):

$$X(\text{photo}) = 680 \int_0^\infty X(\text{rad}).y(\lambda).d\lambda \qquad (2.75)$$

Where $y(\lambda)$ is the luminosity function, eg $y(\lambda) = 0(400), 0.03(450), 0.32(500), 0.99(550), 1.00(555), 0.64(600), 0.11(650), 0(700)$.

Table 2.2: Equivalent radiometric/photometric units
(from Preisendorfer, 1976)

Radiometry	Photometry
Radiant flux $F(\lambda)$ [W]	Luminous flux $\underline{F}$ [lumens]
Radiance $L(\lambda)$ [$q.s^{-1}m^{-2}$]	Luminance (brightness) $\underline{L}$ [lumens m^{-2} = lux]
Irradiance $E(\lambda)$ [$q.s^{-1}m^{-2}$]	Illuminance $\underline{E}$ [lumens m^{-2} = lux]

In discussing Secchi disc visibility (see subsection 2.5.4), Højerslev (1986) points out that the appropriate parameters are the photometric c(lux), K(lux), R(lux) etc. This is a very important distinction which is not generally made in the literature; in this work, photometric (lux) parameters will be indicated by underlining: $\underline{c}$, $\underline{K}$, $\underline{\rho}$, $\underline{R}$, $\underline{L}$ and $\underline{E}$.

2.5.2 Contrast transmittance

The visibility of an object is the maximum range at which it can be visually detected against its background. If the object is a different colour to its background then it may be visible because of its colour contrast. The selective absorption of particular wavelengths (or broad wavelength bands) leads to monochromatic conditions underwater. For example, clear water becomes blue with depth; productive water, due to the presence of gilvin, displays a 'yellow shift' towards sea-green. Moreover, with depth, or in turbid

coastal waters, light levels may be too low for photopic vision. It follows, therefore, that underwater visibility is usually limited by brightness (luminance) contrast, C, defined by:

$$C = \frac{\text{target luminance - background luminance}}{\text{background luminance}} \qquad (2.76)$$

We therefore express the inherent contrast, Co, the contrast a target would have if viewed at zero distance, by: $Co = ({}_t\underline{L}(0) - {}_b\underline{L}(0))/{}_b\underline{L}(0)$, where subscripts t and b indicate target and background. It is convenient at this point, to introduce a sighting angle, γ, measured from the horizontal ($+\gamma$ downwards and $-\gamma$ upwards; $\gamma = \xi - \pi/2$). The inherent contrast of a target viewed vertically downward ($\gamma = \pi/2$) is described by Tyler (1968), and illustrated in Fig.2.11. The object, (eg Secchi disc), has reflectivity $\underline{\rho}$, and the water-background has reflectivity $\underline{R}$. If the downwelling irradiance (illuminance) is Ed then from Eqn.2.76:

$$Co(\underline{\rho}, \pi/2) = \frac{\underline{\rho}.\underline{Ed}/\pi - \underline{R}.\underline{Ed}/\pi}{\underline{R}.\underline{Ed}/\pi} = \underline{\rho}/\underline{R} - 1 \qquad (2.77)$$

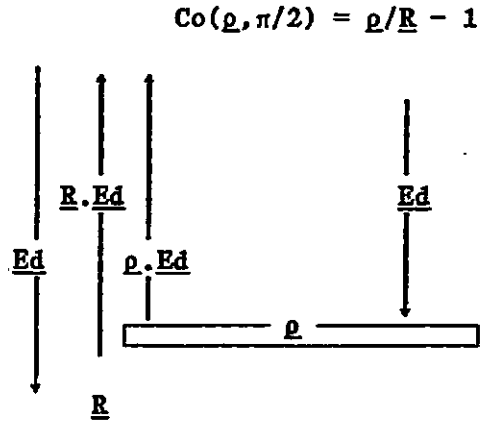

Fig.2.11: Inherent contrast of target sighted vertically downwards

The division by π on the right hand side of Eqn.2.77 indicates that the reflected light is diffuse. It cancels and so, for simplicity, will not be included from here on.

The inherent contrast of non-black targets sighted horizontally ($\gamma = 0$) is not widely discussed in the literature, but we may assume that a form of Eqn.2.77 would not be appropriate as the water-background brightness depends not upon the water's reflectivity, but upon the horizontally invariant spacelight: ${}_b\underline{L}(0) = \underline{L}^*$ (see section 2.3.1). This is illustrated in Fig.2.12, and indicates that:

$$Co(\underline{\rho},0) = \frac{\underline{\rho}.\underline{L}^* - \underline{L}^*}{\underline{L}^*} = \underline{\rho} - 1 = -(1 - \underline{\rho}) \qquad (2.78)$$

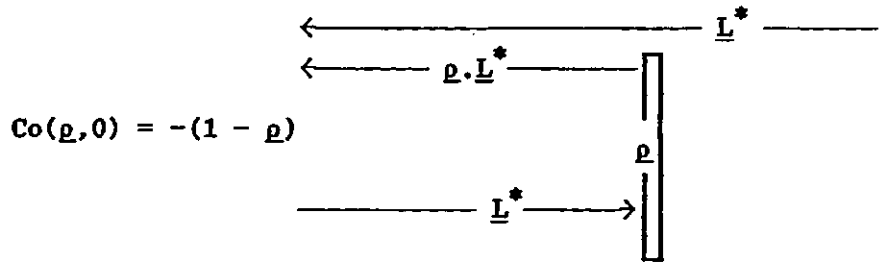

Fig.2.12: Inherent contrast of target sighted horizontally

Equation 2.78 implies that the inherent contrast, and hence the visibility of a horizontally-viewed target decreases with reflectivity; that a white target will be less visible than a grey one. This is so only in very turbid water where the background water is 'milky-white'; generally, $Co(\underline{\rho},0)$ is observed to increase with $\underline{\rho}$. This is because underwater objects tend to be illuminated by high intensity downwelling light rather than lower intensity side light,

as implied by Eqn.2.78. The contrast problem is further complicated by the fact that downwelling and side lights have different spectral intensity curves so that white targets, particularly, will differ slightly in colour from the water-background. In experiments off Malta, at a depth of 15m, Hemmings and Lythgoe (1965) found that the ratio of intensity of side light to downwelling light was about 10% at 450 nm, decreasing to about 4% at 570 nm. The ratio of target (white) radiance to water-background radiance was 2.5 at 440 nm and 2.2 at 460 nm, increasing to 5.2 at 550 nm. It must follow, therefore, that Eqn.2.78 does not properly describe the inherent contrast of a horizontally-sighted, non-black target.

The first rigorous underwater visibility theory is usually attributed to the work of Duntley and Preisendorfer (1952), who reported an experimental investigation of the reduction of visual contrast underwater, which they had conducted in 1948. Their observations revealed that the apparent contrast, Cr, of a target is exponentially attenuated with distance along any path of sight (ie, that like brightness, brightness contrast follows Beer-Lambert's Law). Further experiments in 1949 showed that along horizontal paths of sight, the contrast transmittance equals the beam transmittance of the same water. Both of these field observations can be derived from the equation of radiative transfer (Eqn.2.46), as now shown.

Suppose a target at depth z_t and range r in infinitely deep water, is observed at angle $0 \leq \gamma \leq \pi/2$ from depth z, as illustrated in Fig.2.12.

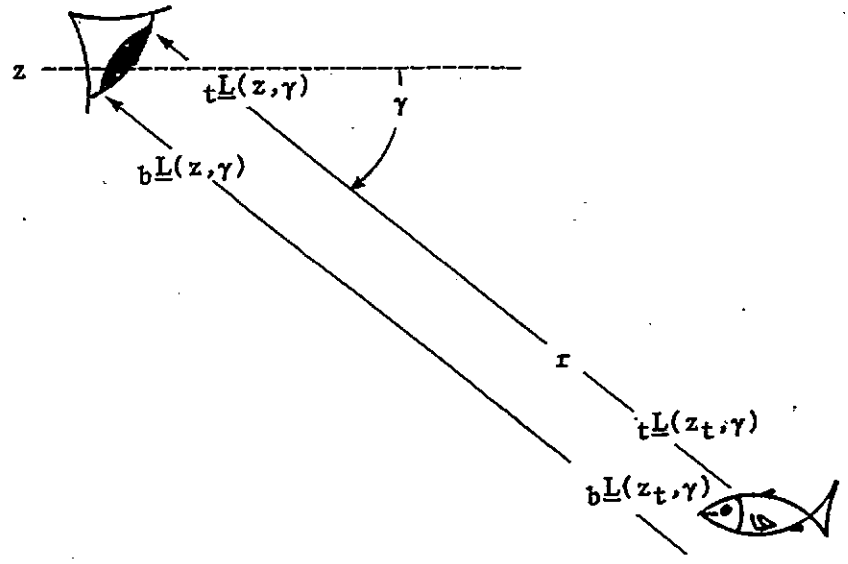

Fig.2.13: Contrast transmittance

We may write, from this figure:

$$Co(\underline{\rho},\gamma,z_t) = \frac{{}_t\underline{L}(z_t,\gamma) - {}_b\underline{L}(z_t,\gamma)}{{}_b\underline{L}(z_t,\gamma)} \tag{2.79}$$

$$Cr(\underline{\rho},\gamma,z) = \frac{{}_t\underline{L}(z,\gamma) - {}_b\underline{L}(z,\gamma)}{{}_b\underline{L}(z,\gamma)} \tag{2.80}$$

The apparent radiance ${}_t\underline{L}(z,\gamma)$ is given by eqn 2.46:

$${}_t\underline{L}(z,\gamma) = {}_t\underline{L}(z_t,\gamma).\exp[-\underline{c}.r] + \frac{\underline{L}^*(z,\gamma)}{\underline{c}+\underline{K}.\sin\gamma}.(1 - \exp[-(\underline{c}+\underline{K}.\sin\gamma).r]) \tag{2.81}$$

The first term on the right describes the loss of image-forming light and the second term describes the gain in veiling or space light (non image-forming diffuse light). The background inherent and apparent

radiances are the radiance of the space light given by Eqn.2.81, viewed from r=∞, ie:

$$ {}_{b}\underline{L}(z,\gamma) = {}_{b}\underline{L}(z_t,\gamma) = \frac{\underline{L}^{*}(z_t,\gamma)}{\underline{c}+\underline{K}.\sin\gamma} \qquad (2.82) $$

By substitution of Eqns 2.81 and 2.82, this equation is reduced, (Preisendorfer, 1976), to:

$$ Cr(\gamma) = Co(\gamma).\exp[-(\underline{c}+\underline{K}.\sin\gamma).r] \qquad (2.83) $$

This is the Contrast Transmittance Law, presented by Duntley and Preisendorfer (1952) for underwater work, and later, by Duntley, Boileau and Preisendorfer (1957) for use in the atmosphere. For observations of horizontal visibility ($\gamma = 0$), Eqn.2.83 reduces to:

$$ Cr(\underline{\rho},0) = Co(\underline{\rho},0).\exp[-\underline{c}.r] \qquad (2.84) $$

For vertically downward sighting ($\gamma = \pi/2$, eg Secchi disc):

$$ Cr(\underline{\rho},\pi/2) = Co(\underline{\rho},\pi/2).\exp[-(\underline{c}+\underline{K}).r] \qquad (2.85) $$

and for vertically upward sighting ($\gamma = -\pi/2$):

$$ Cr(\underline{\rho},-\pi/2) = Co(\underline{\rho},-\pi/2).\exp[-(\underline{c}-\underline{K}).r] \qquad (2.86) $$

Experimental verification of Eqn.2.84 was obtained by Duntley and Preisendorfer (1952), for light and dark objects, by means of photographic and photoelectric telephotometers mounted at five foot intervals along a trackway projecting from a barge. These results strongly supported their hypothesis that the only light from and target reaching an observer is light which has transversed the

intervening space without scattering; scattered light from the target serves solely as a contribution to the scalar irradiance. It has been pointed out by Højerslev (1986), however, that this theory holds only where attenuation is constant for all z,ξ,η which may not be the case in some surface waters.

2.5.3 Visual ranges.

Of course, a range may be reached at which Cr is reduced to a level too low for visual detection by the observer. This limiting apparent contrast is termed the liminal or threshold contrast, Ct. In a pioneering paper on the subject, Blackwell (1946) defined the apparent contrast of an object as threshold if an observer, on repeated attempts under identical conditions to decide whether an object is visible, decides that it is so on 50% of the occasions. Blackwell reported experimental determinations of Ct in which 450,000 observations (out of over two million) by 19 trained observers were analysed to compile threshold tables and diagrams. These tables give: Ct = 0.0033 for circular targets in air. Tyler (1968) suggested that this be doubled for underwater work and so a value of Ct = 0.0066 has been used by many workers (eg Holmes, 1970; Højerslev, 1977, 1986; Preisendorfer, 1976, 1986). Working with a Secchi disc in Goleta Bay, Holmes (1970) deduced a threshold contrast of 0.0013, implying a threshold visual sensitivity twice that found by Blackwell in air. This seems unlikely as in reporting his wartime experiments Blackwell (1946) writes that 'The observers were young women, aged 19-26 years, whose visual acuity in each eye and in both eyes was approximately 20/20 without refractive correction ... Observers were seated at the rear of the observation room in

upholstered chairs ... Observers were allowed to adapt to the observation room brightness... by preliminary adaptation outside the laboratory with standard Polaroid dark adaptation goggles... The overall brightness of the observation room was subject to precise control...'. Clearly this scenario does not typify the optical conditions endured by the middle aged oceanographer as he hangs over the side of a heaving boat peering into the murky depths below.

Lythgoe (1979) has shown that a diver, with normal vision and using a face mask, can perceive a brightness contrast of 2%; a value of Ct = 0.02 will therefore be preferred in this work. Substituting Ct for Cr in Eqn.2.83, and introducing threshold visibility, $V(\gamma)$:

$$Cr = Ct = 0.02 = Co.\exp[-(\underline{c}+\underline{K}.\sin\gamma).V(\gamma)]$$

$$V(\gamma) = \frac{Ln[Co/Ct]}{\underline{c}+\underline{K}.\sin\gamma} = \frac{Ln[Co/0.02]}{\underline{c}+\underline{K}.\sin\gamma} = \frac{Ln[50.Co]}{\underline{c}+\underline{K}.\sin\gamma} \qquad (2.87)$$

In the special case of a zero-reflector, (ρ=0; eg the light-trap described in Chapter 3), the inherent contrast is, from Eqn.2.77: $Co(0,\gamma) = -1$. The negative sign indicates a target darker than its background, so must remain in force to the point of threshold visibility, ie Ct = -0.02. Substituting into Eqn.2.87:

$$V(0,\gamma) = \frac{Ln[(-1)/(-0.02)]}{\underline{c}+\underline{K}.\sin\gamma} = \frac{Ln[50]}{\underline{c}+\underline{K}.\sin\gamma} \qquad (2.88)$$

Duntley and Preisendorfer (1952) coined the term hydrological range, $v(\gamma)$, to define the distance through optically homogeneous water for which the contrast transmittance is reduced to 2%. They were

therefore able to write:

$$Cr/Co = 0.02 = \exp[-(\underline{c}+\underline{K}.\sin\gamma).v(\gamma)]$$

$$v(\gamma) = \frac{Ln[Ct]}{\underline{c}+\underline{K}.\sin\gamma} \qquad (2.89)$$

In general, this equation does not define threshold visibility. In Duntley's definition, the 2% is 2% of the original contrast, Co, ie Cr/Co = 0.02. An absolute visual contrast of 2% must be defined by: Cr = Ct = 0.02., as in Eqn.2.87. However, as is apparent from Eqns. 2.88 and 2.89, the hydrological range is equal to the threshold range of a zero-reflector. This simple equality is much used in the practical visibility experiments described in the current work. In these experiments, threshold visibility measurements are always made vertically downwards, vertically upwards or horizontally, and will be indicated by Z, U and V respectively. Equivalent hydrological ranges will be given by the threshold visibilities of a zero-reflector, indicated by 'h':

$$Zh = \frac{Ln[1/Ct]}{c+K} = \frac{Ln[50]}{c+K} = \frac{3.91}{c+K} \; ; \quad Uh = \frac{3.91}{c-K} \; ; \quad Vh = \frac{3.91}{c}$$

(2.90, 2.91, 2.92)

Equation 2.92 is the origin of the oft-quoted Duntley (1962) rule-of-thumb, that divers can estimate $\underline{c}$ from:

$$\underline{c} = \frac{4}{\text{horizontal visibility of a dark object}} \qquad (2.93)$$

a convenient 'dark object' being the neoprene wet-suit of a fellow diver.

2.5.4 The Secchi depth

Traditionally, oceanographers and marine biologists have assessed water clarity by means of a white Secchi disc, which is lowered through the water column until it just disappears at the Secchi depth, Zs. This depth is given, from Eqns.2.87 and 2.77:

$$Zs = \frac{Ln\left[\frac{\rho/R - 1}{Ct}\right]}{\underline{c} + \underline{K}} = \frac{Fs}{\underline{c} + \underline{K}} \qquad (2.94)$$

Strictly, from this equation, measurement of Zs can produce only an estimate of the combination $(\underline{c}+\underline{K})$, which is not a useful optical parameter. In practice, empirical formulae incorporating Zs have been formulated to estimate the single coefficients $\underline{c}$ and $\underline{K}$, or even suspended particle concentration (eg Pilgrim, 1984).

The coupling factor, Fs, depends upon the assumed values of ρ, $\underline{R}$ and Ct.

(i) Disc reflectivity, ρ. It is generally agreed in the literature, (eg Tyler, 1968), that the reflectivity of white paint is about 80%. In an experiment with flat white paint, Holmes (1970) measured a reflectance of 84% when dry, increasing to 93% on immersion in pure water. However, as pointed out by Højerslev (1977 , 1986), small variations in ρ make very little difference to Fs; as is apparent from Table 2.3.

(ii) Water reflectance, $\underline{R}$. Reflectance must vary from water type to water type. Tyler (1968) says that the reflectance of most natural

Table 2.3: Range of Fs produced by selected values of $\underline{\rho}$, $\underline{R}$ and Ct (%).

		$\underline{R}$ = 1	$\underline{R}$ = 2	$\underline{R}$ = 5	$\underline{R}$ = 10	$\underline{R}$ = 20
Ct = 2	$\underline{\rho}$ = 0	3.912	3.912	3.912	3.912	3.912
	$\underline{\rho}$ = 24	7.048	6.310	5.247	4.248	2.303
	$\underline{\rho}$ = 70	8.146	7.438	6.477	5.704	4.828
	$\underline{\rho}$ = 80	8.281	7.576	6.620	5.858	5.010
	$\underline{\rho}$ = 90	8.401	7.696	6.745	5.991	5.165
	$\underline{\rho}$ = 100	8.507	7.804	6.856	6.109	5.298
Ct = 1	$\underline{\rho}$ = 0	4.605	4.605	4.605	4.605	4.605
	$\underline{\rho}$ = 24	7.741	7.003	5.940	4.942	2.996
	$\underline{\rho}$ = 70	8.839	8.132	7.170	6.397	5.521
	$\underline{\rho}$ = 80	8.975	8.269	7.313	6.551	5.704
	$\underline{\rho}$ = 90	9.094	8.389	7.438	6.685	5.858
	$\underline{\rho}$ = 100	9.200	8.497	7.550	6.802	5.991
Ct = 0.66	$\underline{\rho}$ = 0	5.116	5.116	5.116	5.116	5.116
	$\underline{\rho}$ = 24	8.251	7.514	6.451	5.452	3.507
	$\underline{\rho}$ = 70	9.350	8.642	7.681	6.908	6.032
	$\underline{\rho}$ = 80	9.485	8.780	7.824	7.062	6.215
	$\underline{\rho}$ = 90	9.605	8.900	7.949	7.195	6.369
	$\underline{\rho}$ = 100	9.711	9.008	8.060	7.313	6.502
Ct = 0.13	$\underline{\rho}$ = 0	6.645	6.645	6.645	6.645	6.645
	$\underline{\rho}$ = 24	9.781	9.043	7.980	6.982	5.036
	$\underline{\rho}$ = 70	10.88	10.17	9.210	8.437	7.562
	$\underline{\rho}$ = 80	11.02	10.31	9.353	8.591	7.744
	$\underline{\rho}$ = 90	11.13	10.43	9.479	8.725	7.899
	$\underline{\rho}$ = 100	11.24	10.54	9.590	8.843	8.032

waters, measured for the photopic band width, is about 2%. In a series of measurements in Goleta Bay (California), Holmes (1970) measured $5.9\% \leq R \leq 9.5\%$ (mean R = 8.0%; sd = 1.3%), but he does not state how, ($R(\lambda)$ or $\underline{R}$(lux)?). Højerslev (1986) believes that these unexpectedly high values may have been due to bottom reflection effects; he quotes the following observed values of $\underline{R}$: 0.75% in the

Baltic (Højerslev, 1974), 0.95% in Crater Lake (Tyler et al, 1972) and 1.3% in the Sargasso Sea (Lundgren and Højerslev, 1971). He also reports lux reflectances of 0.75% and 1% in the Baltic (personal communication, 1986) and concludes that $\underline{R}$ = 1.0% is a very likely value for most waters. He agrees, however, that $\underline{R}$ may attain much higher values in the so-called 'milky waters', (eg Prieur, 1976) who reports a value of $\underline{R}$ = 5.3%.

(iii) Threshold Contrast, Ct. As discussed in subsection 2.5.3, many workers appparently assume ideal observation conditions and use a value, Ct=0.66%, as proposed by Tyler (1968). Lythgoe (1979) recommends a value Ct = 2% for divers, and this is used here.

2.5.5 Duntley discs

Duntley (1949) has proposed a method of deducing c and K separately by using two discs, one white and one grey viewed from above and from below. This method is sometimes referred to by other workers, (eg Preisendorfer 1976,1986; Højerslev, 1987), but it requires that the observer be a diver, and apart from our own work (Pilgrim et al, 1988), no other report has been found in the literature of such discs being constructed and used. Preisendorfer (1976) outlines the optical theory of Duntley discs; essentially, his argument is as follows.

If the white and grey discs are lowered to the same depth, z_1, then there is a luminance mismatch between them; the white disc appears brighter than the grey one. For luminance match, the white disc must be lowered to a greater depth z_1+d_1, (see Fig.2.14), where its

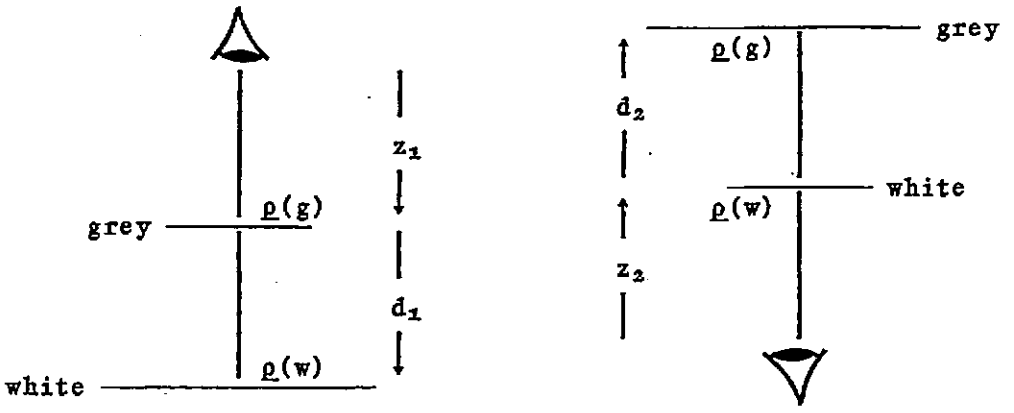

Fig.2.14: Duntley discs sighted vertically upwards and vertically downwards (from Preisendorfer, 1976)

apparent contrast is, from Eqns.2.83 and 2.77

$$Cr(w,z_1+d_1) = (\underline{\rho}(w)/\underline{R} - 1).\exp[-(\underline{c}+\underline{K}).(z_1+d_1)] \qquad (2.95)$$

The apparent contrast of the grey disc is therefore given by:

$$Cr(g,z_1) = (\underline{\rho}(g)/\underline{R} - 1).\exp[-(\underline{c}+\underline{K}).z_1] \qquad (2.96)$$

As there is luminance match then:

$$Cr(w,z_1+d_1) = Cr(g,z_1) \qquad (2.97)$$

and so, from Eqns 2.95 and 2.96:

$$(\underline{\rho}(w)/\underline{R} - 1).\exp[-(\underline{c}+\underline{K}).(z_1+d_1)] = (\underline{\rho}(g)/\underline{R} - 1).\exp[-(\underline{c}+\underline{K}).z_1]$$

from which:

$$(\underline{c} + \underline{K}) = \frac{1}{d_1}.\mathrm{Ln}\left[\frac{Co(w)}{Co(g)}\right] = \frac{1}{d_1}.\mathrm{Ln}\left[\frac{\underline{\rho}(w) - \underline{R}}{\underline{\rho}(g) - \underline{R}}\right] \qquad (2.98)$$

and as $\rho(w)$, $\rho(g) \gg \underline{R}$, then:

$$(\underline{c} + \underline{K}) = \frac{\mathrm{Ln}[\rho(w)/\rho(g)]}{d_1} \qquad (2.99)$$

When the diver looks upwards at the discs, the white disc is at distance r and the grey one is at greater distance $r+d_2$. Preisendorfer (1976) argues that: '.. by simply appealing to Eqn.2.83 with $\gamma = -\pi/2$, we could deduce that, analogously to Eqn.2.99....':

$$(\underline{c} - \underline{K}) = \frac{1}{d_2}.\mathrm{Ln}\left[\frac{Co(w)}{Co(g)}\right] = \frac{\mathrm{Ln}[\rho(w)/\rho(g)]}{d_2} \qquad (2.100)$$

Adding and subtracting Eqns.2.99 and 2.100:

$$\underline{c} = \frac{\mathrm{Ln}[\rho(w)/\rho(g)]}{2} \cdot \left[\frac{1}{d_1} + \frac{1}{d_2}\right] \qquad (2.101)$$

and

$$\underline{K} = \frac{\mathrm{Ln}[\rho(w)/\rho(g)]}{2} \cdot \left[\frac{1}{d_1} - \frac{1}{d_2}\right] \qquad (2.102)$$

It will be shown in Chapter 4 that Eqn.2.100, and hence 2.101 and 2.102, are in error.

Chapter 3

INSTRUMENTATION AND METHODS

3.1 MEASUREMENT OF THE DIFFUSE ATTENUATION COEFFICIENT

The diffuse attenuation coefficients, $K(\lambda)$, were described and defined in subsection 2.2.1. In subsection 2.4.1 it was shown and illustrated that depth-mean $\langle K(\lambda) \rangle$ may be obtained from the depth profile of $E(z)$. The various practical means of obtaining an $E(z)$ profile, and hence $K(\lambda)$ or $\langle K(\lambda) \rangle$, have been reviewed by Pilgrim and Aiken (1988), and include the Single Sensor System (SSS), the Bio-optical Profiling System (BOPS), the Multichannel Environmental Radiometer (MER), the Visibility Laboratory Irradiance Meter (VLIM), the Undulating Oceanographic Recorder (UOR) and the Multi-depth Sensor Array System (MSAS). In the research programme described in this thesis, only an SSS and a UOR were used to obtain $\langle K(\lambda) \rangle$ data, so only these two will be considered further in this chapter.

Any light-profiling system must incorporate three essential components: a light sensor, a depth sensor and a recorder or some means of transmitting the signals to a display at the surface.

A light sensor comprises of a light collector and a photodetector, either a photodiode or a photomultiplier. The form of irradiance measured by a system depends upon the shape and configuration of its collector. A range of irradiance collectors has been reviewed by Højerslev (1975); these were described in subsection 2.4.2, and illustrated in Fig.2.9.

An important aspect of monitoring the propagation of photo-synthetically useful light is the units of measurement employed.

Ostensibly, a simple measurement of irradiant energy flux ($W.m^{-2}$) should suffice; divided by the velocity of light this gives $J.m^{-3}$, the total influx of radiant energy per unit volume of water. However, photosynthesis is a photochemical mechanism, the rate of which depends upon the rate of interacting photons so that low-energy 'red photons' are just as effective as high-energy 'blue photons'. Clearly, photosynthetic light must be measured in quanta rather than total energy. Working Group 15 (UNESCO, 1965) recommended a standard technique for measuring photosynthetic energy in the sea by means of a conceptionally ideal equivalent detector, ie a detector that, for the same radiant flux input, yields a response equivalent to that of a phytoplankton, (Smith and Wilson, 1972). Although impractical to construct a single instrument with ideal response characteristics, Working Group 15 recommended a sensor which measures total quanta in the 350-700 nm band, with a geometrical response independent of direction. It is widely acknowledged that this approaches a practical optimum for monitoring photosynthetically available radiation (PAR). The relative spectral sensitivity of an ideal quantum meter is compared to that of an ideal radiometer (measuring energy) in Fig.3.1. Also illustrated, is the spectral response of the human eye (lux measurement, as would be appropriate for monitoring underwater visibility). In a series of model calculations, Siegel et al (1986) have illustrated how the spectral characteristics of an irradiance sensor can affect estimates of the vertical structure of the diffuse attenuation coefficient for downwelling irradiance, $Kd(\lambda,z)$. For example, they found that in clear oceanic waters, a substantial portion of the vertical structure for orange-red wavebands may be attributed to the characteristics of the irradiance sensor. The two systems employed in this work will now be considered.

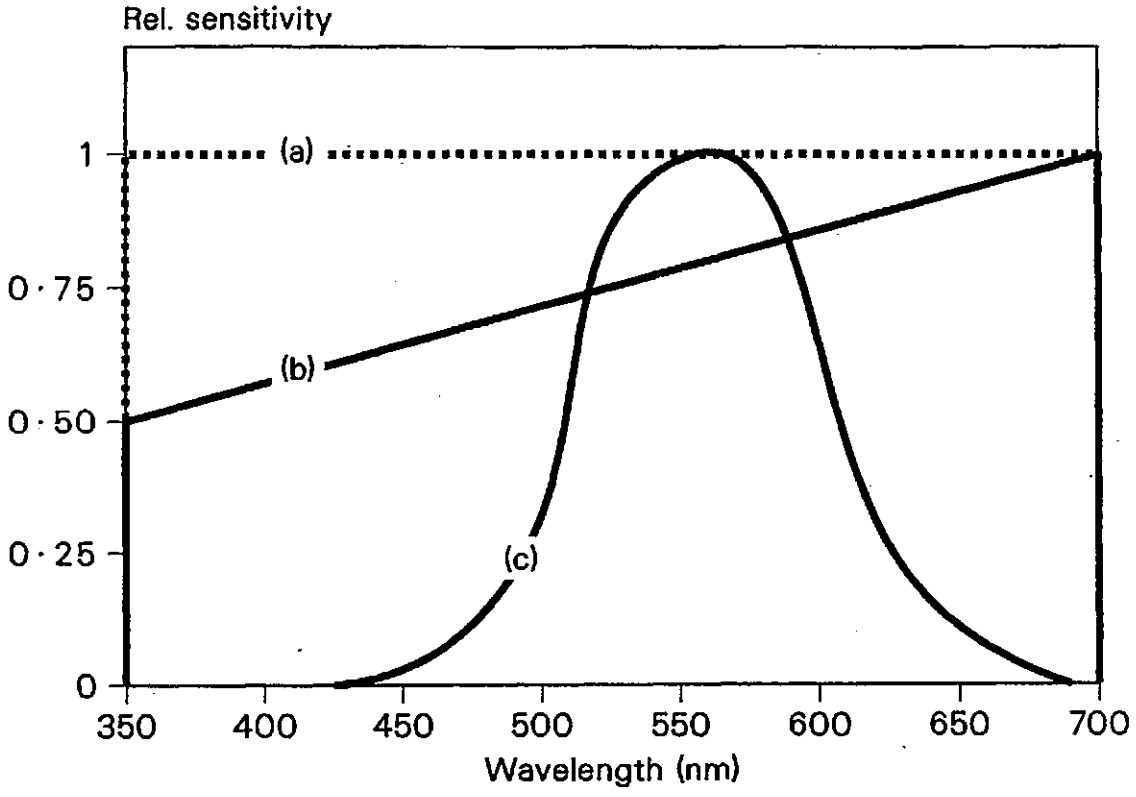

Fig.3.1: Ideal relative sensitivities of, (a) a radiometer measuring Watts, (b) a quantum meter, and (c) a lux meter

3.1.1 The single sensor system

The simplest method of irradiance profiling is to lower a sensor through the water column, recording the light level and depth at convenient intervals. This method was used during the optical surveys of the turbid waters of the Tamar Estuary, and the clearer oceanic waters of the NE Atlantic, (Pilgrim, 1987). In this work use was made of a Biospherical Instruments Inc QSP series Profiling Quantum Scalar Irradiance System. This instrument has been described and evaluated in some detail by Booth (1976). The 4π scalar collector-diffuser is a 1.9 cm diameter solid Teflon sphere with an optic fibre output encased in a stainless steel pipe. The fibre optic guides light to the filter-detector unit where it is

roughly collimated by a lens of short focal length for transmission through the filters. The filters include a Corning 1-62 blue filter, a heat absorbing glass filter, a thin film hot mirror, and Kodak colour-compensating filters. This combination approximates a quantum response between 400 and 700 nm, with sharp cut-off above and below this band. The detector is an EG+G UV-100 photodiode which generates a current (10^{-7} - 10^{-12} amp) in proportion to the incident radiation. This current is amplified by a current to voltage converter before transmission, via cable, to the on-board signal processing unit where the signal is digitally displayed in quanta s^{-1} cm^{-2}. Depth is measured by a pressure transducer built into the underwater unit, and displayed digitally. The sensor is rated to 200 m, and has an operating temperature range of -1 to 35°C. The instrument used in this study was returned to the manufacturer for calibration before the work began.

From Eqn.2.62:

$$\langle {}^{\circ}Ko \rangle = \frac{-d}{dz} Ln[{}^{\circ}Eo(z)]$$

$\langle {}^{\circ}Ko \rangle$ may therefore be obtained by graphing the $Ln[{}^{\circ}Eo](z)$ data as illustrated in Fig.2.7 or, more usually, by linear regression using a microcomputer to find the gradient of the 'best' line.

Of course, Eqn.2.62, and the method described, assume a constant surface value, ${}^{\circ}Eo(0)$. This is rarely the case; comparatively small changes in cloud cover can give rise to surprisingly large and rapid variations in ${}^{\circ}Eo(0)$. The problem is overcome in the Biospherical

Instruments Inc system by inclusion of a skylight monitoring meter sited on deck. Essentially, this device is a duplicate of the underwater meter, but mounted in a 25 cm diameter non-reflecting pan so that exactly half of the spherical Teflon collector protrudes above the plane of the pan rim. This meter therefore functions as a hemispherical collector, and produces an output proportional to the downwelling skylight. After amplification, this signal is displayed digitally at the signal display unit. Suppose fraction, F, of the skylight penetrates the sea surface so that, from Eqn.2.62:

$$^{0}Eo(z) = F.^{0}Eref.\exp[-\langle^{0}Ko\rangle.z]$$

therefore, $Ln[^{0}Eo(z)/^{0}Eref] = Ln[F] - \langle^{0}Ko\rangle.z$, so that:

$$\frac{-d}{dz} Ln[^{0}Eo(z)/^{0}Eref] = \langle^{0}Ko\rangle \qquad (3.1)$$

Underwater light levels may therefore be normalized by division by $^{0}Eref$, and $\langle^{0}Ko\rangle$ obtained from the depth-gradient of $Ln[^{0}Eo(z)/^{0}Eref]$.

In practice, it has been found that skylight levels can change significantly during the time that it takes to switch between underwater and skylight sensors, and make the necessary scale adjustment. In this study the system was modified to take the two sensor outputs to a voltage divider with its own digital display which gave the ratio $^{0}Eo(z)/^{0}Eref$ directly. The digital display of the signal processor was set to give depth. Alternatively, analogue outputs from the signal processor may be taken to a chart recorder, or via an interface to a microcomputer.

In the experiment described in Chapter 4, it was necessary to measure the scalar reflectivity of the water: $^{0}Ro(z) = {}^{0}Eou/{}^{0}Eod(z)$. To obtain the 2π and -2π scalar irradiances, ^{0}Eou and ^{0}Eod, the sensor was fitted with a black, horizontal mask as illustrated in Fig.2.9(c). The lowering frame supplied by Biospherical Instruments Inc keeps the sensor pointing vertically upwards. A new frame was therefore built in house which allowed the masked sensor to be inverted whilst under water.

When using the Single Sensor System, (or the BOPS, MER, or VLIM), care must be taken to obtain all measurements on the sunny side of the ship/boat. Voss et al (1986) have studied the effects of ship shadow on apparent optical properties, and have found that in cloudless conditions the effect of ship shadowing on the derived value of Ed and K may be considerable. The effect upon R was found to be negligible.

3.1.2 The Undulating Oceanographic Recorder (UOR) Mark 2

The Single Sensor System method of profiling from a stationary vessel limits the acquisition of $\langle K(\lambda) \rangle$ data to just a few per day.

To extend the coverage geographically and seasonally, Aiken and Bellan (1986b) have fitted a suite of light sensors (Aiken and Bellan, 1986a) to the Undulating Oceanographic Recorder (Aiken 1981a, 1985) which can be towed at speeds of 4 to 10 $m.s^{-1}$ (8 to 20 knots), and provide measurements over distances of 200 to 300 km d^{-1} (at 20

km h^{-1}, 11 knots). The UOR is a multi-sensor, oceanographic sampler which automatically profiles from near surface to 60 or 70 m, with an undulation pitch typically 1 nautical mile (1.85km). A schematic diagram of the UOR and its sensor suite is shown in Fig.3.2.

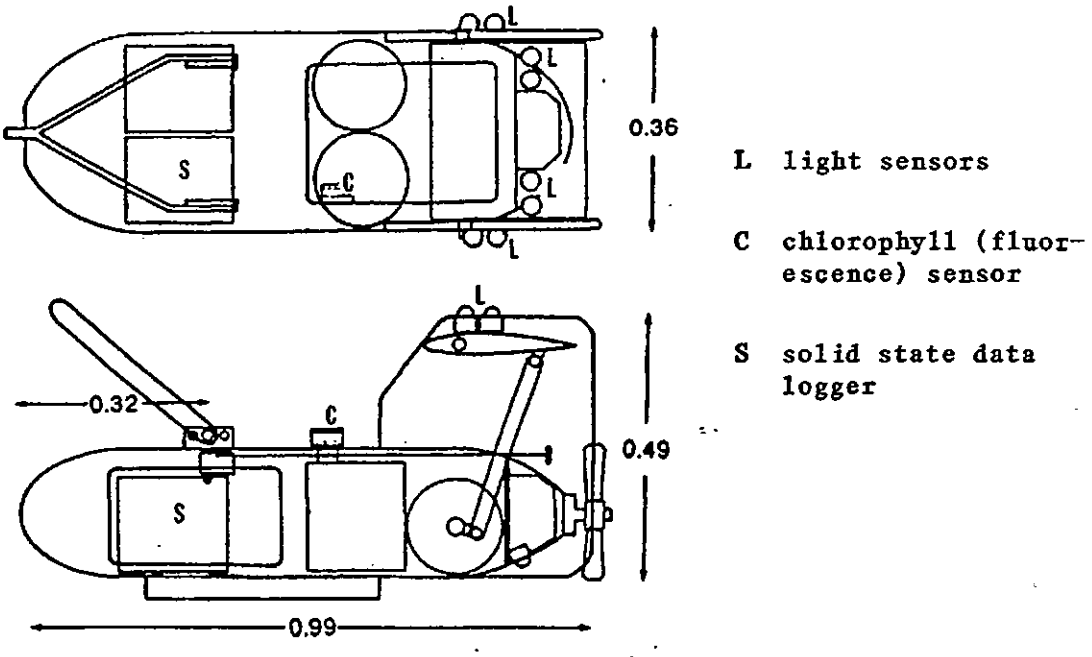

Fig.3.2: Schematic diagram of the UOR Mark 2 (Aiken, 1987, from unpublished report with permission)

In addition to the light sensors, the UOR measures depth, temperature and chlorophyll concentrations (fluorometer). Data from up to 15 sensors are logged in situ by a digital tape recorder or solid state data logger at rates of 10.8k data.h^{-1} (5 s scan rate). The light sensors are arranged in downwelling/upwelling pairs at 5 or 6 different wavelengths so that the water reflectance, $R(\lambda) = Eu(\lambda)/Ed(\lambda)$ can be determined. Data determined by the UOR have been compared with those obtained by conventional sensors, such as the MER, and thus it has been shown that UOR measurements are free from any artefact which might be induced by the towing method (Aiken, personal communication). However, it is suggested here that self-

shading by the body of the UOR may affect readings of some upwelling irradiances in some oceanographic conditions. Data from upwelling-downwelling pairs of sensors are used to determine the reflectance, $R(\lambda)$, which may then be used in the interpretation of remotely sensed images of ocean colour. The question is: can shading by the UOR body be enough to influence the intensity of upwelling irradiances, $Eu(\lambda)$? Of course, the shape, orientation and relative 'intensity' of any shading must depend upon such variables as the amount of cloud cover, the altitude of the sun, the scattering of light in the water (effectively $K(\lambda)$), the state of the sea surface, and the depth of the UOR below the surface. Precise definition in any particular circumstance would therefore be complex and difficult. However, a feel for the situation may be gained by considering where, below the sensor, the received upwelling light actually comes from, and hence, whether this zone is likely to be influenced by the shading from a 1.0 x 0.3 m UOR body.

The situation is depicted in Fig 3.3. The UOR is at some arbitrary depth, $z = 0$, where downwelling irradiance is $Ed(0)$. The upwelling irradiance, ${}^{z}Eu(0)$, received by the UOR <u>from depth z</u>, (<u>not</u> from the sub-UOR water column as a whole), is given by:

$$\begin{aligned} {}^{z}Eu(0) &= {}^{z}Eu(z).\exp[-Ku.z] \\ &= b_b(z).Ed(z).\exp[-Ku.z] \\ &= b_b(z).Ed(0).\exp[-Kd.z].\exp[-Ku.z] \end{aligned} \qquad (3.2)$$

where $b_b(z)$ is the back-scattering coefficient at depth z. Assuming that $Kd \simeq Ku \simeq K$, and that $b_b(z)$ = constant with depth = b_b, then the <u>total</u> upwelling irradiance received at the UOR from the water column

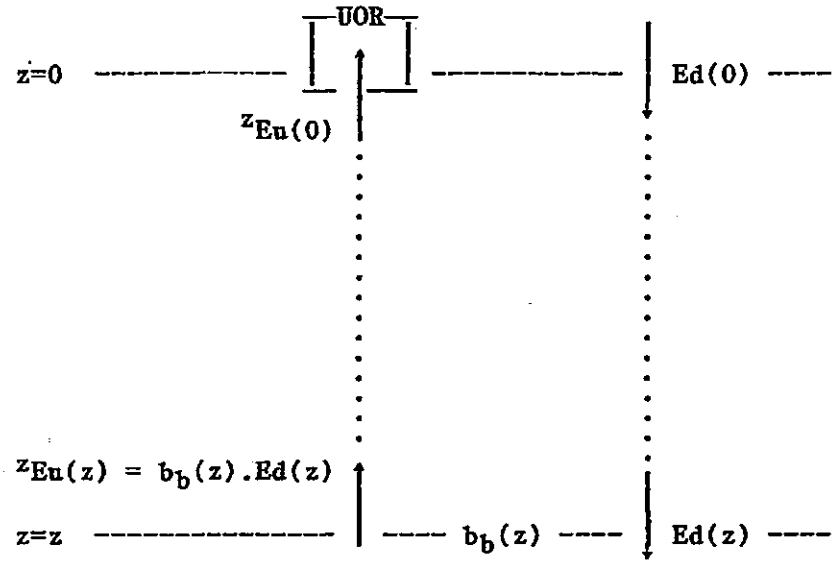

Fig.3.3: Upwelling light received at sensor from depth z

below is given by:

$$^{\infty}Eu(0) = \int_0^{z=\infty} {}^{z}Eu(0) = b_b.Ed(0).\int_0^{z=\infty} \exp[-2.K.z]$$

$$= b_b.Ed(0).\left[\frac{1}{-2.K}.\exp[-2.K.z]\right]_0^{z=\infty}$$

$$= \frac{b_b.Ed(0)}{2.K} \qquad (3.3)$$

Now consider the total upwelling irradiance received from the first diffuse optical depth, (J = K.z = 1, so z = 1/K), below the UOR:

$$^{J}Eu(0) = b_b.Ed(0).\left[\frac{1}{-2.K}.\ \exp[-2.K.z]\right]_0^{z=1/K}$$

$$= 0.865\ \frac{b_b.Ed(0)}{2.K} \qquad (3.4)$$

Therefore, from Eqns.3.3 and 3.4:

$$\frac{J_{Eu(0)}}{\infty_{Eu(0)}} = 0.865 \qquad (3.5)$$

ie 86.5% of the measured upwelling light comes from the first diffuse optical depth below the UOR. The question is now one of scale: is one optical depth large or small compared to the size of the UOR (say 1 m)? In Chapter 4, one set of UOR data (Tow 15, Lynch cruise, 1987) is considered in detail. At 450 nm: $0.060 \leq K \leq 0.161$, and so $16.7 \geq 1/K \geq 6.2$ m, depths large compared to 1 m. However, at 670 nm: $0.192 \leq K \leq 0.560$, and so $5.2 \geq 1/K \geq 1.9$ m, ie depths comparable to the size of the UOR, and so cannot be ignored. It may be, therefore, that self-shading will give rise to significant error in measurements of $Eu(\lambda)$ and $R(\lambda)$:

(i) in clear oceanic waters, at long wavelengths where K will be high due to the selective absorption by H_2O

(ii) in turbid waters at all wavelengths.

Valuable experience of the operation of the UOR was gained during a 3 week research cruise (29 July to 18 August,1987) on board USNS Lynch, organised by the Visibility Laboratory, Scripps Institution of Oceanography, University of California. The objective of this cruise was to measure the 3-dimensional distribution of bio-optical properties, and the associated physical structure and biogenic components of the water column throughout the cruise area (eastern N.Atlantic Ocean, and Norwegian and Greenland Seas). Of particular interest was a mini-survey of the bio-optical properties along the Arctic front located, at the time, to the West of Jan Mayen. Analyses

of data collected by the UOR have been presented in a report (Aiken, 1987), which also outlines the survey routine followed throughout the cruise. Essentially, this routine comprised of detailed profiling at 28 stations (see map, Fig.3.4), and along-track measurements between the stations.

Usually, two stations were occupied each day at approximately 0900 and 1330. At each station, the following measurements were made:

(i) CTD (vertical cast to 500 m).

(ii) Optical properties/vertical cast to 200 m of the Marine Environmental Radiometer, the Visibility Laboratory Irradiance Meter and the Visibility Laboratory Multispectral transmissometer.

(iii) Chlorophyll and accessory pigment concentration (by HPLC) from filtered water samples from various depths throughout the euphotic zone).

Continuous along-track measurements of chlorophyll fluorescence (Turner fluorometer), temperature (thermistor probe), and beam transmission at 660 nm (Sea Tech Inc transmissometer; details of measurements presented in Chapter 4), were recorded from the pumped sea water supply and logged by Apple IIe microcomputer. At the start and end of each UOR tow, and at significant bio-optical features along the track, surface water samples were taken for analysis (HPLC) and filtered for subsequent identification of phytoplankton species (stored in buffered formaldehyde and Lygols iodine solution). Expendable bathythermograph profiles were also obtained at six-hourly intervals and at significant features.

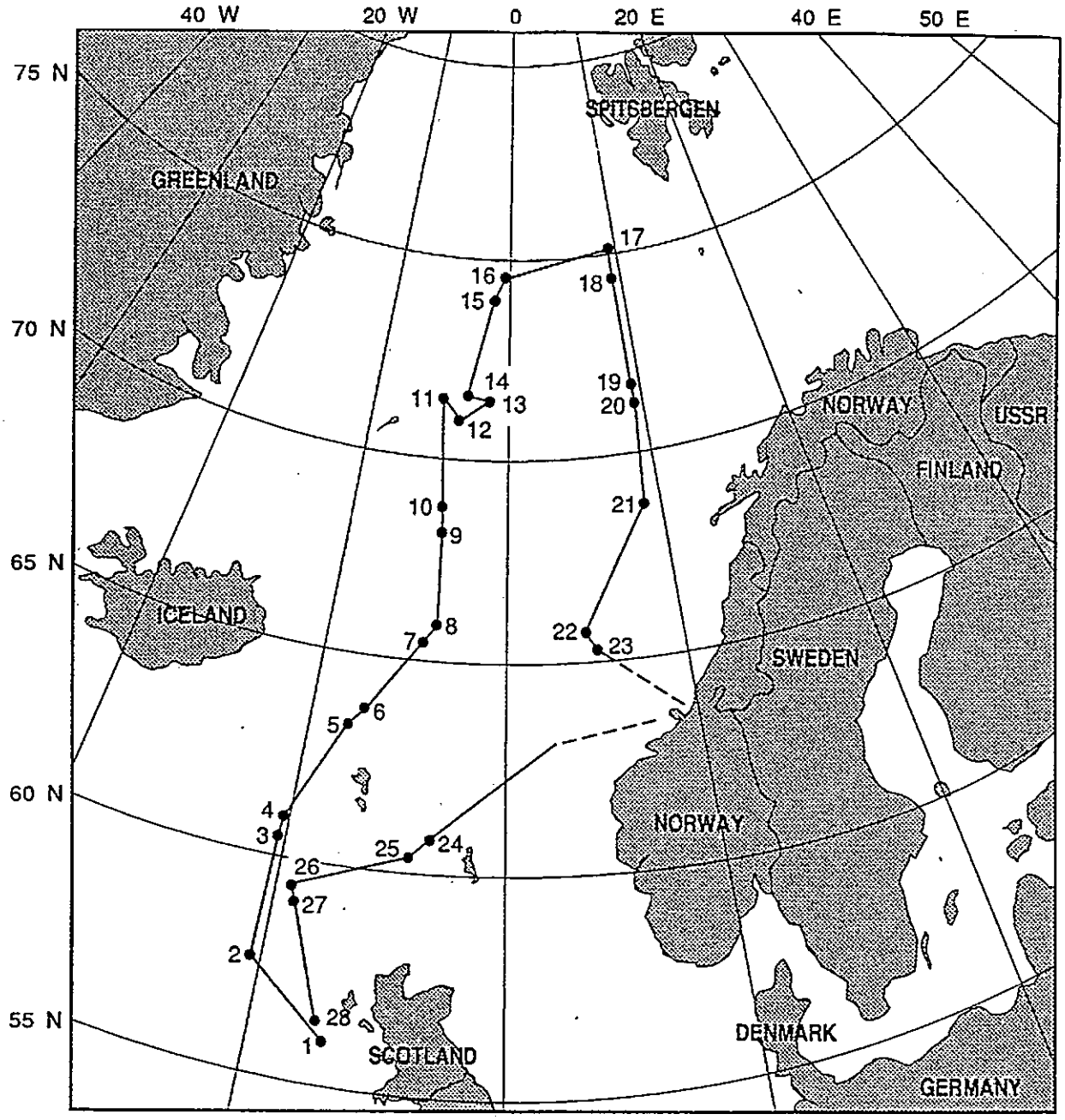

Fig.3.4: Trackline of cruise of USNS Lynch, 30 July to 16 August 1987. Figures are station numbers; Tow 15 was between Stations 10 and 11. (from SIO/IMR Tech Memo OcOp-88t-001, Jan 1988)

The UOR was towed at full speed (ca 10 knots), and set to undulate from surface to 60 m, into the morning station (for about 3 hours at 3 s scan rate), between stations (for about 3 hours at 3 s scan rate) and out of the afternoon station for a longer tow (typically 5 to 6 hours at 10 s scan rate). Adjacent to each station, the UOR was towed at slow speed (2-4 knots) to obtain a deep (>100 m), almost vertical profile.

During the 3 week cruise, the UOR was towed 40 times, covering a total distance of 1364 miles (2526 km); this amounts to some 54% of the total cruise distance (station 1 to station 28) of 2541 miles (4706 km). Seven deployments (tows 15 - 21) were made across the Arctic front. In all, 1407 undulations were made, and the 15 sensors produced a total of 1.7 million data!

3.1.3 Højerslev-type Janus collectors

In chapter 4 is described an experiment in which the average cosine, $\overline{\cos}\xi$, and diffuse absorption coefficient, $^{o}a_{o}$, are determined from measurements with an Højerslev-type sensor as illustrated in Fig.2.8(e) and 2.9, and described in subsection 2.4.2. The sensor system was built in house. The collector was manufactured and donated by Plymouth Marine Laboratory, and was identical to that described by Aiken and Bellan (1986a) for fitting to the UOR, but modified by masking the tapered base so as to more closely resemble the sensor in Fig.2.8(e).

3.2 MEASUREMENT OF BEAM TRANSMISSION

Throughout this programme of research, beam transmission was measured at 660 nm by means of a Sea Tech Inc 25 cm path-length transmissometer. This instrument, widely used in optical oceanography, was developed at the Oregon State University. Transmission is measured using a modulated LED and synchronous detector; the collimated LED transmitter has a beam divergence of less than 3 m.rad and the optical receiver has an acceptance angle of less than 18 m.rad. The LED produces a 20 mm diameter beam with a radiated power output of 3×10^{-7} at 660 nm. Bartz et al (1978) record that '... this wavelength choice was generated by our desire to eliminate attenuation due to dissolved humic acids ... yellow matter absorbs light strongly at shorter wavelengths ... can be ignored for wavelengths larger than 660 nm'. This is true - however, it is also known that it is extremely difficult to maintain a stable output from an LED at shorter wavelengths. Certainly there is a long overdue need for transmissometers of comparable quality, performance and stability to measure transmissions at, for example, 450 nm (peak absorption of Chl.a), and 555 nm (peak of sensitivity spectrum of human vision).

A significant error which arises in measuring beam transmission is due to the inclusion of forward-scattered light. Petzold and Austin (1968), and Austin and Petzold (1977), have discussed the optical design of beam transmissometers, including the problem of receiving foward-scattered light within the acceptance angle of the receiver,

(the half-angle, ω, of the receiver is given by the ratio of beam radius, r, to beam length, L). They quote an equation from Preisendorfer (1958), which gives the percentage error, Δ, in beam attenuation coefficient, c, in terms of the measured (erroneous) attenuation coefficient, c', and the forward scattering function, β_f:

$$\Delta = \frac{c'-c}{c} \times 100 = \frac{-2.\pi.\beta_f}{c}.\left[\frac{r}{L}\right]^2 \times 100 \qquad (3.5)$$

For the Sea Tech Inc transmissometer r/L = 10 mm/25 cm = 0.04. The forward scattering function may be large, however. Bartz et al (1978) have shown that when the volume scattering function is $\beta(\sigma)$, then the attenuation coefficient will be underestimated by:

$$g = 2\pi\int_0^{\omega} \beta(\sigma).\sin\sigma.d\sigma \qquad (3.6)$$

The measured transmission will therefore be overestimated by a factor of exp[-g]. Bartz et al (1978) have tabulated solutions to Eqn.3.6 (Table 3.1), appropriate to the optics of the Sea Tech Inc transmissometer, using a forward scattering function, β_f, based upon a hyperbolic particle size distribution with a slope of 2.9, and a refractive index of 1.05. Inspection of Table 3.1 shows that the correction to c may be considerable. The worst tabulated case is: β_f = 1000, c = 11.30, % error in T = 53.93. For a 25cm path length, transmission will be given by:

$$T' = 1.5393\ T = 0.09128$$

Using this value to calculate c, without allowing for forward

scattering, then the erroneous beam attenuation coefficient is:

$$c' = \frac{-Ln[T]}{r} = \frac{-Ln[0.09128]}{0.25} = 9.58, \quad \text{ie } c = 1.18\ c' \qquad (3.7)$$

So, errors of the order of 20% may be expected in turbid estuarine waters (see, for example, Fig.4.19), and it is a matter of concern that some workers may not have corrected their data – or, at least, it is not apparent from their publised results whether they have or not! All beam attenuations presented in this thesis have been corrected, using an algorithm deduced from Table 3.1

Table 3.1: Percentage error in T by which the transmissometer overreads for a forward scattering function given by β_f, a hyperbolic particle size distribution with a slope of 2.9, and a particle refractive index of 1.09 (Bartz *et al*, 1978)

β_f (m^{-1} sr^{-1})	1	10	50	100	250	500	750	1000
c (m^{-1})	0.01	0.11	0.56	1.13	2.83	5.65	8.48	11.30
% error in T	0.077	0.77	3.80	7.46	17.62	32.13	44.08	53.93

3.3 UNDERWATER OPTICAL TARGETS AND INSTRUMENTATION

A significant component of this research programme was the measurement by divers, of the limiting distance of visibility of several 'standard' targets. These are now described.

3.3.1 The Secchi disc

The Secchi disc is simply a flat white 30cm diameter horizontal plate which is lowered through the water column until it is observed to just disappear at the Secchi depth, Zs. The idea of assessing the transparency of water by making visual observations of a submerged white disc is not a new one but may have originated with a casual observation by a certain Captain Alexandre Bérard in the early 19th century (Tyler, 1968). During a passage from Wallis Island to the Mulgraves, Bérard noticed a white dish entangled in a fishing net at a depth of 40 m. This observation was mentioned in the writings of Dominique Argo the French astronomer and physicist, and subsequently read by Commander Alessandro Cialdi who, in 1865, was head of the Papal Navy and interested in the transparency of the sea and visibility of the sea bed. Cialdi prepared a number of discs of different colours and sizes (Cialdi, 1866), and engaged the services of Professor P A Secchi to organise and conduct a programme of observations from on board the papal barge L'Immacolata Concezione. Secchi measured the depth of disappearance of Cialdi's discs off a graduated line. In his report (Secchi, 1865; translation by Collier et al, 1968), Secchi records that the largest disc deployed was of

3.73m diameter '... formed of an iron circle covered with oiled sailcloth and varnished with white lead'. Smaller discs were 0.4 m in diameter and '... of diverse substances. One was pure white earthenware plate ... others were cloth discs supported by iron circles ... but of different colours: white, yellow and the colour of sea-slime.' these various discs were deployed 6-12 miles off the coast of Civitavecchia in Mediterranean water which was '... perfectly clear, of a beautiful colour and of a great purity ... which for a long time had not been strongly agitated'. During the voyage Secchi carefully examined and recorded the effects of many variables upon the visibility of Cialdi's submerged discs; these are summarised in Pilgrim (1984). After 1866 the Secchi disc became established as a standard instrument for measuring turbidity at sea. It's simplicity and cheapness guaranteed its survival, even after the introduction early this century of the photoelectric cell for the measurement of underwater illumination.

It is not common practice today to construct a Secchi disc with a 3.73 m diameter iron ring covered with oiled sailcloth and varnished with white lead. Nor is sea-slime a fashionable choice of colour. Curiously, exact size and reflectivity have not yet been standardised internationally, though it is usual to use flat white painted discs of 30 cm diameter. All estuarine Secchi depths obtained in the course of this research were observed through a glass-bottomed bucket or diver's face mask to avoid image problems associated with surface refraction and reflection. Discs were lowered on a plastic-covered steel surveyor's tape for ease of measurement. For measuring Secchi depths of less than 1.5 m, a disc was fitted to the end of a graduated pole. This was especially useful in turbid, fast flowing

water as the pole maintained a vertical line of sight. In really fast flowing water, a line was attached to the bottom of the pole and secured at the fore part of the anchored survey vessel.

3.3.2 The light trap, corner reflector and neutral filter.

It will be shown in Chapter 4 that a useful optical theory can be developed for the threshold visibility of an absolutely black, non-reflecting target. It will also be demonstrated in Chater 4 that a flat black surface will usually reflect some light and is therefore unsuitable. However, a matte-black, sheet metal cone with an open base diameter of 30 cm serves as a very efficient light trap underwater. The inside of the cone is observed along its axis. Any light entering the core is reflected away from the observer towards the apex so that the light trap appears absolutely dark, has a reflectance of zero, and an inherent contrast (Eqn.2.77) of -1. Such a light trap is mentioned by Højerslev (1986).

In the same way, the 100% reflector provides the basis for some useful optical theory in Chapter 4. It is believed that the first reference to such a target, the corner reflector, is in Pilgrim *et al* (1988). The reflector was constructed of wood strengthened by angle iron; it is about 30 cm across and plated internally with 4 mm mirror glass. A silicon sealant was applied to all mirror edges and joints to prevent the ingress of seawater. The three mirrored surfaces, set at right-angles to each other in three planes, ensures that any photon entering the corner is reflected back in the appropriate direction.

Also introduced in Pilgrim et al (1988), and considered in Chapter 4, is the use of neutral filters as underwater targets. This is a very attractive proposition for two important reasons. Firstly, it is much easier to specify or measure the transmission of a target than it is to specify or measure its reflectivity. Secondly, when observing the contrast of a neutral filter against its background, then the target and background share the same source of illumination. Consequently, the inherent contrast of the target can be specified without knowing the reflectivity of the water, (eg compare the equations presented in Table 4.3). A 30 cm disc of almost any material with a flat transmission between 400 and 700nm would be suitable. In this study, sheets of neutral filter (of specified transmssion) were obtained from a local theatrical lighting supplier, and sandwiched between sheets of perspex. Perspex has a refractive index very close to that of water, so is non-reflecting and non-refracting underwater.

All underwater threshold distances were measured from the faceplate of the diver's mask or glass of the glass-bottomed bucket, to the nearest 10 cm or, in the case of very short distances, 5 cm.

3.3.3 Duntley discs

The 50 cm and 30 cm diameter Duntley discs (see Fig.2.14) were painted matte-white on one side and grey on the other. The larger was fitted with an axial rod, and the other with an axial tube through which passed the measuring tape to the larger disc. Floats supported the targets during vertically upwards sightings.

The Duntley disc principle depends upon knowing the reflectivities of the grey and white discs, or rather the ratio of their reflectivities $\rho(g)/\rho(w)$. This was determined by measuring the illuminance (reflected irradiance) of the discs in a large laboratory tank by means of an underwater photometer, under exactly the same lighting conditions. The average of a number of readings indicated a reflectance ratio of $\rho(g)/\rho(w) = 23\%$.

3.3.4 Diver held photometer

A photometer suitable for diver use was constructed in house. The collector-sensor was a standard Crump Scientific Instruments system, the output from which was amplified and displayed on a Radio Spares voltmeter. The amplifier and display was housed in an aluminium box with a perspex window. The external cosine collector was fitted with a removable tube to produce radiance measurements.

Chapter 4

RESULTS AND DISCUSSION OF FIELDWORK

Essential to the theme of this research programme is the observation of optical coefficients in the natural environment. Five approaches to the problem of acquiring meaningful data have been investigated: direct measurement, estimation from empirical relationships, estimations from models and special sensors, observations of underwater visibility, and lastly, the deduction of time-series patterns in light penetration. These five methodologies are considered separately in the five subsections of this chapter, using data collected at three locations: the estuarine environment of the River Tamar and Plymouth Sound, the clearer ocean waters of the NE Atlantic during two voyages of RRV Frederick Russell, and the frontal areas of the Norwegian and Greenland Seas during a voyage of USNS Lynch.

In subsection, 4.1, are considered direct measurements of the diffuse attenuation coefficients, $^{o}K_{o}$ and $K(\lambda)$, by instrumentation designed specifically for that purpose, namely the Biospherical Instruments Irradiance Profiler which was used in the estuary and NE Atlantic, and the PML Undulating Oceanographic Recorder which was deployed during the Lynch cruise.

Irradiance profiling is a tricky and time consuming procedure for which the vessel must be stopped; few data per day can be collected in this way. By means of a UOR, vast numbers of continuous data over a considerable geographical area may be obtained in a single day's work. However, UOR deployment is expensive in terms of instrumentation costs and the need for skilled operators. In some circumstances, therefore, it may be acceptable to estimate the diffuse attenuation coefficient or, at least, its temporal or

geographical variation, by means of a continuous recording of the closely related, and easily measured beam attenuation coefficient. The estimation of $\langle {}^{o}Ko \rangle$ and $\langle K(\lambda) \rangle$ from beam transmissometer measurements of c(660nm) is considered in subsection 4.2.

During the Lynch cruise deployment of the UOR, $Kd(\lambda)$ and $Ku(\lambda)$ at a number of wavelengths were measured but not the quantum coefficient ${}^{o}Ko$. A means of estimating ${}^{o}Ko$ from a range of $K(\lambda)$ readings is also included in subsection 4.2.

Thus far, only the measurements of diffuse and beam attenuation coefficients have been considered. Two procedures are considered in subsection 4.3 by which it is possible to obtain values of the average cosine, $\overline{\cos\xi}$, and the absorption and scattering coefficients a and b. The first is Kirk's Monte Carlo Model for which it is necessary to measure the water reflectivity. Modification of the Biospherical profiler for this purpose was described in Chapter 3. The second method involves the use of a Janus-pair of special Højerslev-type sensors, also detailed in Chapter 3.

It is recognised (eg Eqn.2.87) that underwater visibility is limited by the combined effect of the beam and diffuse attenuation coefficients. It must therefore follow that visibility measurements of underwater objects of known optical quality must tell us something about the controlling attenuation coefficients. This is not a new idea; for example, it is well known that the traditional Secchi depth is proportional to the sum (c + K). In subsection 4.4 the scope of this simple idea is greatly extended by using several 'standard' targets other than the matte-white painted Secchi disc, and by using

divers to make observations not only vertically downwards, but also vertically upwards and horizontally. The 'standard' targets include the non-reflecting light trap referred to by Højerslev (1986), and the two novel targets developed in the course of this research and described in Chapter 3, namely the corner reflector and neutral filter.

In broad terms, the smaller the attenuation coefficients, c and/or K, then the clearer the water and the greater the propagation of illuminating and/or visual light. It might therefore be implied that the propagation of light is controlled solely by the attenuation coefficients, ie by the transparency of the water. This is not the case, however, where the thickness of water through which the light must propagate is also subject to variation. In this situation we must consider the combined effect of coefficient and photon path-length, ie the optical depth/distance, $j = c.r$, or the diffuse optical depth, $J = K.z$. An apt example is the cyclic variation in diffuse light reaching the bed of an estuary, where the diffuse optical depth is subject to the cyclic variation in tidal <u>height</u> and, approximately 2π out of phase, the cyclic variation in turbidity induced by tidal <u>flow</u>. This phenomenon is explored in detail in subsection 4.5 where analyses of data collected in the Tamar estuary reveal interesting and predictable patterns.

4.1 DIRECT MEASUREMENT OF $\langle {}^{o}K_o \rangle$ AND $\langle K(\lambda) \rangle$

4.1.1 Direct measurement of $\langle {}^{o}K_o \rangle$ from ${}^{o}E_o$ profiles

In the course of this research programme, over 200 determinations of $\langle {}^{o}K_o \rangle$ were made from the gradients of $Ln[{}^{o}E_o(z)]$ profiles (Eqn.2.62) measured with a Biospherical Instruments Inc QSP series Profiling Quantum Scalar Irradiance System, (as described in Chapter 3). Of these data, about 50 were obtained in the clear oceanic waters of the NE Atlantic, from on board RV Frederick Russell (26 February - 4 March 1985, 27 February - 14 March 1987); the remainder were measured in the turbid waters of the the Tamar Estuary over a period of 5 years (April 1982 to June 1987). These $\langle {}^{o}K_o \rangle$ data have been incorporated into analyses:

(i) to determine relationships between $\langle {}^{o}K_o \rangle$ and other optical properties such as the Secchi depth, Zs, and beam attenuation coefficient, $c(\lambda)$, (subsections 4.2 and 4.3, and Pilgrim, 1987).

(ii) to study the tidal variations in optical properties in an estuary, especially the cyclic variations in irradiance reaching the estuary bed (subsection 4.5, and Pilgrim and Millward, 1988),

Some 80 determinations of $\langle {}^{o}K_o \rangle$ were made at sea from $Ln[{}^{o}E_o(z)]$ profiles measured with a pair of back-to-back Højerslev-type $\frac{1}{2}(E_o + E)$ sensors (as described in Chapter 3). These data are considered in connection with the determination of $\overline{\cos\xi}$ and ${}^{o}a_o$ in subsection 4.3.

4.1.2 Direct measurement of $\langle K(\lambda) \rangle$ by UOR

The UOR Mark 2, and its deployment during the 1987 Cruise of USNS Lynch was described in Chapter 3. The 15 parameters measured were:

- Depth, z(m)
- Temperature, T(°C)
- Chlorophyll concentration, Chl ($mg.l^{-3}$)
- Downwelling and upwelling scalar irradiances, Eod(450), Eod(490), Eod(520), Eod(550), Eou(450), Eou(490), Eou(520) and Eou(550)
- Downwelling and upwelling vector irradiances, Ed(490), Ed(670), Eu(490) and Eu(670).

From the 12 light measurements it was possible to calculate the 12 equivalent diffuse attenuation coefficients: Kod(450), Kod(490), Kod(520), Kod(550), Kou(450), Kou(490), Kou(520), Kou(550), Kd(490), Kd(670), Ku(490) and Ku(670), the 4 scalar irradiance reflectances: Ro(450), Ro(490), Ro(520), Ro(550), and the 2 vector irradiance reflectances: R(490) and R(670).

To demonstrate the scope and value of UOR data, a particularly interesting tow carried out during the Lynch cruise has been analysed, namely Tow 15, across the Arctic front during the night of 5-6 August, 1987. The UOR was launched at 2056 GMT (69° 48.9'N, 04° 37.6'W), and recovered at 0752 GMT (71° 27.1'N, 04° 53.5'W); on the map (Fig.3.4), Tow 15 is located between stations 10 and 11. The tow lasted 10h 56m, during which time the UOR made 103 undulations and covered a distance of 98.5 miles; all 15 channels were logged throughout at 10s intervals. The frontal structure which existed at the time of Tow 15 is illustrated in Figs.4.1(a), (b), (c)

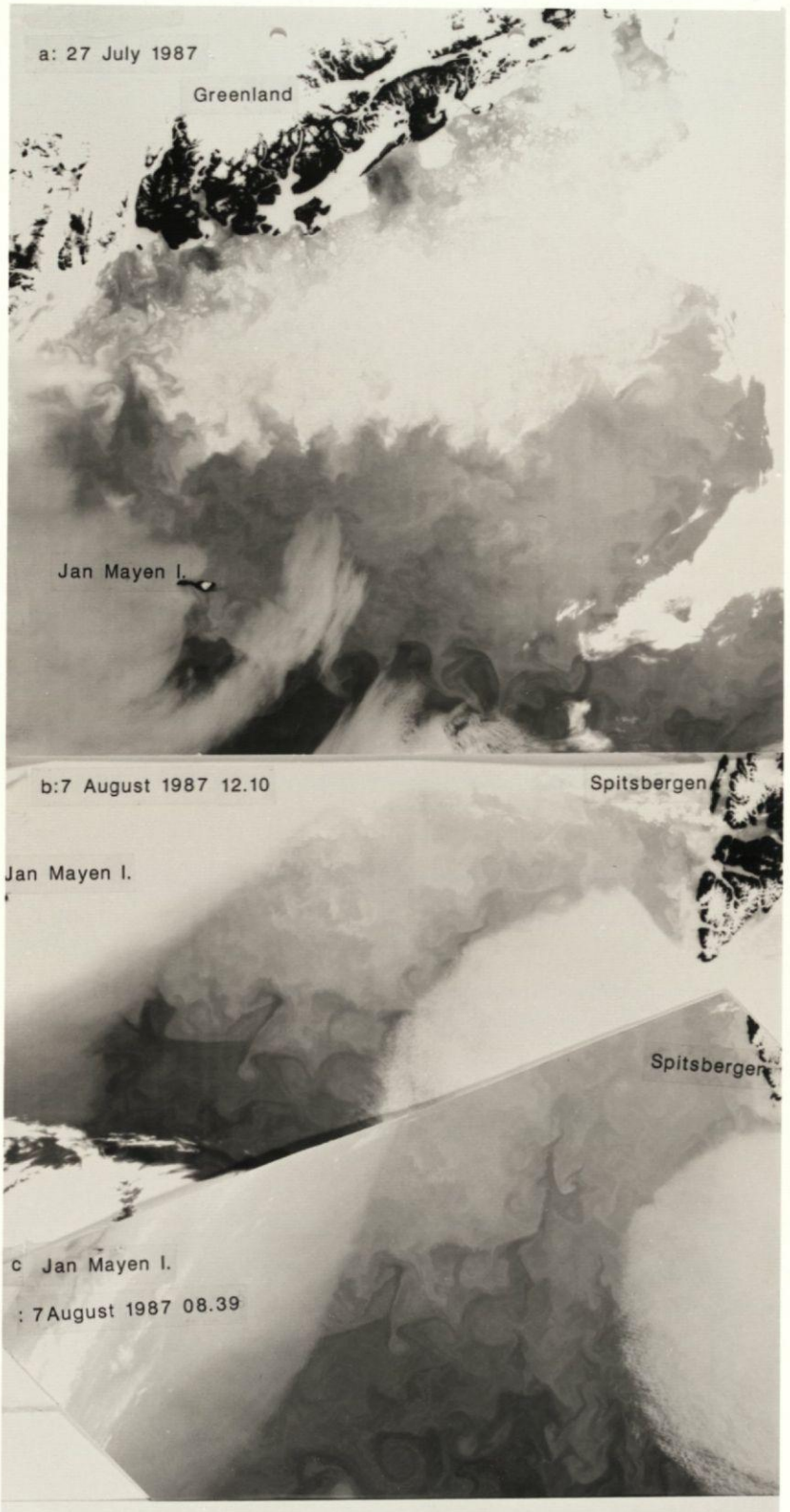

Fig. 4.1: AVHRR Images (Univ.of Dundee)

which are AVHRR images of SST in the Jan Mayen region on 27 July and 7 August 1987. The photographs indicate a strong temperature front (light = cold, dark = warm) running in a general E-W direction at 70°N in the Greenland Sea south of Jan Mayen. On the basis of these images, and temperatures observed during the Lynch cruise, Aiken (1987) has identified the following water masses:

(i) The most northerly waters were characterised by surface temperatures of 4-6°C, <-1°C at 40-60m and >0°C at 120 -140m. As these were the only sub-zero temperatures encountered, then these must be Arctic Waters. On this basis, the Jan Mayen front which was crossed during Tow 15 is identified as the Arctic front.

(ii) Sea surface temperatures to the south of this front are typically 8-10°C with sub-surface temperatures always >0°C. Because the observations showed mixing of Arctic Waters in this part of the Norwegian Sea, then these waters could be described as Modified Arctic Waters or Modified Polar Water. However, in recognition of the generally high surface temperatures at this time of the year, then it may be appropriate to describe them as Modified North Atlantic Waters.

Figures 4.2(a)-(c) are three different illustrations of the frontal temperature structure deduced from UOR measurements during Tow 15. Figure 4.2(a) is a depth-distance plot of isotherms, T(z,x), produced by SDS (Surface Display System) on an IBM-XT microcomputer. Figure 4.2(b) is an SDS 3-dimensional version, and Fig.4.2(c) is a time-plot of the mean temperature (0-20 m). It is apparent from each of these

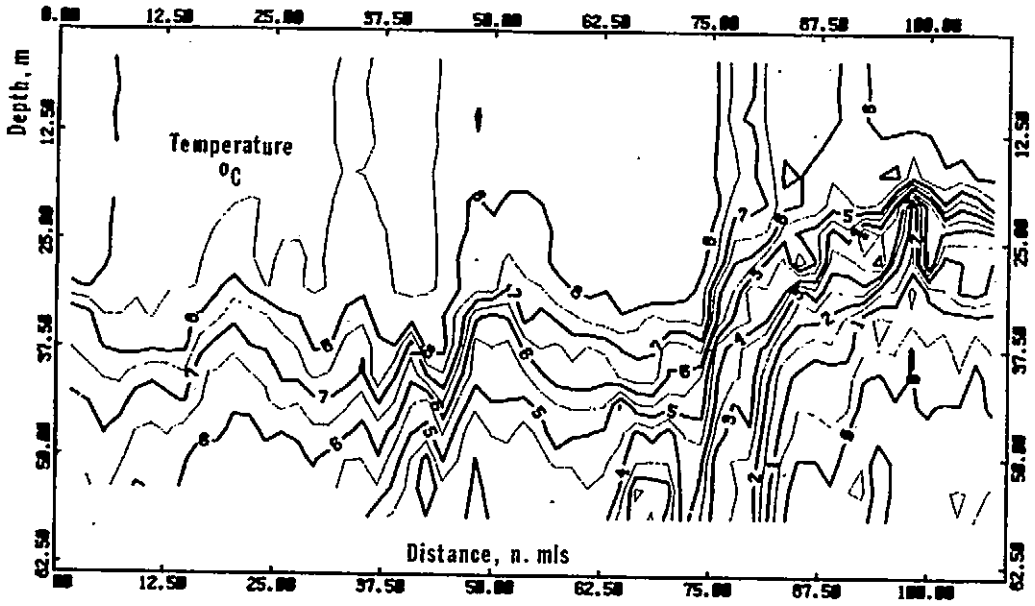

Fig.4.2(a): Plot of isotherms as a function of depth (m) and distance (n.miles) for Tow 15, Lynch 1987

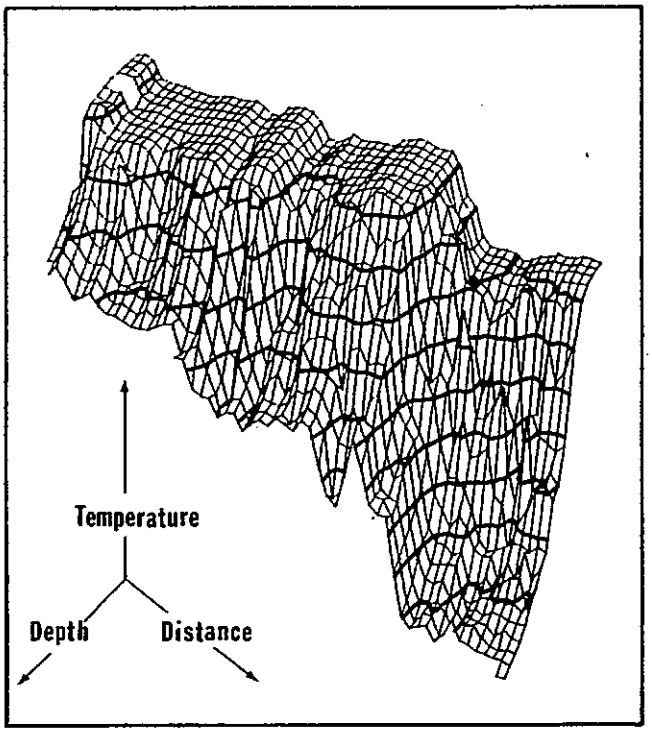

Fig.4.2(b): 3-dimensional plot of Temperature as a function of depth (m) and distance (n.miles) for Tow 15, Lynch 1987

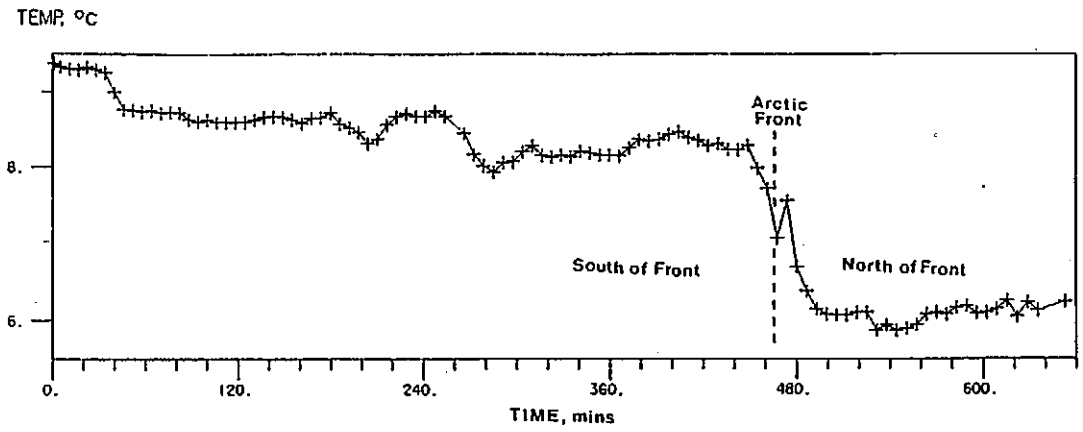

Fig.4.2(c): Time-plot of mean temperature (°C, 0-20 m) for Tow 15, Lynch 1987

plots that there was a steady decrease in temperature on approach to the front (0-450 mins from the start of the tow), and a very marked drop in temperature as the UOR passed through the front at 450-490 mins (c.0425 - 0505, 6 August). The bunching of isotherms in Fig.4.2(a) marks the thermocline, so it is apparent that on approach to the front the surface mixed layer (SML) decreased from >30 m to <15 m, and that the SML temperature fell from ca 8°C to ca 6°C.

Figure 4.3(a)-(c) are equivalent plots of chlorophyll concentration ($mg.m^{-3}$) during tow 15. In the Modified N.Atlantic Waters, south of the front, the chlorophyll was concentrated in the SML with values of >1 - 1.5 $mg.m^{-3}$. North of the front the chlorophyll distribution became very patchy with some concentrations of >2 $mg.m^{-3}$. This extreme patchiness is best illustrated in Fig.4.3(b), the 3-dimensional plot, as a cluster of spikes which contrasts markedly with the smooth pattern south of the front. This spiky signature is usually an indicator of Phaeocystis pouchetii in its colonial form, (Aiken, 1987). Notwithstanding these peaks, chlorophyll

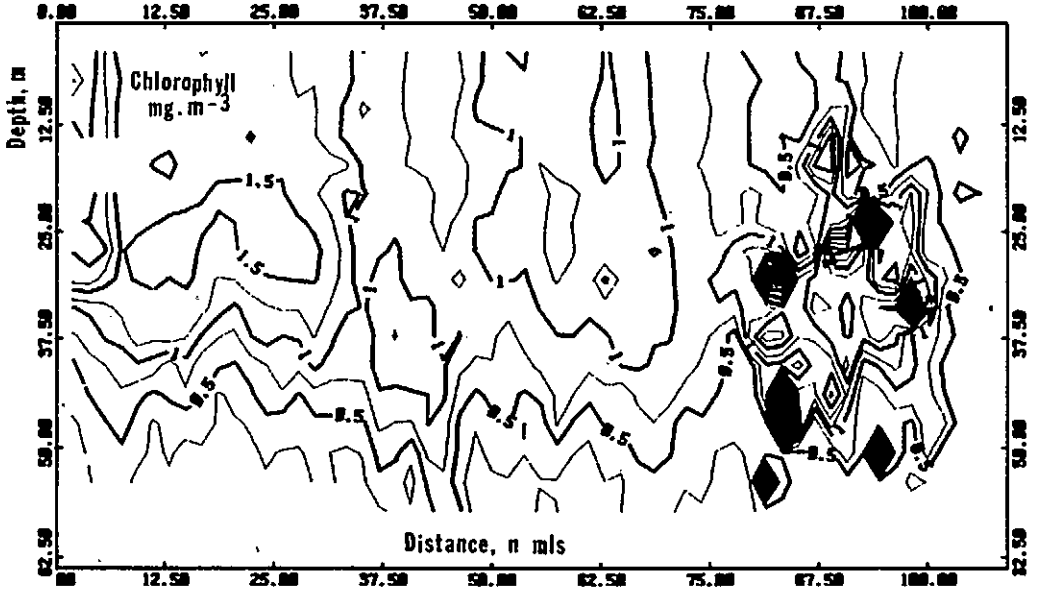

Fig.4.3(a): Plot of isotachs of chlorophyll concentration ($mg.m^{-3}$) as a function of depth (m) and distance (n.miles) for Tow 15, Lynch 1987

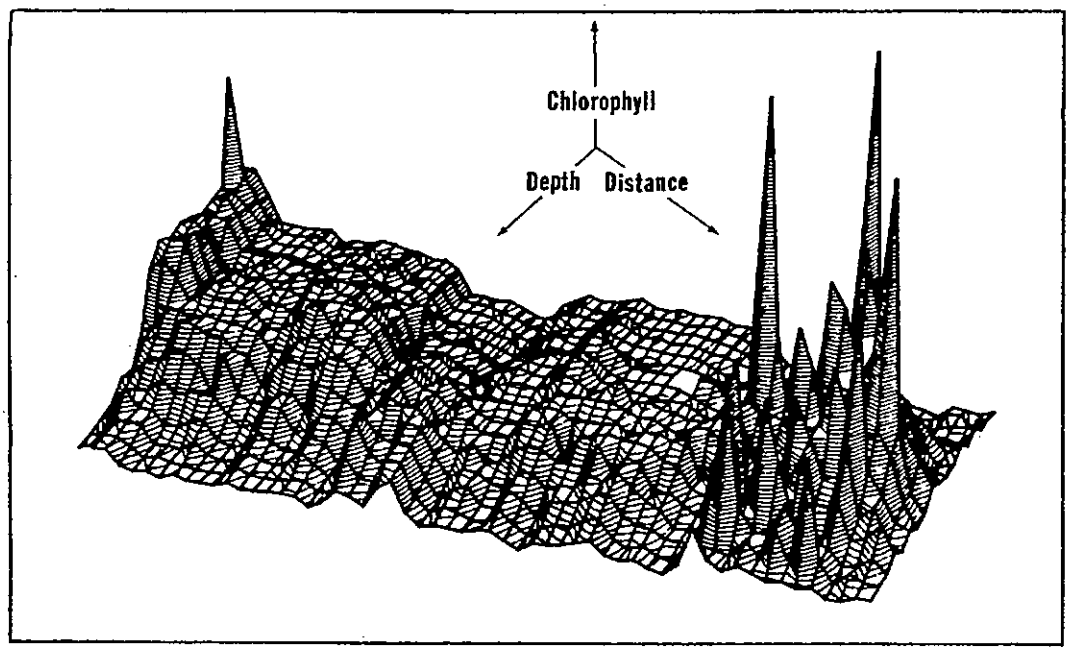

Fig.4.3(b): 3-dimensional plot of Chlorophyll concentration ($mg.m^{-3}$) as a function of depth (m) and distance (n.miles) for Tow 15, Lynch 1987

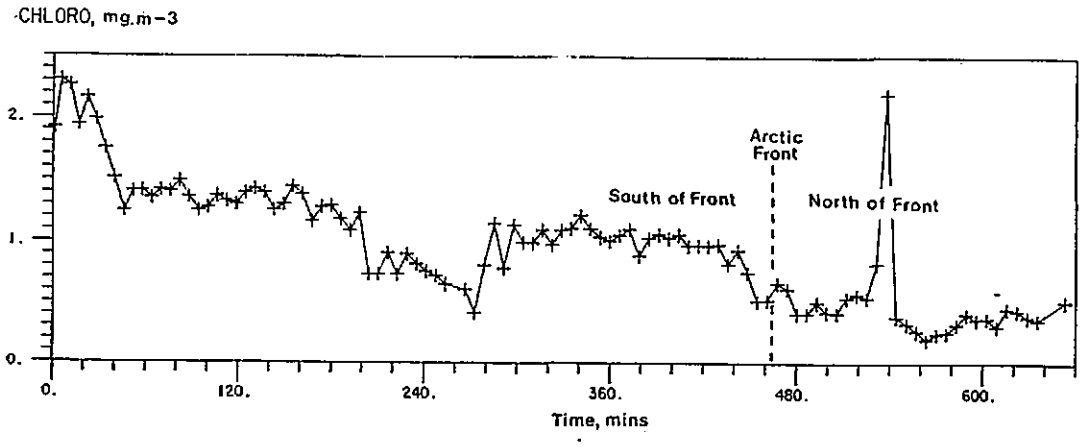

Fig.4.3(c): Time-plot of mean chlorophyll concentration (mg.m^{-3}, 0-20 m) for Tow 15, Lynch 1987

concentration decreased with the frontal drop in temperature. This is apparent from the two time-plots, (Fig.4.2.(c) and Fig.4.3(c)), and from Fig.4.4, a plot of chlorophyll concentration against temperature. Although Tow 15 took place from evening to early morning, there was sufficient light throughout the Arctic summer night to measure downwelling irradiances at all wavelengths except the red; Ed(670) was not recorded during the five darkest hours. Upwelling irradiances were recorded only during the last few (morning) hours of the tow. The overnight variation in ambient light is illustrated in Fig.4.5, a timeplot of the surface values of Eod(450). These values were determined by the extrapolation of Eod(450,z) data to z=0, for each undulation. Figure 4.6 is a plot of Eod(450,z,x). The vertical spacing of the Eod isoirrads is an indication of the diffuse attenuation coefficient, Kod(450,z). The time variation in the mean value of Kod(450,z) between the surface and 20 m is illustrated in Fig.4.7. Similar sets of diagrams were produced for the other wavelengths.

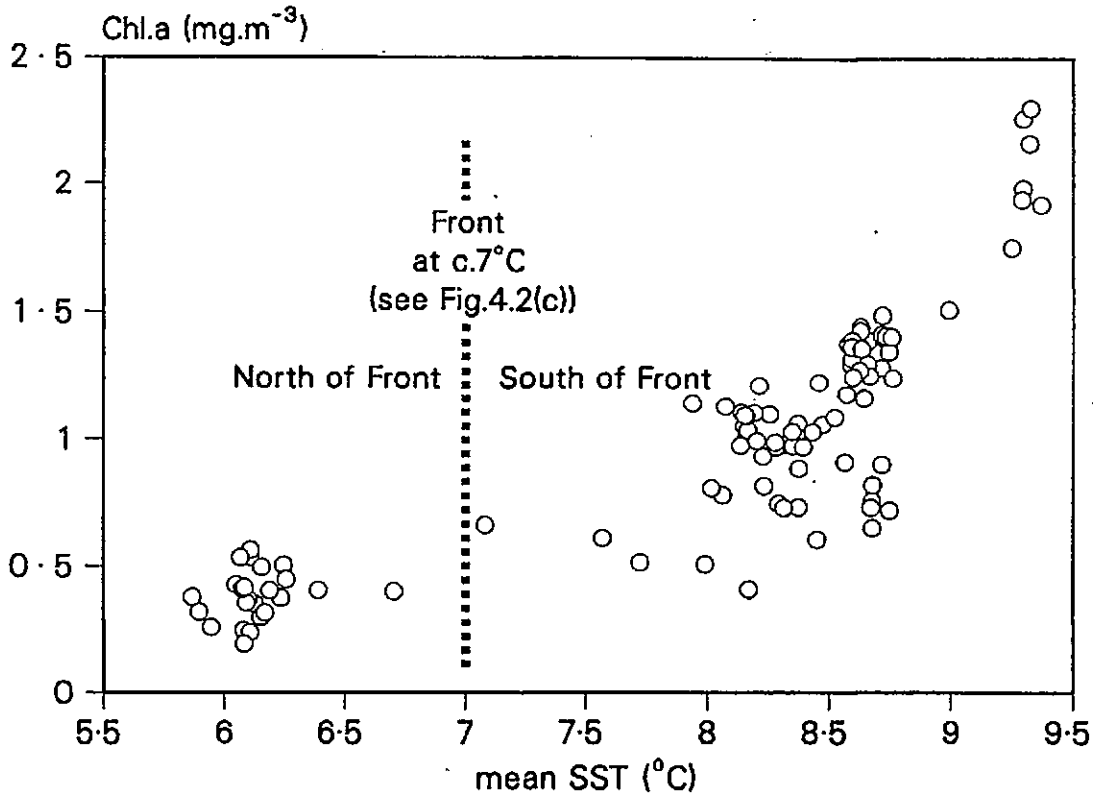

Fig.4.4: **Marked changes in Chlorophyll concentration (mg.m^{-3}) and mean surface Temperature (°C, 0-20 m) across the Arctic Front during Tow 15, Lynch 1987**

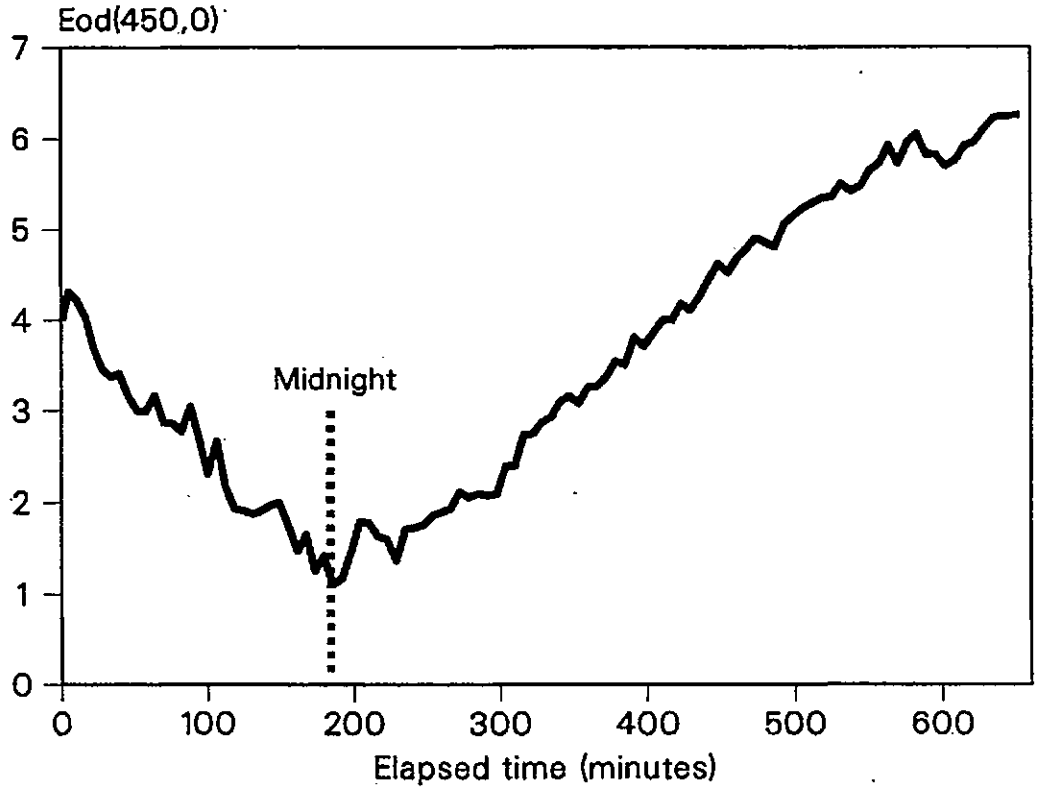

Fig.4.5: **Time-plot of Eod(450,z=0) for Tow 15,Lynch 1987**

We have from Eqn.2.33 (Kirk, 1983):

$$K(\lambda) = Kw(\lambda) + Kg(\lambda) + Kt(\lambda) + Kph(\lambda)$$

On the basis of measurements of the spectral variation of $Kd(\lambda)$ in various ocean waters, Smith and Baker (1978b) have concluded that in regions away from terrigenous influences, the attenuation (apart from that due to water) is mainly due to the phytoplankton and the pigmented detrital products that covary with it. A practical measure of these planktonic materials is the concentration of chlorophyll, indicated by its first absorption peak at 450 nm. We may therefore write:

$$Kd(450) = k_2(450).Chl + Kw(450) + Kx(450) \qquad (4.1)$$

where Chl is chlorophyll concentration ($mg.m^{-3}$), k_2 is the specific diffuse attenuation coefficient due to chlorophyll and chlorophyll-like pigments associated with chlorophyll, and Kx is the contribution by particles and dissolved compounds which are not related in any way to the concentration of chlorophyll.

The relationship between Kod(450) and chlorophyll concentration during Tow 15 is illustrated in Fig.4.8, and indicates that:

$$Kod(450) = 0.0402\ Chl + 0.0597 \quad (r^2=0.782,\ n=101) \qquad (4.2)$$

The intercept, 0.0597, is the sum Kw(450) + Kx(450). Smith and Baker (1981) give Kw(450) = 0.0168, in which case for Tow 15: Kx(450) = 0.0429. The gradient, dK/dChl = 0.040 in Eqn.4.2 is k_2. According to Smith and Baker (1978b), $k_2(450) = 0.037$. The difference, δk_2, is only 0.003 in this case. Similar analyses of the other $Kod(\lambda)$ and

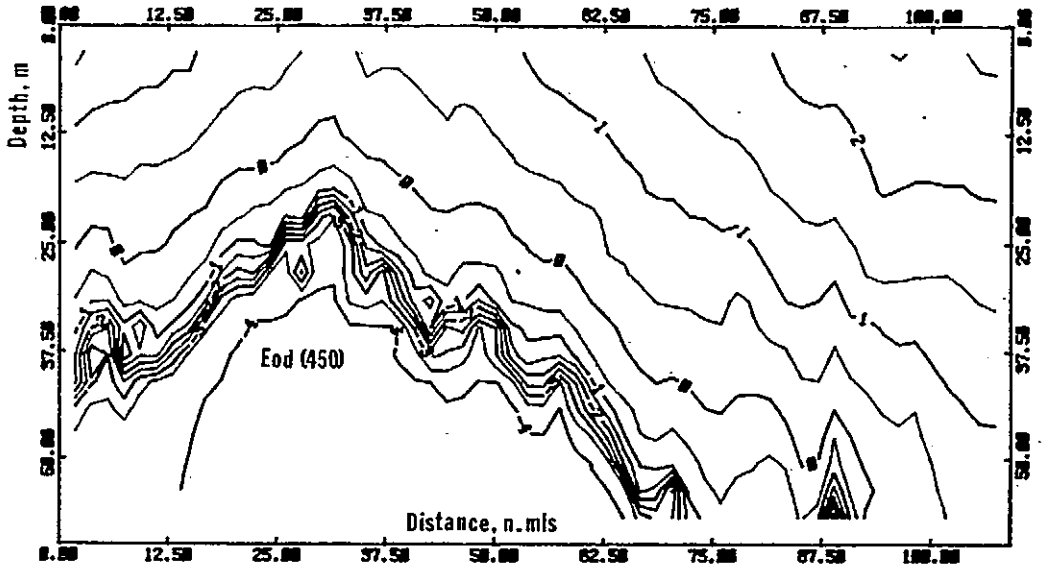

Fig.4.6: Plot of Eod(450) isoirrads as a function of depth (m) and distance (n.miles) for Tow 15, Lynch 1987

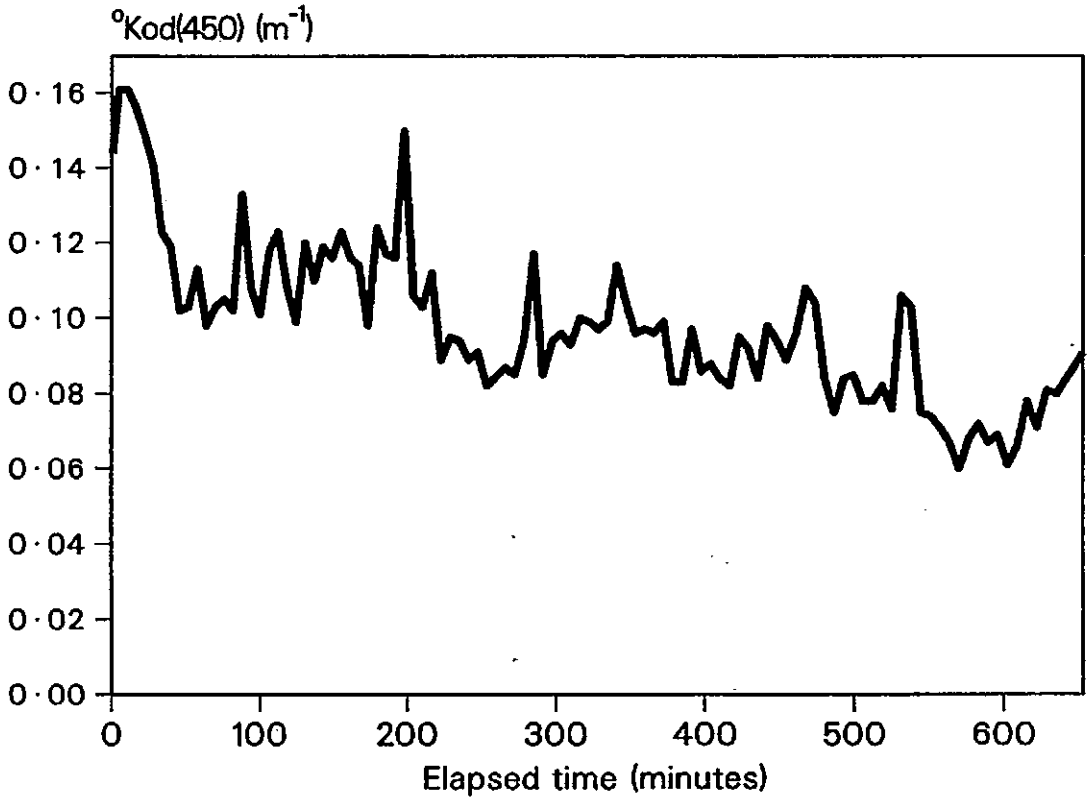

Fig.4.7: Time-plot of mean Kod(450, 0-20 m) for Tow 15, Lynch 1987

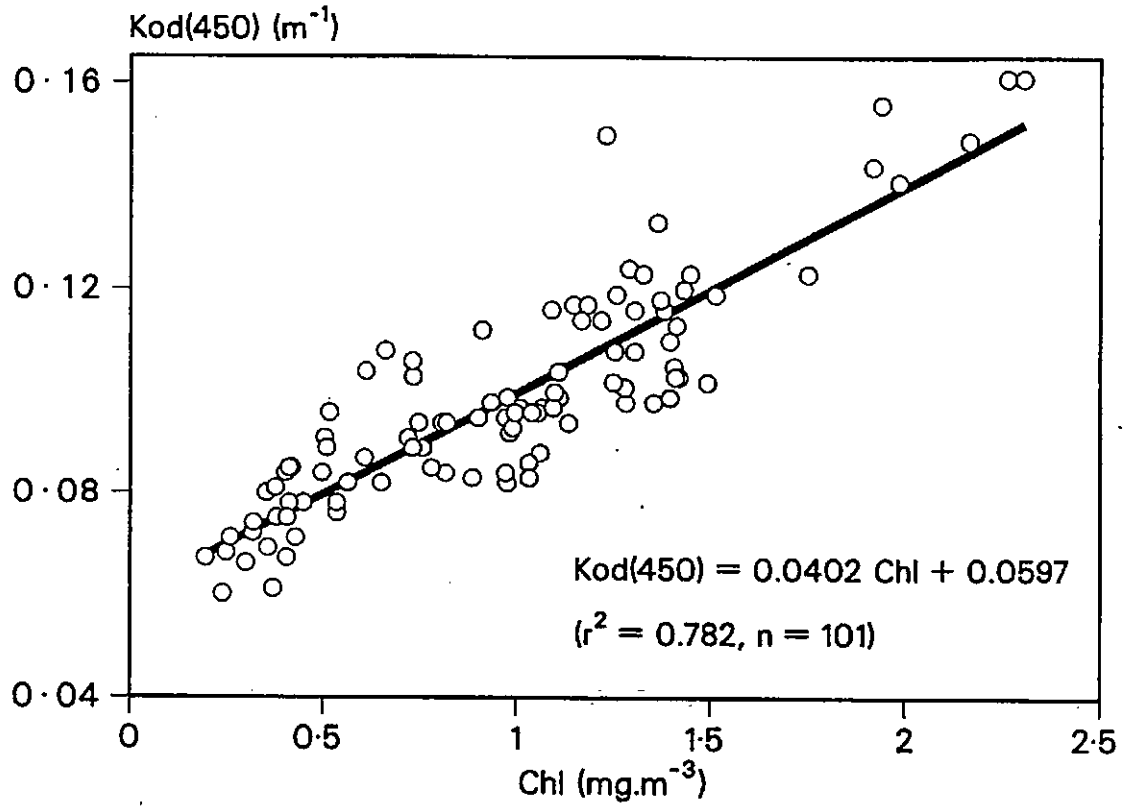

Fig.4.8: Relationship between Kod(450 nm) and Chlorophyll concentration (mg m^{-3}) during Tow 15, Lynch 1987.

Table 4.1: Simple analyses (see text) of the contributing components of Kod(λ), Kd(λ) for UOR Tow 15 (Lynch cruise, 1987). Values of Kw(λ) and $k_2(\lambda)$ are from Smith and Baker (1981) and (1978b), respectively.

K(λ)	Kw(λ)+ Kx(λ)	Kw(λ)	Kx(λ)	$\frac{dK(\lambda)}{dChl}$	$k_2(\lambda)$	$\delta k_2(\lambda)$
Kod(450)	0.0597	0.0168	0.0429	0.040	0.037	0.003
Kod(490)	0.0545	0.0212	0.0333	0.029	0.026	0.003
Kod(520)	0.0547	0.0489	0.0058	0.031	0.019	0.012
Kod(550)	0.0908	0.0648	0.0260	0.012	0.012	0
Kd(490)	0.0638	0.0212	0.0426	0.028	0.026	0.002
Kd(670)	0.3500	0.4300	(−0.08)	0.080	0.015	0.065

Kd(λ) data are presented in Table 4.1

It is apparent from Table 4.1 that throughout Tow 15 values of Eod(670) were too low for proper deduction of Kod(670). The value of $\delta k_2(520) = 0.012$ is, perhaps, a little high; it was subsequently discovered that the Eod(520) sensor had leaked, so Kod(520) values must be considered suspect.

Only one wavelength, 490 nm, was monitored by both scalar and vector collectors on the UOR. Comparison of Kd(490) with Kod(490) during Tow 15 produced the relationship:

$$Kod(490) = 0.864\ Kd(490) + 0.004 \quad (r^2=0.883,\ n=103) \tag{4.3}$$

and through 0,0: $$Kod(490) = 0.906\ Kd(490) \tag{4.4}$$

This is in agreement with Kirk (1983), and others, that $Kod \simeq Kd$.

4.2 ESTIMATION OF $\langle {}^{o}Ko \rangle$ AND $\langle K(\lambda) \rangle$

The measurement of an irradiance profile is a time-consuming procedure. Moreover, irradiance profiles cannot be obtained at night nor in very dull conditions. A number of experiments were therefore conducted to find empirical relationships between $\langle {}^{o}Ko \rangle$ and other, more easily obtained, optical parameters.

4.2.1 Estimation of $\langle {}^{o}Ko \rangle$ from c(660 nm)

Where a continuum of observations is required, or where data are obtainable only at night, then reasonable estimates of $\langle {}^{o}Ko)$ can be made from the easily measured beam attenuation coefficient, $c(\lambda)$. The ratio $c(\lambda)/K(\lambda)$ is about 2.7 in clear ocean water (Tyler, 1968), but increases in turbid waters; it must therefore be determined for the particular waters under investigation.

Values of c(660) were obtained in the northeast Atlantic and Tamar using a 0.25 m path-length, Sea Tech Inc transmissometer (see Chapter 3). The attenuation of 660 nm light by gilvin is negligible compared with that due to the waters and their suspended particulate matter. The c(660):$\langle {}^{o}Ko \rangle$ data were partitioned for oceanic ($^{o}Ko<0.27$) and turbid ($^{o}Ko>0.27$) analyses, this separation being about midway between Jerlov's oceanic type III and coastal type 1 waters (see Jerlov, 1976; Table 27). Linear regression of c:K data obtained by Williams et al (1984) in the Patuxent River, Chesapeake Bay and Atlantic Ocean produced different slopes for the three cases.

Observations made in the course of this work revealed a similar difference, as is apparent from the logarithmic regressions presented below (Pilgrim, 1987). Figure 4.9 shows the relationship between $\langle {}^{o}Ko \rangle$ and c(660) for the combined, oceanic and turbid waters, data.

All observations; $0.0517 \leq {}^{o}Ko \leq 4.276$

$$\langle {}^{o}Ko \rangle = 0.113\ c^{1.288} \quad (r^2=0.996,\ n=37) \qquad (4.5)$$

Oceanic ($^{o}Ko < 0.27$); $0.0517 \leq {}^{o}Ko \leq 0.2677$

$$\langle {}^{o}Ko \rangle = 0.127\ c^{1.575} \quad (r^2=0.955,\ n=14) \qquad (4.6)$$

Turbid ($^{o}Ko \geq 0.27$); $0.2902 \leq {}^{o}Ko \leq 4.276$

$$\langle {}^{o}Ko \rangle = 0.107\ c^{1.314} \quad (r^2=0.927,\ n=23) \qquad (4.7)$$

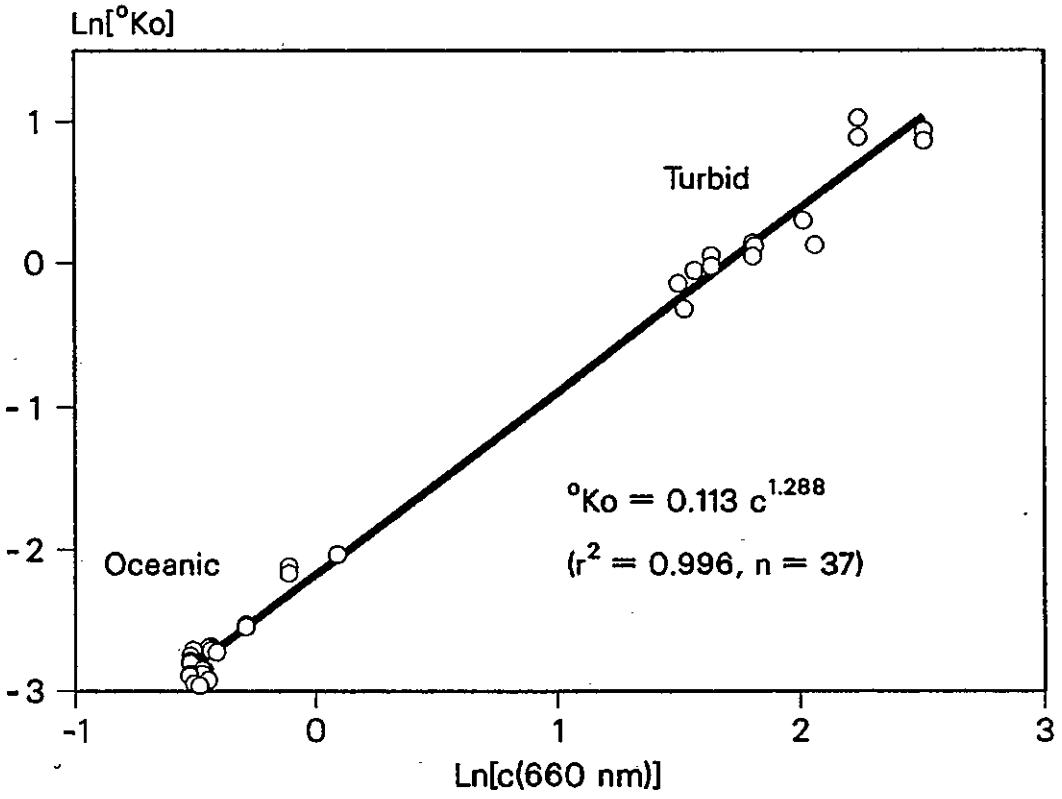

Fig.4.9: **Relationship between Ln[$\langle {}^{o}Ko \rangle$] and Ln[c(660)] from all observations. c(660) values were corrected for forward scattering by the method given by Bartz et al (1978) for a hyperbolic particle size distribution with a slope of 2.9, and a refractive index of 1.05, (see Table 3.1)**

4.2.2 Estimation of K(λ) from c(660)

Beam transmissions were measured during the Lynch 1987 cruise with a Sea Tech Inc transmissometer, and logged by means of a WDC 131/132 interface and Apple IIe microcomputer as described in Chapter 3. Sampling intervals were 1 minute during tows and 5 minutes between tows. Figure 4.10 is a time-plot of hourly means of c(660) for the entire cruise.

UOR data presented the only apportunity, throughout this programme of research, of comparing values of the attenuation and diffuse attenuation coefficient at nearly the same wavelength, namely: c(660) and Kd(670). These data are presented in Fig.4.11, and show that:

$$Kd(670) = 0.230\ c(660) + 0.203 \quad (r^2 = 0.773,\ n=40) \tag{4.8}$$

and through 0,0:

$$c(660)/Kd(670) = 2.173 \tag{4.9}$$

Logarithmic least squares regression produces:

$$Kd(670) = 0.433\ c(660)^{0.509} \tag{4.10}$$

At c(660) = 0.93, the mean value during Tow 15, Eqn.4.10 reduces to:

$$c(660)/Kd(670) = 2.23 \tag{4.11}$$

Tyler (1968) says that $c/K \simeq 2.7$ in oceanic waters, and this figure is widely quoted. However, the photon survival probability model of

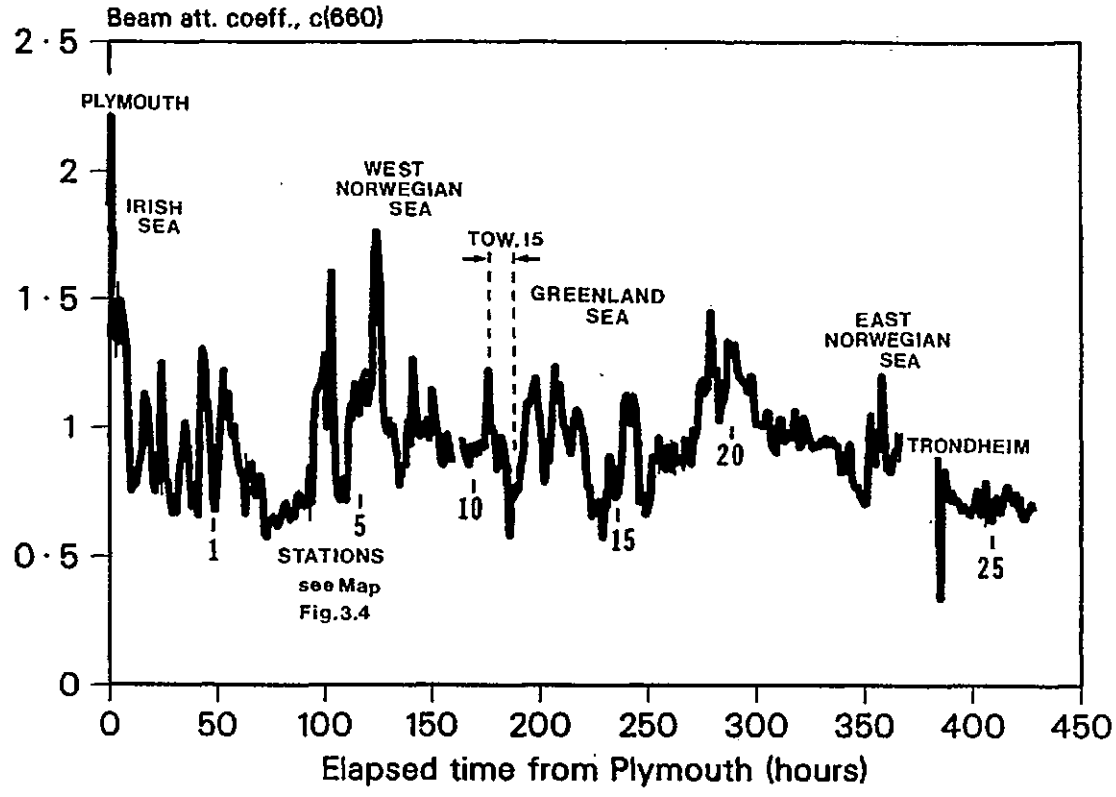

Fig.4.10: Time-plot of hourly means of c(660), Lynch 1987.

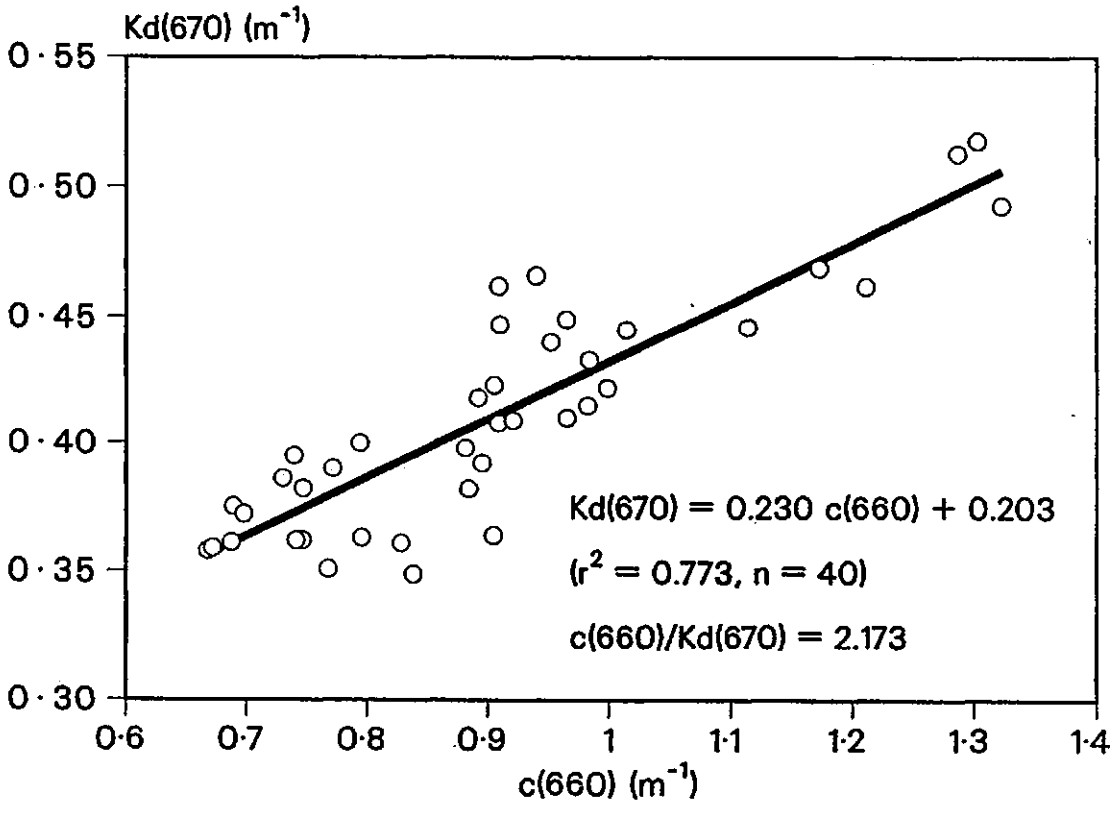

Fig.4.11: Relationship between <Kd(670)> and c(660) during Tow 15, Lynch 1987. c(660) values were corrected as for the c(660) data in Figure.4.9

Timofeeva (1973) (see Table 4.4), indicates that ratios smaller than this are to be expected in comparatively clear (low scattering, small b/c) oceanic waters.

4.2.3 Estimation of $\langle {}^{o}Ko \rangle$ from $Ed(\lambda_1,z)$ ... $Ed(\lambda_n,z)$

During the Lynch 1987 cruise, the UOR was not fitted with a broad-band PAR quantum sensor, so that $\langle {}^{o}Ko \rangle$ was not directly calculated. An attempt was made, however, to estimate $\langle {}^{o}Kod \rangle$ from the available $Eod(\lambda,z)$ data.

Suppose that Fig.4.12 represents an $Eod(\lambda,0)$ spectrum constructed from measurements of $Eod(\lambda_1)$, $Eod(\lambda_2)$ ... $Eod(\lambda n)$, and assumed cut-off at 400 and 700 nm.

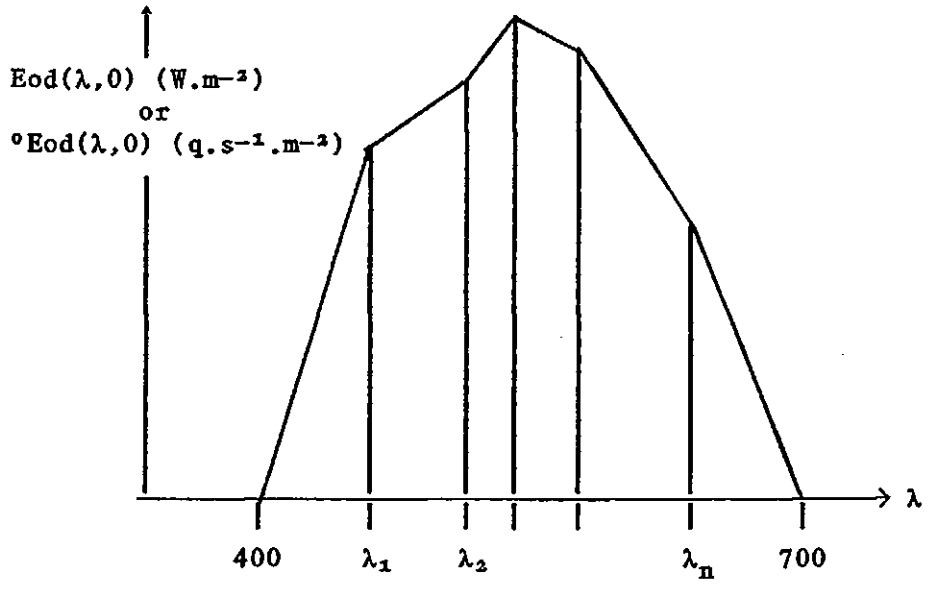

Fig.4.12: Constructed $Eod(\lambda,0)$ or ${}^{o}Eod(\lambda,0)$ spectrum

To convert each value of $Eod(\lambda,0)$ from $W.m^{-2}$ to $q.s^{-1}.m^{-2}$, use is made of the Morel and Smith (1974) equation:

$$W.(q.s^{-1})^{-1} = \lambda/h.c = \lambda(nm) \times 0.5035 \times 10^{16} \qquad (4.12)$$

The spectrum, (Fig.4.12), now becomes one of $^{0}Eod(\lambda,0)$, and the total quantum PAR at z=0 is given by:

$$\begin{aligned}\sum {}^{0}Eod(\lambda,0) = {} & \tfrac{1}{2}\left[{}^{0}Eod(\lambda_1,0).(\lambda_1-400)\right] \\ & + \tfrac{1}{2}\left[({}^{0}Eod(\lambda_1,0) + {}^{0}Eod(\lambda_2,0)).(\lambda_2-\lambda_1)\right] \\ & + \tfrac{1}{2}\left[({}^{0}Eod(\lambda n-1,0) + {}^{0}Eod(\lambda n,0)).(\lambda n-\lambda n-1)\right] \\ & + \tfrac{1}{2}\left[{}^{0}Eod(\lambda n,0).(700-\lambda n)\right] \qquad (4.13)\end{aligned}$$

At some depth, z, each value of $^{0}Eod(\lambda)$ is reduced to:

$$^{0}Eod(\lambda,z) = {}^{0}Eod(\lambda,0).\exp[-{}^{0}Kod(\lambda).z]$$

According to Kirk (1983), and others, $^{0}Kod \simeq Kod \simeq Kd$, so:

$$^{0}Eod(\lambda,z) = {}^{0}Eod(\lambda,0).\exp[-Kod(\lambda).z]$$

We may therefore write for $^{0}Eod(\lambda,z)$ at, say, z=1:

$$^{0}Eod(\lambda,1) = {}^{0}Eod(\lambda,0).\exp[-Kod(\lambda)] \qquad (4.14)$$

and for total PAR quanta at z = 1, a modified form of Eqn.4.13:

$$\sum^{o}Eod(\lambda,1) = \tfrac{1}{2}\left[{}^{o}Eod(\lambda,1).(\lambda_1-400)\right] + \ldots\ldots \qquad (4.15)$$

It is apparent that:

$$\sum^{o}Eod(\lambda,1) = \sum^{o}Eod(\lambda,0).\exp[-\langle{}^{o}Kod\rangle.1]$$

where $\langle{}^{o}Kod\rangle$ is the required estimation of the PAR extinction coefficient, ie:

$$\langle{}^{o}Kod\rangle = Ln\left[\sum^{o}Eod(\lambda,0) \;/\; \sum^{o}Eod(\lambda,1)\right] \qquad (4.16)$$

Six downwelling irradiances, (Eod(450), Eod(490), Eod(520), Eod(550), Ed(490) and Ed(670)), were measured during the Lynch 1987 cruise. Because of sensor leakage, Eod(520) was not used in this calculation, and Eod(490) was preferred to Ed(490). Possibly, the 4 downwelling irradiances at 450, 490, 550 and 670 nm do not give an adequate cover of the constructed 400–700 nm spectrum (Fig.4.12); however, the analysis was carried out to test its feasibility

The irradiance data and Eqns.4.12–4.16 were entered into a Minitab worksheet (Prime), and $\langle{}^{o}Kod\rangle$ (Eqn.4.16) was calculated. The relationship between estimated $\langle{}^{o}Kod\rangle$ and c(660) was found to be:

$$\langle{}^{o}Ko\rangle = 0.201\ c(660)^{0.398} \quad (r^2=0.527,\ n=41) \qquad (4.17)$$

For c(660) = 0.93, the average value during Tow 15, Eqn.4.17 is reduced to:

$$c(660)/\langle {}^{o}Kod\rangle = 4.76 \qquad (4.18)$$

This may be compared to the result that would be given by using c(660) = 0.93 in Eqn.4.6 (Pilgrim, 1987), which was derived from direct measurements of $\langle {}^{o}Ko\rangle$ by means of a Biospherical Instruments Inc profiling system:

$$c(660)/\langle {}^{o}Ko\rangle = 8.21 \qquad (4.19)$$

The rather large difference between Eqns.4.18 and 4.19 is almost certainly due to inherent errors in the estimation method. For example, the measured (UOR) irradiances have significant bandwidths which must distort the shape of the constructed spectrum of Fig.4.12.

Tow 15 was made in the low-light conditions of an Arctic night so that upwelling irradiances were insignificant. In brighter, daylight conditions, values of Eou(λ), Eu(λ) should be added to equivalent Eod(λ), Ed(λ) measurements at the start of the analysis outlined here. This would produce an estimate of $\langle {}^{o}Ko\rangle$ rather than $\langle Kod\rangle$.

Jerlov (1974) and Højerslev and Jerlov (1977) have proposed two simple methods of estimating downwelling quantum irradiance, °Eod(z). In the first, °Eod(z) is estimated from measurements of Ed(465). In the second, the depths at which °Eod(z)/°Eod(0) = 30%, 10%, 3% and 1% are estimated from measurements of the colour index: F(z=1) = Lu(450,1)/Lu(525,1) ≃ Eu(450,1)/Eu(525,1). These methods are further considered in Chapter 5 where proposed future work is discussed.

4.3 ESTIMATION AND INDIRECT MEASUREMENT OF THE ABSORPTION AND SCATTERING COEFFICIENTS

4.3.1 Estimation of $\overline{\cos\xi}$, $^{o}a_o$ and $^{o}b_o$ from Kirk's Monte Carlo Model

Kirk's Monte Carlo model was illustrated in Fig.2.10 , and described in Chapter 2, where it was shown that the average cosine, and absorption and scattering coefficients, may be estimated from measured values of Ko and the scalar irradiance reflectivity, Ro.

The PAR scalar irradiance reflectivity, $^{o}Ro = {}^{o}Eou/{}^{o}Eod$, is readily determined from measurements of upwelling and downwelling scalar irradiance. Twenty-seven observations of ^{o}Eou,^{o}Eod were made in the NE Atlantic and Tamar Estuary by masking and inverting the Biospherical Instruments Inc QSP series profiling Quantum Scalar Irradiance System as described in Chapter 3.

It is theoretically possible to determine $^{o}Ro(z)$ by lowering the instrument to depth z to measure $^{o}Eod(z)$, and then inverting it to measure $^{o}Eou(z)$. This is not a practical solution, however, as inversion of the instrument involves a change in collector depth; moreover, the ambient (sky) light level may vary substantially during the time interval involved. A method was therefore designed by which ^{o}Ro was calculated from separate profiles of ^{o}Eou and ^{o}Eod. We may write: $^{o}Ro = {}^{o}Eou/{}^{o}Eod = Yu/Yd$, where $Yu,Yd = {}^{o}Eou/Eref,{}^{o}Eod/Eref$, the normalised upwelling and downwelling values.

Therefore:

$$^{o}Ro(z) = \frac{Yu(z)}{Yd(z)} = \frac{Yu(0).\exp[-^{o}Kou.z]}{Yd(0).\exp[-^{o}Kod.z]} \qquad (4.20)$$

These derived values of $^{o}Ro(z)$ were subsequently used in the Kirk (1986) version of his Monte Carlo model, where z = Zm, the 10% level. This is the depth at which $^{o}Eo(z)/^{o}Eo(o) = 0.1$, and corresponds to the mid-depth of the euphotic (1%) zone, therefore:

$\frac{^{o}Eo(Zm)}{^{o}Eo(0)} = 0.1 = \exp[-^{o}Ko.Zm]$, whence:

$Zm = Ln(0.1)/-^{o}Ko = 2.303/^{o}Ko$, therefore, from Eqns.4.20:

$$^{o}Ro(Zm) = \exp\left[Ln[Yu(0)] - Ln[Yd(0)] + \frac{2.303}{^{o}Ko}(^{o}Kou + ^{o}Kod)\right] \qquad (4.21)$$

This equation is illustrated in Fig.4.14, and implies that it is also necessary to find ^{o}Ko, ie necessary to take a separate profile with the instrument unmasked. This would be inconvenient, so an equation for finding ^{o}Ko from ^{o}Kod, ^{o}Kou, Yu(o), Yd(o) was derived. We have, from Eqn.3.1:

$$^{o}Ko = \frac{Ln[Y(0)] - Ln[Y(z)]}{z}$$

and as $Y(z) = \frac{^{o}Eo(z)}{Eref} = \frac{^{o}Eou(z) + ^{o}Eod(z)}{Eref} = Yu(z) + Yd(z)$ then:

$$^{o}Ko = \frac{Ln[Yu(o)+Yd(o)] - Ln[Yu(z)+Yd(z)]}{z}$$

Therefore:

$$^{o}Ko.z = Ln\left[\frac{Yu(o) + Yd(o)}{Yu(z) + Yd(z)}\right]$$

$$= Ln\left[\frac{Yu(o) + Yd(o)}{Yu(0).exp[-^{o}Kou.z] + Yd(0).exp[-^{o}Kod.z]}\right]$$

whence, for z = 1, say:

$$^{o}Ko(du) = Ln\left[\frac{Yu(o) + Yd(o)}{Yu(0).exp[-^{o}Kou] + Yd(0).exp[-^{o}Kod]}\right] \qquad (4.22)$$

As upwelling irradiances are so low, particularly in turbid estuarine waters, measurements of ^{o}Eou are subject to considerable fluctuation. Therefore, during these reflectivity experiments, incoming signals were not read from the display unit in the usual way but were directed, via a WDC 131/132 data-logging interface, to an Apple IIe

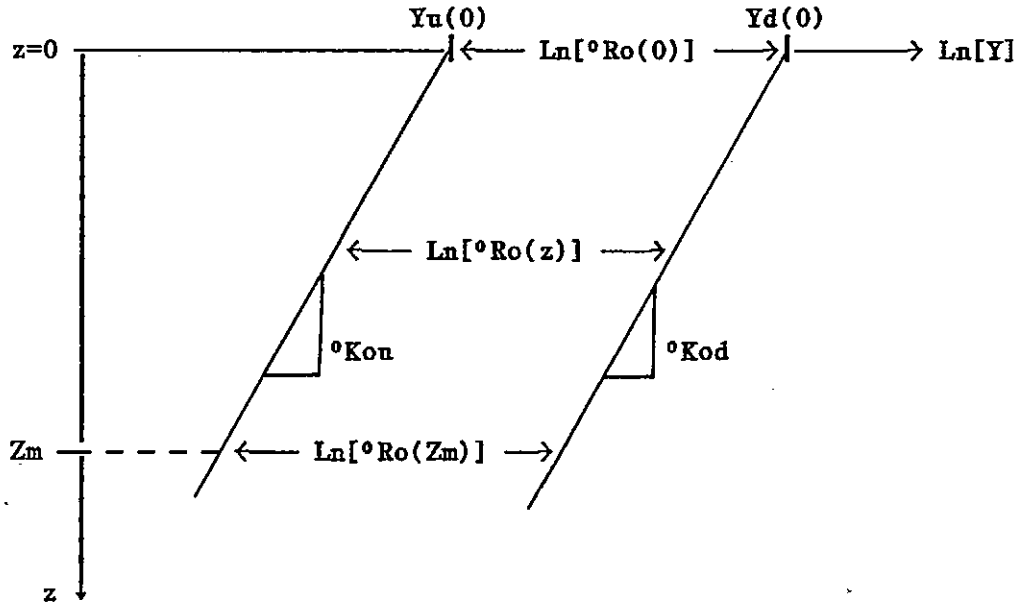

Fig.4.14: Relationship between Ln[$^{o}Ro(Zm)$] and profiles of Ln[$^{o}Eou/Eref$ and Ln[$^{o}Eod/Eref$]

microcomputer. Readings were obtained at 5 sec intervals, and mean values were calculated (programme: MEANER) and displayed by the computer. This system worked satisfactorily.

The Monte Carlo Model of Kirk (1981a, 1981c, 1986) was described in Chapter 2 and illustrated in Fig.2.10. Entering this graph with $^{o}Ro(Zt)$, then values of the average cosine, $\overline{\cos\xi}$, and the ratio of diffuse scattering to absorption coefficients, $^{o}b_o/^{o}a_o$, may be extracted. Now $a = \overline{\cos\xi}.Ke$, and assuming that $^{o}Ko \simeq Ke$ (Kirk, 1986), then: $^{o}a_o = \overline{\cos\xi}.^{o}Ko$. Also, we have $^{o}b_o/^{o}a_o$, so: $^{o}b_o = (^{o}b_o/^{o}a_o).^{o}a_o$ and $^{o}c_o = ^{o}a_o + ^{o}b_o$.

Results of the 27 observations are presented in Table 4.2. Column 1 is of profile numbers prefixed: (27) NE Atlantic, (28) Tamar-Lynher Estuarine confluence, (25) Tamar Estuary, and (29) Plymouth Sound. Column 2 comprises of $^{o}Ko(du)$, (values of ^{o}Ko calculated by Eqn.4.22) and ^{o}Ko measured directly with an unmasked instrument. Reflectivities, $^{o}Ro(Zm)$, and Secchi coefficients, 1/Zs, are listed in column 3. Values of $\overline{\cos\xi}$ and $^{o}b_o/^{o}a_o$ extracted from Fig.2.10 (Kirk's Monte Carlo model) are presented in column 4. Columns 5, 6 and 7 contain the calculated values of $^{o}a_o$, $^{o}b_o$, $^{o}c_o$, $^{o}c_o/^{o}Ko(du)$ and $^{o}c_o + ^{o}Ko(du)$. Values of c(660nm) obtained by transmissometer are also listed in column 7.

Calculated values of $^{o}Ko(du)$ (Eqn.4.22) are plotted against measured values of ^{o}Ko in Fig.4.15. Least-square regression indicates that:

$$^{o}Ko(du) = 1.022\ ^{o}Ko - 0.009;\ ^{o}Ko(du) = 1.015\ ^{o}Ko\ (r^2=0.992,\ n=18) \qquad (4.23)$$

Table 4.2: Results of analyses using Kirk's Monte Carlo model

Prof	*Ko(du) / *Ko	*Ko(Zm) / 1/Zs	$\overline{\cos\xi}$ / *(b/a)$_o$	*s_o / *b_o	*c / c(660)	*(c+K)o(du) / *(c/K)o(du)
2701	0.0525	5.63	0.636	0.0334	0.1373	0.1898
	-	-	3.116	0.1040	0.6040	2.6160
02	0.0538	4.30	0.655	0.0353	0.1202	0.1740
	-	-	2.409	0.0850	0.6404	2.235
09	0.0796	4.19	0.657	0.0515	0.1724	0.2520
	0.0783	0.0526	2.351	0.1210	0.7482	2.202
10	0.1143	3.69	0.668	0.0803	0.2469	0.3612
	0.1202	0.0667	2.076	0.1666	0.8950	2.054
12	0.0605	5.04	0.644	0.0411	0.1563	0.2168
	0.0638	0.0323	2.803	0.1152	0.5943	2.450
13	0.0560	5.32	0.640	0.0355	0.1401	0.1961
	0.0554	0.0435	2.951	0.1047	0.5922	2.530
14	0.0561	5.61	0.644	0.0398	0.1638	0.2199
	0.0618	0.0323	3.115	0.1240	0.5943	2.651
15	0.0664	3.61	0.681	0.0466	0.1411	0.2075
	0.0684	0.0476	2.031	0.0945	0.6465	2.063
16	0.0578	3.42	0.686	0.0385	0.1125	0.1703
	0.0561	0.0476	1.924	0.0740	0.6234	2.005
17	0.1307	13.13	0.541	0.0709	0.5921	0.7228
	0.1311	0.0833	7.355	0.5212	1.0935	4.516
18	0.2027	11.86	0.556	0.1103	0.8247	1.0274
	0.1985	0.1540	6.475	0.7140	-	4.155
2801	2.538	10.07	0.576	1.3662	9.074	11.612
	2.372	1.5600	5.642	7.7080	12.276	3.825
04	0.866	12.67	0.544	0.3950	3.216	4.082
	0.726	0.5714	7.141	2.8210	4.538	4.430
05	0.943	9.710	0.577	0.5646	3.719	4.662
	0.978	0.588	5.588	3.155	4.961	3.803
06	1.050	11.49	0.519	0.5956	5.753	6.803
	1.148	0.606	8.659	5.157	5.587	5.011
07	1.051	15.32	0.496	0.5589	6.264	7.315
	1.126	0.714	10.208	5.705	6.118	5.563
2516	1.145	13.86	0.521	0.5539	5.291	6.436
	1.064	0.910	8.552	4.737	-	3.999
19	1.256	14.30	0.505	0.6325	6.639	7.895
	1.252	-	9.496	6.006	-	5.148
22	1.201	19.13	0.512	0.6331	6.363	7.564
	1.236	1.110	9.051	5.730	-	5.302
25	1.701	9.560	0.566	0.9796	6.927	8.628
	1.732	1.670	6.072	5.948	-	4.972
2901	0.6123	12.49	0.476	0.2914	3.746	4.358
	-	-	11.859	3.455	4.788	6.119
03	0.5389	22.50	0.478	0.2574	3.274	3.813
	-	-	11.720	3.016	4.961	6.074
04	0.5157	22.18	0.512	0.2639	2.661	3.177
	-	-	9.087	2.398	4.320	5.161
05	0.5773	11.06	0.564	0.3258	2.321	2.898
	-	-	6.125	1.995	4.691	4.021
06	0.6290	14.48	0.567	0.3566	2.502	3.131
	-	-	6.018	2.146	4.480	3.978
07	0.6249	16.90	0.566	0.3536	2.497	3.122
	-	-	6.061	2.143	4.936	3.995
08	0.6265	14.95	0.588	0.3683	2.266	2.893
	-	-	5.152	1.897	4.813	3.616

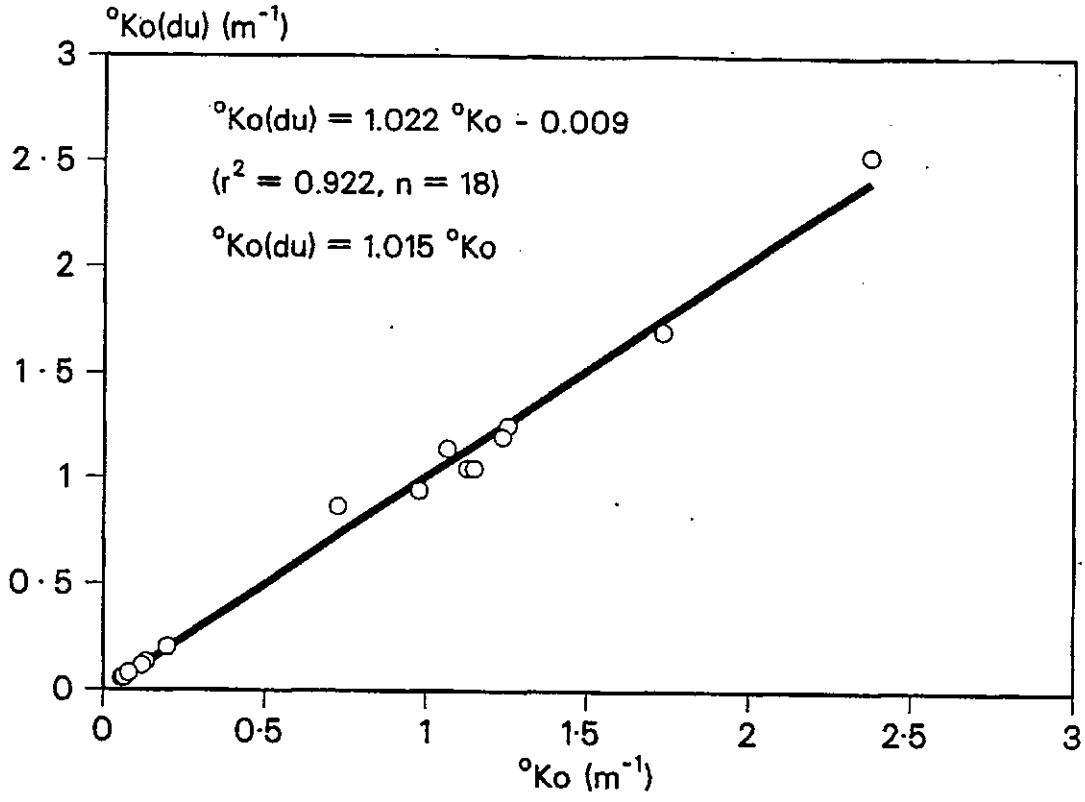

Fig.4.15: Relationship between calculated values of °Ko(du) and measured values °Ko

Equation 4.23 shows that it is in order to calculate the total extinction coefficient from Eqn.4.22.

We may write, from Eqn.2.94, for the Secchi depth:

$$^{o}(c + K)o = \frac{^{o}Fs}{Zs} \qquad (4.24)$$

Regression of $^{o}(c + K)_o$ values with values of Secchi coefficient, 1/Zs, is illustrated in Fig.4.16 and shows that:

$$^{o}(c + K)o = 6.719\ Zs^{-1} + 0.299;\ ^{o}Fs = ^{o}(c + K)_o = 6.998 \approx 7 \qquad (r^2 = 0.916,\ n = 17) \qquad (4.25)$$

It will be shown later that analysis of photopic observations by divers produces the equivalent estimate : $\underline{Fs} = (\underline{c}+\underline{K}) = 5.98 \approx 6$

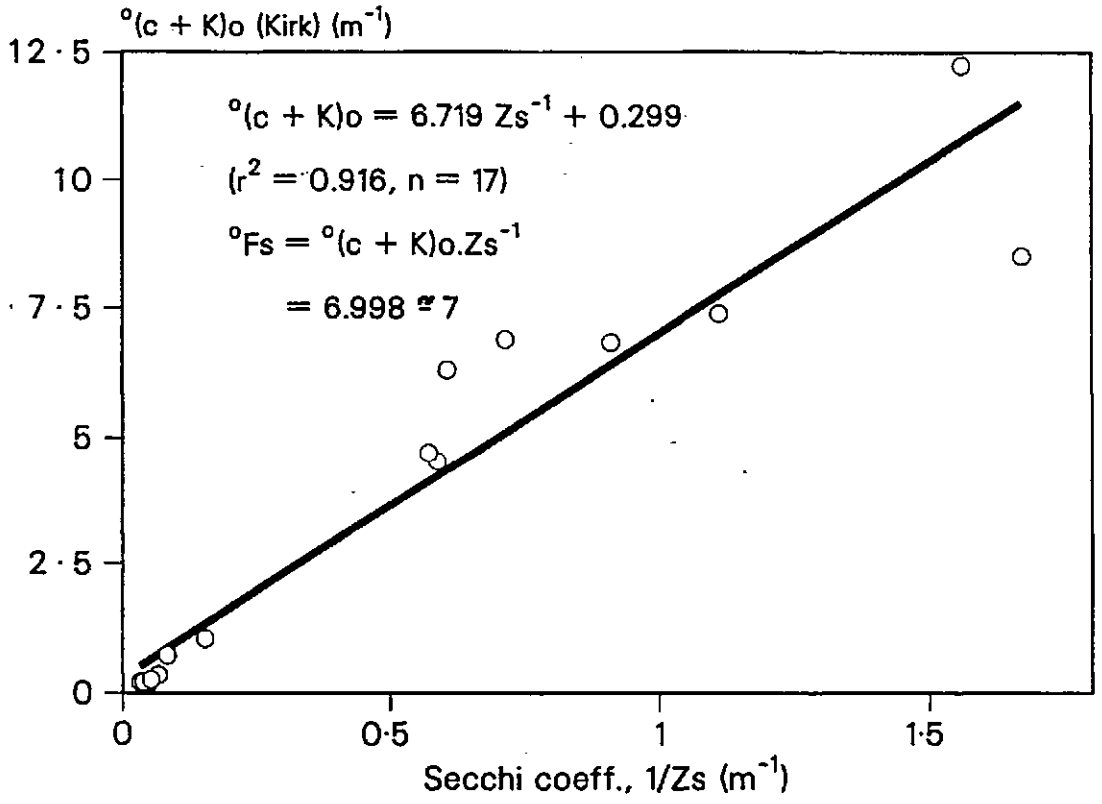

Fig.4.16: Relationship between °(c + K)o, calculated from Kirk's Monte Carlo model, and the measured Secchi coefficient

Other least-squares regressions of data extracted from Table 4.2 are now considered.

Regression of calculated values of $^{\circ}c_o$ with measured values of c(660) produces:

$$^{\circ}c_o = 0.816\ c(660) + 0.479;\ ^{\circ}c_o = 0.733\ c(660)\ (r^2=0.937,\ n = 22) \qquad (4.26)$$

The correlation is reasonable. We would not expect to find that $^{\circ}c_o = c(660)$ as c(660) is the beam attenuation of narrow-band, collimated light, whereas $^{\circ}c_o$ applies to broad-band, diffuse light.

Regression of $^{\circ}c_o = {}^{\circ}K_o(du)$ data gives:

$$^{\circ}c_o = 4.679\ {}^{\circ}K_o{}^{1.223}\ \ (r^2 = 0.982\ n = 27) \qquad (4.27)$$

The non-linearity of this relationship is due to the increase in the ratio ${}^{0}c_0/{}^{0}K_0$ with increase in turbidity, indeed, we may write, from Eqn.4.27:

$${}^{0}c_0/{}^{0}K_0 = 4.679\ {}^{0}K_0\ {}^{0.223} \qquad (4.28)$$

As expected, reflectivity ${}^{0}R_0(Zm)$ is shown to increase with the attenuation coefficient ratio, ${}^{0}c_0/{}^{0}K_0$:

$${}^{0}R_0(Zm)\% = 3.739\ {}^{0}c_0/{}^{0}K_0 - 3.489 \quad (r^2 = 0.748,\ n = 27) \qquad (4.29)$$

4.3.2 Indirect determination of $\overline{\cos\xi}$ and ${}^{0}a_0$ from measurements with a Højerslev-type sensor

Højerslev (1975) describes a sensor-pair which measures ½(Eo + E) and ½(Eo − E). The sensor was illustrated in Figs.2.8 and 2.9, and described in Chapter 2 where it was also shown that data obtained with this type of meter may be used to calculate ⟨Ko⟩ (Eqns.2.70 and 2.71), ⟨K⟩ (Eqn.2.72), a(z) (Eqn.2.73) and $\overline{\cos\xi}(z)$ (Eqn.2.74).

A Højerslev-type sensor was constructed in house, as described in Chapter 3 , and was used to obtain observations in the NE Atlantic during the 1987 Frederick Russell cruise. As the sensors began to leak water early in the cruise, the number of these data is limited.

Figure 4.17 illustrates values of ⟨Ko⟩, calculated from Højerslev-type meter measurements and Eqns.2.70 and 2.71, compared to values of ⟨^{0}Ko⟩ obtained by direct measurement with a Biospherical Instruments

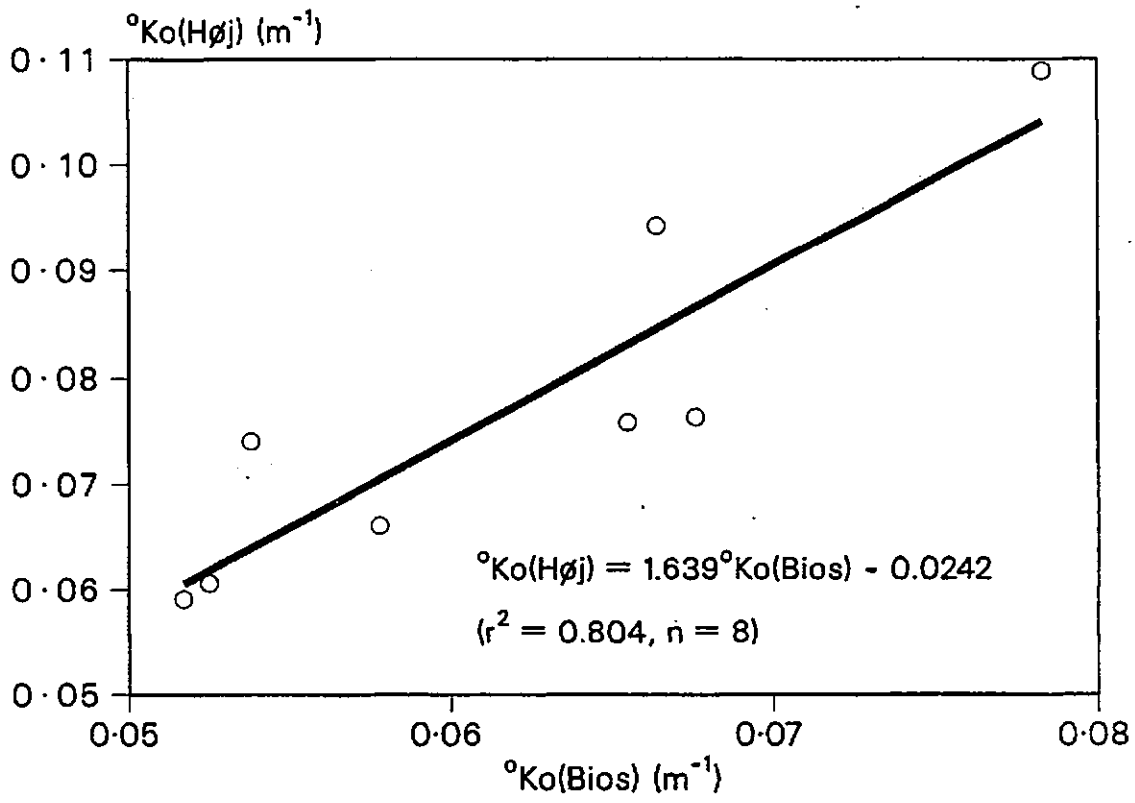

Fig.4.17: Comparison of values of <Ko> calculated from Højerslev-type meter measurements, and values of <°Ko> obtained by measurements with a Biospherical QSP meter

Inc QSP system. Least-squares regression shows that:

$$\langle Ko \rangle \text{ (Højerslev)} = 1.639 \langle {}^{\circ}Ko \rangle \text{ (Biospherical)} - 0.0242 \qquad (r^2=0.804,\ n=8) \qquad (4.30)$$

and through 0,0:

$$\langle Ko \rangle \text{ (Højerslev)} = 1.254 \langle {}^{\circ}Ko \rangle \text{ (Biospherical)} \qquad (4.31)$$

There should not, of course, be such a marked difference between these two data sets.

We have, from the derivation of Eqn.2.73, that $dE/dz = -a(z).Eo(z) = -K(z).E(z)$, whence: $a(z) = K(z).E(z)/Eo(z)$. It must therefore

follow that:

$$a_o.(z) = Ko(z).E(z)/Eo(z) \qquad (4.32)$$

Figure 4.28 shows values of $\langle a \rangle$ (O) and $\langle a_o \rangle$ (Δ), calculated from Højerslev-type meter data and Eqn.4.32, plotted against values of $^{\circ}a_o$ estimated from Kirk's Monte Carlo model (Fig.2.10) and measurements of $\langle {}^{\circ}Ro \rangle$ obtained with a masked Biospherical Instruments Inc QSP system as described in Chapter 3. The data points, particularly Δ , should be close to the 1:1 line.

This considerable discrepancy will be discussed in Chapter 5.

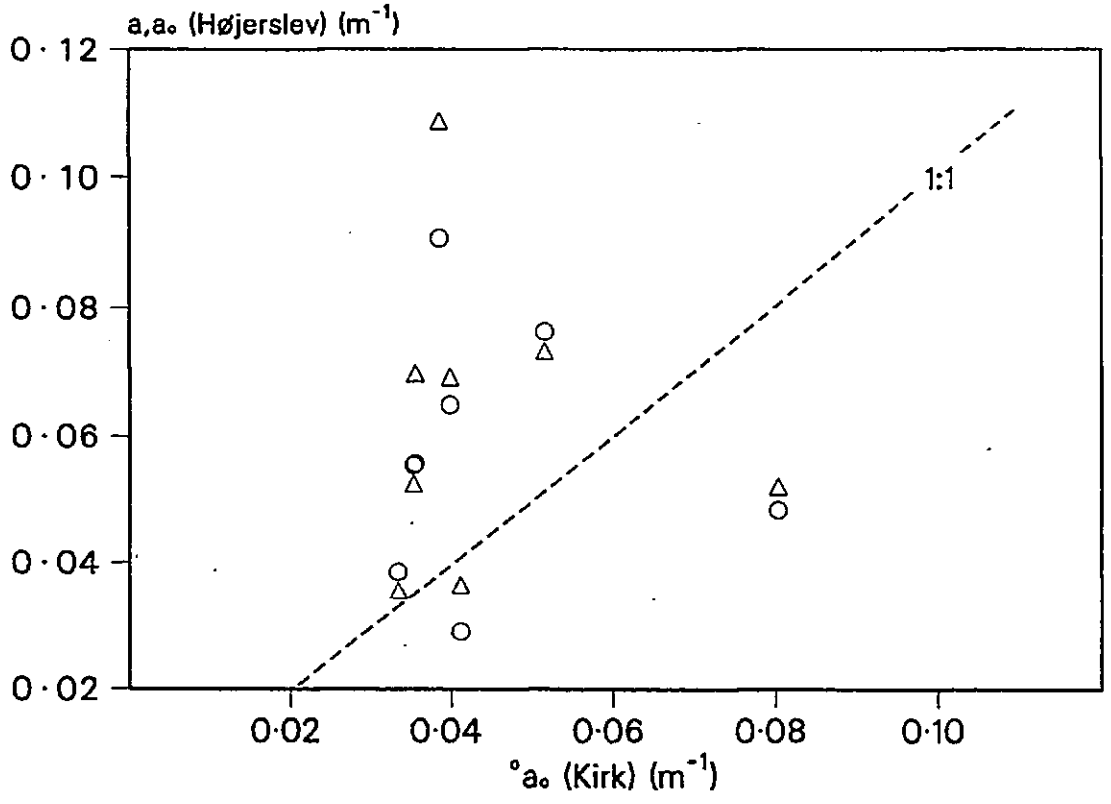

Fig.4.18: Poor comparison between values of $\langle a \rangle$ (O) and $\langle a_o \rangle$ (Δ), calculated from Højerslev-type meter data, and values of $\langle {}^{\circ}a_o \rangle$ estimated from Kirk's Monte Carlo model

4.4 ESTIMATION OF OPTICAL COEFFICIENTS FROM VISUAL RANGES

All of the threshold visual ranges referred to in this subsection are observed vertically downwards (Z), vertically upwards (U) or horizontally (V). We have, Eqn.2.87:

$$v(\gamma) = \frac{\text{Ln}[Co/Ct]}{\underline{c} + \underline{K}.\sin\gamma}$$

from which we may write:

$$Z = \frac{\text{Ln}[Co/Ct]}{\underline{c} + \underline{K}} \qquad (4.33)$$

$$V = \frac{\text{Ln}[Co/Ct]}{\underline{c}} \qquad (4.34)$$

$$U = \frac{\text{Ln}[Co/Ct]}{\underline{c} - \underline{K}} \qquad (4.35)$$

The targets used in the underwater observations have been described in Chapter 3 and were: Secchi disc (s), white disc/target (w), grey disc/target (g), black disc/target (b) or light-trap (h), corner reflector (x) and neutral filter (f).

It was made clear in Chapter 2, and is apparent from Eqns.4.33-4.35 above, that underwater visibility depends upon the transmittance of inherent contrast. The inherent contrast of a target of reflectivity $\underline{\rho}$, sighted vertically downwards ($\underline{\rho}=\pi/2$), is illustrated in Fig.2.11, and again in Fig.4.19(a).

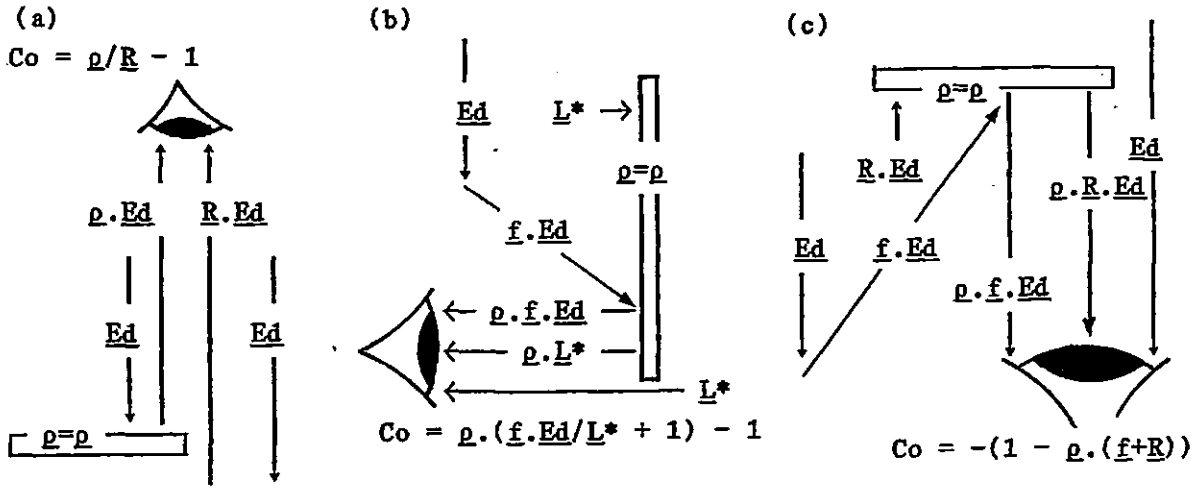

Fig.4.19: Inherent contrast of target of reflectivity ρ

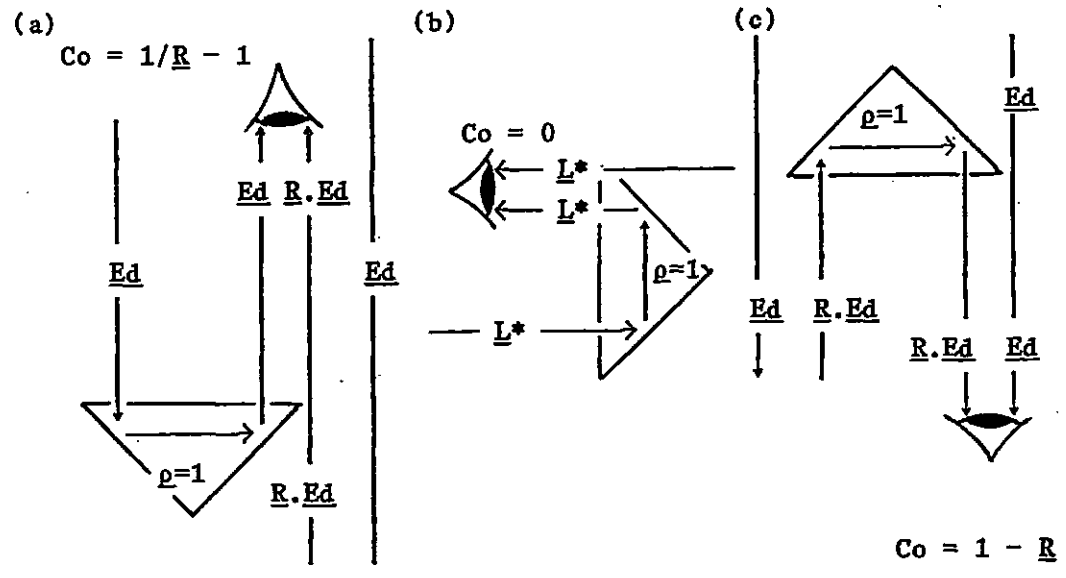

Fig.4.20: Inherent contrast of corner reflector (ρ = 1)

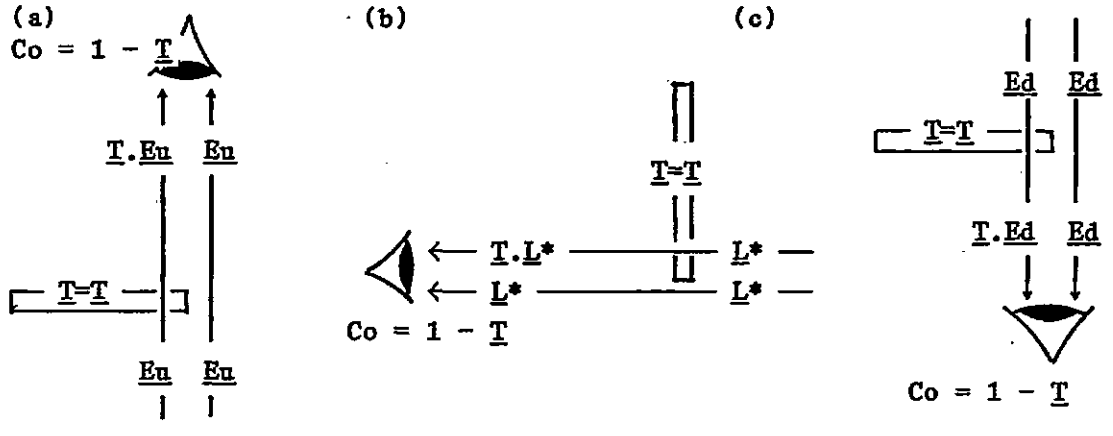

Fig.4.21: Inherent contrast of neutral filter (T = T)

The inherent contrast of such a target is expressed by Eqns.2.76 and 2.77:

$$Co(\underline{\rho}=\underline{\rho},\gamma=\pi/2) = \frac{{}_t\underline{L}(0) - {}_b\underline{L}(0)}{{}_b\underline{L}(0)} = \frac{\underline{\rho}.\underline{Ed} - \underline{R}.\underline{Ed}}{\underline{R}.\underline{Ed}} = \underline{\rho}/\underline{R} - 1 \qquad (4.36)$$

The corner reflector is designed to give practically 100% reflection ($\underline{\rho}=1$). The vertically downward sighting of a corner reflector is illustrated in Fig.4.20(a), and shows that:

$$Co(\underline{\rho}=1,\gamma=\pi/2) = \frac{\underline{Ed} - \underline{R}.\underline{Ed}}{\underline{R}.\underline{Ed}} = 1/\underline{R} - 1 \qquad (4.37)$$

Figure 4.21(a) illustrates the vertically downward sighting of a neutral filter of transmission T. It is apparent that:

$$Co(\underline{\rho}=\underline{T},\gamma=\pi/2) = \frac{\underline{T}.\underline{Eu} - \underline{Eu}}{\underline{Eu}} = \underline{T} - 1 = -(1 - \underline{T}) \qquad (4.38)$$

The negative sign in Eqn.4.38, and several subsequent equations, indicates that the target is darker than its background. The 'maximum' contrast of a dark target against a light background, no matter how bright, is -1 (for $\underline{T}=0$, or $\underline{\rho}=0$); in theory there is no limit to the (positive) contrast of a bright target against a dark background.

It is apparent, without illustration, that a perfect zero-reflector, eg a light-trap (see Chapter 3), has zero reflectivity ($\underline{\rho}=0$), then:

$$Co(\underline{\rho}=0,\gamma=\pi/2) = \frac{0 - \underline{Eu}}{\underline{Eu}} = -1 \qquad (4.39)$$

The inherent contrast of a target, of reflectivity $\underline{\rho}$, sighted horizontally ($\gamma=0$), was illustrated in Fig.2.12, and expressed by Eqn.2.78 as: $Co(\underline{\rho}=\underline{\rho},\gamma=0) = -(1 - \underline{\rho})$. However, it was pointed out in Chapter 2 that Eqn.2.78 implies that the inherent contrast of a horizontally-sighted target decreases with reflectivity; that a white target, for example, would be less visible than a grey one. The problem was recognised as being that of target illumination by high intensity downwelling light rather than lower intensity side light. Suppose, as illustrated in Fig.4.19(b), that some fraction, $\underline{f}>\underline{R}$, of the downwelling irradiance is scattered onto the target surface and so becomes available for reflection. The inherent contrast is therefore given by:

$$Co(\underline{\rho}=\underline{\rho},\gamma=0) = \frac{\underline{\rho}.\underline{f}.\underline{Ed} + \underline{\rho}.\underline{L_*} - \underline{L_*}}{\underline{L_*}} = \underline{\rho}.(\underline{f}.\underline{Ed}/\underline{L_*} + 1) - 1 \qquad (4.40)$$

It is to be noted that $\underline{\rho}$ and $\underline{f}$ may be large enough for $\underline{\rho}.\underline{f}.\underline{Ed}>\underline{L_*}$, in which case Eqn.4.40 becomes positive, ie the target appears brighter than its background, which is often the observed case. Unfortunately Eqn.4.40 defies simplification so that horizontal observations of targets of reflectivity $0<\underline{\rho}<1$ are of little practical use.

The horizontal sighting of a corner reflector is illustrated in Fig. 4.20(b), which shows that:

$$Co(\underline{\rho}=1,\gamma=0) = \frac{\underline{L_*} - \underline{L_*}}{\underline{L_*}} = 0 \qquad (4.41)$$

This is **invisibility** - of the type employed by silver-sided fish. In a shoal, such fish signal their presence to neighbours by occasional side-rolls; the silver sides then reflect brighter downwelling

irradiance, $\underline{Ed}$, which contrasts nicely against background $\underline{L_*}$.

The inherent contrast of a neutral filter, sighted horizontally, is illustrated in Fig 4.21(b) which shows that:

$$Co(\underline{T}=\underline{T},\gamma=0) = \frac{\underline{T}.\underline{L_*} - \underline{L_*}}{L_*} = \underline{T} - 1 = -(1 - \underline{T}) \qquad (4.42)$$

Of course, such a target will always appear darker than its background, so $Co(\underline{T},\gamma=0)$ is always negative.

Clearly, the inherent contrast of a horizontally sighted zero-reflector (perfectly black target or light trap) will be:

$$Co(\underline{\rho}=0,\gamma=0) = \frac{0 - \underline{L_*}}{\underline{L_*}} = -1 \qquad (4.43)$$

Figures 4.19(c), 4.20(c) and 4.21(c) illustrate vertically upward sighting ($\gamma=-\pi/2$) of targets. It is apparent that we may write:

$$Co(\underline{\rho}=\underline{\rho},\gamma=-\pi/2) = \frac{\underline{\rho}.\underline{f}.\underline{Ed} - \underline{Ed}}{\underline{Ed}} = \underline{\rho}.\underline{f} - 1 = -(1 - \underline{\rho}.(\underline{f}+\underline{R})) \qquad (4.44)$$

$$Co(\underline{\rho}=1,\gamma=-\pi/2) = \frac{\underline{R}.\underline{Ed} - \underline{Ed}}{\underline{Ed}} = \underline{R} - 1 = -(1 - \underline{R}) \qquad (4.45)$$

$$Co(\underline{T}=\underline{T},\gamma=-\pi/2) \frac{\underline{T}.\underline{Ed} - \underline{Ed}}{\underline{Ed}} = \underline{T} - 1 = -(1 - \underline{T}) \qquad (4.46)$$

$$Co(\underline{\rho}=0,\gamma=-\pi/2) = \frac{0 - \underline{Ed}}{\underline{Ed}} = -1 \qquad (4.47)$$

[illegible]

[illegible]

The use of a light trap as a black target is mentioned in Højerslev (1986) and in Højerslev (1987, personal communication). It is believed that the theory, construction and use underwater of both the corner reflector and neutral filter is original to Pilgrim et al (1988). These three targets possess the particular advantages of being of known reflectivity/transmission, and of being unaffected by side/top lighting. The neutral filter, moreover, may be chosen to have any desired transmision. All of the inherent contrast equations derived in this subsection are summarised in Table 4.3.

Table 4.3: Inherent contrasts of four 'standard' targets with allocated equation numbers; all optical parameters are photometric.

	Sighting angle, γ		
Target	Vertically downwards $\gamma = \pi/2$	Horizontally $\gamma = 0$	Vertically upwards $\gamma = -\pi/2$
painted reflector $\rho = \rho$	$Co(\rho,\pi/2) = \rho/R - 1$ (4.36)	$Co(\rho,0) = \rho.(f.Ed/L^* + 1) - 1$ (4.40)	$Co(\rho,-\pi/2) = -(1 - \rho.(f+R))$ (4.44)
corner reflector $\rho = 1$	$Co(1,\pi/2) = 1/R - 1$ (4.37)	$Co(1,0) =$ 0, invisible (4.41)	$Co(1,-\pi/2) = -(1 - R)$ (4.45)
light-trap $\rho = 0$	$Co(0,\pi/2) = -1$ (4.39)	$Co(0,0) = -1$ (4.43)	$Co(0,-\pi/2) = -1$ (4.47)
neutral filter $T = T$	$Co(T,\pi/2) = -(1 - T)$ (4.38)	$Co(T,0) = -(1 - T)$ (4.42)	$Co(T,-\pi/2) = -(1 - T)$ (4.46)

4.4.1 Estimation of ($\underline{c}$+$\underline{K}$) and $\underline{c}$,$\underline{K}$ from Zs

The sum of the coefficients $\underline{c}$ and $\underline{K}$ is provided by the Secchi disc equation, Eqn.2.94:

$$\underline{c} + \underline{K} = \frac{\mathrm{Ln}[(\rho/\underline{R} - 1)/Ct]}{Zs} = \frac{Fs}{Zs}$$

As discussed in Chapter 2, the value of the coupling constant, Fs, depends in practice upon the choice/estimation of values of ρ, R and Ct. These are given in Table 2.3.

Over 300 Secchi disc depths were observed in the course of this work ($0.35 \leq Zs \leq 31$), in estuarine and coastal waters, and in relatively clear oceanic waters.

It is almost universally recognised among Secchi disc cognoscenti that given a good estimate of Fs, the disc provides an estimate of $\underline{c}$+$\underline{K}$ but not of the separate values $\underline{c}$,$\underline{K}$. Clearly $\underline{c}$,$\underline{K}$ could be deduced from $\underline{c}$+$\underline{K}$ only if the ratio $\underline{K}/\underline{c}$ were a constant for all waters, but this is not the case. However, Højerslev (1986) claims that it is possible to separate $\underline{c}$ and $\underline{K}$, within reasonable errors, from a single Secchi depth. The same argument is reproduced by Preisendorfer (1986).

Højerslev uses $\rho = 0.8$ and $Ct = 0.0066$, which, substituted into Eqn.2.94, gives:

$$(\underline{c} + \underline{K}).Zs = 4.80 - \mathrm{Ln}[\underline{R}] \qquad (4.48)$$

whence:

$$\underline{c}.Zs = \frac{4.80 - Ln[\underline{R}]}{1 + \underline{K}/\underline{c}} \qquad (4.49)$$

Højerslev then uses the optical model of Timofeeva (1974) which gives $\underline{R}$ and $\underline{K}/\underline{c}$ in terms of photon survival probability $\underline{b}/\underline{c}$, (cols.1-3 in Table 4.4), and calculates, from Eqn.4.56, the equivalent value of $\underline{c}.Zs$ (col.4 in Table).

Table 4.4: Secchi disc parameters as a function of photon survival probability, $\underline{b}/\underline{c}$, from Timofeeva (1974) [cols.1-3], Højerslev (1978) [col.4], and a calculation presented here [col.5 = col.2 x col.4].

(1)	(2)		(3)	(4)	(5)
$\underline{b}/\underline{c}$	$\underline{K}/\underline{c}$	$\underline{c}/\underline{K}$	$\underline{R}$	$\underline{c}.Zs$	$\underline{K}.Zs$
0.1	0.93	1.08	0.0014	5.89	5.48
0.2	0.85	1.18	0.0021	5.93	5.04
0.3	0.77	1.30	0.0032	5.96	4.59
0.4	0.68	1.47	0.0050	6.01	4.09
0.5	0.60	1.67	0.0075	6.06	3.64
0.6	0.50	2.00	0.0123	6.13	3.07
0.7	0.40	2.50	0.0203	6.21	2.48
0.8	0.30	3.33	0.0334	6.31	1.89
0.9	0.19	5.26	0.0508	6.43	1.22

He then takes the average value of $\underline{c}.Zs$ from col.4, and writes:

$$\underline{c}.Zs = 6.10 \qquad (4.50)$$

Observations of $\underline{c}$ and Zs obtained in this study produced a similar estimate: $\underline{c}.Zs = 4.75$ (Eqn.4.95).

Substituting Eqn.4.50 into Eqn.4.49 gives:

$$\underline{K}.Zs = -1.3 - Ln[\underline{R}] \qquad (4.51)$$

At this point, Højerslev argues that since, from Timofeeva (1974), $\underline{R} = 0.15 \exp[-5\underline{K}/\underline{c}]$, then:

$$\underline{K}.Zs = 3.3 \qquad (4.52)$$

In effect this must mean that Table 4.4 was again used to extract an 'average' value of $\underline{K}/\underline{c} = 0.54$, appropriate to $\underline{c}.Zs = 6.10$. In a similar argument, (Højerslev, personal communication, 1986), he says that as '$\underline{R} = 0.01$ is a very likely value for most oceanic waters', then substituting this mean approximation into Eqn.4.51 produces Eqn.4.52.

It is considered that this method of separating $\underline{c}$,$\underline{K}$ is unsatisfactory for three main reasons:

(i) As stated earlier, solution for two unknowns requires two equations unless the two unknowns bear a constant relationship.

(ii) Division of Eqn.4.52 by Eqn.4.50 gives $\underline{K}.Zs/\underline{c}.Zs = \underline{K}/\underline{c} = 3.3/6.10 = 0.54$ always, no matter what the Secchi depth. This ratio was also assumed in converting Eqn.4.51 into Eqn.4.52. However, it is widely recorded (eg Tyler, 1968), that $\underline{K}/\underline{c}$ decreases with turbidity, as is quite clear from Table 4.4, the basis of Højerslev's argument. Topliss (1982) has found $\underline{K}/\underline{c}$ values as low as 0.1 in Liverpool Bay, and similar values will be indicated by observations made during this study and presented later in this chapter. Indeed, if $\underline{K}/\underline{c} = \text{const}$ is to be a tenet of this proof, then

Eqns.4.50 and 4.52 could be derived directly from the Secchi disc equation (Eqn.2.94), without the tortuous journey through Timofeeva's photon survival probability model.

(iii) In Table 4.4, the range in $\underline{c}$.Zs is small ($5.48 \leq \underline{c}.Zs \leq 6.43$), so that it may seem not unreasonable to extract the mean value: $\underline{c}.Zs = 6.10$. However, associated with this range is a comparatively larger $\underline{K}/\underline{c}$ range ($0.93 \geq \underline{K}/\underline{c} \geq 0.19$). If we now add to Højerslev's table with col.5 = col.2 x col.4, then we deduce that $1.22 \leq \underline{K}.Zs \leq 5.48$ which is not reasonably approximated by the proposed universal $\underline{K}.Zs = 3.3$ of Eqn.4.52.

It is stressed that no case is being made against Eqns.4.50 and 4.52 as general approximations for, say, most oceanic waters; the objection is to Højerslev's claim that it is possible to solve for the two unknowns, $\underline{c}$ and $\underline{K}$, from a single observation. It is surely apparent that two Secchi-type equations are required. It will be demonstrated in the next two subsections that this may be achieved by combining both downward and upward, or downward and horizontal observations.

4.4.2 Estimation of $\underline{c}$,$\underline{K}$ from Duntley disc distances

In the previous subsection it was argued that separation of ($\underline{c}$+$\underline{K}$) into $\underline{c}$,$\underline{K}$ could be achieved only by obtaining <u>two</u> different observations in the same water.

We have, from Eqns.2.98, 2.99 and 2.100 (Preisendorfer, 1976):

$$(\underline{c} + \underline{K}) = \frac{1}{d_1}.\mathrm{Ln}\left[\frac{Co(w)}{Co(g)}\right] = \frac{\mathrm{Ln}[\rho(w)/\rho(g)]}{d_1} \qquad (4.53)$$

$$(\underline{c} - \underline{K}) = \frac{1}{d_2}.\mathrm{Ln}\left[\frac{Co(w)}{Co(g)}\right] = \frac{\mathrm{Ln}[\rho(w)/\rho(g)]}{d_2} \qquad (4.54)$$

where d_1 and d_2 are the separation, upwards and downwards, of a pair of white (w) and grey (g) Duntley discs. So, Eqns.2.101 and 2.102:

$$\underline{c} = \frac{\mathrm{Ln}[\rho(w)/\rho(g)]}{2} \cdot \left[\frac{1}{d_1} + \frac{1}{d_2}\right] \qquad (4.55)$$

$$\underline{K} = \frac{\mathrm{Ln}[\rho(w)/\rho(g)]}{2} \cdot \left[\frac{1}{d_1} - \frac{1}{d_2}\right] \qquad (4.56)$$

So, these last two equations apparently satisfy the requirement, and are the basis of the method proposed by Duntley, and described by Preisendorfer (1976). Now Eqn.4.53 is based upon the same reasoning as the Secchi disc equation so must be correct, but from Eqns.4.53 and 4.54, because ($\underline{c}$+$\underline{K}$)>($\underline{c}$-$\underline{K}$), then $1/d_1 > 1/d_2$, ie $d_2 > d_1$. Also, from Eqn.4.56, to keep $\underline{K}$ positive, then $d_2 > d_1$. However, observations in Plymouth Sound and Malaysian waters, (Pilgrim <u>et al</u>, 1988), have shown that $d_1 > d_2$ always. Equation 4.54 is clearly suspect, and the question now is: is it viable to follow Preisendorfer's argument

and '..simply appeal to Eqn.2.83 with $\gamma=-\pi/2$..' and thereby transform Eqn.2.99 into Eqn.2.100? The pair of discs are not only turned upside-down; the white disc is placed nearer to the observer. Preisendorfer's reasoning produces the apparent contrasts:

$$Cr(w,r) = (\underline{\rho}(w)/\underline{R} - 1).\exp[-(\underline{c}-\underline{K}).r]$$

and

$$Cr(g,r+d_2) = (\underline{\rho}(g)/\underline{R} - 1).\exp[-(\underline{c}-\underline{K}).(r+d_2)]$$

Equating at luminance matching:

$$(\underline{\rho}(w)/\underline{R} - 1).\exp[-(\underline{c}-\underline{K}).r] = (\underline{\rho}(g)/\underline{R} - 1).\exp[-(\underline{c}-\underline{K}).(r+d_2)]$$

which reduces to:

$$(\underline{c} - \underline{K}) = \frac{1}{d_2}.\mathrm{Ln}\left[\frac{Co(g)}{Co(w)}\right] = \frac{\mathrm{Ln}[\underline{\rho}(g)/\underline{\rho}(w)]}{d_2} \qquad (4.57)$$

which is <u>not</u> the same as the result given in Eqn.4.54, from Preisendorfer (1976). Moreover, Eqn.4.57 implies that $\underline{K}>\underline{c}$ so is entirely wrong, unless the grey disc should be nearer to the observer than the white disc (to make d_2 effectively negative). This cannot be. Both discs must appear darker than the bright sea-surface background; the grey disc must therefore be further away from the observer to reduce the greater contrast. Observations in Plymouth Sound have confirmed that this is always so. By 'inverting' Eqn.4.53 to derive Eqn.4.54, it is implied that when observing the discs from below, then the background brightness is comprised of $\underline{R}.\underline{Eu}$ (analagous to $\underline{R}.\underline{Ed}$ in Eqn.2.77 when looking down), ie just a percent or so of the

upwelling irradiance. This is illustrated in Fig.4.22(a), but cannot represent the true case; the overwhelming component of the background brightness seen when looking upwards is the very bright downwelling irradiance, Ed. This was recognised in the model proposed in Fig.4.19(c), and reproduced in Fig.4.22(c).

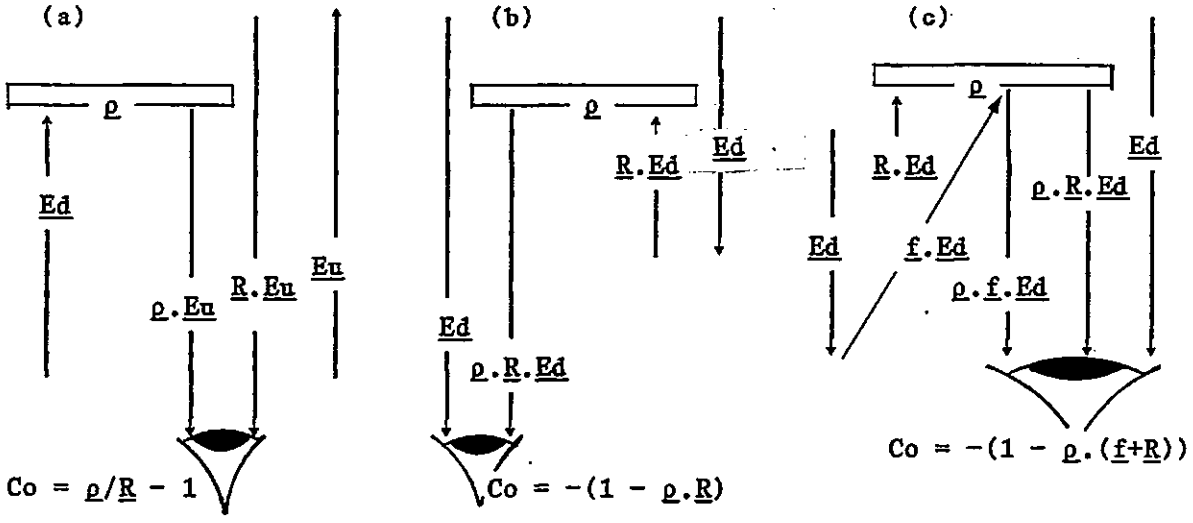

Fig.4.22: Inherent contrast of Duntley disc sighted vertically upwards,
(a) as implied by Preisendorfer (1976), and comparable to Fig.2.11
(b) improved but unrealistic model which takes no account of side-lighting.
(c) proposed here as a realistic model

This model also takes account of the side-lighting which must arise, and it is interesting to note that if this allowance were not made then the situation would be as depicted in Fig.4.22(b). The inherent contrast would then be given by:

$$Co(\underline{\rho},0) = \frac{\underline{\rho}.\underline{R}.\underline{Ed} - \underline{Ed}}{\underline{Ed}} = \underline{\rho}.\underline{R} - 1 = -(1 - \underline{\rho}.\underline{R}) \qquad (4.58)$$

Substitution of Eqn.4.58 for $\rho(g)$ and $\rho(w)$ in Eqn.4.51 gives:

$$(\underline{c} - \underline{K}) = \frac{1}{d_2} .\mathrm{Ln}\left[\frac{Co(g)}{Co(w)}\right] = \frac{\mathrm{Ln}[(1 - \underline{\rho}(g).\underline{R})/(1 - \underline{\rho}(w).\underline{R})]}{d_2} \qquad (4.59)$$

Equation 4.59 is a great improvement on Eqn.4.57 in that it gives $\underline{c} > \underline{K}$, however, as $\underline{\rho}.\underline{R} << 1$ then it implies that $Co(\underline{\rho},0) \rightarrow 1$, ie that a white target, for example, would self-shade and appear almost black. Observations in Plymouth Sound have shown that this is not the case; the disc is illuminated by side-light (see Fig.4.19(c)), and appears dull but not black. We are therefore justified in using derived equation Eqn.4.44:

$$Co(\underline{\rho},-\pi/2) = -(1 - \underline{\rho}.(\underline{f}+\underline{R}))$$

where $\underline{f}$ ($>\underline{R}$) is the fraction of the downwelling irradiance which is back-scattered onto the underside of the target. So, Eqn.4.59 becomes viable in the form:

$$(\underline{c} - \underline{K}) = \frac{1}{d_2} .\mathrm{Ln}\left[\frac{Co(g)}{Co(w)}\right] = \frac{\mathrm{Ln}[(1 - \underline{\rho}(g).(\underline{f}+\underline{R}))/(1 - \underline{\rho}(w).(\underline{f}+\underline{R}))]}{d_2} \qquad (4.60)$$

Adding and subtracting Eqns.4.53 and 4.60:

$$\underline{c} = \frac{1}{2}\left[\frac{\mathrm{Ln}[\underline{\rho}(w)/\underline{\rho}(g)]}{d_1} + \frac{\mathrm{Ln}[(1 - \underline{\rho}(g)(\underline{f}+\underline{R}))/(1 - \underline{\rho}(w)(\underline{f}+\underline{R})]}{d_2}\right] \qquad (4.61)$$

$$\underline{K} = \frac{1}{2}\left[\frac{\mathrm{Ln}[\underline{\rho}(w)/\underline{\rho}(g)]}{d_1} - \frac{\mathrm{Ln}[(1 - \underline{\rho}(g)(\underline{f}+\underline{R}))/(1 - \underline{\rho}(w)(\underline{f}+\underline{R})]}{d_2}\right] \qquad (4.62)$$

These new equations, easily solved by microcomputer, are therefore proposed as solutions to Duntley disc observations. Unfortunately, this means of finding $\underline{c},\underline{K}$, which for convenience will be called

c,K method I, suffers from two serious practical difficulties.

Firstly, reliable observations of d_1 and d_2 are not easily obtained. Experience of measuring d_1 and d_2 over a period of two years has shown that it is extremely difficult for a diver to decide the exact point of luminance matching, as this type of assessment is too subjective. Judging a threshold distance is more objective ('see' or 'not see'), and hence comparatively simple, and it will now be shown that the Duntley distances, d_1 and d_2, can be derived from the threshold ranges Zw, Zg, Uw and Ug of the white and grey discs:

$$Ct = Co(w).\exp[-(\underline{c}+\underline{K}).Zw)] = C(g).\exp[-(\underline{c}+\underline{K}).Zg] \qquad (4.63)$$

therefore:

$$Co(g)/Co(w) = \exp[-(\underline{c}+\underline{K}).(Zw-Zg)] \qquad (4.64)$$

but at luminance matching, from Eqn.2.97: $Cr(w,z_1+d_1) = Cr(g,z_1)$, in which case, for $z_1=0$:

$$Cr(w,d_1) = Cr(g,0) = Co(g) \qquad (4.65)$$

ie, <u>at luminance matching the apparent contrast of the white disc is, simply, the inherent contrast of the grey one</u>, and so we may write:

$$Co(g)/Co(w) = Cr(w,d_1)/Co(w) = \exp[-(\underline{c}+\underline{K}).d_1] \qquad (4.66)$$

Equating 4.64 and 4.66, and by a similar argument for upward sighting:

$$d_1 = Zw - Zg;\ d_2 = Ug - Uw \qquad (4.67)$$

The second problem with $\underline{c},\underline{K}$ method I, and hence Eqns.4.68 and 4.69, is that the significant value of $\underline{f}$ must depend upon the volume scattering function $\underline{\beta}(\sigma)$, and so constitutes yet another variable with which one must contend; nor is it readily assessed by observation. Also, one must know the more easily measured reflectivities: $\underline{\rho}(w)$ and $\underline{\rho}(g)$.

The solution to these problems is to be found in the use of a corner reflector and light trap, both of these targets being of known reflectivity and unaffected by side-lighting. Using the values of inherent contrast given in Table 4.3, Eqns.4.53 and 4.59 become:

$$\underline{c} + \underline{K} = \frac{1}{d_1}.\mathrm{Ln}\left[\left|\frac{Co(1,\pi/2)}{Co(0,\pi/2)}\right|\right] = \frac{\mathrm{Ln}[1/\underline{R} - 1]}{Zx - Zh} \tag{4.68}$$

$$\underline{c} - \underline{K} = \frac{1}{d_2}.\mathrm{Ln}\left[\frac{Co(0,-\pi/2)}{Co(1,-\pi/2)}\right] = \frac{\mathrm{Ln}[1/(1-\underline{R})]}{Uh - Ux} \tag{4.69}$$

and so:

$$\underline{c} = \frac{1}{2}\left[\frac{\mathrm{Ln}[1/\underline{R} - 1]}{Zx - Zh} + \frac{\mathrm{Ln}[1/(1-\underline{R})]}{Uh - Ux}\right] \tag{4.70}$$

$$\underline{K} = \frac{1}{2}\left[\frac{\mathrm{Ln}[1/\underline{R} - 1]}{Zx - Zh} - \frac{\mathrm{Ln}[1/(1-\underline{R})]}{Uh - Ux}\right] \tag{4.71}$$

These novel equations represent proposed c,K method II and are rather elegant in that they require only one assumption: the value of $\underline{R}$. The major disadvantage of method II is apparent from Eqn.4.69: because $d_2 \propto 1/(\underline{c}-\underline{K})$, then in clear water where $\underline{c},\underline{K}$ and hence $\underline{c}-\underline{K}$ are small, Uh may become greater than the observer's safe or convenient

maximum diving depth. This has not been a problem in turbid Plymouth waters.

It is suggested that this diving-depth problem may be overcome in clear water by using two neutral filters (see Chapter 3), unaffected by side-lighting, for the upward observations. The inherent contrast of such filters is given, in Table 4.3, as $-(1-\underline{T})$ in which case Eqn.4.70 becomes:

$$\underline{c} - \underline{K} = \frac{1}{d_2} \text{Ln}\left[\frac{Co(f_2)}{Co(f_1)}\right] = \frac{\text{Ln}[(1-\underline{T}_2)/(1-\underline{T}_1)]}{Uf_2 - Uf_1} \qquad (4.72)$$

where $\underline{T}_1 > \underline{T}_2$. Adding and subtracting Eqns.4.68 and 4.72:

$$\underline{c} = \frac{1}{2}\left[\frac{\text{Ln}[1/\underline{R} - 1]}{Zx - Zh} + \frac{\text{Ln}[(1-\underline{T}_2)/(1-\underline{T}_1)]}{Uf_2 - Uf_1}\right] \qquad (4.73)$$

$$\underline{K} = \frac{1}{2}\left[\frac{\text{Ln}[1/\underline{R} - 1]}{Zx - Zh} - \frac{\text{Ln}[(1-\underline{T}_2)/(1-\underline{T}_1)]}{Uf_2 - Uf_1}\right] \qquad (4.74)$$

This is proposed c,K method III, cumbersome in that it uses four different targets but probably the most practical for use in clear water. As deep clear water tends to look dark when sighted vertically downwards (low $\underline{R}$), then the obvious simplification - using neutral filters both upwards and downwards - may not be practicable. If it is viable, then the equations for c,K method IV are :

$$\underline{c} = \frac{1}{2}\left[\frac{\text{Ln}[(1-\underline{T}_1)/(1-\underline{T}_2)]}{Zf_1 - Zf_2} + \frac{\text{Ln}[(1-\underline{T}_2)/(1-\underline{T}_1)]}{Uf_2 - Uf_1}\right] \qquad (4.75)$$

$$\underline{K} = \frac{1}{2}\left[\frac{\text{Ln}[(1-\underline{T}_1)/(1-\underline{T}_2)]}{Zf_1 - Zf_2} - \frac{\text{Ln}[(1-\underline{T}_2)/(1-\underline{T}_1)]}{Uf_2 - Uf_1}\right] \qquad (4.76)$$

4.4.3 Estimation of $\underline{c}/\underline{K}$, and $\underline{c},\underline{K}$ from diver observations of U,V,Z

Further methods of estimating c,K and c/K from diver observations of U,V and Z will now be explored. For convenience, expressions for threshold visibilities are summarised in Table 4.5; they are derived from the inherent contrasts of Table 4.3 and the threshold visibility equation, Eqn.2.87.

Table 4.5: Threshold visibilities of four 'standard' targets with allocated equation numbers; all optical parameters are photometric

	Sighting angle, γ		
Target	Vertically downwards $\gamma = \pi/2$	Horizontally $\gamma = 0$	Vertically upwards $\gamma = -\pi/2$
painted reflector $\rho = \rho$	$Z\rho = Zs = \frac{Ln[(\rho/R - 1)/Ct]}{c + K}$ (4.77)	$V\rho = \frac{Ln\left[\frac{\rho(f.Ed/L_* + 1) - 1}{Ct}\right]}{c}$ (4.78)	$U\rho = \frac{Ln[(1-\rho.(f+R))/Ct]}{c - K}$ (4.79)
corner reflector $\rho = 1$	$Zx = \frac{Ln[(1/R - 1)/Ct]}{c + K}$ (4.80)	Vx: invisibility	$Ux = \frac{Ln[(1 - R)/Ct]}{c - K}$ (4.81)
light trap $\rho = 0$	$Zh = \frac{Ln[1/Ct]}{c + K}$ (4.82)	$Vh = \frac{Ln[1/Ct]}{c}$ (4.83)	$Uh = \frac{Ln[1/Ct]}{c - K}$ (4.84)
neutral filter $T = T$	$Zf = \frac{Ln[(1-T)/Ct]}{c + K}$ (4.85)	$Vf = \frac{Ln[(1-T)/Ct]}{c}$ (4.86)	$Uf = \frac{Ln[(1-T)/Ct]}{c - K}$ (4.87)

The estimation of $\underline{c}$,$\underline{K}$ from diver observation of a pair of Duntley discs was considered, in some detail, in the previous subsection, and $\underline{c}$,$\underline{K}$ methods I to IV were proposed. As these methods produce separate estimates of $\underline{c}$ and $\underline{K}$, then $\underline{c}/\underline{K}$, effectively a measure of scattering, can also be calculated.

Better estimates of $\underline{c}/\underline{K}$ and $\underline{c}$,$\underline{K}$ may be obtained from the two simple light trap observations Vh and Zh. From Eqns.4.82 and 4.83:

$\text{Ln}[1/\text{Ct}] = (\underline{c}+\underline{K}).\text{Zh} = \underline{c}.\text{Vh}$, whence:

$$\underline{c}/\underline{K} = \frac{\text{Zh}}{\text{Vh} - \text{Zh}} \qquad (4.88)$$

an equation <u>quite independent of ρ, R or Ct</u>. From Eqn.4.83, and by combining Eqns.4.83 and 4.88:

$$\underline{c} = \frac{\text{Ln}[\text{Ct}]}{\text{Vh}} = \frac{3.9}{\text{Vh}} \qquad (4.83)$$

$$\underline{K} = (\underline{c}/\underline{K})^{-1}.\underline{c} = \frac{\text{Vh} - \text{Zh}}{\text{Zh}}.\frac{\text{Ln}[\text{Ct}]}{\text{Vh}} = 3.9\left[\frac{1}{\text{Zh}} - \frac{1}{\text{Vh}}\right] \qquad (4.89)$$

The comparative ease of these two novel measurements - horizontal and vertically downwards observations of a light trap - and the elegant simplicity of Eqns.4.88, 4.83 and 4.89 compare favourably with the difficulties associated with Duntley disc type observations and their analyses. This is $\underline{c}$,$\underline{K}$ method V and is <u>strongly recommended for routine diver observations</u>.

Similarly, from observations of a light trap vertically downwards and

vertically upwards, from Table 4.5:

Eqn.4.82: $\underline{c}+\underline{K} = \frac{\mathrm{Ln}[1/Ct]}{Zh}$

Eqn.4.84: $\underline{c}-\underline{K} = \frac{\mathrm{Ln}[1/Ct]}{Uh}$

whence, by addition and subtraction:

$$\underline{c} = (\mathrm{Ln}[Ct]/2).\left[\frac{1}{Zh} + \frac{1}{Uh}\right] = 1.95\left[\frac{1}{Zh} + \frac{1}{Uh}\right] \qquad (4.90)$$

$$\underline{K} = (\mathrm{Ln}[Ct]/2).\left[\frac{1}{Zh} - \frac{1}{Uh}\right] = 1.95\left[\frac{1}{Zh} - \frac{1}{Uh}\right] \qquad (4.91)$$

from which, again independent of $\underline{\rho}$, $\underline{R}$ or even Ct:

$$\underline{c}/\underline{K} = \frac{Uh + Zh}{Uh - Zh} \qquad (4.92)$$

This is $\underline{c},\underline{K}$ method VI which may suffer the same disadvantage as discussed for $\underline{c},\underline{K}$ method II: in clear water the diver may need to go uncomfortably deep for threshold observation Uh.

Some results of diver observations of Vh, Zh, Uh, Vb, Zb, Ub, Zx, Ux and Zs, analysed by methods II, V and VI, are now presented. It is convenient to combine the very similar Vh, Zh, Uh and Vb, Zb, Ub. However, although a matt-black surface should, in theory, have a reflectivity of zero, this is rarely the case; moreover, it has been noted in the course of these experiments that a vertical matt-black surface receives and reflects a significant amount of the intense downwelling irradiance (see Fig.4.19(b)). This is also true of the

black neoprene wetsuit of a diver (see, for example, Eqn.2.93). Observations in Plymouth Sound have indicated that the hydrological range, Vh, is about 15% greater than the threshold range of a black target, Vb, ie:

$$1.15\ Vb = Vb' = Vh \qquad (4.93)$$

From Eqn.2.94, Secchi depth, Zs = f($\underline{c}$+$\underline{K}$) and so, as $\underline{c}$>$\underline{K}$ (see eg Table 4.4), then Zs is controlled more by $\underline{c}$ than by $\underline{K}$. Figure 4.23 compares values of $\underline{c}$, calculated by methods V, VI and II, with concurrent observations of Zs^{-1}. Figure 4.24 compares similar values of $\underline{K}$ with Zs^{-1}. It is apparent that:

(i) values of $\underline{c}$ and $\underline{K}$ calculated by methods V and VI (O and Δ) compare closely with each other, particularly in the case of $\underline{c}$

(ii) values of $\underline{c}$ and $\underline{K}$ calculated by method II (●) do not compare closely with those found by methods V and VI

(iii) as expected, there is a better correlation between $\underline{c}$ and Zs^{-1} than between $\underline{K}$ and Zs^{-1} and so, from method V only:

$$\underline{c} = 4.711\ Zs^{-1} + 0.109 \quad (1.95 \leq Zs \leq 19.0,\ r^2=0.925,\ n=66) \qquad (4.94)$$

$$\text{and through 0,0:} \quad \underline{c}.Zs = 4.75 \qquad (4.95)$$

$$\underline{K} = 0.634\ Zs^{-1} + 0.192 \quad (r^2=0.269,\ n=33) \qquad (4.96)$$

$$\text{and through 0,0:} \quad \underline{K}.Zs = 1.39 \qquad (4.97)$$

This analysis supports the earlier recommendation that method V is to be preferred for routine diver observation.

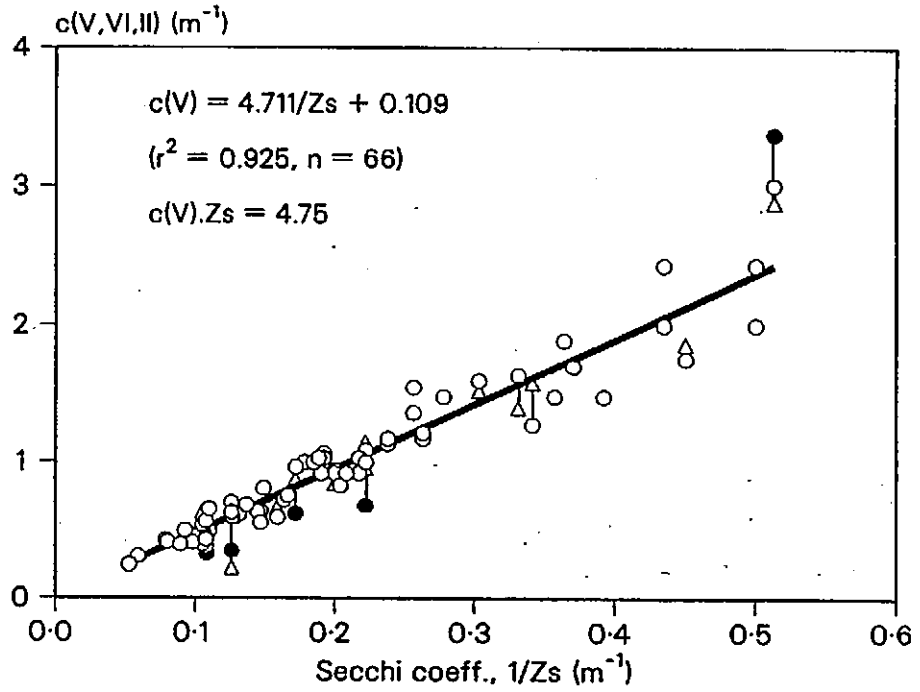

Fig.4.23: Relationship between the Secchi coefficient, Zs^{-1} and the photopic beam attenuation coefficient, c, found by method V (O) in Plymouth Sound, Burrator Reservoir and Malaysian waters, and by methods VI (Δ) and II (●) in Plymouth Sound and Burrator Reservoir, (Pilgrim et al, 1988)

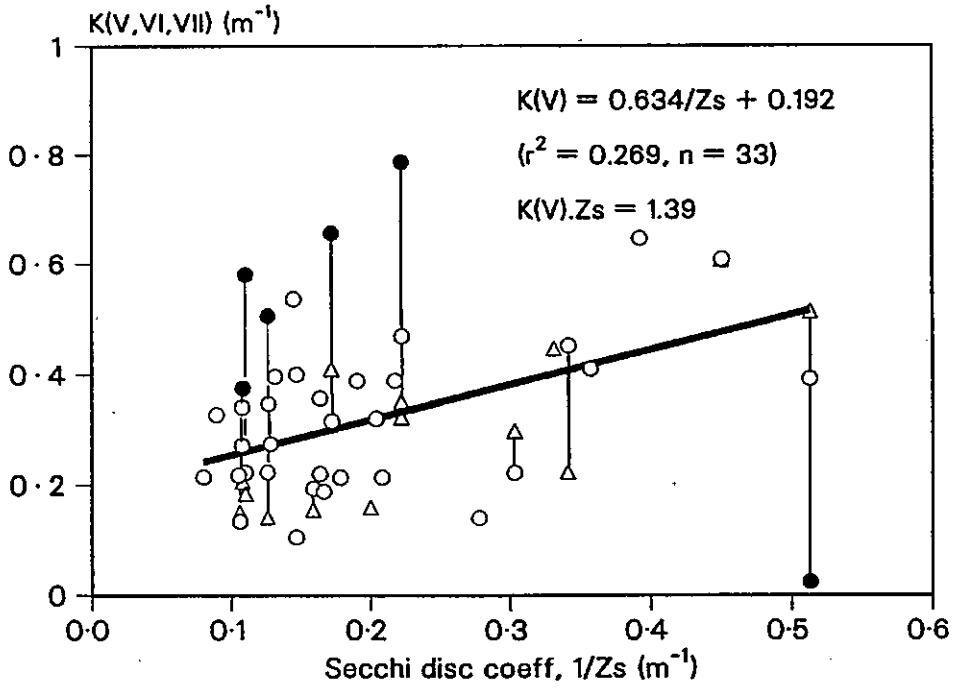

Fig.4.24: Relationship between the Secchi coefficient, Zs^{-1} and the photopic diffuse attenuation coefficient, K, found by method V (O) in Plymouth Sound, Burrator Reservoir and Malaysian waters, and by methods VI (Δ) and II (●) in Plymouth Sound and Burrator Reservoir

We have the Secchi disc equation, Eqn.2.94: $\underline{c}+\underline{K} = \underline{Fs}/Zs$, where $\underline{Fs}$ is a function of disc reflectivity, $\underline{\rho}$, threshold contrast, Ct, and water reflectivity, $\underline{R}$. Figure 4.25 presents values of $\underline{c}+\underline{K}$ calculated by method V from 34 diver observations of Vh and Zh, regressed against concurrent observations of Zs^{-1}.

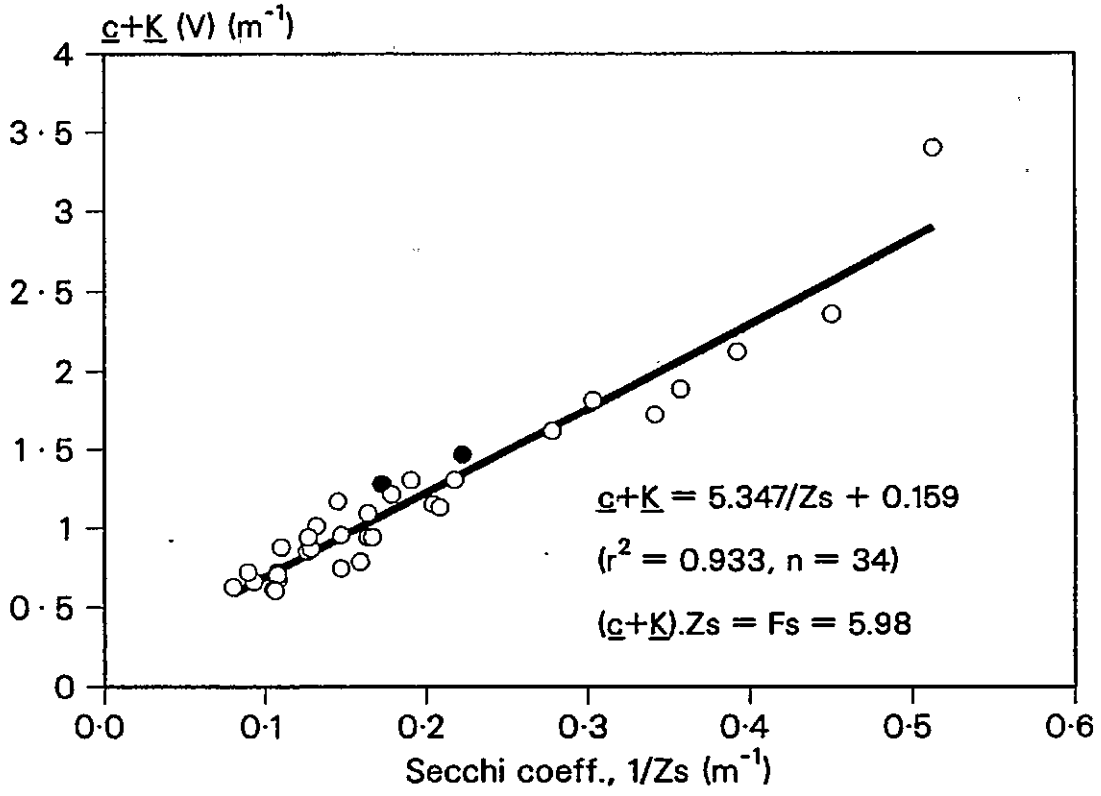

Fig.4.25: Relationship between values of $\underline{c}+\underline{K}$ and Zs^{-1} in Plymouth Sound (0) and Burrator Reservoir (●), calculated by method V

These data produce the regression:

$$\underline{c}+\underline{K} = 5.347\ Zs^{-1} + 0.159 \quad (1.95 \leq Zs \leq 12.5,\ r^2=0.933,\ n=34) \qquad (4.98)$$

and through 0,0: $\underline{c}+\underline{K} = 5.98\ Zs^{-1}$, ie $\underline{Fs} \simeq 6$ (4.99)

Values of $\underline{Fs} = f(\underline{\rho},Ct,\underline{R})$ are presented in Table 2.3, and it can be seen that $\underline{Fs} = 6$ corresponds to, say: $\underline{\rho}$ = 80%, Ct = 2% and $\underline{R}$ = 9%.

However, $\underline{R}$ = 9% must be seen only as an average condition of the waters observed. Indeed, a major problem in using a Secchi disc is that whilst $\underline{\rho}$ and Ct are essentially constant for a given disc and observer, water reflectance varies with turbidity – the parameter being measured. This is illustrated in Fig. 4.26 in which reflectances, Rp, observed by a diver with a hand-held photometer, (see Chapter 3), in Plymouth Sound and Burrator Reservoir (Dartmoor) are compared with concurrent observations of the Secchi depth. Burrator Reservoir is a shallow and dark-bottomed lake; consequently, its reflectance is anomalously low.

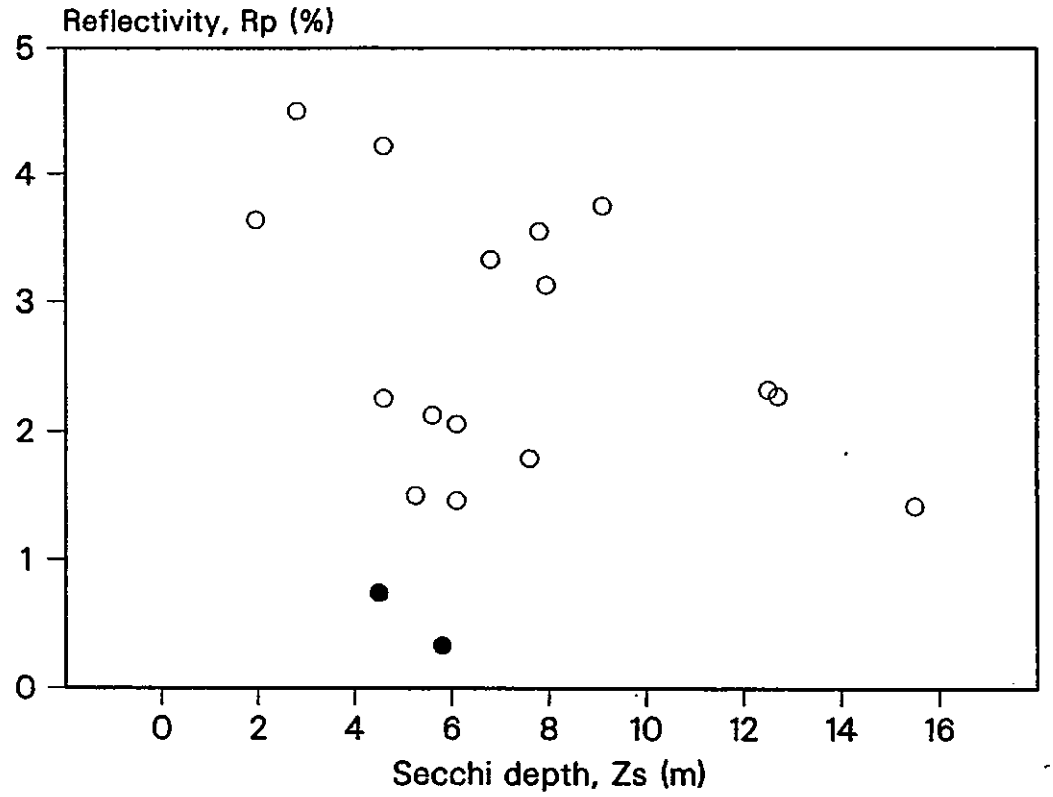

Fig 4.26: Illustration of the general trend for water reflectivity to decrease with increasing Secchi depth. Measurements of Rp were obtained by a diver with a hand-held photometer in Plymouth Sound (O), and the comparatively shallow waters of dark-bottomed Burrator Reservoir, Dartmoor (●).

Figure 4.26 well illustrates the important general trend for water reflectance to increase with decreasing Secchi depth (increasing turbidity), but it would be neither appropriate nor useful to fit a curve to these particular data. We now see that a Secchi Disc Equation should, properly, incorporate the varying nature of $\underline{R}$, and hence $\underline{Fs}$, with Zs. We have from Eqn.2.94:

$$Zs = \underline{Fs}.(\underline{c}+\underline{K})^{-1}$$

but assuming that $\underline{Fs} = f(Zs)$, then this would be improved as:

$$Zs = \underline{Fs}_1.(\underline{c}+\underline{K})^{-\underline{Fs}_2}$$

$$\text{ie } Ln[Zs] = Ln[\underline{Fs}_1] - \underline{Fs}_2.Ln[\underline{c}+\underline{K}] \qquad (4.100)$$

Using the data presented in Fig.4.25, and Eqns.4.98 and 4.99:

$$\underline{c}+\underline{K} = 4.8\ Zs^{-0.84};\quad Zs = 6.4\ (\underline{c}+\underline{K})^{-1.1}\ (1.95 \leq Zs \leq 12.5,\ r^2=0.916,\ n=34) \qquad (4.101)$$

Equation 4.101 is therefore presented as an 'improved' Secchi Disc Equation which properly incorporates the variation in water reflectance with turbidity.

As is apparent from Table 4.4 (Timofeeva's model), increased photon scattering ($\underline{b}/\underline{c}$), and consequent decreased Secchi depth, Zs, also gives rise to an increase in the ratio $\underline{c}/\underline{K}$. Method V was used to obtain estimates of $\underline{c}/\underline{K}$ from diver observations of Vh and Vz; these are compared to concurrent observations of Zs^{-1} in Fig.4.27.

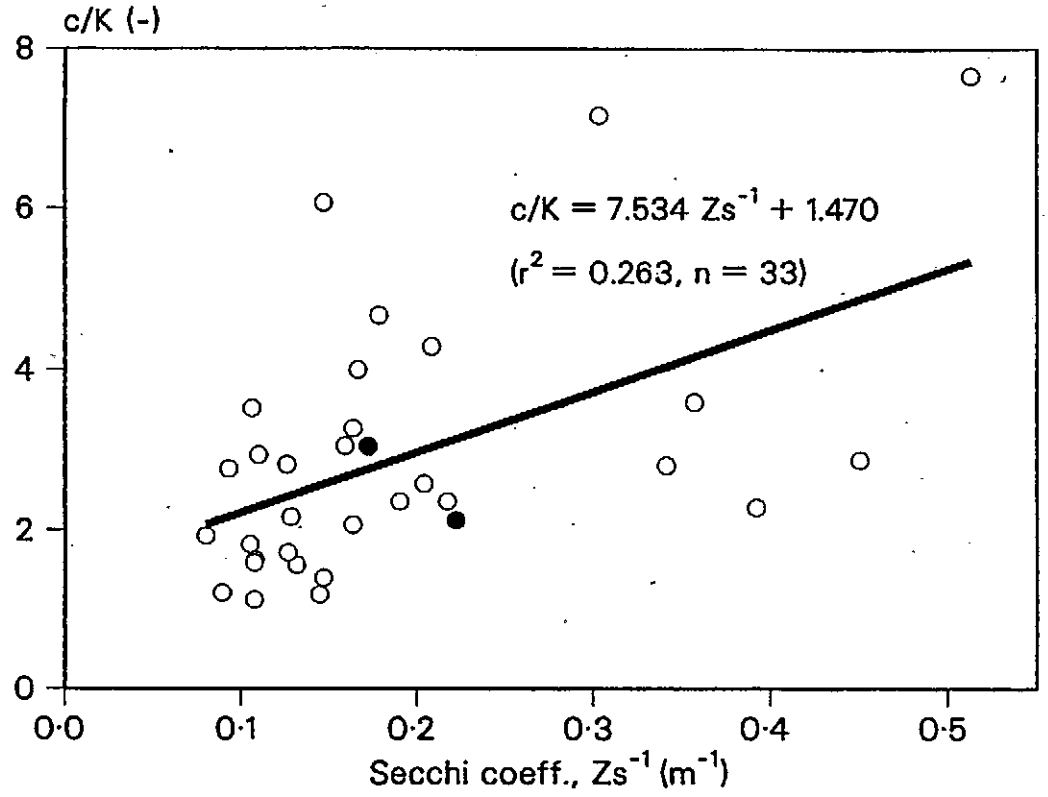

Fig.4.27: Observed relationship between Secchi coefficient, Zs^{-1} and c/K from diver observations in Plymouth Sound (O) and Burrator Reservoir (●), by method V. Both c/K and Zs^{-1} are expected to increase with increased scattering

4.4.4 Estimation of Vh from Zs

In optical work, it is frequently useful to be able to estimate horizontal visibility from an on-board observation, (eg in the assessment of net visibility in an *in situ* study of 'ghost-net' fishing; Pilgrim *et al*, 1985). Fifty-eight concurrent observations of horizontal visibility and Secchi depth have been obtained by divers in the waters of Plymouth Sound, SE Malaysia and Singapore (Pilgrim *et al*, 1988), and are presented in Fig.4.28. Some of these visibilities were the hydrological range, Vh, of a light trap; some

were the threshold visibilities of a matt-black disc, Vb, adjusted by Eqn.4.93.

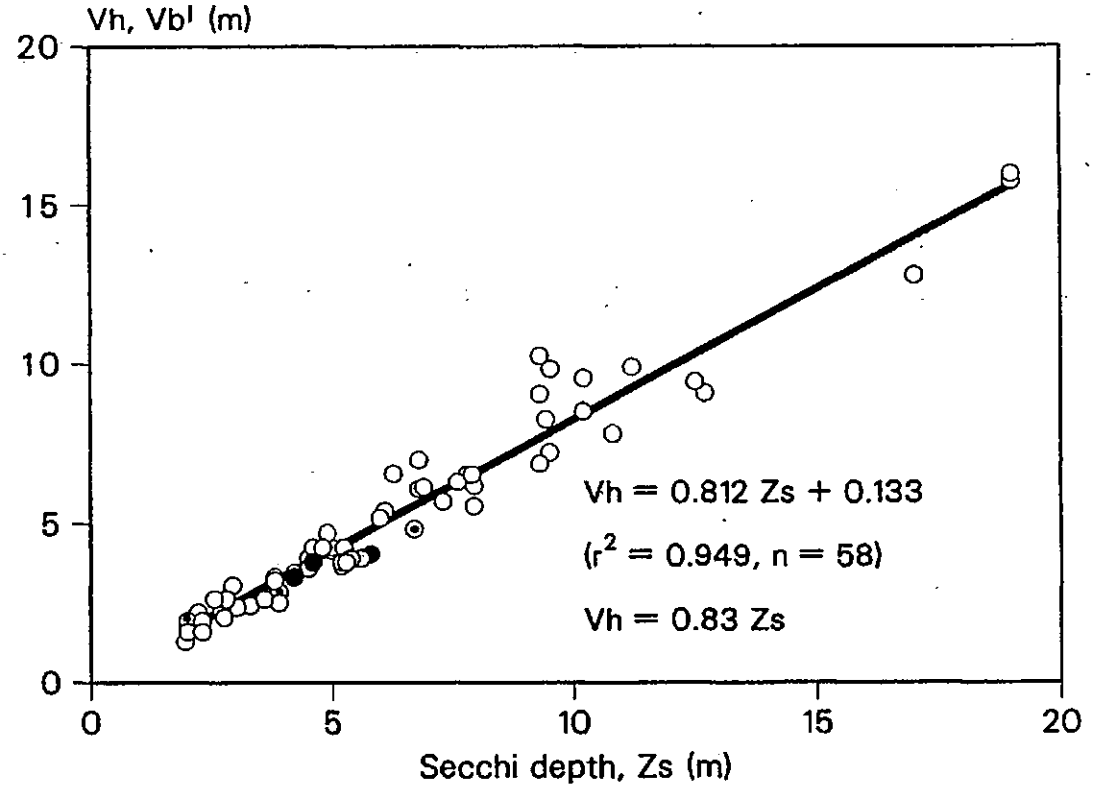

Fig.4.28: Relationship between the hydrological range, Vh, and the Secchi depth, Zs, in Plymouth Sound (O), Burrator Reservoir (●) and SE Malaysian waters (⊖)

Regression of the data presented in Fig.4.28 produces the equations:

$$Vh = 0.812\ Zs + 0.133 \quad (1.95 \leq Zs \leq 19.0,\ r^2 = 0.949,\ n = 58) \tag{4.102}$$

and through 0,0: $Vh = 0.83\ Zs$ (4.103)

For practical purposes, and incorporating Eqn.4.93, we may write:

$$Vh = 0.8\ Zs \tag{4.104}$$

$$Vb = 0.7\ Zs \tag{4.105}$$

4.4.5 Estimation of $\underline{c}+\underline{K}$, ρ, $\underline{R}$ and Ct from on-board observations of Z

If diver observations are unobtainable or inconvenient, then only vertically downward measurements ($Z\rho$, Zh, Zx and Zf) are viable. Likely useful rearrangements of Eqns.4.77, 4.80, 4.82 and 4.85 (Table 4.5), for our 4 standard targets, are tabulated in Table 4.6.

Table 4.6: Useful rearrangements of equations for vertically downwards threshold visibility with allocated equation numbers; all optical parameters are photometric.

	Standard target type			
	painted reflector $\rho = \rho$	light-trap $\rho = 0$	corner reflector $\rho = 1$	neutral filter $T = T$
$c+K =$	$\dfrac{\mathrm{Ln}\left[\frac{\rho-R}{R.Ct}\right]}{Z\rho}$ (4.106)	$\dfrac{\mathrm{Ln}[Ct]}{Zh}$ (4.107)	$\dfrac{\mathrm{Ln}\left[\frac{1/R-1}{Ct}\right]}{Zx}$ (4.108)	$\dfrac{\mathrm{Ln}\left[\frac{1-T}{Ct}\right]}{Zf}$ (4.109)
$\rho =$	$R.(Ct.\exp[(c+K).Z\rho] + 1)$ (4.110)	–	–	
$R =$	$\dfrac{\rho}{Ct.\exp[(c+K).Z\rho] + 1}$ (4.111)		$\dfrac{1}{Ct.\exp[(c+K).Zx] + 1}$ (4.112)	
$Ct =$	$\dfrac{\rho/R - 1}{\exp[(c+K).Z\rho]}$ (4.113)	$\dfrac{1}{\exp[(c+K).Zh]}$ (4.114)	$\dfrac{1/R - 1}{\exp[(c+K).Zx]}$ (4.115)	$\dfrac{1 - T}{\exp[(c+K).Zf]}$ (4.116)

The sum $\underline{c}+\underline{K}$ has little theoretical value but is the parameter estimated from the Secchi disc equation (Eqn.4.106), and is useful as a broad measure of optical turbidity. Values of $\underline{\rho}$, $\underline{R}$ and Ct must be assumed, and this is particularly risky in very turbid waters where

$\underline{R}$ may be high and unknown. By using the corner reflector, the target reflectivity is known (ρ=1) but an assumed value for $\underline{R}$ is still required:

$$\text{Eqn.4.108:} \quad \underline{c}+\underline{K} = \frac{\text{Ln}\left[\frac{1/\underline{R} - 1}{\text{Ct}}\right]}{\text{Zx}}$$

In turbid water it is better to use the light trap (this has also been recommended by Højerslev, 1986), or neutral filter, as it is then necessary to assume only a value for Ct, say 2%, (Højerslev uses 0.66%); so:

$$\text{Eqn.4.107:} \quad \underline{c}+\underline{K} = \frac{-\text{Ln}[\text{Ct}]}{\text{Zh}} = \frac{3.91}{\text{Zh}}$$

or

$$\text{Eqn.4.109:} \quad \underline{c}+\underline{K} = \frac{\text{Ln}\left[\frac{1-\underline{T}}{\text{Ct}}\right]}{\text{Zf}} = \frac{\text{Ln}[1-\underline{T}] + 3.91}{\text{Zf}}$$

In the unlikely event of the observer preferring an estimate of $\underline{R}$ to one of Ct, then an estimate of $\underline{c}+\underline{K}$ may be obtained by using the light trap and corner reflector together. Equating Eqns.4.114 and 4.115:

$$\text{Ct} = \frac{1}{\exp[(\underline{c}+\underline{K}).\text{Zh}]} = \frac{1/\underline{R} - 1}{\exp[(\underline{c}+\underline{K}).\text{Zx}]}$$

so, $-(\underline{c}+\underline{K}).\text{Zh} = \text{Ln}[1/\underline{R} - 1] - (\underline{c}+\underline{K}).\text{Zx}$, whence:

$$(\underline{c}+\underline{K}) = \frac{\text{Ln}[1/\underline{R} - 1]}{\text{Zx} - \text{Zh}} \qquad (4.117)$$

The light-trap and corner reflector pair may also be used to estimate

the unknown reflectivity of a third disc:

Eqn.4.110: $\underline{\rho} = \underline{R}.Ct.\exp[(\underline{c}+\underline{K}).Z\rho] + 1$

Eqn.4.117: $\underline{c}+\underline{K} = -Ln[Ct]/Zh$

Eqn.4.112: $\underline{R} = 1/(Ct.\exp[(\underline{c}+\underline{K}).Zx] + 1)$

Substituting $\underline{c}+\underline{K}$ and $\underline{R}$ from Eqns.4.107 and 4.112, into Eqn.4.110:

$$\underline{\rho} = \frac{Ct.\exp\left[\frac{-Ln[Ct]}{Zh}.Z\rho\right] + 1}{Ct.\exp\left[\frac{-Ln[Ct]}{Zh}.Zx\right] + 1}$$

$$= \frac{\exp[-Ln[Ct]\ Z\rho/Zh] + 1}{\exp[-Ln[Ct]\ Zx/Zh] + 1} \qquad (4.118)$$

and as $Z\rho/Zh$, $Zx/Zh \sim 2$, then $\exp[] \gg 1$, and so:

$$\underline{\rho} = \frac{\exp[-Ln[Ct]\ Z\rho/Zh]}{\exp[-Ln[Ct]\ Zx/Zh]} = \exp\left[\frac{3.91}{Zh}\ (Z\rho - Zx)\right] \qquad (4.119)$$

Table 4.7 lists observations of Zx, Zh and Zs in different waters. The 'unknown' ρ is that of a matt-white painted Secchi disc - generally assumed to be about 80%, (eg Tyler, 1968).

By equating Eqns.4.107 and 4.108, water reflectivity, $\underline{R}$, may be estimated:

$$\underline{c}+\underline{K} = \frac{-Ln[Ct]}{Zh} = \frac{Ln\left[\frac{1/\underline{R} - 1}{Ct}\right]}{Zx}$$

therefore, $\mathrm{Ln}\left[\frac{1/\underline{R} - 1}{Ct}\right] = 3.91\ Zx/Zh$, and so:

$$\underline{R} = (0.02 \exp[3.91\ Zx/Zh] + 1)^{-1} \qquad (4.120)$$

Table 4.7: Some calculations of ρ by Equation 4.119

Observation			Reflectivity of Secchi disc calculated from Equation 4.119
Zh	Zs	Zx	
5.55	9.30	9.55	0.839
2.66	4.50	4.57	0.902
5.90	10.76	11.22	0.737
			Mean: 0.826

This result agrees closely with the 80% suggested by Tyler (1968).

Lastly, consider a means of estimating the observer's threshold contrast, Ct. The corner reflector is not useful in this case as Eqn.4.121 contains both R and c+K. However, use may be made of a neutral filter of known transmission, T, and a light trap. Equating Eqns.4.107 and 4.109:

$$\underline{c+K} = \frac{-\mathrm{Ln}[Ct]}{Zh} = \frac{\mathrm{Ln}[1-\underline{T}] - \mathrm{Ln}[Ct]}{Zf}$$

therefore, $-\mathrm{Ln}[Ct].\left[\frac{1}{Zh} - \frac{1}{Zf}\right] = \frac{\mathrm{Ln}[1-\underline{T}]}{Zf}$, and so:

$$Ct = \exp\left[\frac{-\mathrm{Ln}[1-\underline{T}]}{Zf/Zh - 1}\right] \qquad (4.121)$$

4.4.6 Estimation of $\langle {}^{o}K_o \rangle$ from Zs

The Secchi disc depth is a function of photopic c and K, (Eqn.4.106). Traditionally, however, workers have estimated the euphotic depth, Ze_p, a function of diffuse attenuation only, by assuming an empirical relationship of the form: $\langle {}^{o}K_o \rangle . Zs = {}^{o}J_s$, where ${}^{o}J_s$ is the PAR diffuse optical depth of the Secchi depth (eg Poole and Atkins, 1929; Clarke, 1941; Gall, 1949; Duntley and Preisendorfer, 1952; Graham, 1966; Tyler, 1968; Williams, 1968; Quasim et al, 1968; Holmes, 1970; Idso and Gilbert, 1974; Weinberg, 1976; Otobe et al, 1977; Walker, 1982; Højerslev, 1986). Most agree that $1.3 \leq K.Zs \leq 1.8$, but debate the exact figure, (where $K = \langle K \rangle, \langle K_d \rangle, \langle {}^{o}K_o \rangle$ or, often, an unspecified form of K; they are, in any case, approximately equal). There is little to be gained from this search for great accuracy since Zs is a function of c and K, and c is several times as big as K. The expression: K.Zs = constant, (or c.Zs = constant), represents a parabola, and some workers, (eg Idso and Gilbert, 1974; Højerslev 1977 , 1978, 1986), have presented their data closely scattered about a curve of this form. In fact, the shape of this parabola is rather insensitive to small changes in the chosen constant, particularly at large or small Secchi depths (eg clear ocean or turbid estuarine waters). This is illustrated in Fig.4.29 by the two parabolas: K.Zs = 1 and K.Zs = 2 within which, seemingly, would fit all of the curves specified by the listed workers. Of greater significance, the listing includes the number of observations (n) and range of Secchi depths on which these 'laws' were based. It is apparent that some were based on too few observations and too limited a range of turbidities for universal application; the scope of Pilgrim (1987) compares well with most.

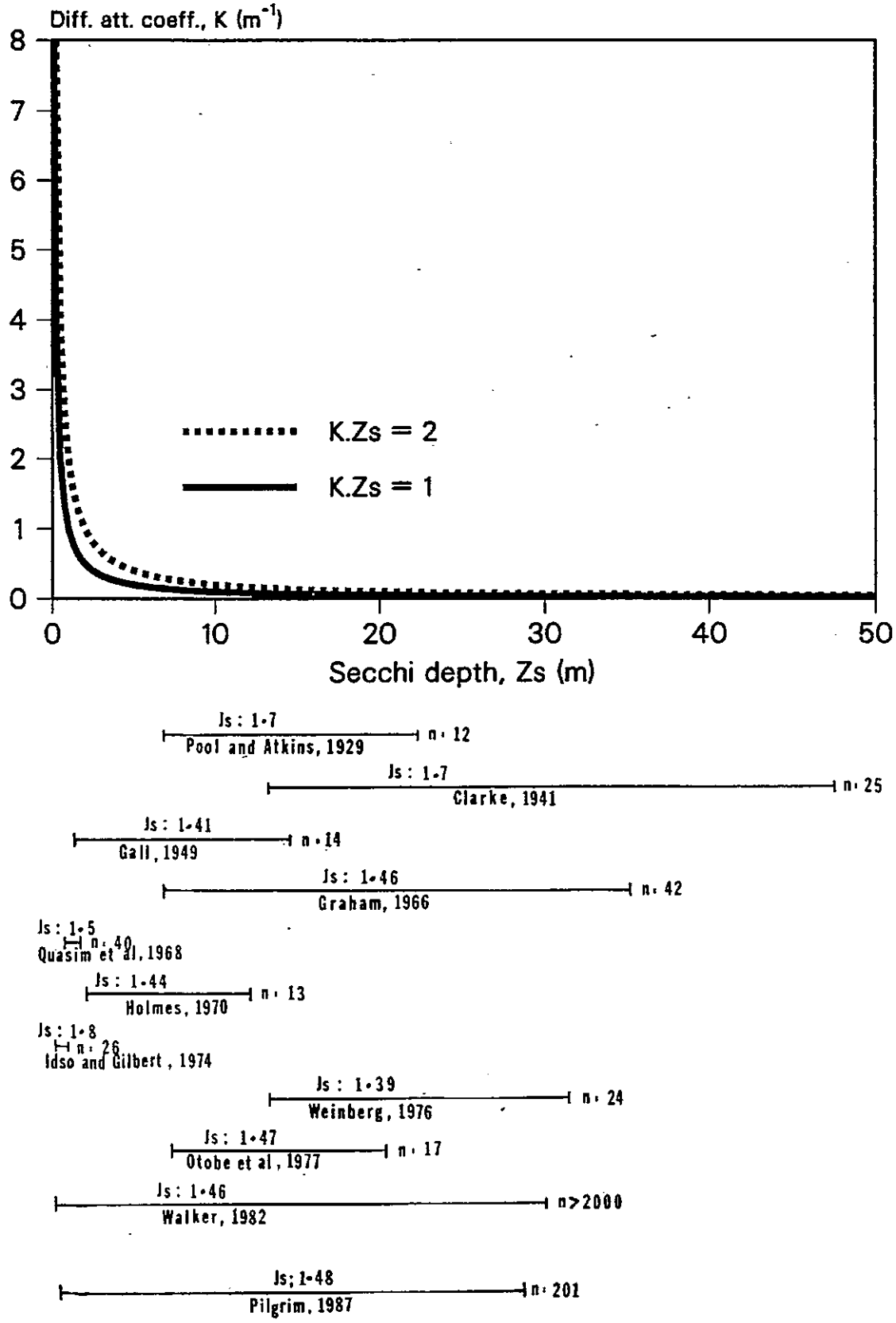

Fig.4.29: The two parabolas K.Zs = Js = 1,2; and values of K.Zs = Js published by eleven workers (including Pilgrim, 1987) with the number (n) and range (⊢——⊣) of Secchi depths measured

Figure 4.30 illustrates 201 ⟨°Ko⟩:Zs data-pairs collected in the NE Atlantic and Tamar Estuary.

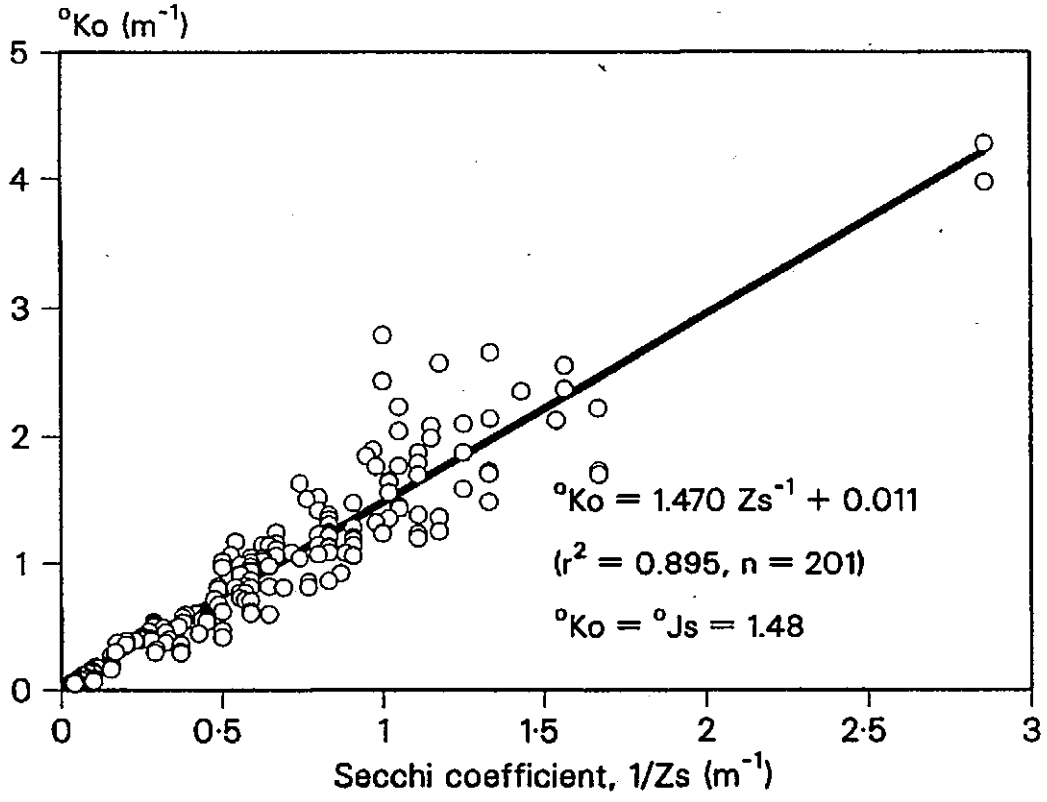

Fig.4.30: Relationship between ⟨°Ko⟩ and Zs from data collected at 201 stations in the NE Atlantic and Tamar Estuary

Least-squares regression analysis gives:

$$\langle {}^{\circ}Ko \rangle = 1.470\ Zs^{-1} - 0.0114 \qquad (4.122)$$

$(0.35 \leq Zs \leq 31,\ 0.0517 \leq {}^{\circ}Ko \leq 4.276,\ r^2 = 0.895,\ n = 201)$

and through 0,0: $\langle {}^{\circ}Ko \rangle . Zs = {}^{\circ}Js = 1.48 \qquad (4.123)$

Secchi disc data were also partitioned for 'oceanic' (Ko < 0.27) and 'turbid' (°Ko ≥ 0.27) analyses. This separation is about midway between Jerlov's oceanic type III and coastal type I waters (see

Jerlov, 1976, Table 27). The equations derived from these analyses are:

Oceanic ($^{o}Ko < 0.27$)

$$\langle {}^{o}Ko \rangle = 1.309\ Zs^{-1} + 0.0073 \qquad (4.124)$$

$(6.5 \leq Zs \leq 31,\ 0.0517 \leq {}^{o}Ko \leq 0.2677,\ r^2=0.811,\ n=48)$

and through 0,0: $\langle {}^{o}Ko \rangle .Zs = {}^{o}Js = 1.38$ (4.125)

Turbid ($^{o}Ko \geq 0.27$)

$$\langle {}^{o}Ko \rangle = 1.450\ Zs^{-1} + 0.0327 \qquad (4.126)$$

$(0.35 \leq Zs \leq 2.7,\ 0.2902 \leq {}^{o}Ko \leq 4.2767,\ r^2=0.834,\ n=153)$

and through 0,0: $\langle {}^{o}Ko \rangle .Zs = {}^{o}Js = 1.48$ (4.127)

The 153 'turbid' data-pairs were obtained in the same waters in which Poole and Atkins (1929) derived: K.Zs= 1.7 (based on 12 data points). Recalculation of their data (Walker, 1980) gave a more accurate estimate: K.Zs = 1.4, a value closer to the 1.48 presented here. Unless the local value of ^{o}Js has recently been derived from direct observations of $\langle {}^{o}Ko \rangle$, then it is suggested that biologists adopt the working relationship:

$$^{o}Js = \langle {}^{o}Ko \rangle .Zs = 1.5 \qquad (4.128)$$

and hence, from Eqn.2.63, for the euphotic depth, Ze:

$$Ze = \frac{{}^{o}Je}{\langle {}^{o}Ko \rangle} = \frac{4.6}{1.5/Zs} = 3\ Zs \qquad (4.129)$$

The regression analyses reveal a small difference between turbid (^{o}Js= 1.48) and oceanic (^{o}Js = 1.38) waters, which may be real, or possibly a consequence of the fact that all of the turbid

observations were made using a glass-bottomed bucket or diver's face mask, (to avoid the adverse effects of surface reflection and refraction), whereas the oceanic observations were made from the deck of a research ship.

That there should be markedly better correlation between Zs, a function of $\underline{c}+\underline{K}$, and Vh, a function of $\underline{c}$ only ($r^2 = 0.949$, Eqn.4.102) than between Zs^{-1} and $\langle^0Ko\rangle$ ($r^2 = 0.895$, Eqn.4.122) may be attributed to the fact that $\underline{c}$ is several times as big as $\underline{K}$ or $\langle^0Ko\rangle$, and so the more significant part of the parameter $\underline{c}+\underline{K}$.

The regressions presented in Eqns.4.122 - 4.127 are very slightly different to those published in Pilgrim (1987) for the same data. In that paper, regressions were calculated by the method given by Pedoe (1970), in which it is assumed that both x and y, (in this case Zs^{-1} and $\langle^0Ko\rangle$), are subject to observational error. This is certainly correct, but it is now appreciated that adoption of this method may not allow proper comparison with the published results of other workers, who almost certainly use the standard method of least squares. Throughout this current work, all least-squares regressions have been obtained from the MINITAB package on PRIME. Of course, these small differences are of no practical significance; the important conclusions (Eqns.4.128 and 4.129) are unchanged.

4.4.7 Estimation of ⟨°Ko⟩ from Vh

The Marine Conservation Society is currently organising a nationwide observation scheme, Viswatch, in which divers are asked to note the depth of the deepest kelp plant and the horizontal visibility at the seabed. The reasoning here is apparent: the better the visibility, then the clearer the water and so the deeper the penetration of sunlight for photosynthesis. This researcher was invited to analyse the collected data. The question therefore arose: what is the most appropriate empirical relationship between the depth of the euphotic zone, Ze, a function of ⟨°Ko⟩, and the hydrological range, Vh, a function of c? No doubt a solution of sorts could be derived from the c(660):⟨°Ko⟩ data which produced Eqn.4.5 - 4.7. However, transmission at 660 nm is not a good representation of broad-band vision. A more direct approach was therefore taken by using the real observations of horizontal visibility. Combining Eqns.4.129 and 4.103:

$$\frac{Ze}{Vh} = \frac{(4.6/1.5).Zs}{0.83\ Zs} \quad \text{ie } Ze = 3.7\ Vh \qquad (4.130)$$

If preferred, ⟨°Ko⟩ may be estimated from Eqns.4.127 and 4.103:

$$\langle {}^{\circ}Ko\rangle .Vh = \frac{1.48}{Zs}\ 0.83\ Zs, \text{ ie } \langle {}^{\circ}Ko\rangle = \frac{1.23}{Vh} \qquad (4.131)$$

Unfortunately, the Marine Conservation Society gave no instructions to divers on how to observe 'horizontal visibility', whilst the observations of Vh, which produced the relationships given in

Eqn.4.130 and 4.131 are of the hydrological range as defined by Eqn.2.92, ie the threshold visual range of a zero-reflector. In a series of experiments in Plymouth Sound and the waters of East Malaysia and Singapore, divers were asked to estimate the 'horizontal visibility' near the bed, no indication being given on how this should be done. These estimates (Vis) are compared to measured values of Vh (light trap) and Vb' (black disc, adjusted) in Fig.4.31.

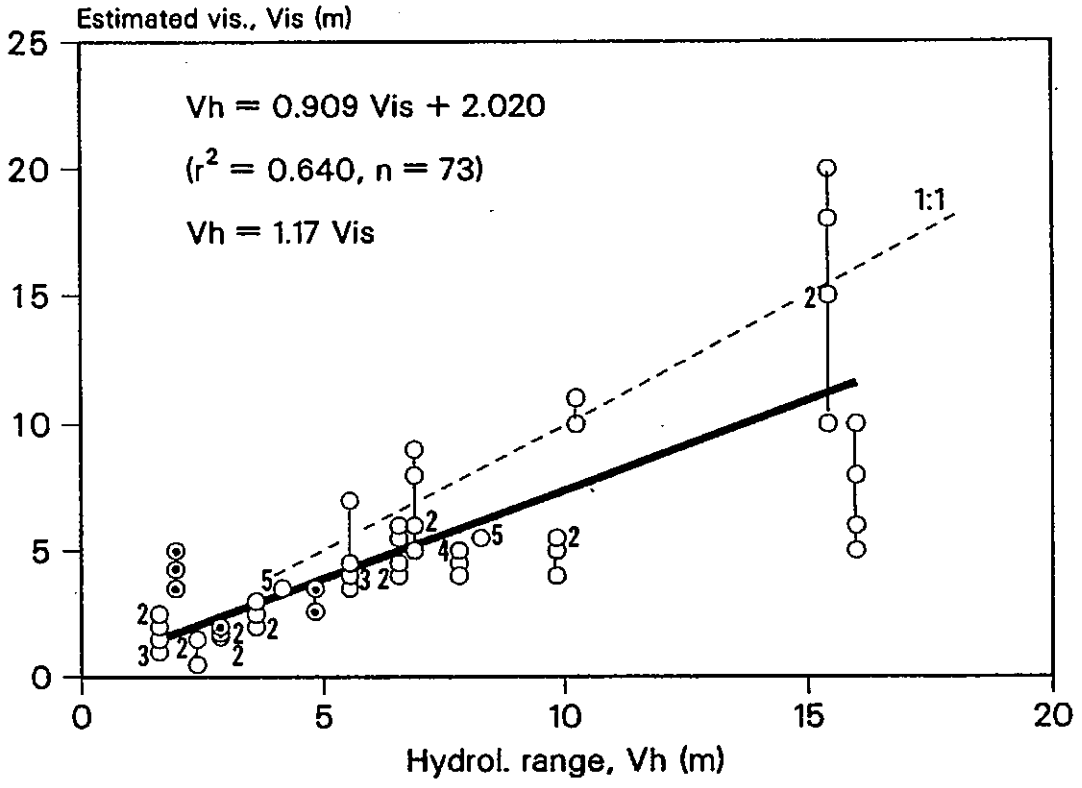

Fig.4.31: Relationship between measured values of the hydrological range (Vh,Vb') and 73 divers' estimates of 'visibility' (Vis). Vertical lines join estimates offered by several divers on the same occasion. Observations were made in the waters of: Plymouth Sound (O) and SE Malaysia (⊖) The broken line indicates the equality: Vis = Vh. (Pilgrim et al, 1988)

Least-squares regression of the data in Fig.4.31 produces the relationship (Pilgrim et al, 1988):

$$Vh = 0.909\ Vis + 2.020 \quad (1.6 \leq Vh \leq 16.0,\ r^2=0.640,\ n=73) \qquad (4.132)$$

and through 0,0: $Vh = 1.17\ Vis$ (4.133)

That $Vis < Vh$ is to be expected; an uninstructed observer will not judge 'the visibility' to be the absolute threshold range of a zero reflector, but rather the maximum range at which common objects are just visible.

4.4.8 Estimation of particle concentration from Zs

It is apparent that the Secchi depth must decrease with increased suspended particle concentration, P, usually expressed in parts per million (ppm). There is no governing theory which gives P in terms of Zs so this relationship must be determined empirically. The data plotted in Fig.4.32 were obtained from on board 3 boats anchored in the lower reaches of the River Tamar on two separate occasions (30 June and 7 July, 1982); these data are included in the two tidal time-plots, Figs.4.33(a) and (b). The particle concentration P (ppm) was obtained by turbidity meters which had been calibrated against international standard formazin. The least-squares regression equations are:

$$P = 24.71\ Zs^{-1} - 9.16;\ Zs^{-1} = 0.033\ P + 0.45 \quad (r^2=0.823,\ n=52) \qquad (4.134)$$

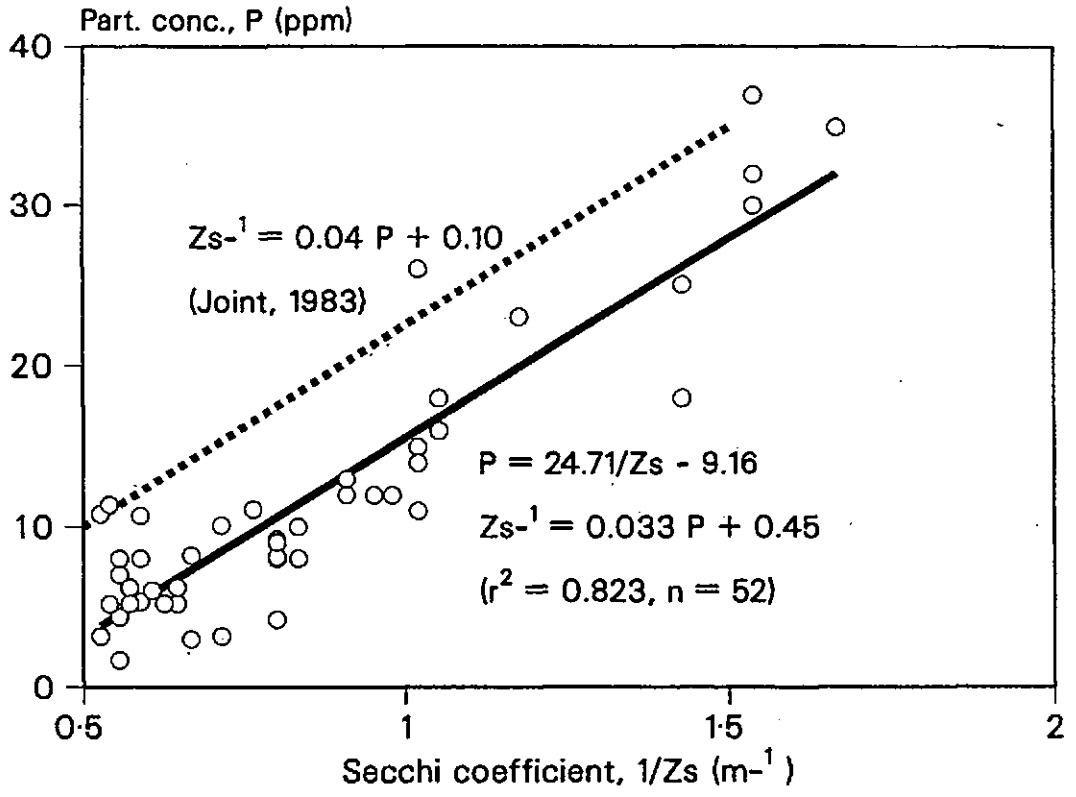

Fig.4.32: Relationship between Secchi coefficient, 1/Zs, and the gravimetric particle concentration, P, during two surveys on the River Tamar: 30 June 1982 (neaps) and 7 July 1982 (springs).

The rather high degree of scatter in Eqn.4.134 is not unexpected. The turbidity meter effectively measures beam transmission which is a function of particle size as well as concentration (Gibbs, 1974); the scatter therefore suggests a range of particle sizes different to that of the formazin standard.

The relationship between particle concentration and Secchi depth presented in Eqn.4.134 compares very closely with that found by Joint (1983) from gravimetric measurements in the Bristol Channel in 1973 and 1974:

$$Zs^{-1} = 0.040\ P + 0.10 \qquad (4.135)$$

This equation is plotted (broken line) in Fig.4.32. The intercepts in Eqns.4.134 and 4.135 represent Secchi depths of 2.2 (Tamar) and 10.0 (Bristol Channel) at P=0, and may reflect differences in concentrations of dissolved organics in the two rivers. The gradients, $d(Zs^{-1})/dP$, are very similar: 0.033 $(m^{-1}).ppm^{-1}$ in the Tamar, and 0.040 $(m^{-1}).ppm^{-1}$ in the Severn.

4.5 TIDAL VARIATIONS IN OPTICAL PROPERTIES

4.5.1 Tidal variation in <°Ko>, Zs etc

Although internal cycling of sediment within the Tamar estuary is predominantly driven by seasonal changes in river flow (Bale *et al*, 1985), it has been demonstrated by Uncles *et al* (1985) and Uncles *et al* (1986) that resuspension of sediment is locally enhanced by tidal bed stress with a large springs-neaps variability in a manner similar to that described for the Gironde and Autune by Allen *et al* (1980). Figures 4.33(a) and (b) show the gradual changes in five tide-related parameters measured at half-hourly intervals throughout a neaps and a spring tidal cycle. These parameters are: depth of water under the boat, h, (effectively the height of tide), the depth-mean PAR diffuse attenuation coefficient, <°Ko>, the depth-mean particle concentration P, the Secchi coefficient, 1/Zs, and the fraction of fresh water, FFW, (taken to be: ((35-S)/35)x100%). As the dimension and/or numerical range of each parameter is different, data have been converted to 'percentage of range above minimum', and so each curve covers the full 100% scale. Two controlling factors are apparent. The very distinct control is FFW for it is the fresh river outflow which is responsible for the down-stream flux of suspended particles from the tubidity maximum. The rising tide brings clearer saline water into the estuary. This dependence of suspended sediment concentration upon salinity is also illustrated in Figs.4.34(a) and (b). If sediment concentration depended only upon the influx by river water and sea water, then the sediment concentrations in these

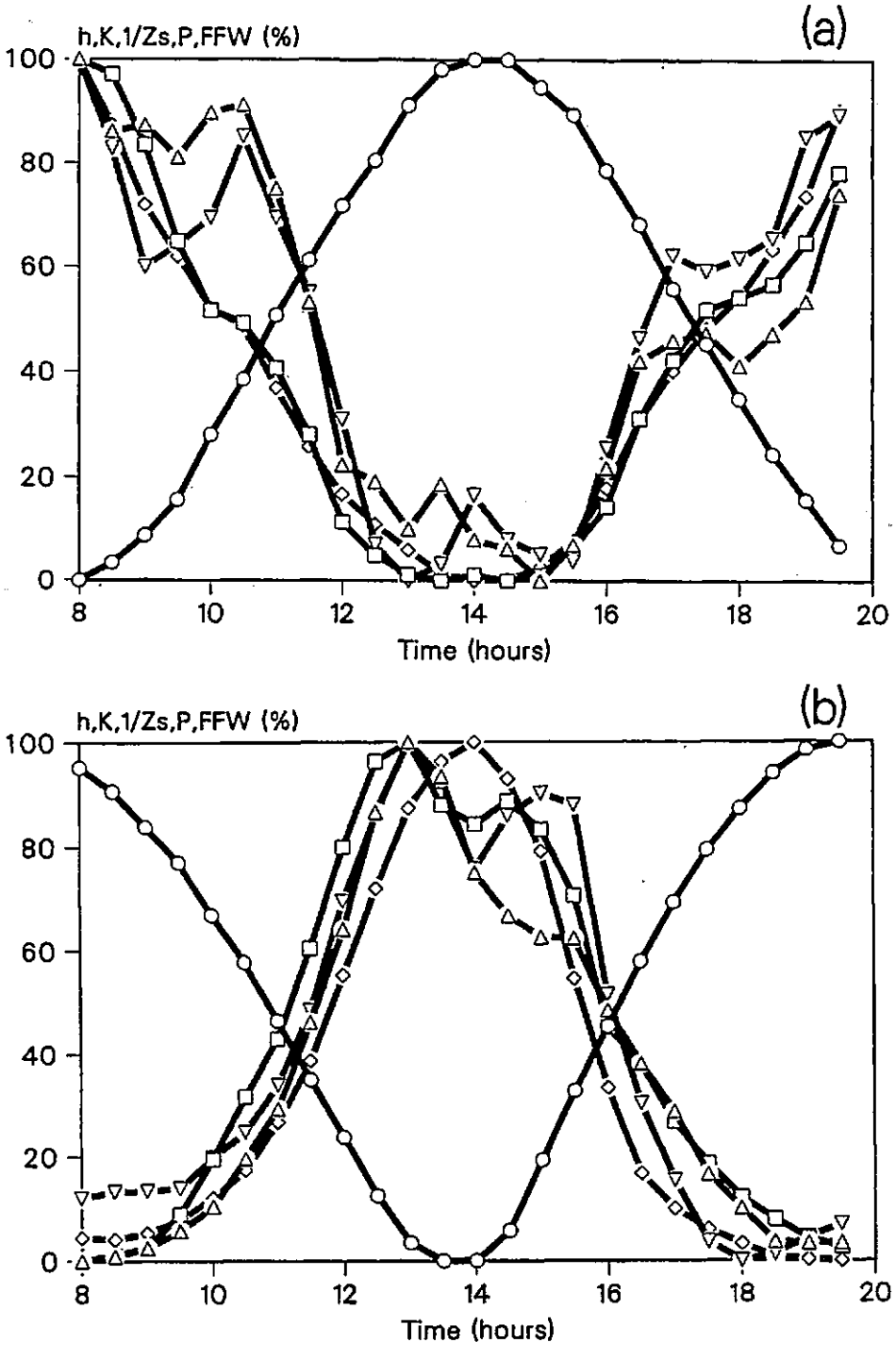

Fig.4.33: Tidal variations in turbidity parameters at Cargreen (19.7 km from Weir, River Tamar) on: (a) 30 June 1982 (neaps), and (b) 7 July 1982 (springs). The curves are:

- height of tide, h
- PAR diffuse attenuation coefficient, ⟨°Ko⟩
- Secchi coefficient, 1/Zs
- particle concentration, P
- fraction of fresh water, FFW

Ordinate scales are: % of range above minimum

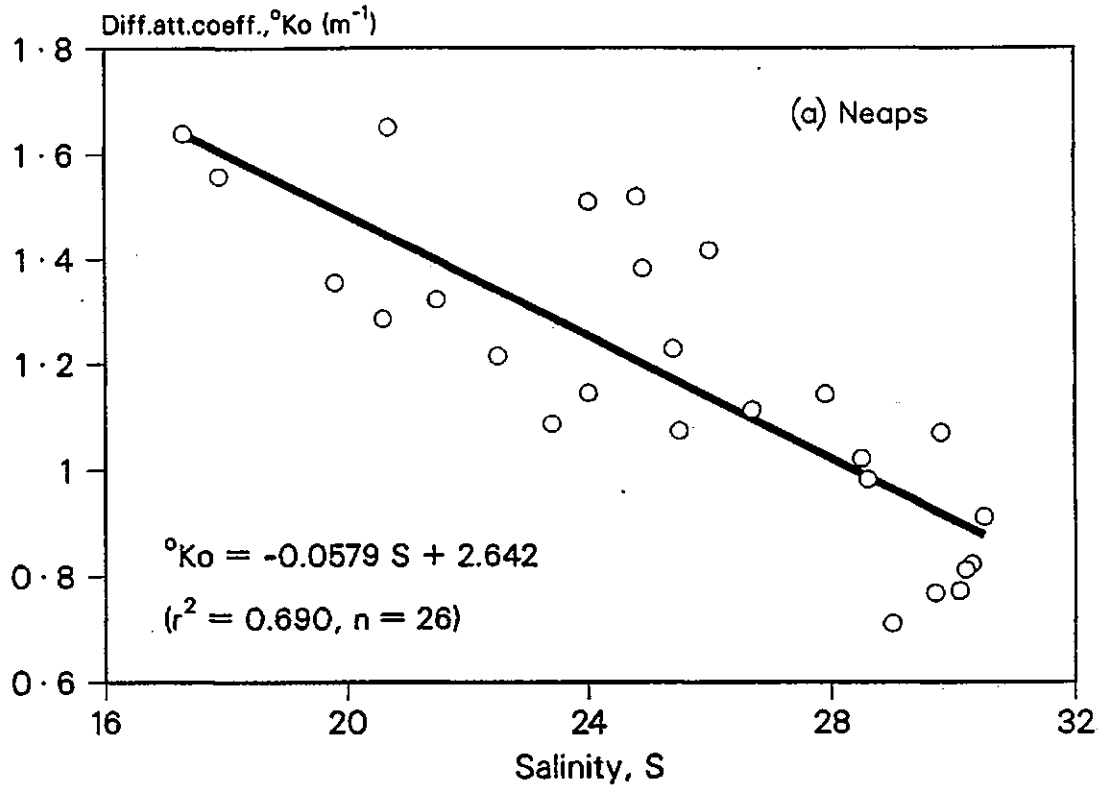

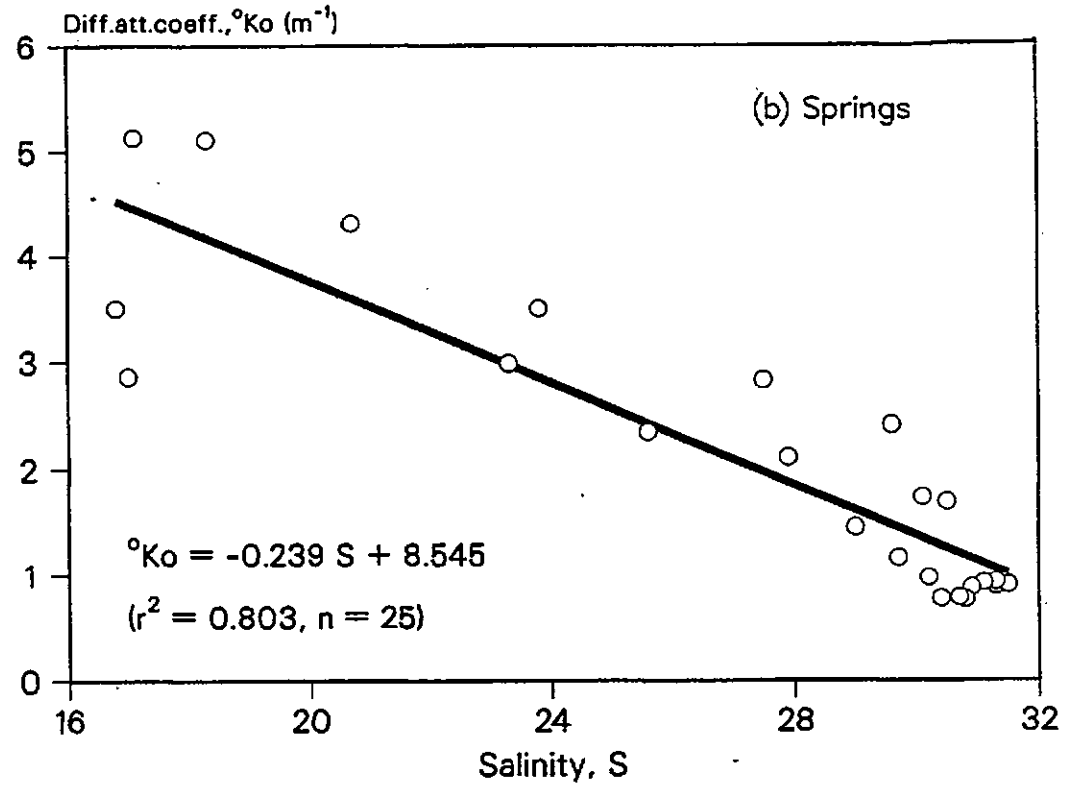

Fig.4.34: Relationship between PAR diffuse attenuation coefficient and salinity at Cargreen (19.7 km from Weir, R.Tamar) on: (a) 30 June 1982 (neaps), (b) 7 July 1982 (springs)

two would be given by extrapolation to S=0 and S=35:

Neaps: $\langle {}^{o}Ko \rangle = -0.0561S + 2.61$ ($r^2=0.793$, n=26) (4.136)

which produces the extrapolations:

S = 0, $\langle {}^{o}Ko \rangle$ = 2.61 (river water)

S = 35, $\langle {}^{o}Ko \rangle$ = 0.647 (sea water)

Springs: $\langle {}^{o}Ko \rangle = -0.206S + 7.61$ ($r^2=0.879$, n=26) (4.137)

which produces the extrapolations:

S = 0, $\langle {}^{o}Ko \rangle$ = 7.61 (river water)

S = 35, $\langle {}^{o}Ko \rangle$ = 0.40 (sea water)

The seawater values of $\langle {}^{o}Ko \rangle$ are of the right order; otherwise these results tell us little. It would be a mistake to assume that the river contribution to $\langle {}^{o}Ko \rangle$ on the two occasions was 2.61 and 7.61 m^{-1} respectively; there must be a considerable contribution by tidal resuspension of the type described by Allen et al (1980), Morris et al (1982a), Uncles et al (1985), Uncles (1986) and others.

The other important control upon turbidity is the water column turbulence, a function of water velocity. Although turbulence was not measured directly, its effect is just noticeable at high water and low water. We see from Figs.4.23(a) and (b) that at slack water $\langle {}^{o}Ko \rangle$, P and 1/Zs decrease for a short period as the larger particles settle out in the temporary low-turbulence conditions. Salinity is not affected in the same way and so the FFW curves do not exhibit perturbations at HW or LW.

It is apparent from Figs.4.33(a) and (b) that the phase angle, ϕ,

between the height of tide, h(t), and the approximately sinusoidal variation in turbidity, say $\langle^{o}Ko\rangle(t)$, is about π. It is given by: $\langle^{o}Ko\rangle(t) = \alpha + \beta.\cos(\sigma t'+\phi)$, where t = time, $t' = t - t(HW)$, $\sigma = 2\pi/$duration of tide, and α,β are constants. Therefore:

$$\langle^{o}Ko\rangle(t) = \alpha + \beta.\cos \sigma t'.\cos\phi + \beta.\sin \sigma t'.\sin \phi$$

$$= \alpha + \beta_1.\cos \sigma t' + \beta_2.\sin \sigma t' \qquad (4.138)$$

where $\beta_1 = \beta.\cos \phi$, $\beta_2 = \beta.\sin \phi$ and $\phi = \tan^{-1}(\beta_2/\beta_1)$ are obtained by multiple regression of $\langle^{o}Ko\rangle(t)$ data against cos $\sigma t'$ and sin $\sigma t'$. Results showed that during the particular tides in question: the $\langle^{o}Ko\rangle(t)$ curve at neaps (Fig.4.33(a)) lagged the tidal curve by 1.08π and at springs (Fig.4.33(b)) by 0.84π.

4.5.2 Tidal variations in irradiance reaching an estuary bed.

A significant proportion of total estuarine primary production takes place on the estuary bed. The most important producers are the intertidal angiosperms such as Zostera spp., and salt-marsh Spartina spp. Also of consideration are the macrophytes, mainly Fucus spp., filamentous algae such as Enteromorpha spp., and diatoms and other microalgae (microphytobenthos) very near the surface of mud flats (McLusky,1981). Colijn (1982) has measured PAR diffuse attenuation coefficients in the Ems-Dollart Estuary and has calculated column irradiances for phytoplankton, and irradiances reaching submerged microphytobenthos over mud-flats at high water. Paterson (1986) has investigated, in a laboratory tidal micro-system, the stabilisation of cohesive sediments by the mucopolysaccharides produced by

intertidal diatoms. Species of Navicula and Nitzchia were observed to migrate to the sediment surface when photon flux densities were increased above 0.5 $\mu E\ m^{-2}s^{-1}$; after 4 hours there was a synchronous appearance of large numbers of Scoliapleura tumida.

The amount of light available to benthic flora must depend on the sky-light level, a function of latitude, season, time of day and cloud cover, and the proportion of surface light which is able to penetrate the overlying water column, a function of water depth and turbidity. In the Tamar Estuary the main component of turbidity is suspended inorganic particles (mainly quartz, with smaller fractions of tourmaline, ilmenite, magnetite, feldspar and granite fragments), and this varies tidally, reaching a maximum at low water with the resuspension of sediment by increased turbulence, and a corresponding minimum at about high-water (Morris et al, 1982; Bale et al, 1985; Uncles et al, 1986), (see eg Figs.4.33(a) and (b)). It is therefore apparent that the two factors limiting light intensity at the bed are about π out of phase and counteract; when the depth is least, so is the transparency and vice versa. It might be assumed therefore that the two opposing factors simply cancel, but this is not the case, as demonstrated by Pilgrim and Millward (1988). The time variation in the natural log of the proportion of surface light reaching the bed is expressed by $J_h(t)$, given by: $J_h(t) = h(t).K(t)$ where, for simplicity, we write $J_h(t)$, $K(t)$ for ${}^{o}J_h(t)$, $\langle {}^{o}Ko \rangle(t)$, so:

$$J_h(t) = h(t).K(t)$$

$$= (\bar{h} + \frac{\Delta h}{2}.(\cos\theta)).(\bar{K} + \frac{\Delta K}{2}.(-\cos\theta))$$

whence:

$$J_h(t) = \bar{h}.\bar{K} + \bar{h}.\frac{\Delta K}{2}.(-\cos\theta) + \bar{K}.\frac{\Delta h}{2}.(\cos\theta) - \frac{\Delta h.\Delta K}{4}.\cos^2\theta \qquad (4.139)$$

where Δh, ΔK, $\bar{h}$, $\bar{K}$ are the tidal ranges and mean values of water depth and diffuse attenuation coefficient, and θ is the tidal angle. Suppose that $\Delta K/\bar{K} = \Delta h/\bar{h}$, ie that $\bar{h}.\Delta K = \bar{K}.\Delta h$; clearly the second and third terms would cancel so that:

$$J_h(t) = \bar{h}.\bar{K} - \frac{\Delta h.\Delta K}{4}.\cos^2\theta = \bar{h}.\bar{K} - \frac{\Delta h.\Delta K}{8}.(1 - \cos 2\theta) \qquad (4.140)$$

This function varies at twice the tidal frequency ($\cos.2\theta$) as illustrated in Fig.4.35, curve (a), which indicates maximum light penetration (minimum J_h) at both HW and LW and minima at rising and falling mid-tides. It is also apparent that all the maxima and minima are equal; eg $J_h(HW) = J_h(LW)$, and this may be written:

$$(h + \tfrac{1}{2}\Delta h).(K - \tfrac{1}{2}\Delta K) = (h - \tfrac{1}{2}\Delta h).(K + \tfrac{1}{2}\Delta K) \qquad (4.141)$$

which simplifies to $\Delta h/\bar{h} = \Delta K/\bar{K}$, the special precondition. This situation will therefore be called: equilibrium $J_h(t)$, occurring at the equilibrium depth.

In shallower water (nearer to the bank rather than up-estuary, so giving approximately the same $\Delta K/\bar{K}$), the ratio $\Delta h/\bar{h}$ will be larger and $J_h(HW) > J_h(LW)$. This condition will be called tide-dominated $J_h(t)$, as light penetration is controlled more by the tidal variation in water depth than by the opposing variation in K. It is characterized by $\Delta h/\bar{h} > \Delta K/\bar{K}$ and illustrated in Fig.4.35, curve (b).

It can be seen from curve (c) that as $\Delta h/\bar{h} >> \Delta K/\bar{K}$, the $J_h(t)$ curve tends to follow the depth curve. This will therefore be known as tide-following $J_h(t)$.

In water deeper than the equilibrium depth: $\Delta h/\bar{h} < \Delta K/\bar{K}$. This is the turbidity-dominated $J_h(t)$ type in which $J_h(HW) < J_h(LW)$, and is illustrated in Fig.4.35, curve (d). As $\Delta h/\bar{h} << \Delta K/\bar{K}$ (curve (e)), the $J_h(t)$ curve tends to follow the turbidity curve, K(t), which is identified as turbidity-following $J_h(t)$.

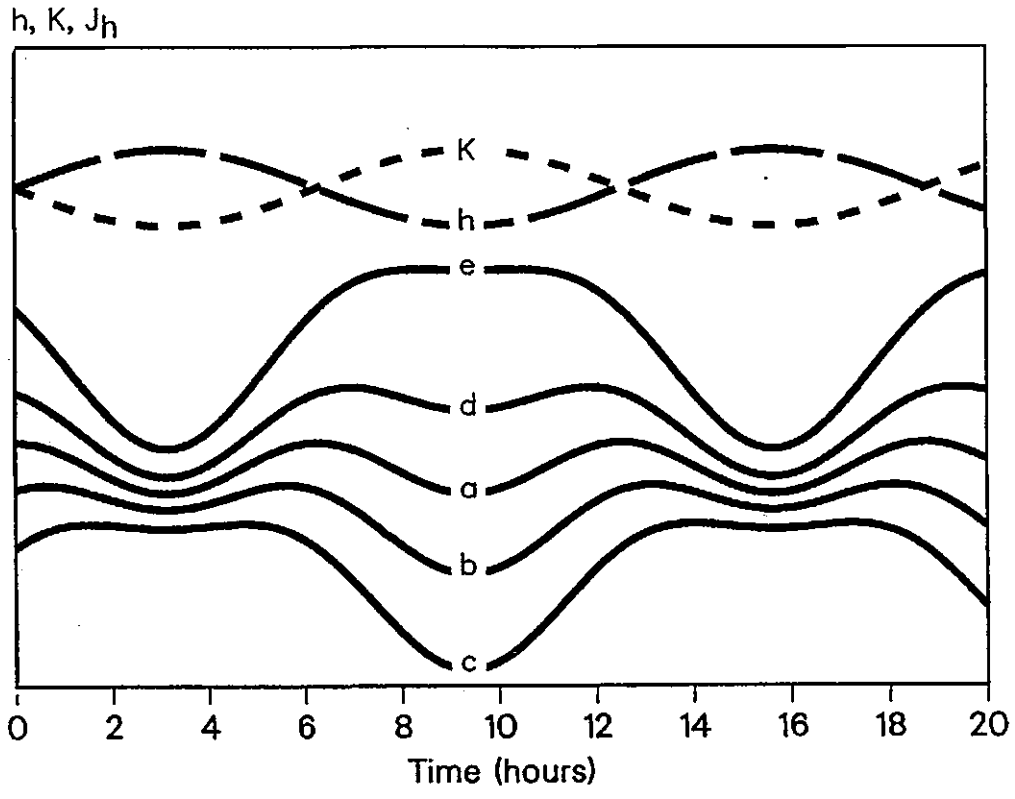

Fig.4.35: Theoretical curves of the time variation in the diffuse optical depth, $J_h(t)$, of an estuary bed.

(a) $J_h(t, \tau=1)$ (b) $J_h(t, \tau>1)$ (c) $J_h(t, \tau>>1)$
(d) $J_h(t, \tau<1)$ (e) $J_h(t, \tau<<1)$

It is sometimes more convenient to estimate K from the Secchi depth, Zs. Although Zs is inversely proportional to the sum c+K, simple empirical formulae are frequently used to give separate values of K and/or c. It has been found, for example, that for work in the Tamar Estuary (Pilgrim, 1987): $\langle {}^{o}Ko \rangle .Zs = J_s = 1.5$, where J_s is the diffuse optical depth of the Secchi depth. We may therefore write: $J_h = K.h = (1.5/Zs).h$ ie $Jh = h/Zs$. The term h/Zs will be recognized as the scaled depth, H, used by Pingree (1978, 1986) in constructing S-H (stability - scaled depth) diagrams which describe the relationship between environmental conditions and the start of the productive season in coastal waters. We may therefore use H as a meaningful substitute for J_h. Similarly, K may be estimated locally from an empirical K:c relationship. In the Tamar Estuary, the correlation: $K = 1.1066\ c^{1.314}$ has been obtained (Pilgrim, 1987) where c is measured at 660 nm and corrected for forward scattering by the method given by Bartz et al (1978). Actual conversion is unnecessary; the general pattern of $J_h(t)$ may be studied from analogous time series of $\gamma_h(t)$. We may therefore predict the $J_h(t)$ curve type by calculation of the ratio τ:

$$\tau = \frac{\Delta h/\bar{h}}{\Delta K/\bar{K}} = \frac{\Delta h/\bar{h}}{\Delta(1/Zs)/(1/\bar{Zs})} = \frac{\Delta h/\bar{h}}{\Delta c/\bar{c}} \qquad (4.142)$$

The characteristics of the five named $J_h(t)$ types are summarised in Table 4.8.

Table 4.8: Summary of $J_h(t)$ curve types and characteristics

$J_h(t)$ curve type	Curve in Fig.4.35	τ	Shape of $J_h(t)$ curve	Situation - one or more of:
Tide-following	c	$\tau>>1$	Follows depth curve; single penetration max (min J_h) at LW	Shallow water Large tidal range High turbidity Small turbidity range
Tide-dominated	b	$\tau>1$	Small penetration max (low J_h) at HW; larger max (min J_h) at LW	
Equilibrium	a	$\tau=1$	Equal penetration maxima (J_h minima) at LW and HW	
Turbidity-dominated	d	$\tau<1$	Small penetration max (low J_h) at LW; larger max (min J_h) at HW	Deep water Small tidal range Low turbidity Large turbidity range
Turbidity-following	e	$\tau<<1$	Follows turbidity curve; single penetration max (min J_h) at HW	

These theoretical patterns have been observed in data obtained in the Tamar Estuary. K(t) and Zs(t) data were obtained during two surveys (30 June, 1982, and 7 July, 1982) at stations 8.8, 19.7, 23.3 and 26.7 km down-estuary of a weir used as the baseline for distances. Another survey, which included the collection of beam transmissometer (660 nm) data, was carried out on 19-20 March, 1987, at the confluence of the Lynher and Tamar (26 km from the weir).

Figures 4.36 - 4.41 illustrate observed tidal variations in h(t), K(t) and $J_h(t)$ (or their Secchi disc or beam transmission

equivalents). Percentage scales covering the full ordinate are again used so that any tidal pattern is immediately apparent. The data relevant to these percentage scales, the τ ratios and the predicted $J_h(t)$ curve types are presented in Table 4.9.

Table 4.9: Data illustrated in Figs 4.36 – 4.41, calculated τ and predicted $J_h(t)$ curve types. The turbidity data are: K in Fig.4.36, 1/Zs in Figs 4.37 – 4.40, and c in Fig.4.41.

Figure	Tide			Turbidity		τ	Predicted $J_h(t)$ curve type
	Np/Sp	h(HW)	h(LW)	max	min		
4.36(a)	Np	7.10	4.25	1.549	0.787	0.770	turbidity-dominated
4.36(b)	Sp	6.36	1.95	4.850	0.770	0.731	turbidity-dominated
4.37(a)	Np	7.10	4.25	1.020	0.561	0.864	turbidity-dominated
4.37(b)	Sp	6.36	1.95	1.538	0.541	1.106	(equilibrium)
4.38(a)	Np	7.95	5.30	0.811	0.400	0.589	turbidity-following
4.38(b)	Sp	7.80	3.85	0.884	0.403	0.908	equilibrium
4.39(a)	Np	4.45	1.70	0.646	0.408	1.978	tide-following
4.39(b)	Sp	5.10	1.15	0.546	0.278	1.945	tide-following
4.40(a)	Np	4.20	1.25	10.00	2.443	0.891	equilibrium
4.40(b)	Sp	4.85	0.80	10.00	1.867	1.046	equilibrium
4.41	-	20.43	14.96	12.04	1.17	0.188	turbidity-following

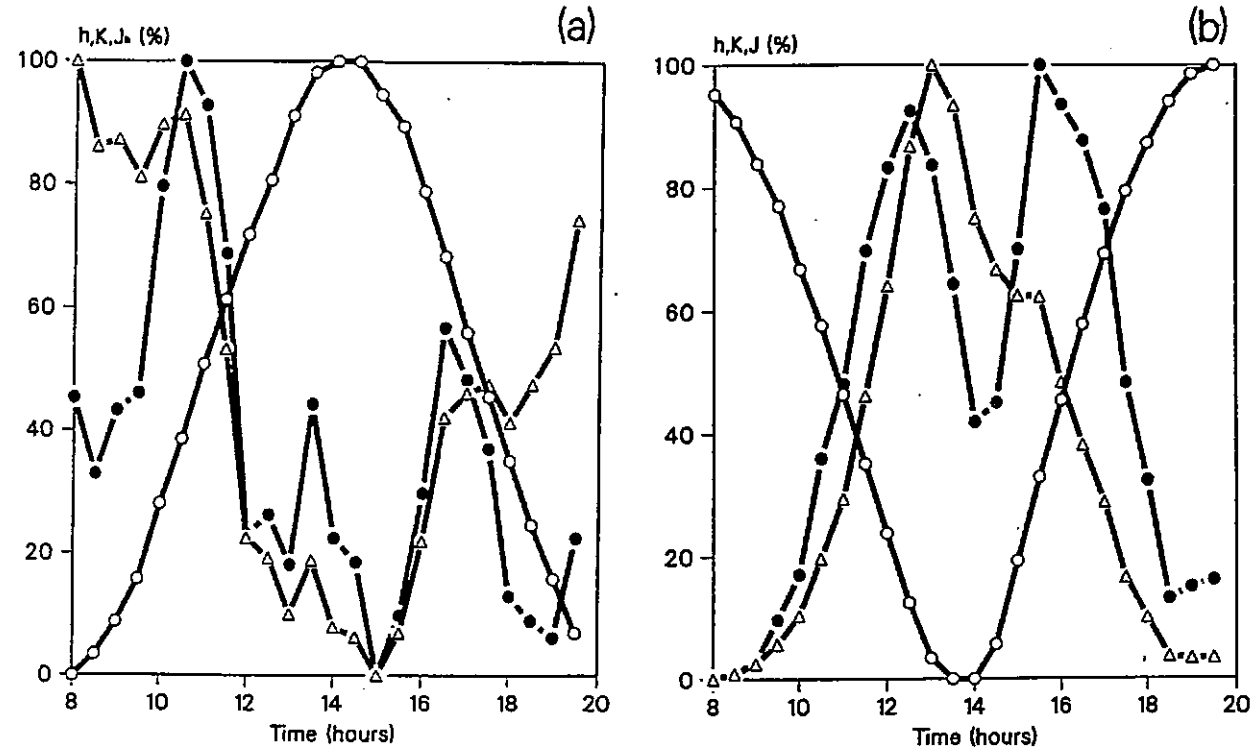

Fig.4.36: Variation in K(t) (Δ), h(t) (O), and J_h(t) (●) at Cargreen (19.7 km), (a) 30 June 82, neaps; (b) 7 July 82, springs

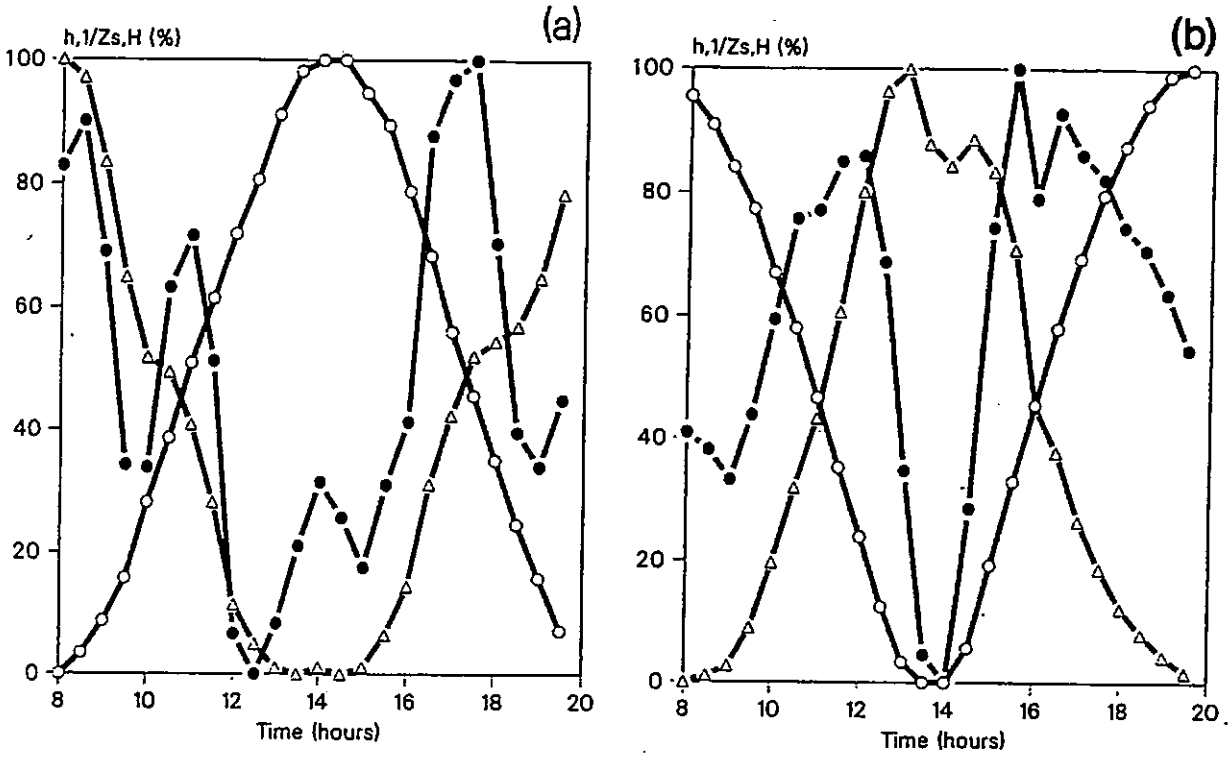

Fig.4.37: Variation in 1/Zs(t) (Δ), h(t) (O), and H(t) (●) at Cargreen (19.7 km), (a) 30 June 82, neaps; (b) 7 July 82, springs

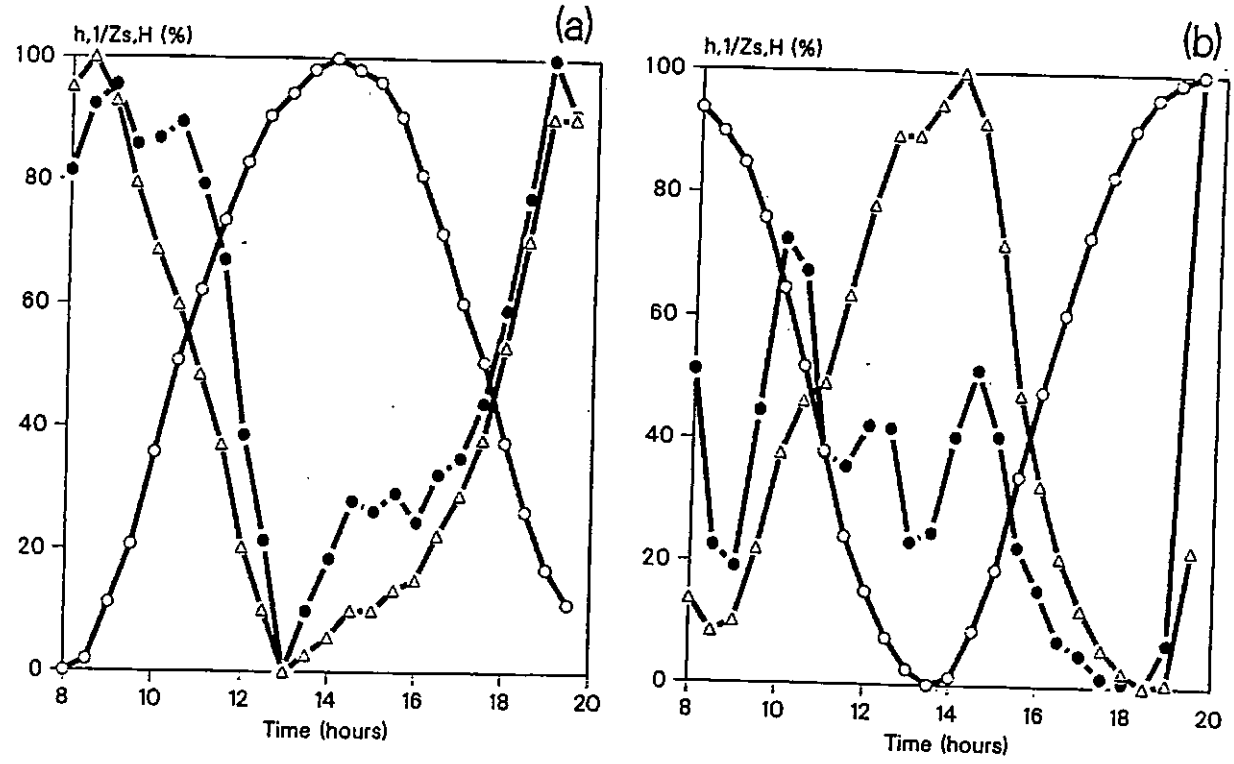

Fig.4.38: Variation in 1/Zs(t) (Δ), h(t) (O), and H(t) (●) at Saltash (23.3 km), (a) 30 June 82, neaps; (b) 7 July 82, springs

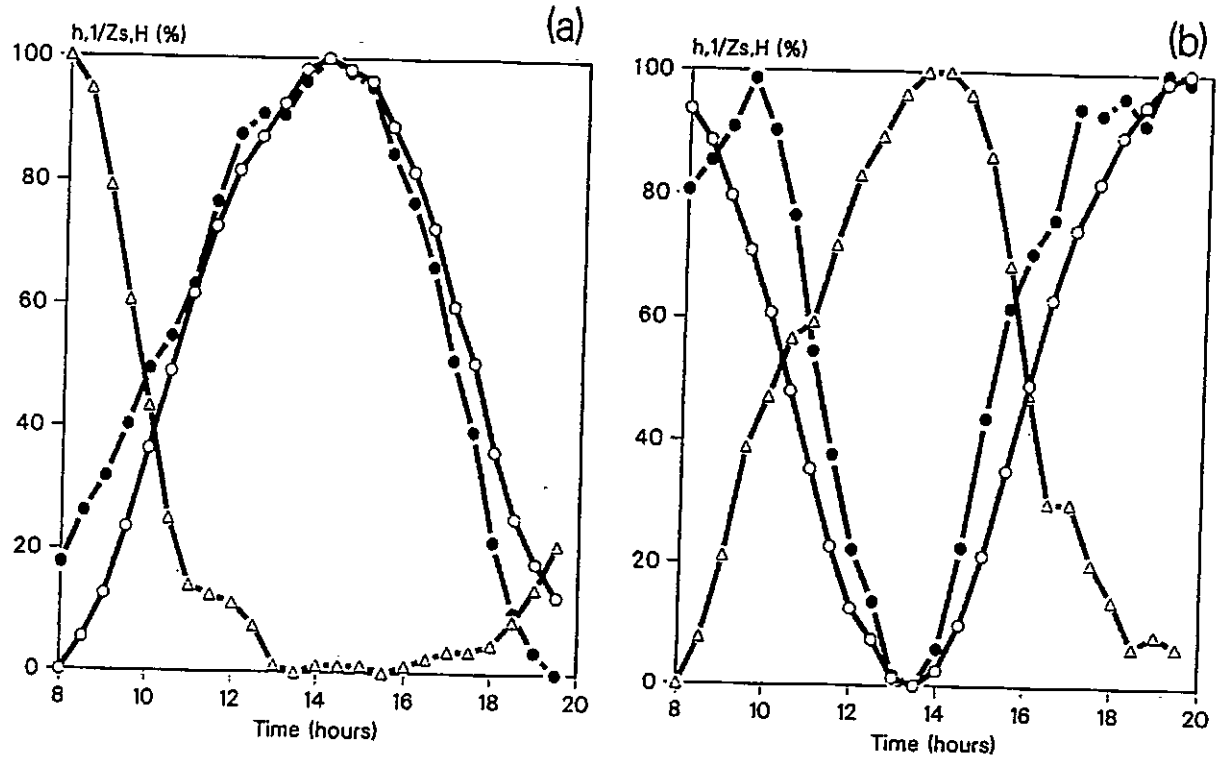

Fig.4.39: Variation in 1/Zs(t) (Δ), h(t) (O), and H(t) (●) at D'port (26.7 km), (a) 30 June 82, neaps; (b) 7 July 82, springs

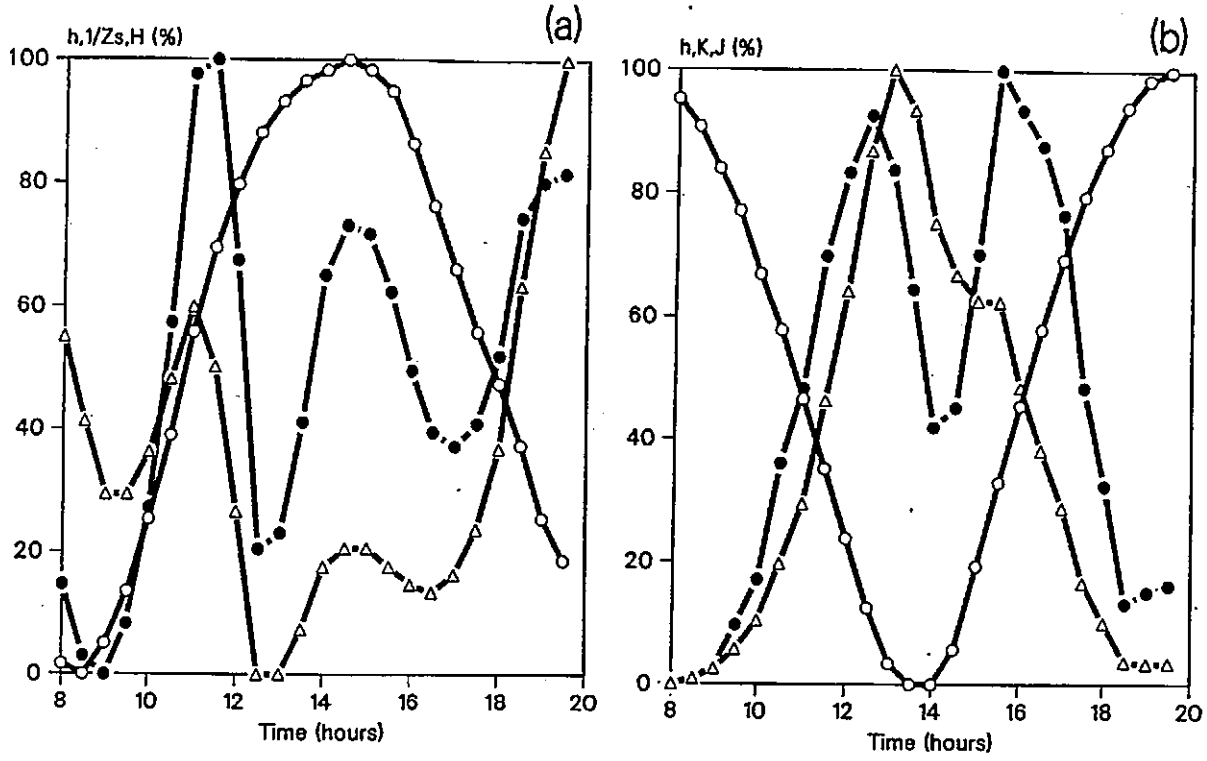

Fig.4.40: Variation in 1/Zs(t) (Δ), h(t) (O), and H(t) (●) at Calstock (8.8 km), (a) 30 June 82, neaps; (b) 7 July 82, springs

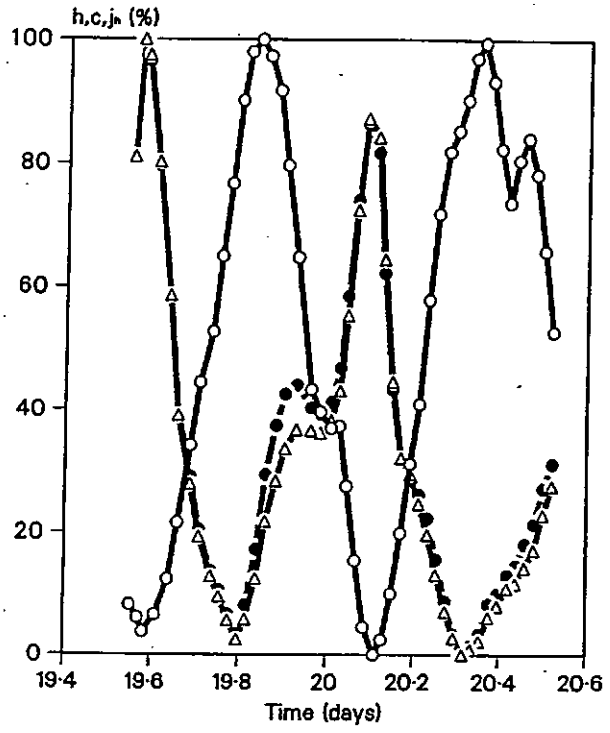

Fig.4.41: Variation in c(t) (Δ), h(t) (O), and γ_h(t) (●) at the Tamar–Lynher confluence (26.0 km), 19–20 March 87

Figures 4.36(a) and (b) show the time series h(t), K(t) and $J_h(t)$ at Cargreen (19.7 km) at neaps (30 June, 1982) and springs (7 July, 1982). From Table 4.9 it is seen that $\tau < 1$, $(\Delta h/\bar{H} < \Delta K/\bar{K})$, in each case, and from Table 4.8 that this turbidity-dominated situation should produce a double-frequency curve with a low J_h at LW and a minimum J_h at HW. This is nicely illustrated in both cases. The same expected pattern is displayed by the neaps scaled-depth curve (Fig.4.37(a)). The springs scaled-depth curve (Fig.4.37(b)) shows the distinct double frequency but H(LW) < H(HW). This may be due to one or two anomalous Secchi depth readings near LW, which would also account for the erroneous 'equilibrium $J_h(t)$' prediction (Table 4.9).

At Saltash (23.3 km), $\tau << 1$ during the neaps observation (Table 4.9). As expected, the H(t) curve closely follows the 1/Zs(t) curve (Fig.4.38(a)) in this turbidity-following situation (Table 4.8). Another turbidity-following situation is shown for the beam transmission observations made at the Tamar-Lynher confluence (26 km); the optical depth curve, $\gamma_h(t)$, follows the attenuation coefficient curve, c(t), almost exactly (Fig.4.41).

At springs at Saltash (Fig.4.38(b)), $\tau = 1$ and we see an equilibrium H(t) curve somewhat distorted by irregularities in the 1/Zs(t) curve.

At neaps and springs at Devonport (26.7 km), $\tau >> 1$, and the curves of H(t) closely follow those of h(t), (Figs.4.39(a) and (b)), as anticipated in this low-turbidity, tide-following situation.

Figures 4.40(a) and (b) present neaps and springs curves obtained at Calstock (8.8 km). Table 4.9 shows that $\tau = 1$ (equilibrium H(t))

on both occasions. Although both H(t) curves display something of a double-frequency pattern, this shape is greatly influenced by the distinct buckle in the 1/Zs(t) curves at LW. This Secchi depth perturbation is to be expected. At this distance up the estuary, mid-tide flow velocities and associated turbulent-suspension turbidities are high; the temporary but marked reduction in 1/Zs at LW must be due to the settling out of larger particles during this period of slack tide. Smaller LW perturbations can be seen in the K, 1/Zs and P curves (Figs.4.33(a) and (b)); it is significant that the associated FFW curves do not display these perturbations.

Chapter 5

SUMMARY AND CONCLUSIONS

The aim of this research programme was to study the optical attenuation coefficients and related optical properties of oceanic and estuarine waters, and the methods of measuring and estimating them. Principally, these are forms of the diffuse attenuation coefficient, $K(\lambda)$, the beam attenuation coefficient, $c(\lambda)$, the absorption coefficient, $a(\lambda)$, the scattering coefficient, $b(\lambda)$, the optical depths, $J(\lambda)$, $j(\lambda)$ and $H(\lambda)$, and the reflectance, $R(\lambda)$. Of special significance are the narrow-band coefficients related to particular conditions of the water, (eg the 450 nm absorption peak of Chl.a), the broad-band attenuation of PAR, and the broad-band photometric coefficients related to vision.

Appropriate and accessible coefficients were studied in two ways: by optical instrumentation (radiometric energy measure, $qs^{-1}m^{-2}$ or Wm^{-2}), and by the visual observation of 'standard' optical targets (photometric measure; lumens m^{-2} = lux). The second approach is not well covered in the literature, and this presented the opportunity of developing improved and novel theory and methodologies.

5.1 DIRECT MEASUREMENTS OF OPTICAL COEFFICIENNTS

In this study, direct measurements of the diffuse attenuation coefficient were obtained from the calculated gradients of the log-irradiance profiles. This was illustrated in Fig.2.7, and expressed by Eqn.2.62: $K = -d/dz(Ln[E(z)])$. Four methods of measuring E(z) were employed in the course of this work, (others are reviewed by Pilgrim and Aiken, 1989); they were: the Biospherical Instruments Inc QSP series Profiling Quantum Scalar Irradiance System measuring $^{o}Eo(z)$, the same instrument modified in house to measure $^{o}Eod(z)$ and $^{o}Eou(z)$, a Højerslev-type Janus pair of sensors, and lastly, both vector and hemispherical sensors mounted on the PML Undulating Oceanographic Recorder.

Some of the earliest recorded irradiance profiles were obtained, near Plymouth, by staff of the Marine Biological Association (Poole, 1925, 1928; Poole and Atkins, 1926, 1928, 1929). Recent work includes measurements in the Western Mediterranean (Højerslev, 1973, 1974a), the Baltic (Højerslev, 1974b), Liverpool Bay (Topliss, 1982), Chesapeake Bay (Williams et al, 1984), the Ems-Dollard Estuary (Colijn, 1982), the Western English Channel (Aiken and Bellan,1968a), the NE Atlantic and Tamar Estuary (Pilgrim, 1987), and an extensive study of Australian waters (Kirk, 1976, 1977, 1979, 1980a, 1980b, 1981a, 1981b, 1983). Clearly, this method is well established in optical oceanography; it has been found altogether satisfactory in the present work.

Particular care must be taken, however, when interpreting the depth

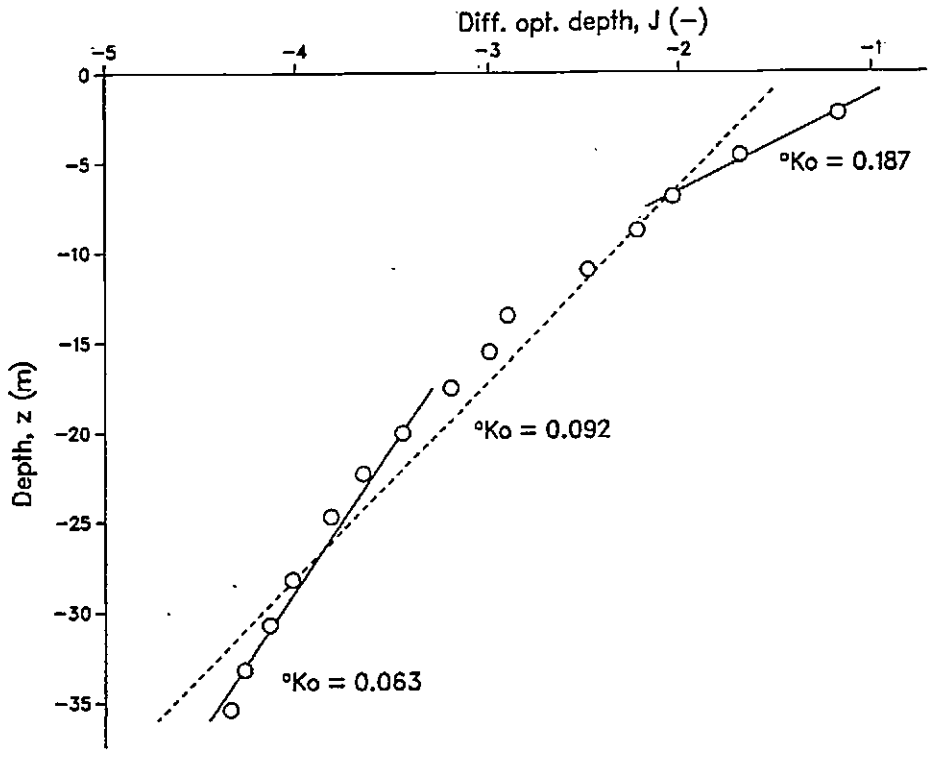

Fig.5.1: Example of a biphasic J(z) profile in clear water, observed in the NE Atlantic before the spring bloom, 6 March 1985.

dependence of broad-band irradiance, such as PAR, in very clear water where the profile is generally biphasic with a higher value of K near the surface. An example of this phenomenon is illustrated in Fig.5.1; the profile was obtained in the clear, pre-bloom waters of the NE Atlantic on 6th March, 1985, (first Frederick Russell cruise). The mean gradient of this profile suggests that $\langle {}^{o}Ko \rangle = 0.092$. Near the surface ($z \leq 7.5m$), however, the water has an extinction coefficient of 0.187, whilst at depth ($z \geq 17.5m$) there is apparently clearer water of $\langle {}^{o}Ko \rangle = 0.063$.

This curiosity is well documented (eg Kirk, 1983) and understood. As solar radiation penetrates a water body, it becomes progressively impoverished in those wavelengths which are absorbed strongly, and so relatively enriched in those which absorb weakly. The diffuse attenuation of PAR is high near the surface where red is strongly

absorbed; it falls to a lower value at depth where the surviving blue is less readily absorbed.

In turbid water there is a tendency for diffuse attenuation to increase with depth due to the flux becoming more diffuse, ie the photons follow longer pathlengths. This effect counteracts that due to the change in spectral composition so that in turbid water it is generally found that the irradiance profile is remarkably linear.

As described in Chapter 3, underwater irradiance measurements obtained by the Biospherical Inc underwater sensor were divided by a sky-light reading to allow for any changes in the sky-light during the profiling period. There is no provision for sky-light monitoring in the UOR system. All of the UOR data included in this present research were obtained in the Norwegian-Greenland Seas in overcast conditions and very steady ambient light (eg see Fig.4.5). However, if the UOR were to be deployed in cloudy-and-clear conditions then significant errors could arise. For example, if the sky-light level were to double or halve during the 2-3 minutes of a half-undulation, then the error in K would be: $Ln[2,\frac{1}{2}]/\Delta z = \pm 0.7/\Delta z$.

Another concern about the performance of the UOR, namely the possibility of self-shading affecting measurements of upwelling irradiance (and hence important reflectance), is dealt with later in this chapter.

Notwithstanding these reservations, experience of using the system during the Lynch cruise, and the subsequent analysis of the collected data, have shown conclusively that the UOR provides by far the best

means of collecting optical data at sea. Working with the Biospherical system in the NE Atlantic (Frederick Russell cruises), it was usually possible to obtain only 2 or 3 profiles each day – for which the ship had to be stopped. The UOR measures two profiles every undulation (ca 5 minutes), for as many hours as is required. Only with a continuously recording system such as this can knowledge be gained of the widespread distribution of optical properties, and perhaps more importantly, the occurrence of local anomalies.

Meaningful measurements of beam transmission, to calculate $c(\lambda)$, can be obtained only from transmissometers of the highest quality and most exacting design. The instrument used throughout this programme was the Sea Tech Inc 25cm path-length transmissometer which operates at 660 nm. A remarkable feature of this excellent instrument is it's stability. Transmissions were successfully logged for 430 hours during the Lynch cruise (see Fig.4.10); although frequent checks were made, recalibration was unneccessary throughout this period.

Transmissometer data must be corrected for forward scattering (see Table 3.1 from Bartz et al, 1978); this correction is very high for turbid water and cannot be ignored.

Unfortunately, Sea Tech Inc transmissometers operate at 660 nm only. There is a great need, in optical oceanography, for high quality transmissometers operating at other wavelengths, eg at 555 nm, the peak of the human photopic spectrum, and at 450 nm, the peak of the Chl.a absorption spectrum.

5.2 INDIRECT MEASUREMENTS AND ESTIMATIONS OF OPTICAL COEFFICIENTS

It has been emphasized throughout this work that the beam attenuation coefficient, $c(\lambda)$, does not bear a fixed relationship to the diffuse attenuation coefficient, $K(\lambda)$. Increased turbidity gives rise to increased scattering, which in turn gives rise to increased path lengths in diffuse propagation, and hence some increase in $K(\lambda)$. In the case of collimated light, however, scattering gives rise to direct photon loss so that $c(\lambda)$ is increased considerably. So, with increased turbidity the ratio c/K must increase.

It must follow, therefore, that $K(\lambda)$ cannot be properly calculated from the more easily measured $c(\lambda)$. However, from the argument above, it is apparent that any empirical equation that is formulated should be of the geometric form $K(\lambda) = f_1.c(\lambda)^{f_2}$, in recognition of the non-linear increase in c/K with turbidity. Three such equations (Eqns.4.5 - 4.7) were presented in Pilgrim (1987) from data collected in the NE Atlantic and Tamar Estuary, for estimating ^{o}Ko from c(660):

All observations; $0.0517 \leq {}^{o}Ko \leq 4.276$

$\langle {}^{o}Ko \rangle = 0.113\ c^{1.288}$ (r^2=0.996, n=37)

Oceanic; $0.0517 \leq {}^{o}Ko \leq 0.2677$

$\langle {}^{o}Ko \rangle = 0.127\ c^{1.575}$ (r^2=0.955, n=14)

Turbid; $0.2902 \leq {}^{o}Ko \leq 4.276$

$\langle {}^{o}Ko \rangle = 0.107\ c^{1.314}$ (r^2=0.927, n=23)

It is theoretically possible to calculate ^{o}Ko almost exactly from a

selection of E(λ) measurements. This was demonstrated in Chapter 4 where values of ⟨°Ko⟩ were estimated from E(λ) measurements obtained by the UOR during Tow 15, Lynch cruise. The UOR was not fitted with a PAR sensor during this cruise, so direct comparison could not be made. An empirical comparison was made through Eqn.4.6, and this cast some doubt on the ⟨°Ko⟩ estimates. The method is theoretically sound; the probable error may be attributed to the fact that each of the E(λ) sensors have a considerable bandwidth which distorts the shape of the constructed spectrum. This is a problem to be considered in future work (see section 5.6).

Kirk's Monte Carlo Method (Fig.2.10) was used to estimate values of $\overline{\cos\xi}(Zm)$, $^{o}a_{o}(Zm)$ and $^{o}b_{o}(Zm)$ from measured values of °Ko(Zm) and °Ro(Zm). Estimates derived from 27 observations were presented in Table 4.2. These were compared to concurrent observations of Zs and c(660), and reasonable correlations were obtained (Eqns.4.25 - 4.29). It is concluded that a Monte Carlo model of this type would be a valuable asset to the hydro-optical work currently under way in Plymouth. However, the model will need a high degree of flexibility to accommodate the diverse problems that will be tested. Also, the model must be based upon parameters which define local, rather than Australian or US, hydro-optical conditions.

As described in 4.3.2, attempts were made, in the North Atlantic and Tamar Estuary, to calculate the average cosine and absorption coefficient from measurements of upwelling and downwelling irradiance obtained from a Højerslev-type sensor-pair (Højerslev, 1975). This sensor-pair is illustrated in Fig.2.8 and 2.9, and was constructed in house using collectors donated by Plymouth Marine Laboratory. These

were identical to the collector described by Aiken and Bellan (1986a) for fitting to the UOR, but modified by masking the tapered base so as to more closely resemble the sensor in Fig.2.8.(e). It is apparent from Fig.4.18 that this experiment was not successful. There was poor comparison between values of $\langle a \rangle$ and $\langle a_o \rangle$ calculated from the Højerslev-type meter data, and values of $\langle {}^{o}a_o \rangle$ estimated from Kirk's Monte Carlo method and measurements of $\langle {}^{o}R_o \rangle$ obtained with a masked Biospherical sensor.

The sensor of Aiken and Bellan (1986a) is almost like sensor (d) in Fig.2.8, and Højerslev (1975) says that the response of this is: ½(Eod + Ed). Of course, the constant ½ is irrelevant in terms of output voltage; the significant factor is the vector component Ed which will decrease from a maximum at $\xi = 0^{o}$ to zero at $\xi = 90^{o}$. Could it be that the sensor responses presented by Højerslev (1975), and reproduced in Fig.2.8, are incorrect? Unfortunately, Højerslev does not provide proofs of his findings, so a simple method of judging the angular response of a diffuse collector has been developed.

The total flux received by an irradiance sensor is the sum, over all angles, of the intensity of the intercepted radiant flux multiplied by the intercept area: $F = Ai \times \int L.d\xi$. As optical constructions are reversible, then the angular reception response of the sensor must be the same as the angular distribution of radiance that it would produce if it were a transmitter. A plot of the angular distribution of tranmitted radiance would then form a curve identical in shape to that of the angular distribution of received radiance. An ideal receiver of radiance is the eye; it must therefore follow that the

response of a sensor at any angle ξ may be judged by 'seeing' the relative size of the exposed sensor area. This method is tested in Fig.5.2 for the five sensors (a)-(e) described by Højerslev (1975) and illustrated in Fig.2.8.

(a) This is a classical pair of back-to-back (Janus) circular cosine collectors. From $\xi = 0$, the collector is seen as a circle (area = 1). For $0 < \xi < \pm\pi/2$, the collector is seen as an ellipse of decreasing area ($L < 1$). At $\xi = \pm\pi/2$ it disappears. For $\pm\pi/2 < \xi \leq \pi$ the eye sees an ellipse increasing in area to a circle. 'Seen areas' are equivalent to radiance, L. A plot of the angular distribution of L produces the expected cosine curve (the upwelling radiance is negative). So, sensor measures Ed,Eu.

(b) This is the classical spherical 4π irradiance sensor. It is seen as a circle ($L = 1$) from all directions. Sensor measures Eo.

(c) The spherical sensor is placed on a black plane. As in the case of (b), it is seen as a circle ($L = 1$) when $0 \leq \xi \leq +\pi/2$. On crossing the plane there is a sharp cut-off and the sphere is not seen ($L = 0$). Sensor measures Eod.

(d) Hemisphere on black plane. It is seen as a circle ($L = 1$) at $\xi = 0$, and as an ellipse of decreasing area ($1 > L > \frac{1}{2}$) when $0 < \xi < \pm\pi/2$. At $\xi = \pm\pi/2$ it is seen as a semicircle ($L = \frac{1}{2}$), followed by cut-off ($L = 0$). Sensor measures $\frac{1}{2}$(Eod + Ed).

(e) This is the well known 'Højerslev collector'. It looks like (d) for $0 \leq \xi \leq \pm\pi/2$. There is no cut off at $\pm\pi/2$; the eye sees a

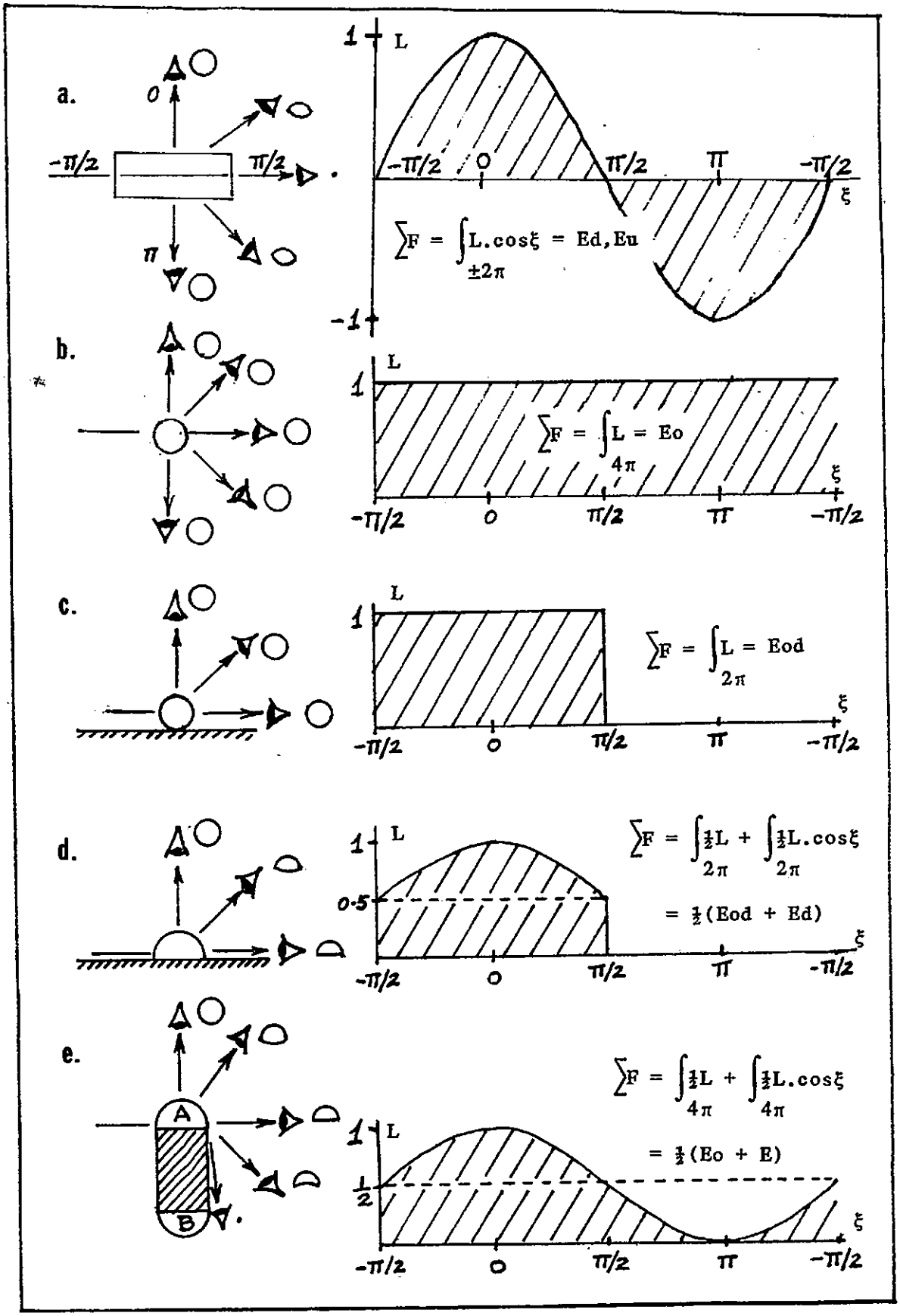

Fig.5.2: Five examples of a proposed 'seen area' method for judging the angular response of a diffuse collector; (these are the same collectors as depicted in Fig.2.8 and 2.9, from Højerslev, 1975)

crescent of decreasing area ($\frac{1}{2} > L \geq 0$) for $\pm\pi/2 < \xi \leq \pi$. From the plot it is to be seen that the angular distribution of L is equivalent to $\frac{1}{2}L + \frac{1}{2}L.\cos\xi$, whence $F = \frac{1}{2}L + \frac{1}{2}L.\cos\xi = \frac{1}{2}(Eo$ E). So, sensor A measures $\frac{1}{2}(Eo + E)$ and sensor B measures $\frac{1}{2}(Eo -$ E).

All of these deductions, (a)-(e), are in total agreement with the findings of Højerslev (1975) as reproduced in Figs.2.8 and 2.9. It is therefore reasonable to suppose that this technique of judging the response of a sensor may be used in the study of any existing light collector (with a diffusing surface), or in the design of new ones. For example, teflon spheres are not easy to produce, and their mounting is fragile. So is there a hemisphere type of sensor that has a response that approximates to, say, type (c)? Seen from $\xi = 0$, the sensor will be circular (area = πr^2). It must therefore have an apparent area of πr^2 when seen from $\xi = \pm\pi/2$. Two possibilities are illustrated in Fig.5.3. One is a hemisphere mounted on a cylindrical base of height $\pi r/4 = 0.785$ r; the other is a cone of height πr.

The original problem remains. On the basis of Fig.5.2, the sensor of Aiken and Bellan (1986a) should have a response somewhere between types (d) and (e), probably more like (d). This has been checked by calibration (Aiken 1988, personal communication), and the anticipated $\frac{1}{2} + \frac{1}{2}\cos\xi$ response has been found. Therefore, there should be much better agreement, in Fig.4.18, between absorption coefficients a and a_o (Hojerslev's method), and $^{o}a_o$ (Kirk's model).

A simple analysis was performed (Table 4.1) on the $K(\lambda)$ data from UOR Tow 15 (Lynch cruise, 1987) to assess the contribution to $K(\lambda)$ by the

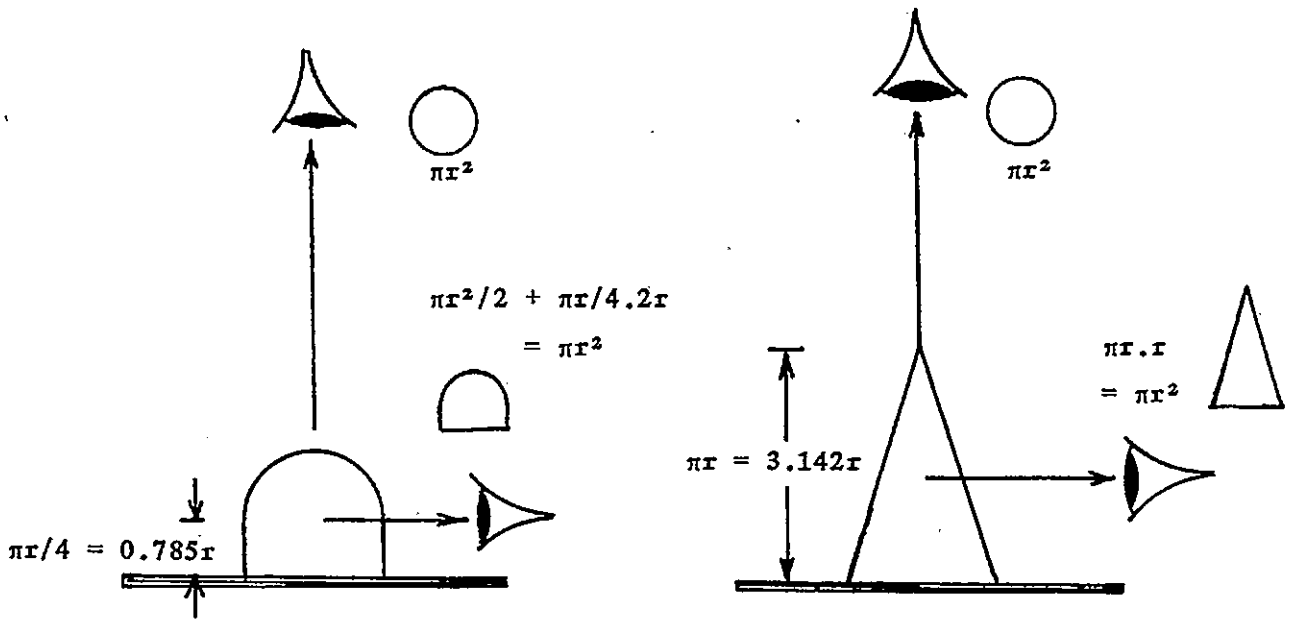

Fig.5.3: Two approximate 2π collectors proposed by means of the 'seen area' method of judging a sensor's angular response

components: water ($K(\lambda)$), planktonic materials measured as chlorophyll concentration ($k_2(\lambda).Chl$), and particles plus dissolved compounds not related to the concentration of chlorophyll ($Kx(\lambda)$). The calculated values of k_2, the specific diffuse attenuation coefficient due to chlorophyll-like pigments associated with chlorophyll, agree closely with those from Smith and Baker (1978b). In the case of λ = 450 nm, it is apparent from Fig.4.7 that for Tow 15 the average value of °Kod is about 0.110 m^{-1}, and from Table 4.1 that Kw(450) = 0.017 m^{-1} and Kx(450) = 0.043 m^{-1}. So, in the particular example considered, the approximate contributions to °Kod(450) were: water 15.5%, chlorophyll and chlorophyll-like pigments 45.5%, and particulates plus non-chlorophyll related compounds 39%.

5.3 MEASUREMENTS OF WATER REFLECTANCE

Since the launch of the Coastal Zone Colour Scanner (CZCS) in 1978, inceasing use has been made, in oceanography, of information gathered by the remote sensing of radiation emanating from the sea surface. The scope of remote sensing is global, and provides a synoptic view of widespread phenomena such as phytoplankon blooms. Radiometers in the CZCS measure in six bands: blue (443±10 nm), green (520±10 nm), yellow (550±10 nm), red (670±10 nm), near infra-red (750±50 nm), and infra-red (11500±1000 nm). The measured radiance is strongly dominated by atmospheric scattering and absorption. Even under favourable conditions, this may be as much as 80% in the red and 90-95% in the blue, so that subsurface optical properties change the measured radiance by only 10-20% or less (Sørensen, 1981). Of this emergent flux, about 90% originates from the first diffuse optical depth, J = 1/K, (Kirk, 1983).

Values of upward radiance may be of interest in themselves; however, by far the most important use of remote sensing is in assessing the concentrations of optically significant constituents in the surface layer: plankton, suspended sediments, dissolved materials etc. It is the task of the optical oceanographer to study and measure the relationships between the spectral quality of upwelling light and the particular hydrological conditions of the water: physical, biological and/or chemical. The quality of upwelling light must also depend upon that of the downwelling field, and this will vary with cloud cover, sun's altitude etc. The hydrological influence of interest may be isolated by dividing the upwelling by the downwelling flux,

and this amounts to measuring the water's irradiance reflectance: $Ro(\lambda,z) = Eou(\lambda,z)/Eod(\lambda,z)$, where $z \to 0$.

It is to be expected that reflectance will increase with an increase in backscattering, and decrease with an increase in the absorption of downwelling photons; in fact $R \propto b_b/(a+b_b)$, (Kirk 1983). As $b_b << a$ in natural water, then this may be simplified to: $R \propto b_b/a$, eg Prieur (1976) proposes the approximation: $R(0) = 0.33\ b_b/a$. Kirk (1981a) found that R(0) increases with decrease in the sun's altitude, and proposed the very similar expression: $R(0) = f.b_b/a$, where f = 0.328, 0.391, 0.449, for sun's altitude = 90°, 45°, 30°. Both the diffuse attenuation cofficient, Ko, and the Secchi coefficient, Zs^{-1}, must increase with b_b/a (eg see Fig.2.10). It is therefore to be expected that reflectance will increase with an increase in Ko or Zs^{-1}, assuming that scattering material is present, (Gordon and Clark,1981, have shown that in water containing pigments only, then reflectance increases in the red and decreases in the blue with increase in pigment concentration, whilst in the green and blue-green it is unchanged).

Water reflectances were obtained by four different methods in the course of this research, and these produced five different types of reflectance measurement: °Ro(Zm), Rp, $\langle R(\lambda,z)\rangle$, $\langle Ro(\lambda,z)\rangle$ and $\underline{R}$. These data are summarised in Fig.5.4, from which the following conclusions may be drawn:

(i) The expected overall increase in °Ro(Zm), Rp(z) and $\underline{R}$, with turbidity, is apparent.

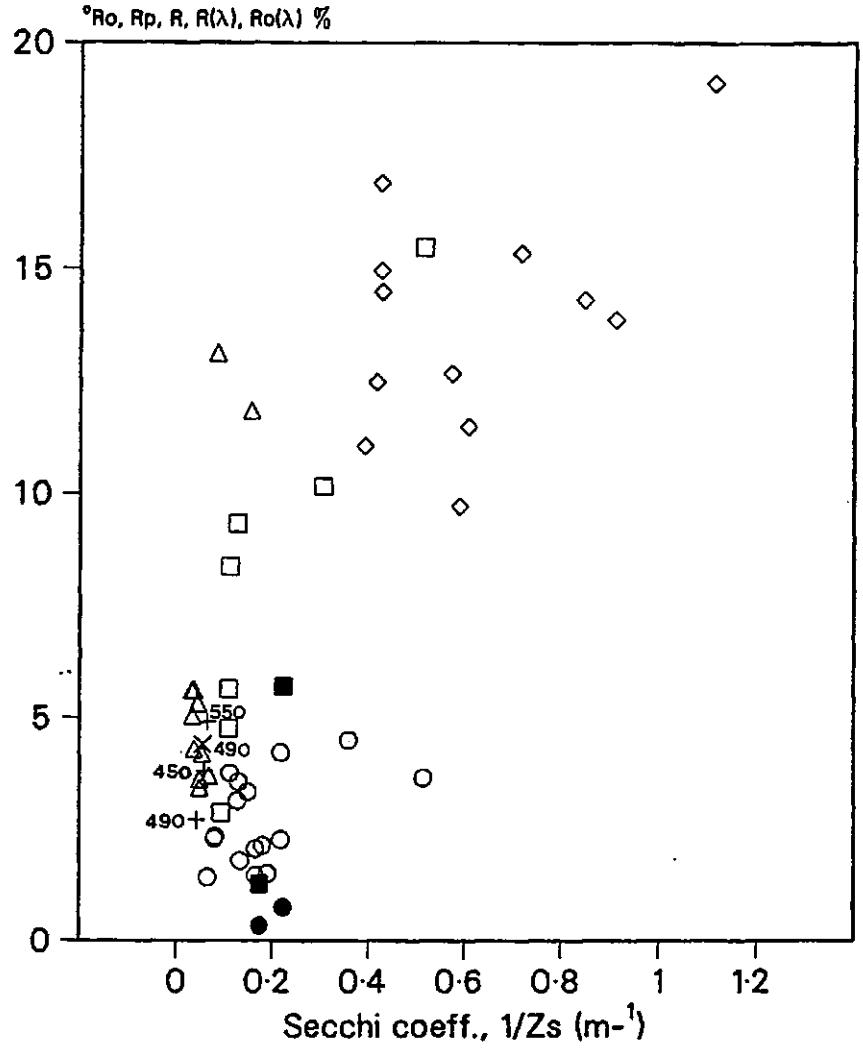

Fig.5.4: Summary of measured water reflectances. Symbols are:

△,◇ °Ro(Zm) measured by adapted Biospherical irradiance meter in the NE Atlantic (△) and Tamar Estuary/Plymouth Sound (◇). These data were listed in Table 4.2.

○,● Rp(z) measured by hand-held (diver) photometer in Plymouth Sound (○) and Burrator Reservoir (●). These data were plotted in Fig.4.26.

□,■ R calculated (Eqn.4.120) from visual observations of Zx and Zh in Plymouth Sound (□) and Burrator Reservoir (■).

+450,+490,+550,X490
Average values of $\overline{Ro(450,z)}$, Ro(490,z), Ro(550,z) and R(490,z) measured by $\overline{UOR}$ during tow 15, Lynch cruise 1987.

Where °Ko or K(λ) but not Zs was measured, then conversion for plotting was by: K.Zs = 1.48 (Eqn.4.123)

(ii) This trend is particularly marked in the °Ro(Zm) data which cover the full range of the plot. In the Tamar Estuary and Plymouth Sound, °Ro(Zm)$\geq$9.6%. In the NE Atlantic, °Ro(Zm)$\leq$5.6%, except for two very high values, 11.9% and 13.1%, which were measured at a station 70 n.miles west of the Scillies in water that was rich in coccoliths. The sea surface appeared remarkably 'milky white' at the time.

(iii) As noted earlier, in discussing Fig.4.26, reflectances measured in Burrator Reservoir (● and ■) are markedly low. This is because of the strong absorption of short-wave irradiation in water rich in dissolved organics (Gelbstoff), but low in particulate (scatterer) concentration, as described by Gordon and Clark (1981). (In fact, a decrease in $\underline{R}$ must also increase the inherent contrast of the Secchi disc and lead to a corresponding increase in Zs. However, Eqn.2.94 or inspection of Table 2.3 shows that a decrease in $\underline{R}$ gives rise to a proportionally smaller increase in Fs, eg Ct = 2, $\underline{\rho}$ = 80, $\underline{R}$ = 10, Fs = 5.858; but Ct = 2, $\underline{\rho}$ = 80, $\underline{R}$ = 5, Fs = 6.620).

5.4 VISIBILITY OBSERVATIONS

In the visibility work carried out in the course of the present study, it was recognised that since underwater visibility is limited by the attenuation coefficients $\underline{c}$ and $\underline{K}$, then diver observations of targets of known optical quality provide a means of estimating these coefficients and other closely related parameters. The most useful of these are summarised, in Table 5.1, for each of four categories: diver/surface observer, and theoretical/empirical. Where more than one approach is possible then only the best, as determined by this study, is listed; for example, measurements based upon Method V are preferred to the use of Duntley Discs. Three points of particular note, from Table 5.1, are:

- Methods (vii)-(xi) use the new types of targets introduced in this study.

- Methods (vii) and (viii) are presented as preferred alternatives to using a Secchi disc. Unlike the Secchi depth equation (Eqn.2.94), neither (vii) nor (viii) requires an estimate of the disc reflectivity, $\underline{\rho}$, or water reflectance, $\underline{R}$.

- Method (xiii) is a proposed alternative to (xii), the traditional Secchi disc equation, for use in very turbid waters ($Zs<2$ m; $Zs^{-1}>0.5$ m). It allows for the significant increase in reflectance, $\underline{R}$, that occurs in high turbidity water. Equations for (xii) and (xiii) are plotted together in Fig.5.5

Table 5.1: Summary of recommended threshold visibility methods

	to find	measure	Equation	
DIVER ONLY				
Theoretical				
i	$\underline{c}$	Vh	$\underline{c} = 3.9/Vh$	(4.83)
ii	$\underline{K}$	Vh,Zh	$\underline{K} = 3.9\left[\frac{1}{Zh} - \frac{1}{Vh}\right]$	(4.89)
iii	$\underline{c}/\underline{K}$	Vh,Zh	$\underline{c}/\underline{K} = Zh/(Vh - Zh)$	(4.88)
Empirical				
iv	$\langle°Ko\rangle$	Vh	$\langle°Ko\rangle = 1.23/Vh$	(4.131)
v	Ze	Vh	$Ze = 3.7\ Vh$	(4.130)
vi	Vis	Vh	$Vis = 1.17\ Vh$	(4.133)
SURFACE OBSERVER				
Theoretical				
vii	$\underline{c} + \underline{K}$	Zh	$\underline{c} + \underline{K} = 3.9/Zh$	(4.107)
viii		Zf	$\underline{c} + \underline{K} = \frac{Ln[1-\underline{T}] + 3.9}{Zf}$	(4.109)
ix	$\underline{\rho}$	Zs,Zx	$\underline{\rho} = \exp\left[\frac{3.9}{Zh}(Zs - Zx)\right]$	(4.119)
x	$\underline{R}$	Zh,Zx	$\underline{R} = [(0.02\ \exp[3.9\ Zx/Zh]) + 1]^{-1}$	(4.120)
xi	Ct	Zf,Zh	$Ct = \exp\left[\frac{-Ln[1-\underline{T}]}{Zf/Zh - 1}\right]$	(4.121)
Empirical				
xii	$\underline{c} + \underline{K}$	Zs	$\underline{c} + \underline{K} = 6\ Zs^{-1}$	(4.99)
xiii			$\underline{c} + \underline{K} = 4.8\ Zs^{-0.84};\ (Zs \leq 2)$	(4.101)
xiv	$\underline{c}$	Zs	$\underline{c} = 4.8\ Zs^{-1}$	(4.95)
xv	$\underline{K}$	Zs	$\underline{K} = 1.2\ Zs^{-1}$	(5.1)
xvi	$\langle°Ko\rangle$	Zs	$\langle°Ko\rangle.Zs = Js = 1.5$	(4.128)
xvii	Ze	Zs	$Ze = 3\ Zs$	(4.129)
xviii	Vh	Zs	$Vh = 0.83\ Zs$	(4.103)
xix	P	Zs	$P = 24.7\ Zs^{-1} - 9.16$	(4.134)

V,Z = horizontal and vertically downward threshold visibilities
h = light trap
f = neutral filter
s = Secchi disc
x = corner reflector

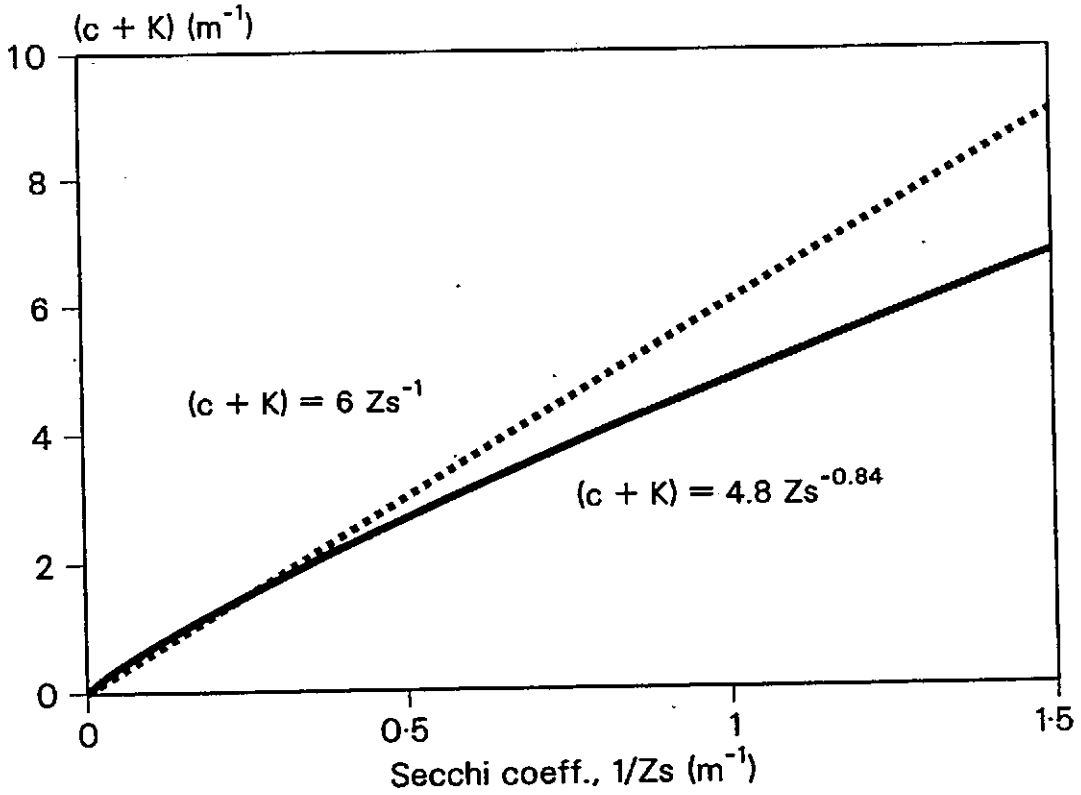

Fig.5.5: Comparison of Secchi disc equations for photometric c+K

5.5 TIDAL VARIATIONS IN THE DIFFUSE OPTICAL DEPTH

In subsection 4.5, the curious and unexpected phenomenon of tidal variation in light penetration to the bed of an estuary was examined in some detail. It was demonstrated that the combination of sinusoidally varying water depth and turbidity results in a sinusoidal variation in the diffuse optical depth of the bed at double the tidal frequency. A range of possible curves of light penetration with time were illustrated in Fig.4.35 and, for clarity, were classified in Table 4.8 as: Tide-following, Tide-dominated, Equilibrium, Turbidity-dominated or Turbidity-following. Predicted curve types were found in data obtained in the Tamar Estuary, as illustrated in Figs.4.36-4.41, and detailed in Table 4.9. It is worth noting here that suitable data for analysis can be obtained with the simplest of instrumentation: a Secchi disc and a sounding lead!

The question arises as to whether these findings are applicable outside of the estuarine system, and whether these cyclic variations in light level occur in clearer coastal waters. This phenemenon must occur where waters are tidal and matched by a significant tidal variation in turbidity; for example, off headlands where high tidal velocities and associated sediment resuspension may occur at mid-tide. Suppose that there is an 8% variation in K, ie $\Delta K/K = 0.08$, and a tidal range (Δh) of 4m. It follows that there will be an equilibrium type variation (curve a, Fig.4.35) at a depth of 50 m where $\tau = (\Delta h/h)/(\Delta K/K) = 1$. At shallower depths ($\tau>1$) there will be a tide following/dominated pattern (curve b,c). In deeper water ($\tau<1$) the cyclic variation will be turbidity following/dominated; of

course, it is assumed that $\overline{K}$ is low enough to allow light to penetrate to these depths.

The magnitude of the variation, ΔJh, in the diffuse optical depth, is given by:

$$\Delta Jh = \overline{h}.\overline{K} - (\overline{h} + \tfrac{1}{2}\Delta h).(\overline{K} - \tfrac{1}{2}\Delta K)$$
$$= \tfrac{1}{2}\overline{h}.\Delta K - \tfrac{1}{2}\overline{K}.\Delta h + \tfrac{1}{4}\Delta h.\Delta K$$

but in equilibrium conditions: $\Delta h/\overline{h} = \Delta K/\overline{K}$, in which case $\tfrac{1}{2}\overline{K}.\Delta h = \tfrac{1}{2}\overline{h}.\Delta K$, so that:

$$\Delta Jh = \tfrac{1}{4}\Delta h.\Delta k \qquad (5.2)$$

$$\frac{\Delta Jh}{\overline{Jh}} = \frac{1}{4} \cdot \frac{\Delta h}{\overline{h}} \cdot \frac{\Delta K}{\overline{K}} \qquad (5.3)$$

In the example quoted above, where $\Delta K/\overline{K} = \Delta h/\overline{h} = 8\%$, then $\Delta Jh/\overline{Jh} = 0.16\%$. The effect of a 0.16% change in Jh will, of course, depend upon the actual value of $\overline{Jh}$; in this example it will depend upon the prevailing value of $\overline{K}$. Suppose that $\overline{K} = 0.1$ (equivalent to a Secchi depth of about 15 m), so that at 50 m depth:

$$\frac{E_{max}}{E_{min}} = \frac{E(0).\exp[-Jh_{min}]}{E(0).\exp[-Jh_{max}]} = \frac{\exp[-0.104 \times 48]}{\exp[-0.1 \times 50]} = 1.01$$

and $\overline{Jh} = 0.102 \times 49 \simeq 5$

So, in this example ($\overline{h} = 50$, $\Delta h = 4$, $\overline{K} = 0.1$, $\Delta K = 0.008$), there will be an equilibrium type cyclic variation in the diffuse optical depth. However, the amplitude of this variation will amount to only about 1% of the light level at that depth. The mean light level at 50 m will

be 0.7% (Jh = 5) of the surface intensity, (the 1% level is at 46 m).

Other possible combinations of $\overline{h}$,$\overline{K}$ and ΔK which produce an equilibrium type variation in Jh from a 4 m tidal range, may be extracted from Fig.5.6. The graph also gives the ratio E_{max}/E_{min} and the aproximate Secchi depths from Eqn.4.128. For example, suppose that over a tidal cycle $0.5 \leq K \leq 2.5$; entering Fig.5.6 with $\overline{K} = 1.5$ and $\Delta K = 2$ shows that an equilibrium type variation will occur at a depth of 3 m, and that the maximum light levels (occurring at HW and LW) will be 7.4 times the minimum (occurring at mid-tide).

The shaded part of Fig.5.6 is an impossible, no-go area which would involve negative values of h and K. Also plotted on the diagram, are curves of J = 4.6,18,34. The J = 4.6 curve represents the approximate limit of net primary production (J = 4.6 is equivalent to 1% of surface illumination). Photosynthesizing organisms will therefore experience an equilibrium type varation only within the area bounded by this line and the shaded corner. Most of this permitted area specifies shallow, turbid water with a large tidal variation in turbidity, ie typical estuarine conditions. The bottom part of the area shows that equilibrium type conditions are possible in deeper, clearer waters; however, below about 30 m the amplitude of variation (E_{max}/E_{min}) may be too small to have any significant effect upon photosynthesis.

According to Parsons *et al* (1977), colour vision is possible to a diffuse optical depth of about J=18, and detection of light by man or deep sea fish is limited to $J \leq 34$. These curves are also shown on

Fig.5.6, from which it is apparent that significant tidal variations in light levels appropriate to the visual responses of animals could occur over a wide range of turbidities and depths in coastal waters.

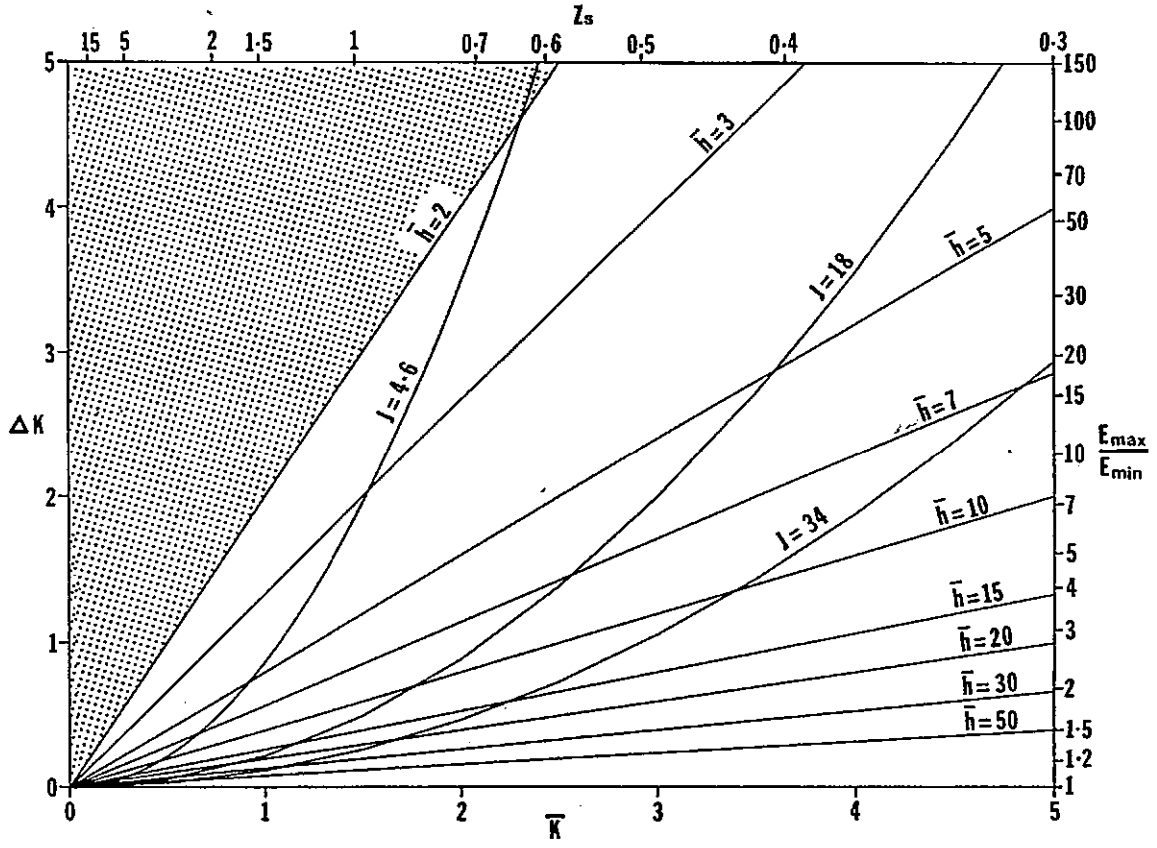

Fig.5.6: Possible combinations of h, K (or Zs) and ΔK which will produce equilibrium type variations in the diffuse optical depth of the bed, Jh(t), with a 4 m tidal range; the three J curves represent the approximate limits of net photosynthesis (4.6), colour vision (18) and detection by man and deep sea fishes (34)

5.6 FUTURE WORK

The most valuable conclusion that can be drawn from this programme of study is that there are clearly identifiable areas of hydro-optical research that urgently require further work. The six most important are now discussed, and it will be apparent that these proposed programmes are closely interrelated.

5.6.1 UOR instrumentation and data analyses

Among the biologically most significant hydro-optical parameters is $^{o}K_{o}$, the 4π diffuse attenuation coefficient in the 350-700 nm PAR band (UNESCO, 1965). In Chapter 4, several methods of estimating broadband PAR from simpler measurements were considered and tested. If the UOR were to carry a 350-700 nm quantum sensor fitted with a scalar collector, then this would provide the means of fully testing several estimation methods over a wide range of hydro-optical conditions. (Because self-shading by the UOR may affect the measurement of upwelling irradiance, it would be best to fit only an upward-looking sensor, and measure $^{o}E_{od}$). Four estimation methods, (i)-(iv), which could then be tested are now considered.

(i) In Chapter 4, a method was proposed for constructing the full PAR quantum spectrum from available $E(\lambda)$ data, (see Fig 4.12). It was recognised that the bandwidths of the $E(\lambda)$ measurements may give rise to some uncertainty. Given proper $^{o}E_{o}$ data for

comparison, then this problem could be fully analysed and a better algorithm deduced.

(ii) A very attractive proposition is that of finding a good correlation between °Eo and a single E(λ) measurement. Such an algorithm would be very valuable in the analysis of remote sensing data. Jerlov (1974) has proposed a method by which °Eo may be estimated from E(465).

(iii) Højerslev and Jerlov (1977) have proposed a method of estimating quanta irradiance from the colour index, F, at 1m depth, where: $F(z=1) = [Lu(450,1)/Lu(525,1] \simeq [Eu(450,1)/L(525,1)]$.

(iv) In Chapter 4, °Ko data were compared to surface measurements of the beam attenuation coefficient, c, at 660 nm. A more reliable comparison could be made, especially in coastal and estuarine waters, by mounting the beam transmissometer on the UOR. The Sea Tech Inc transmissometer is fitted with a bracket for this purpose.

It is to be noted that methods (ii) and (iii) are strongly dependent upon the measured water having an absorption spectrum which conforms to the scheme of water types specified by Jerlov (1976). These methods may prove less useful in the study of hydro-optical anomalies such as may occur at an oceanic front or in coastal/estuarine waters. Of course, a similar reservation must be made in the case of method (iv).

5.6.2 Water reflectance and the problem of instrumental self shading

In discussing the measurement of water reflectance, and its relevance to obtaining ground truths for remote sensor calibration, it was noted that nearly all of the remotely detectable flux comes from within the first diffuse optical depth of the surface. It is vital, therefore, that sound techniques be used in measuring upwelling and downwelling radiances/irradiances, and hence reflectances, at a minimum practical depth below the sea surface. This constraint gives rise to three hydro-optical problems which call for early investigation:

(i) There are serious physical difficulties associated with near-surface measurement, particularly in bad weather. With depth, however, there must be changes in $R(\lambda)$ due to the vertical structure of the water column. The question therefore arises as to what is the maximum depth at which meaningful measurements of reflectance can be obtained.

(ii) Having discovered, from (i), how shallow the sensors must be set, how is this to be done? Are data obtained during, or at the top of a normal UOR undulation adequate, or must the UOR or similar sledge be towed much closer to the surface? Must a special vehicle be developed?

(iii) In Chapter 3, the problem of self-shading by an instrument as large as a UOR was considered. It was estimated (Eqn.3.5), that over 85% of the measured upwelling light comes from within a distance of one diffuse optical depth of the sensor.

It was then suggested that this could present a real problem at long wavelengths and/or in turbid waters. It is proposed that a temporary boom be extended from the UOR to locate a pair of sensors well clear of any shading. Reflectance data from these sensors could then be compared to that obtained from an identical pair fitted to the body of the UOR.

5.6.3 Underwater visibility theory and measurements

The study of underwater visibility has made a significant contribution to this programme of research. Some published theory has been found wanting, and improvements have been proposed. Novel methodologies for use by divers and surface oceanographers have been recommended. In all this work it has been assumed that the basic theory of underwater visibility, and especially contrast visibility as provided by Eqn.2.76, is correct. However, there are aspects of this simple equation which give rise for concern. For example, it implies that the inherent contrast of a non-reflector, eg a light trap, is -1 no matter what the background luminance. It also implies that when the background is absolutely black, then the inherent contrast is ∞ for a target of any reflectivity. From Duntley's contrast transmission law (Eqn.2.83 and Fig.2.13), the apparent contrast must also be ∞ at any distance r. In fact this has no practical meaning underwater where, in the presence of illumination, the background cannot be absolutely black since this would imply zero-scattering water. Always, $\beta(\sigma) \neq 0$, so there must always be some background space-light, L^*. But what if this is very low, as in very clear water?

Also, it would be useful to examine the inherent contrast equation (Eqn.2.76) in the more common situation in which neither the target nor the background is black, but rather different intensities of the same tone. The real situation may be further complicated by the fact that the underwater environment is rarely absolutely monochromatic, (Lythgoe, 1988, personal communication).

Another underwater visibility problem concerns the effect of the ambient light level upon the observer's threshold contrast. Consider, as a practical example, the Secchi disc equation (Eqn.2.94):

$$Zs = \frac{Ln\left[\frac{\rho/\underline{R} - 1}{Ct}\right]}{\underline{c} + \underline{K}}$$

The inherent contrast of the disc is represented by the constant term ($\rho/\underline{R}$-1). The threshold contrast, Ct, varies with the observer and the observing conditions, including the ambient light level. There must be an increase in threshold contrast to account for the obvious and observable decrease in Secchi depth that occurs at low ambient light levels. It is unlikely that this phenomenon has had a significant effect upon the measurements obtained so far in the course of this research, as all of the observations were made in near-surface waters in fairly bright conditions. However, if these studies are to be applied to low ambient light situations, such as the visibility of fishing nets in deeper, darker waters, then Ct can no longer be considered constant.

Clearly, there is a need to re-examine the theory and practical

applications of inherent and threshold contrasts underwater, but in controlled conditions of illumination (intensity, wavelength and bandwidth), water transmission (type of dissolved substances, and particle type, size and size distribution), and target-background colour and intensity. This will not be achieved in the field, and so a laboratory model is presently under construction; see Fig.5.7.

Basically, the visibility tank is a long aquarium-type vessel with the bottom, ends and one side comprising of frosted, mirrored glass. These surfaces will maintain the diffused light field emanating from the controlled light source via the frosted glass side of the tank. The target-background will comprise of neutral filters sandwiched between perspex sheets. This arrangement will avoid all the problems associated with sidelighting (eg see Fig.4.22, and Eqn.4.78), and with the measurement of target and background reflectivity. A miniature light trap and corner reflector may also be used. The water may be natural, diluted natural or, more likely, made up with exact concentrations of known particles and dissolved organics and/or inorganics. The water will be circulated through a spectrophotometer and/or transmissometer flow cell to obtain spectral and transmission information. Ambient light levels within the tank will be monitored by means of a photometer with a photometric response spectrum, (UDT model PIN 10AP).

It is anticipated that many useful experiments will be possible with this visibility tank. Initially, however, attention will be directed towards the two problems outlined earlier:

(i) A more comprehensive definition of inherent contrast

(ii) A study of the variation in threshold contrast with such factors as: different observers, different conditions of light-dark adaptation, different types and conditions of face mask and, particularly, different levels and spectral quality of ambient light.

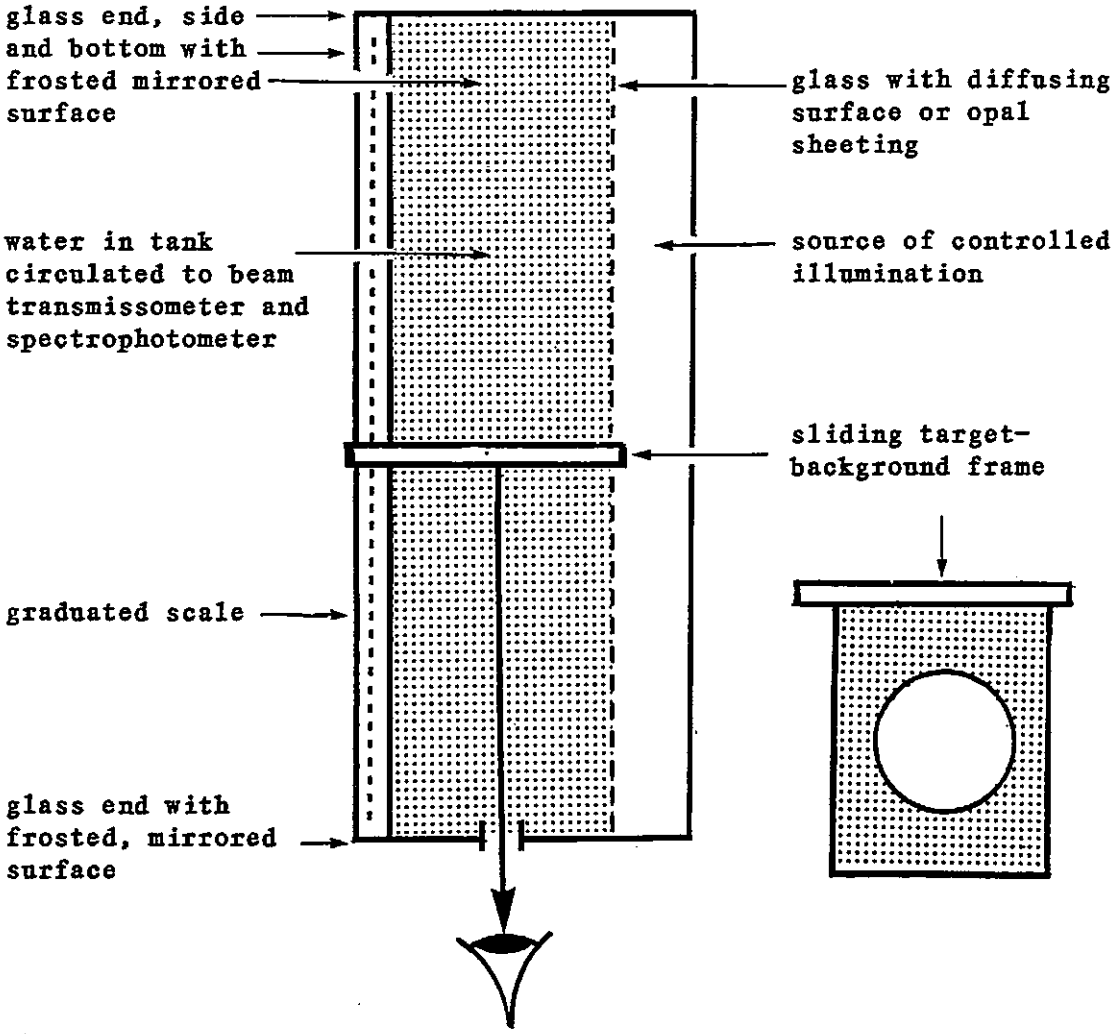

Fig.5.7: Plan view of proposed visibility tank, presently under construction

Visibility experiments in the sea will certainly continue; for example, the results of visibility tank experiments will need to be

confirmed in the field. Also, use of the corner reflector + light trap + neutral filter disc suite of targets from a surface boat, (rather than diver), has yet to be tested. The equations concerned were presented in Table 4.6. Of particular interest will be the calculation of water reflectivity, R, by Eqn.4.120, and the observer's threshold contrast, Ct, by Eqn.4.121.

The inspiration for this whole study originated in an underwater investigation of the problem of 'ghost net' fishing by lost and abandoned monofilament gill nets in shallow water (Pilgrim et al, 1985). Subsequently, attempts were made to produce equally invisible nets by colour-pattern camouflage of environmentally more acceptable multifilament netting. Results of these experiments were promising, but statistically inconclusive. This potentially valuable work will be reassessed and continued in the field and in the visibility tank.

5.6.4 Influence of particle size and size distribution upon light propagation

Optical turbidity is a function of at least the following parameters: particle concentration, particle size, particle shape, particle size distribution and particle mineral (refractive index). Moreover, particle size, shape and refractive index must be greatly influenced by the scale and nature of any organic or inorganic coating (Glegg et al, 1985), and these will vary in the environment with: location, depth, state of tide, river flow and salinity (flocculation). These variables cannot be selected to order in the field. To study their effect upon optical turbidity it will be necessary to design a

laboratory model, and then to contrive turbidities of selected and controlled minerals, sizes, distributions and concentration. The effect of particle variation upon the beam attenuation coefficient and upon visibility problems may be studied in the transmissometer flow cell and visibility tank described earlier in this chapter. But what of the diffuse attenuation coefficient, K?

Friedman et al (1981) have discussed the problem of measuring the absorption coefficient of turbid water by spectrophotometer; a systematic error results from the increased path lengths followed by scattered particles. Bricaud et al (1981) have noted that even after filtration, seawater remains a scattering medium so that the coefficient obtained from a conventional spectrophotometer is intermediate between $a(\lambda)$ and $c(\lambda)$. It may follow, therefore, that if a spectrophotometer cell were so designed that all of these scattered photons were collected by the receiver, then this measure would be equivalent to the attenuation coefficient for diffuse light, $K(\lambda)$. Shibata (1959) has described seven representative types of attenuance (see Table 5.2) by assigning a preceding subscript to indicate the nature of the incident light, and a following subscript to describe the nature of the light after it has passed through the sample. Rectilinear attenuance, cAc, is the attenuance that would occur in a spectrophotometer when measuring a non-scattering sample; simply, cAc is the generally sought absorbance. Quasi-attenuance, cEf, is of significance to the proposed method of measuring $K(\lambda)$. It is illustrated in Fig.5.8, and is now considered in further detail.

Some of the collimated incident light, cI, is neither absorbed nor scattered, and reaches the detector as Ic. Some fraction, $0<f<1$, of

Table 5.2: Seven types of attenuance (Shibata, 1959)

Type of Attenuance	Incident light Collimated	Diffuse	Definition
Rectilinear	cAc	-	Ln[Io/Ic]
Quasi-	cEf	-	Ln[Io/(Ic + f.Id)]
Semi-integral	cEt	dEt	Ln[Io/It]
Integral	cEtr	dEtr	Ln[Io/(It + Ir)]
R-corrected	crEt	drEt	Ln[(Io - Ir)/It]
Reflex 0<f<1 and Ip+Id = It	cEr	dEr	Ln[Io/Ir]

c = collimated; d = diffuse; r = reflected; t = total transmitted; f = measured fraction of the total diffuse light (0<f<1)

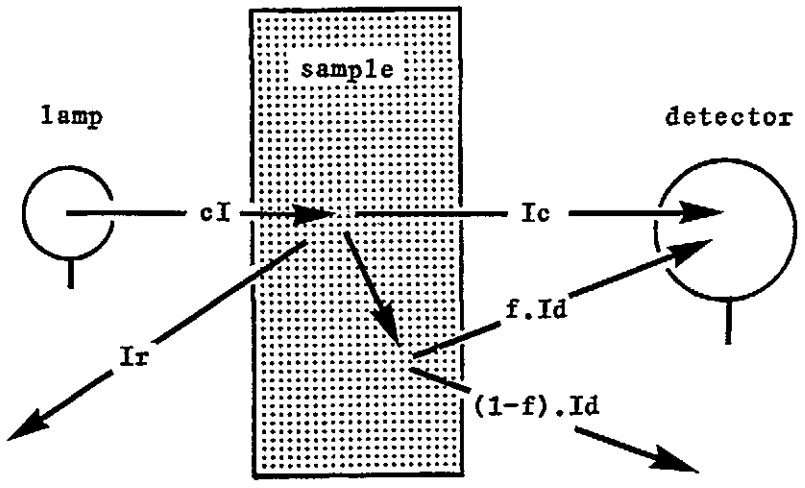

Fig.5.8: The optics of quasi-attenuance measurement in a spectrophotometer (Shibata, 1959).

cI will be scattered into the acceptance angle of the meter as diffuse flux, f.Id. The remaining photons, (1-f).Id, will be lost and treated in the same way as absorbed photons in the instrumental 'calculation' of absorbance. This is the troublesome error which plagues seekers of simple absorbance. Nor, unfortunately, is it a measure of diffuse attenuance (K x cell length). A measure of diffuse attenuance should include all of the forward propagation flux, Ic + f.Id + (1-f).Id, but none of the back-scattered photons of Ir. This suggests one possible technique for measuring K: design a spectrophotometer with a detector large enough to collect all of the forward flux leaving the sample cell.

An alternative approach is prompted by the efforts of Shibata (1959), to remove the error caused by lost flux (1-f).Id. He describes a simple technique in which a small piece of opal glass is placed either between the sample and detector (procedure A), or between the light source and the sample (procedure B; see Fig.5.9), in which case both the reference cell (water) and the sample cell are illuminated by diffuse light. Since the light emerging from the sample and reference cells have been completely diffused, the value of attenuance thus measured is, says Shibata, '... the approximate value of semi-integral attenuance for diffuse incident light, which includes the effect of multiple reflection'. Semi-integral attenuance is the third of those listed in Table 5.2, and is expressed: ln[Io/It] where It is the total transmitted flux. This is, surely, diffuse attenuance, and so:

$$K = (1/r).Ln[Io/It] \qquad (5.4)$$

where r is the cell length.

To increase the accuracy and sensitivity of the system, a 100 mm flow-cell was used. As scattered photons would be lost through the side of the flow-cell, this was silvered. If the flow-cell is imagined to be a column of water in the sea, then the reflected photons in the cell represent the random flux of photons that would be scattered into the column to exactly replace those randomly scattered out. The silvered flow-cell was arranged as illustrated in Fig.5.9 in an Ultrascope 4050 spectrophotometer (LKB Biochrom Ltd). The whole calibration and measuring procedure was controlled by a microprocessor interfaced with an Apple IIe microcomputer which displayed (VDU), recorded (soft disc) and printed all measured spectra.

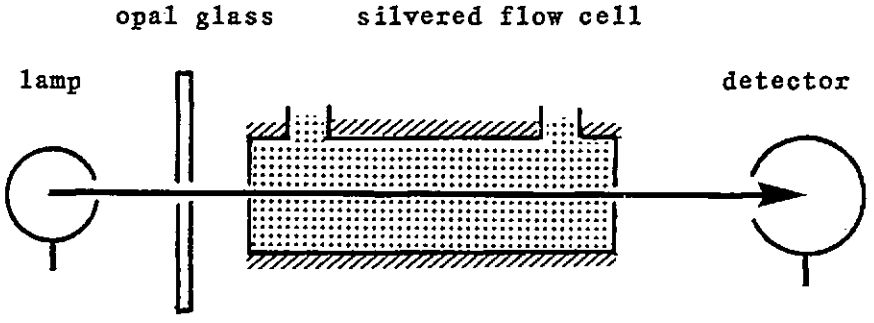

Fig.5.9 Arrangement of opal glass and silvered flow cell in spectrophotometer

A number of attempts have been made to simulate diffuse transmission - and hence measurement of K - in the system illustrated. So far, the results have been unconvincing. It was only during the last of these experiments that the reason for this was fully demonstrated. The spectrophotometer was opened in a darkened room and a white card was placed between the sample tube and the detector to examine the shape and size of the emergent diffuse beam. It was apparent that with increased sample turbidity, and hence increased scattering, the beam

was widening so that the flux density was being reduced (apart from the intended reduction due to increased K). As the receiver does not collect the whole beam, but only a sample through its window (see Fig.5.9), then this gives rise to a large and serious error.

Clearly, some form of lens system will have to be placed between the tube and window so that all of the emergent flux can be collected and focused onto the receiver.

5.6.5 The development of Monte Carlo modelling of underwater light

The technique of Monte Carlo modelling to study or predict the behaviour of light underwater has been employed by several workers including Plass and Kattawar (1969,1972), Kattawar and Platt (1972), Gordon and Brown (1973, 1974, 1975) and Gordon et al (1975). In Chapters 2 and 4, the Monte Carlo modelling of Kirk (1981a, 1981c, 1986a,1986b), was described and a graphical representation (Fig.2.10) of one set of results (Kirk 1986a) was used in the analysis of data obtained in the North Atlantic and Tamar Estuary (Table 4.2, Figs 4.15 and 4.18, and Eqn 4.25).

A mathematical model of light propagation would be most useful to the PML+IMS (Plymouth) work. An early version of Kirk's model was published in Kirk (1981c); however a new model should be produced as:

(i) Kirk's model is not ubiquitous in application; a new model would be tailored to particular needs, such as the study of near-surface reflectance or the problem of instrumental self-shading.

(ii) Mathematical models necessarily incorporate measured constants and empirical algorithms derived from regional data that may not be appropriate for use elsewhere; a new model would include empirical parameters apposite to the area(s) of investigation.

5.6.6 Spectral measurements of irradiance and/or radiance

As demonstrated in this programme of research, a considerable range of optical information can be gathered using instrumentation operating in a single, narrow band (eg c(660)), or in a single, broad band (eg °Ko). The scope would be much widened, however, by measuring optical properties over a range of selected narrow bands, so that the spectral properties of the waters could be defined. For example, by measuring $K(\lambda)$ values, then Jerlov's water type (Jerlov, 1976) may be determined.

Spectral irradiometers/radiometers are commercially available; but they are extremely expensive. A system is therefore suggested by which simple measurements of spectral radiance and/or irradiance can be obtained by means of an underwater camera.

The proposed method (see Fig.5.10) entails taking a photograph of the illustrated filter frame using an industrial quality black and white film (eg Kodak Tmax Professional). The frame will consist of an opaque plastic sheet with a series of circular windows and a single rectangular window. The circular windows will be fitted with coloured filters at the wavelengths of interest. The rectangular window will be fitted with a graduated series of neutral filters. At

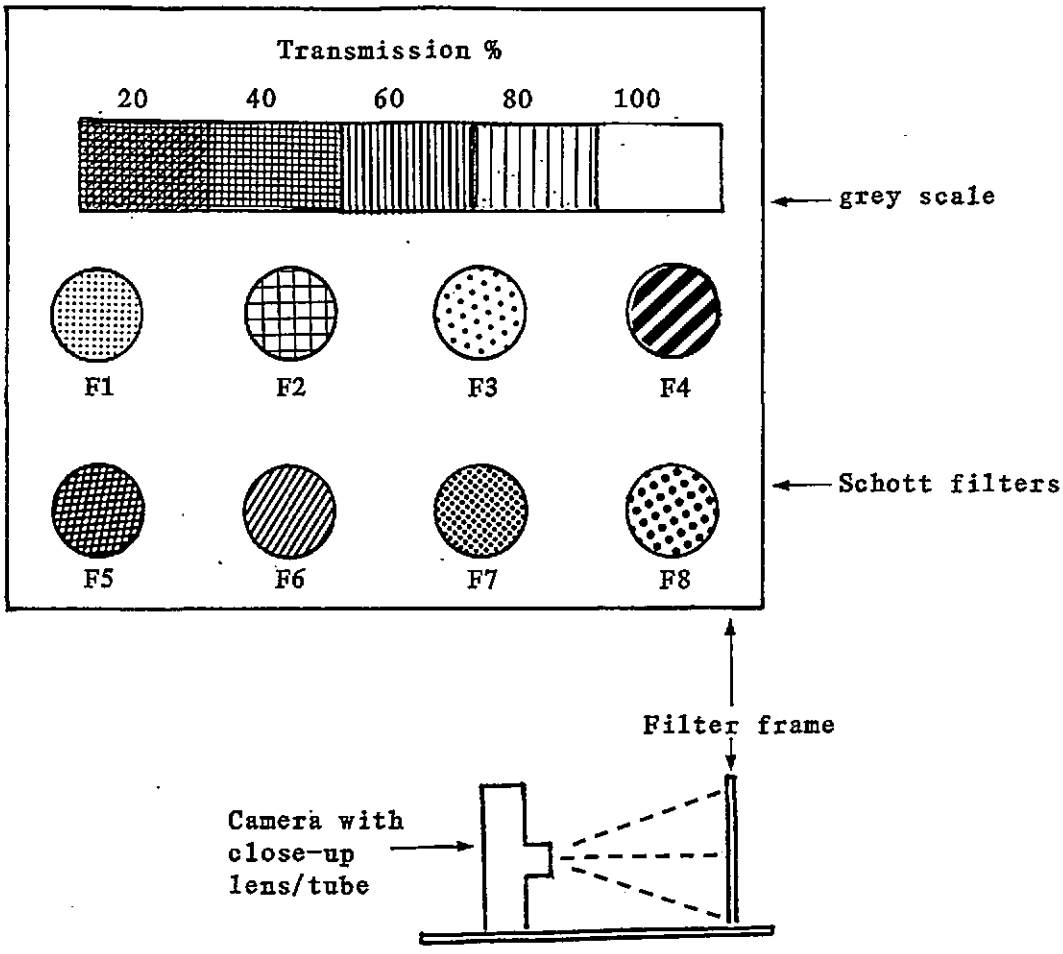

Fig.5.10: Proposed camera + filter frame spectral irradiance/radiance meter

any depth, z, the camera may be pointed in any direction, ξ, to measure the spectral distribution, $E(\lambda,z,\xi)$. After exposure, the film will be developed (negative) but not printed. The graduated neutral filter exposure will be used to calibrate a standard photographic densitometer which will then be used to measure the relative intensities of the coloured filter exposures. If the filter windows were to be fitted with Gershun tubes, then the system would measure radiance, $L(\lambda)$, rather than irradiance, $E(\lambda)$.

The proposed system is very flexible; a set of different filter

frames could be made to monitor different selections of wavelengths) eg:

(i) 555 nm plus several higher and lower wavelengths to cover the human photopic spectrum

(ii) a suitable range of wavelengths to estimate PAR, as discussed in 5.5.1

(iii) the wavelengths monitored by any particular satellite or airborne remote sensing system, eg the CZCS (443, 520, 550, 670, 750 nm)

(iv) the <u>in vivo</u> peak absorption wavelengths of algal pigments (chlorophylls, carotenoids and biliproteins), (see eg Kirk, 1983)

(v) similarly, the peak absorption wavelengths of the visual pigments (rhodopsin) of selected fishes, (see eg the list of references in Partridge, 1988)

(vi) the suite of sensors fitted to a UOR in related experiments

(vii) the selection of filters used by Hemmings and Lythgoe (1965) in their diver-operated device used to compare the relative spectral intensity of top light and side light. By chance, this device was first used off Malta during an underwater science expedition in 1965. The proposed camera system will be used in our own work in these same waters in 1989; indeed, it is likely that the experiment described by Hemmings and Lythgoe will be repeated exactly for comparison.

This system could also be used from a boat for measuring the spectral distribution of upwelling irradiance, $E_u(\lambda)$, by simply dipping it into the water. Also, by pointing it upwards, it could be used to measure the spectral distribution of skylight.

.....

On the whole, the objectives of this study have been fulfilled, though each investigation has raised new questions. Hopefully, this will continue to be the case; it will be a sad day that produces no new questions.

.....

LIST OF REFERENCES

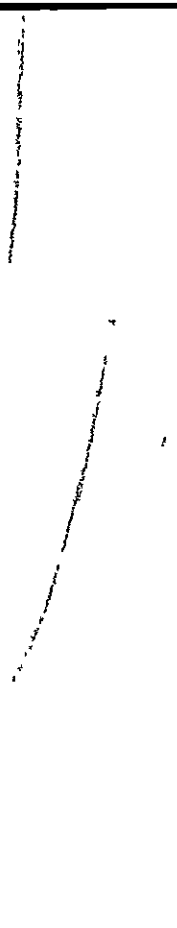

Ackroyd DR, Loring DH, Marsh JG, Millward GE, Morris A (1982)
Physicochemical processes controlling the composition of estuarine sediments.
Invited paper for presentation at 4th Joint Oceanographic Assembly, Halifax, N.Scotia.

Aiken J (1985)
The Undulating Oceanographic Recorder mark 2.
In: Mapping strategies in chemical oceanography (Zirino A, ed.) Amer.Chem.Soc., Washington, 315-322.

Aiken J (1987)
Physical, biological and bio-optical properties of the NE Atlantic Ocean, the Norwegian Sea and Greenland Sea, August 1987.
Data report (incorporating cruise report), File no. OPS 2.14/ PPP DIR 1.3.10, 56pp.

Aiken J and Bellan I (1986a)
A simple hemispherical, logarithmic light sensor.
Proc.SPIE, 637, Ocean Optics VIII, 211-16.

Aiken J and Bellan I (1986b)
Synoptic optical oceanography with the Undulating Oceanographic Recorder.
Proc.SPIE, 637, Ocean Optics VIII, 221-29.

Allen GP, Salomon JC, Bassoullet P, Du Penhoat Y and De Grandpre C (1980)
Effects of tides on mixing and suspended sediment transport in macrotidal estuaries.
Sediment Geog., 6:69-90.

Austin RW, Petzold TJ (1977)
Consideration in the design and evaluation of oceanographic transmissometers.
In: Tyler (1977), 104-20.

Bainbridge R, Evans GC and Rackham O, eds. (1965)
Light as an ecological factor.
Symp.Brit.Ecol.Soc., Cambridge 1965, Blackwell Sc.Publications, 384pp.

Bale AJ and Morris AW (1987)
In situ measurement of particle size in estuarine waters
Est.Coast.Shelf Sci., 24:253-63.

Bale AJ, Morris AW and Howland RJM (1985)
Seasonal sediment movement in the Tamar Estuary.
Oceanol.Acta, 8(1):1-6.

Bartz R, Zaneveld RV and Pak H (1978)
A transmissometer for profiling and moored observations in water.
Proc.SPIE, 160, Ocean Optics VIII, 102-8.

Beardsley GF Jnr, Pak H, Carder K and Lunden B (1970)
Light scattering and suspended particles in the eastern equatorial Pacific Ocean.
J.geophys.res., 75(15):2837-45.

Blackwell HR (1946)
Contrast thresholds of the human eye.
J.Opt.Soc.Amer., 36:624-43.

Booth CR (1976)
The design and evaluation of a measurement system for photosynthetically active quantum scalar irradiance.
Limnol.Oceanogr., 21:326-36.

Bricaud A, Mortel A and Prieur L (1981)
Absorption by dissolved organic matter of the sea (yellow substance) in the UV and visible domains.
Limnol.Oceanogr., 26(1):43-53.

Cialdi Cdr. (1866)
Sul moto ondoso del mare e su el correnti de esso specialmente auquelle littorali.
2nd edition, Rome, 258-288, cited in ONI Transl A-655 Hydrog.Off.,1955

Clarke GL (1941)
Observations on transparency in the southwestern section of the North Atlantic Ocean.
J.Mar.Res, 4:221-30.

Cocking SJ (1976)
Improved underwater viewing.
In: Drew et al (1976), 139-98.

Colijn F (1982)
Light absorption in the waters of the Ems-Dollard estuary and its consequences for the growth of phytoplankton and microphytobenthos.
Netherlands J.Sea Res., 15(2):196-216.

Collier A, Finlayson GM, Cake EW (1968)
On the transparency of the sea.
Limnol.Oceanogr., 13:391-94.

Cooper LHN and Milne A (1938)
The ecology of the Tamar Estuary - underwater illumination.
J.mar.biol.Ass.UK., 22:509-27, 23:391-96.

Drew EA, Lythgoe JN and Woods JD, eds. (1976)
Underwater research.
Academic Press, London, 430pp.

Duntley SQ (1962)
Underwater visibility.
In: Hill (1962), 452-55.

Duntley SQ (1963)
Light in the sea.
J.Opt.Soc.Amer., 53(2):214-33.

Duntley SQ and Preisendorfer RW (1952)
The visibility of submerged objects.
Final report N5ori-07864, Visibility Lab., MIT, 74pp.

Emmerson PG (1984)
Colour constancy underwater - the effects of viewing distance.
Prog.Underwater Sci., 9:9-14.

Emmerson PG (1987)
Predicting target detection distances in visual search tasks underwater.
Prog.Underwater Sci., 12:159-67.

Fay CW (1976)
An investigation into colour vision underwater.
In: Drew et al (1976), 199-207.

Friedman E, Poole L, Cherdak A, Houghton W (1980)
Absorption coefficient instrument for turbid natural waters.
Appl.Optics., 19:1688-93.

Fry ES (1974)
Absolute calibration of a scatterance meter.
In: Gibbs (1974), 101-109.

Gall MHW (1949)
Measurement to determine the extinction coefficients and temperature gradients in the North Sea and English Channel.
J.mar.biol.Ass.UK, 28:757-80.

Gershun A (1936)
Fundamental ideas of the theory of a light field (vector methods of photometric calculations.
Izv.Aked.Nauk SSSR, Otd.Mat.Estestv.Nauk, 417-30.

Gibbs RJ, ed. (1974a)
Suspended solids in water.
Plenum Press, NY and London, 320pp.

Glegg GA, Titley JG, Glasson DR, Millward GE, Morris A (1985)
The microstructures of estuarine particles and their role in heterogeneous chemical reactivity.
Presented before the Division of Environmental Chemistry, Amer.Chem.Soc., Chicago, Sept 1985.

Gordon HR (1980)
Irradiance attenuation coefficient in a stratified ocean: a local property of the medium.
Appl.Optics, 19(13):2092-94.

Gordon HR and Brown OB (1973)
Irradiance reflectivity of a flat ocean as a function of its optical properties.
Appl.Optics, 12:1549-51.

Gordon HR and Brown OB (1974)
Influence of bottom depth and albedo on the diffuse reflectance of a flat, homogeneous ocean.
Appl.Optics, 13:2153-59.

Gordon HP and Brown OB (1975)
Diffuse reflectance of the ocean: some effects of vertical structure.
Appl.Optics, 14:2892-95.

Gordon HR, Brown OB and Jacobs MM (1975)
Computed relationships between the inherent and apparent optical properties of a flat homogeneous ocean.
Appl.Optics, 14(2):417-27.

Gordon HR, Smith RC and Zaneveld JR (1984)
Introduction to ocean optics
Proc.SPIE, 489, Ocean Optics VII, 2-41

Graham JJ (1966)
Secchi disc observations and extinction coefficients in the central and eastern North Pacific Ocean.
Limnol.Oceanog., 11:184-90.

Hemmings CC and Lythgoe JN (1965)
The visibility of underwater objects.
In: Symposium of the Underwater Association for Malta 1965 (Lythgoe JN and Woods JD, eds.), 23-30.

Hill MN, ed. (1962)
The Sea, vol 1.
John Wiley, NY London, 864pp.

Højerslev NK (1972)
A theoretical proof of the existence of a constant vertical radiance attenuation coefficient in a horizontally stratified ocean.
Univ.Copenhagen, Inst.Phys.Oceanogr., Report no.20, 9pp.

Højerslev NK (1974.b)
Inherent and apparent optical properties of the Baltic.
Univ.Copenhagen, Inst.Phys.Oceanogr., Report no.23, 16pp.

Højerslev NK (1975)
A spectral light absorption meter for measurements in the sea.
Limnol.Oceanogr., 20:1024-34.

Højerslev NK (1977)
Spectral daylight irradiance and light transmittance in natural waters measured by means of a Secchi disc only.
ICES, code C.M.1977/C:42, hydrog.committee, 19pp.

Højerslev NK (1978)
Daylight measurements appropriate for photosynthetic studies in natural sea water.
J.cons.int.Explor.Mer., 38(2):131-46.

Højerslev NK (1984)
Fundamentals of the solar radiation field in air and under water.
Univ.Copenhagen, Inst.Phys.Oceanogr., Report no.47, 32pp.

Højerslev NK (1986)
Visibility of the sea with special reference to the Secchi disc.
Proc.SPIE, 637, Ocean Optics VIII, 294-305.

Højerslev NK and Jerlov NG (1977)
The use of the colour index for determining quanta irradiance in the sea.
Univ.Copenhagen, Inst.Phys.Oceanogr., report no.35, 12pp.

Holmes RW (1970)
The Secchi disc in turbid coastal waters.
Limnol.Oceanogr., 15:688-94.

Idso S, Gilbert RG (1974)
On the universality of Poole and Atkins Secchi disc - light extinction equation.
J.Appl.Ecol., 11:399-401.

Jerlov NG (1968)
Optical oceanography.
Elsevier, Amsterdam, 194pp..

Jerlov NG (1974)
A simple method for measuring quanta irradiance in the ocean.
Univ.Copenhagen, Inst.Phys.Oceanogr., report no.24, 10pp.

Jerlov NG (1976)
Marine optics.
Elsevier Oceanogr.Ser., Amsterdam, 203pp.

Jerlov NG (1977)
Classification of seawater in terms of quanta irradiance.
J.cons.int.Explor.Mer., 37(3):281-87.

Jerlov NG and Nielsen ES eds.(1974)
Optical aspects of oceanography.
Academic Press, London and NY, 494pp.

Joint IR (1983)
Measurement of microbial processes
In: Practical procedures for estuarine studies (Morris AW, ed.), NERC, 101-138.

Kattawar GW and Plass GN (1972)
Radiative transfer in the Earth's atmosphere-ocean system - II: Radiance in the atmosphere and ocean.
J.Phys.Oceanogr., 2:146-56.

Kirk JTO (1976)
Yellow substance (gelbstoff) and its contribution to the attenuation of photosynthetically active radiation in some inland and coastal SE Australian waters.
Aust.J.Mar.Freshwater Res., 27:61-71.

Kirk JTO (1977)
Use of a quanta meter to measure attenuation and underwater reflectance of photosynthetically active radiation in some inland and coastal SE Australian waters.
Aust.J.Mar.Freshwater Res., 28:9-21.

Kirk JTO (1979)
Spectral distribution of photosynthetically active radiation in some SE Australian waters.
Aust.J.Mar.Freshwater Res., 30:81-91.

Kirk JTO (1980a)
Relationship between nephelometric turbidity and scattering coefficients in certain Australian waters.
Aust.J.Mar.Freshwater Res., 31:1-12.

Kirk JTO (1980b)
Spectral absorption properties of natural waters: contribution of the soluble and particulate fractions to light absorption in some inland waters of SE Australia.
Aust.J.Mar.Freshwater Res., 31:287-96.

Kirk JTO (1981a)
Monte Carlo study of the nature of the underwater light field in, and the relationships between, optical properties of turbid yellow waters.
Aust.J.Mar.Freshwater Res., 32:517-32.

Kirk JTO (1981c)
Monte Carlo procedure for simulating the penetration of light into natural waters.
CSIRO Aust.Div.Plant Ind.Tech.paper no.36, 1-16.

Kirk JTO (1983)
Light and photosynthesis in aquatic ecosystems.
Cambridge Univ.Press, 401pp.

Kirk JTO (1986)
Estimation of the absorption coefficient of natural waters from hemispherical scalar irradiance measurements.
Unpublished, 3pp.

Kirk JTO (1986b)
Optical properties of picoplankton suspensions.
In: Photosynthetic picoplankton (Platt T and Li WK, Eds), Can.Bull.Fish.Aquat.Sci., 214: 501-520.

Kullenberg G (1974)
Observed and computed scattering functions.
In: Jerlov and Nielsen (1974), 25-49.

Leach JWP (1985)
Underwater inspection and field dependency in turbid water.
Prog.Underwater Sci., 10:7-15.

Lundgren B and Hojerslev NK (1971)
Daylight measurements in the Sargasso Sea - results from the Dana expedition, January-April 1966.
Univ.Copenhagen, Inst.Phys.Oceanogr., Report no.14,25pp.

Lythgoe JN (1971)
Vision.
In: Woods and Lythgoe (1971), 103-39.

Lythgoe JN (1979)
The ecology of vision.
Clarendon Press, Oxford, 244pp.

McLusky DS (1981)
The estuarine ecosystem.
Blackie, Glasgow, 150pp.

Morel A (1974)
Optical properties of pure water and pure sea water.
In: Jerlov and Nielsen (1974), 1-24.

Morel A, Prieur L (1977)
Analysis of variations in ocean colour.
Limnol.Oceanogr., 22:709-22.

Morel A, Smith RC (1974)
Relation between total quanta and total energy for aquatic photosynthesis.
Limnol.Oceanogr., 19:591-600.

Morris AW, Bale AJ, Howland RJM (1982a)
The dynamics of estuarine manganese cycling.
Estuarine, Coastal and Shelf Sci., 14:175-92.

Otobe H, Nakai T, Hattori A (1977)
Underwater irradiance and Secchi disc depth in the Bering Sea and the northern North Pacific in Summer.
Mar.sci.communications, 3:255-70.

OU/S341 (1982)
Photochemistry: light, chemical change and life.
S341 course units, The Open University.

Paterson DM (1986)
The migratory behaviour of diatom assemblages in a laboratory tidal micro-ecosystem examined by low temperature scanning electron microscopy.
Diatom Research, 1(2):227-39.

Pedoe J (1970)
Advanced National Certificate Mathematics, vol II.
Hodder and Stoughton, London, 382pp.

Petzold TJ and Austin RW (1968)
An underwater transmissometer for ocean survey work.
Scripps.Inst.Oceanogr., report ref.68-69, 5pp.

Pilgrim DA (1984)
The Secchi disc in principle and in use.
Hydrogr.J., 33:25-30.

Pilgrim DA (1987)
Measurement and estimation of the extinction coefficient in turbid estuarine waters.
Proceedings of the 16th EBSA Symposium: Dynamics of Turbid Coastal Environments. Continental Shelf Research, 7(11/12):1425-28.

Pilgrim DA and Aiken J (1989)
Measurement of the optical diffuse attenuation coefficient.
Hydrogr.J., in press.

Pilgrim DA and Millward GE (1988)
Measurement of the diffuse optical depth of a bed of a tidal estuary.
Proceedings of the 17th EBSA Symposium: Estuarine and Marine Methodologies, in press.

Pilgrim DA, Redfern TA, MacLachlan GS and Marsh RI (1988)
Estimation of optical coefficients from diver observations of visibility.
Prog.Underwater Sci., 13, in press.

Pilgrim DA, Smith MH and Trotter FJ (1985)
A ghost-net experiment in shallow water near Plymouth.
IDU report no.1232, Sea Fish Industry Authority, Hull, 18pp.

Pingree RD (1978)
Mixing and stabilization of phytoplankton distributions on the north west European continental shelf.
In: Spatial pattern in plankton communities (Steele JH, ed.), Plenum Press, 181-220.

Pingree RD, Mardell GT, Reid PC and John AWG (1986)
The influence of tidal mixing on the timing of the spring phytoplankton development in the southern bight of the North Sea, the English Channel and the Northern Armorican shelf
Lecture Notes on Coastal Estuarine Studies, vol.17, Tidal Mixing and Plankton Dynamics (Bowman J, Yentsch CS and Patterson WT, eds.), Springer-Verlag, Berlin Heidelberg, 164-192.

Plass GN and Kattawar (1969)
Radiative transfer in an atmosphere-ocean system.
Appl.Optics, 8:455-66.

Plass GN and Kattawar GW (1972)
Monte Carlo calculations of radiative transfer in the earth's atmosphere-ocean system - I: Flux in the atmosphere and ocean.
J.Phys.Oceanogr., 2:139-45.

Poole HH (1925)
On the photo-electric measurement of submarine illumination.
Sci.proc.Royal Dublin Soc., 18:99-115.

Poole HH (1928)
A simple form of photo-electric photometer using a neon lamp to measure the current.
Sci.proc.Royal Dublin Soc., 19:17-25.

Poole HH and Atkins WRG (1926)
On the penetration of light into seawater.
J.mar.biol.Ass.UK., 14:177-98.

Poole HH and Atkins WRG (1928)
Further photometric measurements of the penetration of light into seawater.
J.mar.biol.Ass.UK, 15:455-83.

Poole HH and Atkins WRG (1929)
Photo-electric measurements of submarine illumination throughout the year.
J.mar.biol.Ass.UK, 16:297-324.

Preisendorfer RW (1960)
Application of radiative transfer theory to light measurements in the sea.
Symp.Rad.Energy in the Sea, IUGG monogr., no.10, 11-29.

Preisendorfer RW (1976)
Hydrological optics, vol.1.
US Dept.of Commerce, Washington, 218pp.

Preisendorfer RW (1986)
Eyeball optics of natural waters - Secchi disk science.
NOAA Tech.memorandum, Environ.Res.Lab., ref.RL PMEL-67, 90pp.

Prieur L (1976)
Transfert radiatif dans les eaux de mer - application a la determination de parametres optiques caracterisant leur teneur en substances dissonte et leur contenu en particules.
These de doctorat d'Etat et Sciences Physiques, no. dénregistrement au CNRS, AO 12187, 300pp.

Qasim SZ, Bhattathiri PMA and Abidi SAH (1968)
Solar radiation and its penetration in a tropical estuary.
J.exper.mar.biol.ecol., 2:87-103.

Ross HE (1965)
Size and distance judgements under water and on land.
In: Symposium of the Underwater Association for Malta 1965 (Lythgoe JN and Woods JD, eds.), 19-22.

Ross HE (1967)
Steroscopic acuity under water.
Underwater Assoc.Report 1966-67, 61-64.

Ross HE and Rejman MH (1976)
Narcosis and visual attention.
In: Drew et al (1976), 209-16.

Secchi PA (1865)
Relazione delle esperienze fatte a bordo della pontificia Pirocorvetta 1'Immacolata Concezione per determinare la transparenza del mare.
Part translation in: Collier et al (1968)

Shibata K (1959)
Spectrophotometry of translucent biological materials - opal glass transmission method.
Methods of biochemical analysis, 7:77-109.

Smith RC and Baker KS (1978b)
Optical classification of natural waters.
Limnol.Oceanogr., 23(2):260-67.

Smith RC and Baker KS (1981)
Optical properties of the clearest natural waters (200-800nm).
Appl.Optics, 20:177-84.

Smith RC and Tyler JE (1975)
Transmission of solar radiation into natural waters.
In: Photochemical and Photobiological Reviews, vol.1 (Smith KC, ed.)
Plennum, NY, 117-56.

Smith RC and Wilson WH Jnr (1972)
Photon scalar irradiance.
Appl.Optics, 11:934-38.

Smith RC, Austin RW and Petzold TJ (1974)
Volume-scattering functions in ocean waters.
In: Gibbs (1974), 61-72.

Sørensen BM (1981)
Recommendations of the 2nd International workshop on atmospheric correction of satellite observation of seawater colour.
Commission of the European Communities Joint Research Centre, 49pp

Timofeeva VA (1974)
Optics of turbid waters (results of laboratory studies).
In: Jerlov and Nielsen (1974), 177-219.

Topliss BJ (1982a)
Optical monitoring of coastal waters: photic depth estimates.
Marine Environ.Res., 7(4):295-308.

Tyler JE (1968)
The Secchi disc.
Limnol.Oceanogr., 13:1-6.

Tyler JE (1977)
Light in the sea.
Benchmark papers in optics no.3, Dowden Hutchinson and Ross Inc, 384pp

Tyler JE and Preisendorfer RW (1962)
Light.
In: Hill (1962), 397-451.

Tyler JE, Smith RC and Wilson WH (1972)
Predicted optical properties for clear natural water.
J.Opt.Soc.Amer., 62:83-91.

Tyler JE, Austin RW and Petzold TJ (1974)
Beam transmissometers for oceanographic measurements.
In: Gibbs (1974), 51-59.

Uncles RJ, Elliott RCA, Weston SA (1985)
Observed fluxes of water, salt and suspended sediment.
Estuarine Coastal Shelf Sci., 20:147-67.

Uncles RJ, Elliott RCA, Weston SA, Pilgrim DA, Ackroyd DR, McMillan DJ and Lynn NM (1985)
Synoptic observations of salinity, suspended sediment and vertical current structure in a partly mixed estuary.
In: Physics of Shallow Estuaries and Bays (van de Kreeke C, ed.)
Springer-Verlag, Berlin Heidelberg, 58-70.

UNESCO (1965)
Working Group 15: Report of the first meeting of the joint group of experts in photosynthetic radiant energy.
UNESCO Tech.pap.Mar.Sci., 2, 5pp.

Voss KJ, Nolten JW and Edwards GD (1986)
Ship shadow effects on apparent optical properties.
Proc.SPIE, 637, Ocean Optics VIII, 186-90.

Walker TA (1980)
A correction to the Poole and Atkins Secchi disc - light attenuation formula.
J.mar.biol.Ass.UK., 60:769-71.

Walker TA (1982)
Use of a Secchi disc to measure attenuation of underwater light for photosynthesis.
J.Appl.Ecol., 19:539-44.

Weinberg S (1976)
Submarine daylight ecology.
Mar.biol., 37:291-304.

Williams J (1968)
The meaningful use of the Secchi disc.
Chesapeake Bay Inst., Tech.report no.45, 15pp.

Williams J (1970)
Optical properties of the sea.
US Naval Institute series in oceanography, 123pp.

Williams J, Skove F and Forster J (1984)
The effect of suspensoids on optical parameters in a typical estuary.
Proc.SPIE, 489, Ocean Optics VII, 49-54.

Woods JD and Lythgoe JN, eds. (1971)
Underwater science: an introduction to experiments by divers.
Oxford Univ. Press, 330pp.

Appendix

P U B L I S H E D P A P E R S

The Secchi Disc in principle and in use

D.A. Pilgrim, Dept. of Marine Science, Plymouth Polytechnic.

1. *Introduction*

The Secchi disc is simply a flat white 20-30cm diameter horizontal plate which is lowered through the water column until it is observed to just disappear — at the *Secchi depth* Zs. It is apparent that in broad terms Zs must be a function of the turbidity of the water and indeed, the Secchi disc has been used by oceanographers and marine biologists as a means of assessing water clarity for well over a century. To understand the operation of this ostensibly straight forward instrument — and rather more importantly, to understand what it measures exactly — then we shall need to consider certain aspects of established optical theory as applied to the propagation of light underwater and to the concept of contrast visibility. We may then consider the disc's practical uses.

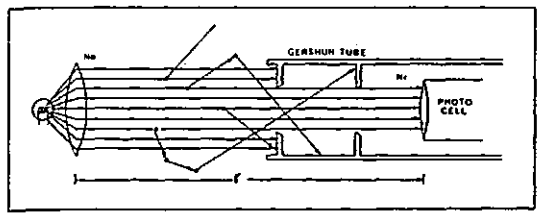

Fig. 1
Attenuation of a collimated beam of light (radiance, N)

2. *Some optical theory*

2.1 *The attenuation of underwater light*

It is observed that when light is propagated through water it suffers a loss in intensity. *Fig. 1* illustrates the path of a beam of collimated light of intensity (radiance) No at the source which is attenuated to intensity Nr during its passage through distance r. This beam attenuation is due to both absorption and scattering. Photons of light are absorbed by organic and inorganic particles in suspension, dissolved inorganic salts, plankton and by molecules of the water itself. As only collimated light is accepted through the Gershun tube of the receiver then any light scattered out of the beam by particles, plankton, salt and water molecules is totally lost. The beam attenuation (or simply attenuation) is therefore the sum of absorption and scattering. It may be demonstrated that the consequent decrease in light intensity with distance is exponential and expressed by *Beer-Lambert's law:*

$$N(r) = N(0) \cdot \exp\left[-(a+b) \cdot z\right] = N(0) \cdot \exp\left[-\alpha z\right] = N(0) \cdot \exp\left[-\gamma\right] \qquad \text{eq. 1}$$

where a is the *absorbtion coefficient,* b is the *scattering coefficient* and the sum of a and b, is the (beam) attenuation coefficient. The geometrical path length r multiplied by the attenuation coefficiient α is termed the *optical length* γ . *A very good example of a receiver which accepts only collimated – direct – rays of light is the eye and its mechanical equivalent, the camera; indeed the attenuation coefficient* α is usually associated with some aspect of visibility or photography.

2.2 *The extinction of underwater light*

Thus far it has been assumed that photons flow in a collimated beam and that scattered light is therefore lost. This is not necessarily the case. Suppose an underwater surface such as that illustrated in *Fig. 2* is *illuminated* by downwelling *irradiance* H; that is to say by light arriving from a range of directions due to scattering. It is apparent that as scattering is essentially a random process then for every photon which is randomly scattered out of the water column above the receiving surface then a photon will be randomly scattered into the column. If this were not the case then presumably the column would brighten or darken. It must therefore follow that there is no net loss from the column directly by scattering; however there will be *additional absorption* associated with the increased path lengths followed by the scattered streams of photons. We may therefore write Beer-Lambert's law for irradiance:

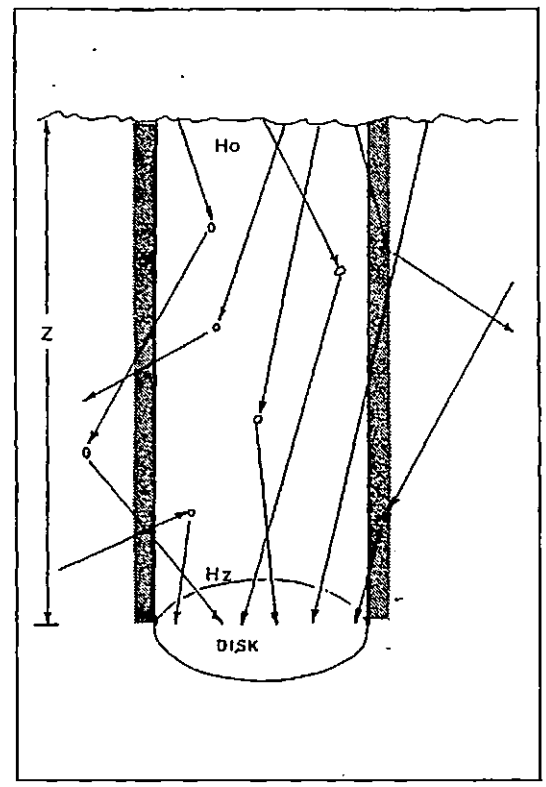

Fig. 2
Extinction of diffused light (irradiance, H)

$$H(z) = H(0) \cdot \exp\left[-(a+a') \cdot z\right] = H(0) \cdot \exp\left[-K \cdot z\right] = H(0) \cdot \exp\left[-J\right] \qquad \text{eq. 2}$$

where a′ represents the increase in the value of the absorption coefficient due to the increased path length followed by the scattered light and K is the *extinction coefficient* or *diffuse attenuation coefficient.* J, the multiple of the geometrical length of the path and the extinction coefficient may be termed the *optical length for irradiance.* Just as beam attenuation is usually associated with visibility so is extinction

generally associated with some form of illumination. The Secchi disc is illuminated by downwelling irradiance and its upwelling radiance is observed by the eye; we should not be surprised therefore to find that the Secchi depth is a function of both α and K.

2.3 *Contrast visibility*

An object may be visually detected against its background if it is a different colour to its background; this is known as *colour contrast*. If the object is the same colour as its background then it may still be detected if it has a different brightness to its background. This is *brightness contrast*, the phenomenon which most often limits visibility in the generally monochromatic subsurface world. Contrast C is defined by:

$$C = \frac{\text{object brightness} - \text{background brightness}}{\text{background brightness}}$$

We may therefore express the *inherent contrast* Co of an object — the contrast that it would have if viewed at zero distance — by the expression:

$$Co = \frac{No - bNo}{bNo}$$

where N is radiance and b indicates background. At some finite distance r the *apparent contrast* will be expressed by:

$$Cr = \frac{Nr - bNr}{bNr}$$

These contrasts are illustrated in *Fig. 3.* Apparent contrast Cr is diminished with increased distance r by two concurrent processes. Light from the object is attenuated by absorption

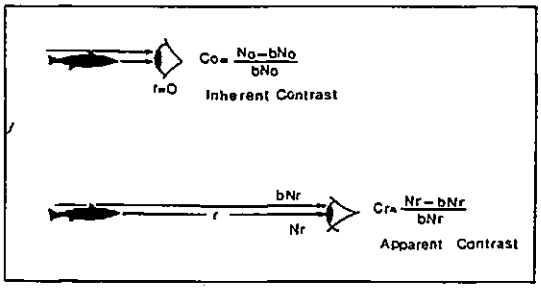

Fig. 3
Brightness contrast

and scattering so that there will be a reduction in object radiance; at the same time incoming daylight is scattered towards the observer throughout the entire length of the path of sight producing a veil of light behind which the object becomes increasingly indistinct. The diminution in apparent contrast to which these two processes contribute is given by *Duntley's law of contrast reduction* (Duntley, 1952):

$$Cr = Co.\exp\underbrace{\left[-(\alpha + K.\sin\theta)r\right]}_{\text{contrast reduction factor}} \qquad \text{eq. 3}$$

The situation in which this equation is derived is illustrated in *Fig. 4.* It can be seen from eq. 3 that the apparent contrast Cr decreases exponentially with range r as a function of both the attenuation and extinction coefficients and sighting angle θ. Of course, a range may be reached at which Cr is reduced to a level too low for visual detection by the observer. This limiting apparent contrast is termed the *threshold contrast* Ct. Duntley (1952) coined the term *hydrological range* V to

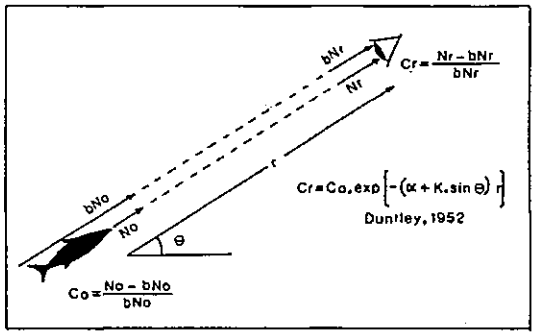

Fig. 4
Duntley's law of contrast reduction

describe this distance of disappearance. Substitution of Ct and V into eq. 3 gives:

$$V = \frac{\text{Ln}\left[\frac{Co}{Ct}\right]}{\alpha + K.\sin\theta} = \frac{\beta}{\alpha + K.\sin\theta} \qquad \text{eq. 4}$$

where β represents the term Ln [Co/Ct], a constant for any given object and observer. Eq. 4 shows that the range of visibility for, say, a fish or diver is maximum when looking vertically upwards ($\theta = -90°$; $\sin\theta = -1$), minimum when looking vertically downwards ($\theta = 0°$; $\sin\theta = 0$). We should now consider the special case of the visibility of a flat white disc viewed from above.

2.4 *The Secchi depth*

Suppose a flat white disc of surface reflectivity ρ is situated at depth z and is observed from above as illustrated in *Fig. 5.* The disc is illuminated by irradiance Hz so that its inherent brightness at depth z must be ρ.Hz. The mass of water itself will reflect (back scatter) light; this property of the water is characterised by its *reflectance* R. It follows that the inherent brightness of the background water against which the disc is observed must be given by R.Hz and so we may write for inherent contrast of the disc:

$$Co = \frac{\rho.Hz - R.Hz}{R.Hz} = \frac{\rho - R}{R}$$

So, the inherent contrast of the submerged disc and indeed, any underwater object, depends only upon its own reflectivity and the reflectance of the water; it is not a function of the ambient light conditions assuming that these are bright enough for efficient vision. The disc will be observed vertically downwards ($\theta = 90°$) so that $K.\sin\theta = K$. At Zs, the depth of disappearance, the apparent contrast will be the threshold contrast Ct so that from eq. 4 we may now write the *Secchi depth equation:*

$$Zs = \frac{\text{Ln}\left[\frac{\rho - R}{Ct.R}\right]}{\alpha + K} = \frac{\beta_s}{\alpha + K} \quad \text{whence} \quad (\alpha + K) = \frac{\beta_s}{Zs} \qquad \text{eq. 5}$$

3.

3.1 *Secchi's experiment*

The idea of assessing the transparency of water by making visual observations of a submerged white disc is not a new one but may have originated with a casual observation by a certain Captain Alexandre Bérard in the early 19th century (Tyler, 1968). It is recorded that on some occasion during a passage from Wallis Island to the Mulgraves, Bérard noticed a white dish entangled in a fishing net at a depth of 40m. This

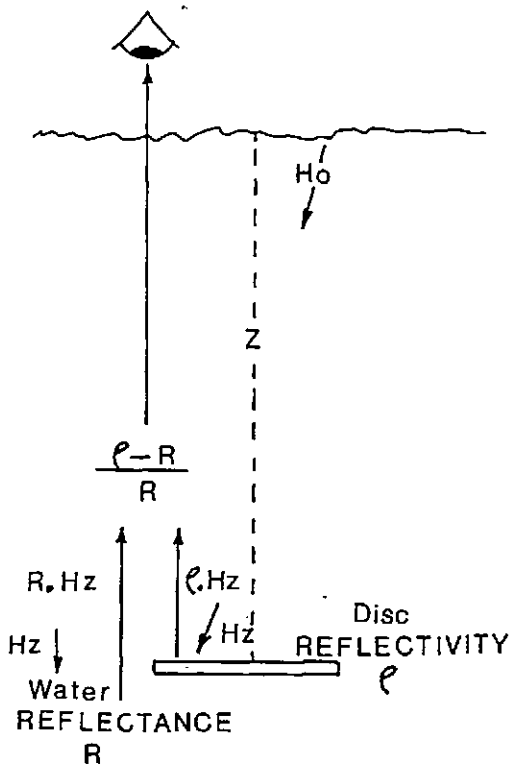

Fig. 5

observation was mentioned in the writings of Dominique Argo the French astronomer and physicist whose optical work included photometric measurements of the brightness of the stars, proof of the relationship between the aurora borealis and magnetic variation and important observations of the total solar eclipse of 1842. The works were subsequently read by Commander Alessandro Cialdi who, in 1865, was head of the Papal Navy and interested in the transparency of the sea and visibility of the sea bed. Cialdi prepared a number of discs of different colours and sizes (Cialdi, 1866) and engaged the services of Professor PA Secchi to organise and conduct a programme of observations from on board the papal barge L'Immacolata Concezione. Secchi measured the depth of disappearance of Cialdi's discs off a graduated line. In his report (Secchi, 1865; translation by Collier et al, 1968) Secchi records that the largest disc deployed was of 3.73m diameter "... formed of an iron circle covered with oiled sailcloth and varnished with white lead". Smaller discs were 0.4m in diameter and "... of diverse substances. One was pure white earthenware plate... others were cloth discs supported by iron circles... but of different colours: white, yellow and the colour of sea mud." These various discs were deployed 6-12 miles off the coast of Civitavecchia in Mediterranean water which was "... perfectly clear, of a beautiful colour and of a great purity... which for a long time had not been strongly agitated".

During the voyage Secchi carefully examined and recorded the effects of many variables upon the visibility of Cialdi's submerged discs. His conclusions were:

(i) *Influence of size of disc.* The large discs were found to have a greater depth of visibility than the smaller ones "... because the images of the latter... are deformed in all directions by refraction, and become so diffused that it is impossible to recognise the object exactly, even when it is sufficiently clear."

(ii) *Influence of shadow of ship.* Secchi recorded that depths of disc visibility were approximately equal on the shaded and sun-lit sides of the ship "... provided that the solar rays reflected by the water were prevented from reaching the eye."

(iii) *Influence of height of observer above the water.* It was determined that "... by placing the eye as near as possible to the water the depth increases...", and that "... between the measurements taken on the deck of the ship and in the smaller craft there was a difference of 2m, but this advantage was more noticeable for the little discs than for the large ones."

(iv) *Influence of altitude of sun and cloud cover.* "The most important factors are the height of the sun and the clearness of the sky.", wrote Secchi who found that a sky even thinly covered with light clouds resulted in "... 4m less of depth..." than a perfectly clear sky.

(v) *Colour of disc and water.* Secchi analysed the light reflected by white discs by means of a spectroscope and, as may be expected in his "... perfectly clear ..." Mediterranean water, he found that the first colour to disappear was red followed by yellow and green whilst "... blue, indigo and violet remain completely unaltered.. that explains the colour of the seawater which is of a lovely blue darkening to violet". Cialdi had also provided discs painted yellow "... and the colour of the sea slime...", (whatever that might be in a 19th century Mediterranean "... of great purity ..."!), and Secchi noted that these disappeared at depths representing hardly half of those of the white ones.

(vi) *Maximum depth of disc visibility* (i.e. maximum Secchi depth). During this original series of experiments Secchi recorded depths no greater than 45m — little more than Bérards 40m observation — but wrote that "... I believe that in seas like our Mediterranean, one could reach at the most only 50m and, with great difficulty 60m..." This is probably about right as Tyler (1968) has calculated an absolute maximum Secchi depth of 67m for pure water.

(vii) *The use of polarizers.* Secchi did try some observations "... using polarizers proposed by Argo... to destroy the reflection of the light on the water which greatly impaired distinct vision... but without any advantage...". He found that the advantage of reduced sunlight reflection was outweighed by the unwanted absorption by the polarizer and "... the necessity of using a single eye...". [In fact I have experimented with modern polarizing sunglasses — two eyes — and have found them to be of some advantage; however I much prefer to use a glass-bottomed bucket as this completely removes both surface reflection and irregularities in surface *refraction,* the phenomenon which causes the disc image deformation referred to by Secchi in (i).]

(viii) *Point of actual disc disappearance.* Even during these first recorded observations Secchi notes that "... in each experiment the disappearance happened in rather narrow limits of depth, varying rarely from one meter in the same circumstances...". [This is an interesting point, I have made many Secchi disc observations and underwater measurements of horizontal visibility and

have always been surprised that the disc or fellow diver should disappear at such an exact depth or range. One might imagine that the target would gradually fade into the background over a considerable range of distance but this is not usually the case except in water rich in planktonic 'bloom'. I have also found remarkable agreement in the observations by several observers or divers in the same water.]

After 1866 the Secchi disc became established as a standard instrument for measuring turbidity at sea. Its simplicity and cheapness guaranteed its survival — even after the introduction, early this century, of the photoelectric cell for the measurement of underwater illumination.

3.2 *The Secchi disc today*

It is not common practice today to construct a Secchi disc with a 3.73m diameter iron ring covered with oiled sailcloth and varnished with white lead. Nor is sea slime a fashionable choice of colour. Curiously, exact size and reflectivity have not yet been standardised internationally though it is usual to use flat white painted discs of 20-30cm diameter. [I did not use painted discs in the collection of the data presented in section 4. To maintain a repeatable standard throughout, I used 30cm discs of ordinary 4mm mirrored glass which had been Frosted by rubbing with a small piece of glass and wet, grade 1 carborundum powder. The mirrors were glued to an aluminium base plate which was rigged with a 3-legged bridle, Of exactly 1m depth, and attached to a plastic covered steel surveyors' tape. The Secchi depth was therefore the tape measurement plus 1m. For measuring Secchi depths of less than 1.5m I have fixed a 20cm mirrored disc to a graduated pole. This is especially useful in turbid, fast flowing water as the pole keeps the line of sight vertical. In really fast flowing water a line may be attached to the bottom of the pole and secured at the fore part of the anchored survey vessel. As mentioned in section 2, a glass-bottomed bucket was used throughout.]

3.3 *A working value of βs*

We have from eq. 5 that $(\alpha + K) = \beta s/Zs$ and that $\beta s = \text{Ln}[(\rho - R)/Ct.R)]$. Clearly we need some realistic values for ρ R and Ct if we are to use the Secchi disc to calculate $(\alpha + K)$, the sum of the attenuation and extintion coefficients.

The reflectivity ρ of bright white paint is generally taken to be 80-85% though Holmes (1970) does mention that in an experiment with flat white paint a reflectance of 84% was measured when dry but this increased to 93% on immersion in pure water. It is usual to assume a value of 82%.

The reflectance of the water R must vary from water type to water type. It is generally agreed (e.g. Tyler, 1968) that R is typically 2%. [Incidently, this means tht when a diver, in deep water, looks up he observes a downwelling irradiance 50 times As bright as that which he sees when he looks downwards.]

The threshold visual contrast Ct is simply the lowest value of contrast detectable by the eye. Blackwell (1946) describes the extensive experimentation that was conducted at the Tiffany Foundation, New York, during the 2nd World War to determine the contrast threshold for the normal human observer under a wide variety of conditions. The results of these experiments are presented in Blackwell's paper as tables of threshold contrast of discs of various sizes (angular subtense) both brighter and darker than their background. Entering these tables with typical Secchi disc angular subtense and reported ambient light levels then it may be deduced (Tyler, 1968) that its liminal visual contrast would be 0.0066.

If we now use these values (ρ = 82%, R = 2% and Ct = 0.7%) in eq. 5 then we get $\text{Ln}[(0.82 - 0.02)/(0.007 \times 0.02)]$ = 8.65 = βs. In experiments in Goleta Bay, Holmes (1970) deduced values of $\beta s = 9.4$ and Ct = 0.0013. Of course this implies a human liminal vision twice as sensitive as that found by Blackwell. This is certainly curious for in reporting his wartime experiments Blackwell (1946) writes that "The observErs were young women, aged 19-26 years, whose visual acuity in each eye and in both eyes was approximately 20/20 without refractive correction... Observers were seated at the rear of the observation room in upholstered chairs... Observers were allowed to adapt to the observation room brightness... by preliminary adaptation outside the laboratory with standard Polaroid dark adaptation goggles... The overall brightness of the observation room was subject to precise control...", and so on. Clearly this scenario does not typify the optical conditions endured by the middle aged oceanographer or hydrographer as he hangs over the side of a heaving boat peering into the murky depths below.

In fact the combination $(\alpha + K)$ is not a very useful parameter anyway. It is more usual to try to calculate the more meaningful single quantities K or α or even suspended particle concentration from empirical formulae incorporating Zs. We shall now consider an example of each of these.

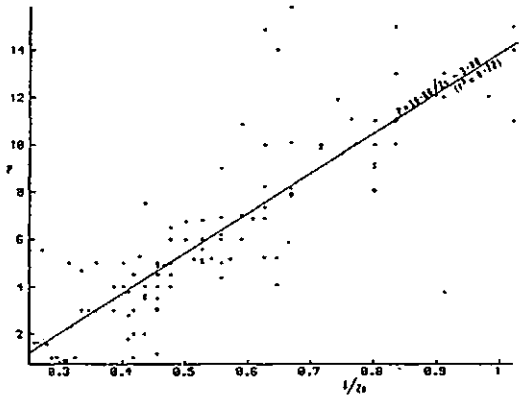

Fig. 6
Turbidity v. Secchi depth

4. *Secchi disc measurements*

4.1 *Turbidity*

It is apparent that the Secchi depth must decrease with increased suspended particle concentration P, usually expressed in parts per million (ppm). There is no governing theory which gives P in terms of Zs so this relationship must be determined by calibration against some known standard. The data plotted in *Fig. 6* were obtained from on board 3 boats anchored in the lower reaches of the River Tamar on two separate occasions (30 June and 7 July, 1982). The particle concentration P (ppm) was obtained by turbidity meters which had been calibrated against international standard formazin. In *Fig. 6* P is plotted against 1/Zs; the least squares regression equation is $P = 16.86/Zs - 3.00$, $r^2 = 0.722$. The rather high degree of scatter is not unexpected. The turbidity meter effectively measures beam transmission which is a function of particle size as well as concentration (Gibbs, 1974); the scatter therefore suggests a range of particle sizes different to that of the formazin standard.

4.2 *Extraction coefficient*

We have from eq. 5 that Zs is a function of both the attenuation and extinction coefficients i.e. $Zs = \beta s/(\alpha + K)$. It is far more useful, however, to know the value of the extinction coefficient alone; for example it is the extinction of downwelling *photosynthetically active radiation* (PAR) the band of light between 400 and 700 nanometers (about the same band as visible light) which is of such interest to marine biologists and oceanographers in the study of photosynthesis by phytoplankton. Again an empirical approach must be made to the problem. Some of the earliest work with photoelectric cells was carried out near Plymouth by H.H. Poole and W.R.G. Atkins (Poole, 1925; Poole and Atkins, 1926; Poole and Atkins, 1928; Poole and Atkins, 1929) who were the first to offer the marine biologist a relationship between the extinction coefficient and the Secchi depth. They gave this relationship as K.Zs = 1.7. Neither these workers, nor the several others who have published a value for K.Zs have specifically mentioned the fact that the constant K.Zs is, of course, the optical depth of irradiance of the Secchi depth — the term that I labelled Js in eq. 2. Published values of K.Zs range from about 1.3 to 1.7 and include those listed in the table following.

Table 1 - Published values of K.Zs = Js

K.Zs = Js	Area	Reference
1.7	English Channel	Poole and Atkins (1929)
1.59	Tamar estuary	Cooper and Milne (1938)
1.7	South of Bermuda	Clarke (1914)
1.42	North Sea & English Channel	Gall (1949)
1.46	North Pacific	Graham (1966)
1.5	Cochin estuary	Quasim et al (1968)
1.44	California coast	Holmes (1970)
1.7	(sewage ponds)	Idso and Gilbert (1974)
1.39	Mediterranean	Weinberg (1976)
1.47	Bering Sea & North Pacific	Otobe et al (1977)
1.45	(by recalculation of the pioneering data of Poole and Atkins, 1929)	Walker (1980)
1.46	North East Australia	Walker (1982)

We know that K and Zs are not theoretically related and the values of Js given in Table 1 were obtained from data obtained in many different kinds of water. There is then, a remarkable agreement between these results. *Fig. 7* illustrates the combined observations obtained from on board the Plymouth Polytechnic research vessel *Catfish* whilst anchored at 4 different stations in the Tamar estuary on 30 June 1982, 7 July 1982, 31 May 1984 and 1 June 1984. The least squares regression is 1/K = 0.95 Zs — 0.42 ($r^2 = 0.89$). The best straight line through 0,0 is 1/K = 0.716 Zs, a result which gives Js = K.Zs = 1.4 for the range of small values of Secchi depth obtained in this way very turbid estuarine water.

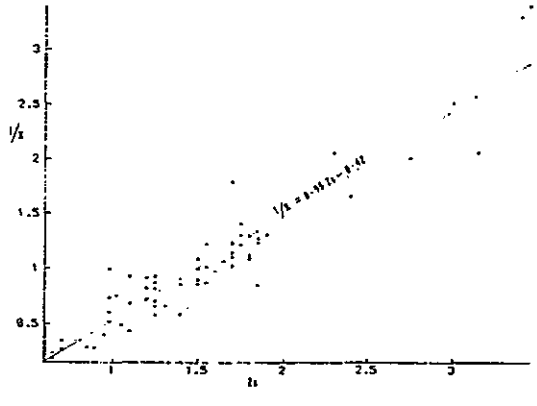

Fig. 7
1/Extinction coefficient v. Secchi depth

Of very special interest to the marine biologist is an estimate of the *compensation depth* Zc. At this depth the light level — the *compensation light intensity* — is such that a plankton fixes carbon at exactly the same rate as it loses it by respiration. The compensation depth therefore represents the limiting depth at which real growth can take place. It is widely observed that at the compensation depth there is increased photosynthetic activity within a layer about 10m thick Kirk (1983). It is generally assumed that at the compensation depth the light level is 1% of that at the surface. Hence, from eq. 2 we may write for the optical depth of the compensation depth: Js = Ln [1%] = 4.6. Using a value of 1.5 for Js (see Table 1) we may write:

$$\frac{Zc}{Js} = \frac{K.Zc}{K.Zs} = \frac{4.6}{1.5} \sim 3$$

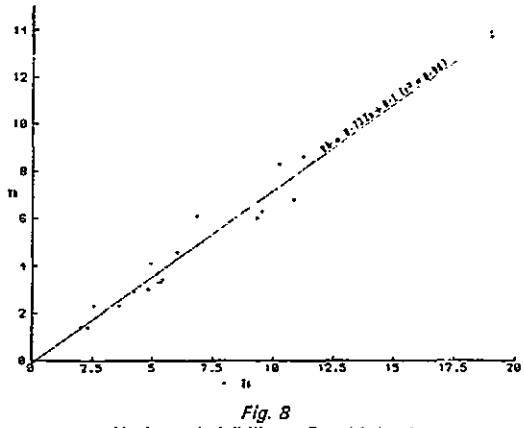

Fig. 8
Horizontal visibility v. Secchi depth

i.e. the compensation depth is approximately 3 times the Secchi depth (Zc ~ 3Zs).

4.3 *Horizontal visibility*

The hydrological range V is given by eq. 4. If the sighting is horizontal then $\theta = 0$ and we may therefore say that $Vh = \beta/\alpha$ i.e. the horizontal visibility is a function of attenuation only. Underwater visibility is generally reckoned in terms of a black object such as a neoprene-suited diver. Assuming that black represents a reflectivity of zero then we can write for the inherent contrast of such a black body: $Co = (e - R)/R = -1$. The negative sign has no physical significance beyond indicating that we are dealing with a dark object against a brighter background rather than a bright object viewed against a dark background. It is quite in order therefore, to say that for a black body: $Co = |Co| = 1$. It is most unlikely that a diver wearing a face mask will have a threshold contrast Ct of less than about 2% (Gazey, 1970) whence β = Ln [Co/Ct] = Ln [1/0.02] = 3.9. This result agrees with the rule of thumb given by Duntley (1952) that $Vh = 4/\alpha$. *Fig. 8* presents data obtained during dives in the Plymouth area and it will be seen that there is a very strong correlation ($r^2 = 0.975$) between the horizontal visibility Vh and the Secchi depth Zs. The equation is Vh = 0.73 Zs + 0.1 but as the least squares regression line passes almost through 0,0 then we may neglect the small intercept and say Vh = 0.73 Zs.

5. *In conclusion*

The Secchi disc is a cheap and simple instrument that gives an immediate indication of water turbidity. Although, strictly, we should interpret disc observations only in terms of $(\alpha + K)$ we may take an impirical approach to obtaining more useful parameters such as the compensation depth (a function of K only), the horizontal visibility (a function of α only) or even the turbidity (ppm) — theory notwithstanding.

References

Blackwell H.R. (1946) *Contrast thresholds of the human eye.* J.Pt.Soc.Am., *36,* 624-643, 1946.

Cialdi Cdt. A. (1866) *Sul moto ondoso del mare e su el correnti de esso specialmente auquelle littorali.* 2nd Ed., Rome, 1866.

Clarke G.L. (1941) *Observations on transparency in the southwestern section of the North Atlantic Ocean.* J.Mar.Res., *4,* 221-230, 1941.

Collier A. Finlayson G.M., Cake E.W. (1968) *On the transparency of the sea.* Limnol. Oceanogr., *13,* 391-394, 1968.

Cooper L.H.N. and Milne A. (1938) *The ecology of the Tamar Estuary II Underwater illumination.* J.mar.biol.Ass.UK., *22,* 509-527, 1938.

Duntley S.Q. (1952) *The visibility of submerged objects.* final report, Visibility Lab., MIT, 1952.

Gall M.H.W. (1949) *Measurements to determine extinction coefficients and temperature gradients in the North Sea and English Channel.* J.mar.biol.Ass.UK., *28,* 757-780, 1949.

Gibbs R.J. (1974) *Suspended solids in water.* Plenum Press, 1974.

Gezey B.K. (1970) *Visibility and resolution in turbid waters.* Underwater Sc. and Technology J., *2(2),* 105-115, 1970.

Graham J.J. (1966) *Secchi disc observations and extinction coefficients in the central and eastern North Pacific Ocean.* Limnol.Oceanogr., *11,* 184-190. 1966.

Hemmings C.C. (1965) *Factors influencing the visibility of objects underwater.* In: Light as an ecological factor; Evans et al (ed.), Blackwell Sc. Pub., 1965.

Hemmings C.C. and Lythgoe J.N. (1965) *The visibility of underwater objects.* Symp. of Underwater Ass., Malta, 1965, pp. 23-30.

Holmes R.W. (1970) *The Secchi disc in turbid coastal waters.* Limnol.Oceanogr., *15,* 688-694, 1970.

Idso S.B. and Gilbert R.G. (1974) *On the universality of the Poole and Atkins Secchi disc – light extinction equation.*

Kirk J.T.O. (1983) *Light and photosynthesis in aquatic ecosystems.* Cambridge University Press, 1983.

Otobe, H, Nakai T. and Hattori A. (1977) *Underwater irradiance and Secchi disk depth in the Bering Sea and the northern North Pacific in Summer.* Mar.Sc.Communications, *3,* 255-270, 1977, 1977.

Poole H.H. (1925) *On the photo-electric measurement of submarine illumination.* Sci.Proc.Royal Dublin Soc., *18,* 99-115, 1925.

Poole H.H. and Atkins W.R.G. (1926) *On the penetration of light into seawater* J.Mar.Biol.Ass.UK., *14,* 177-198, 1926.

Poole H.H. and Atkins W.R.G. (1926) *Further photoelectric measurements of the penetration of light into sea water.* J.Mar.Biol.Ass.UK., *15,* 455-483, 1928.

Poole H.H. and Atkins W.R.G. (1929) *Photo-electric measurements of submarine illumination throughout the year.* J.Mar.Biol.Ass.UK., *16,* 297-324, 1929.

Qasim S.Z., Bhattathiri P.M.A. and Abidi S.A.H. (1968) *Solar radiation and its penetration in a tropical estuary.* J.Exp.Mar.Biol. and Ecol., *2,* 87-103, 1968.

Secchi P.A. (1865) *Relazione delle esperienze fatte a bordo della pontificia Pirocorvetta L'Immacolata Concezione per determinare la transparenza del mare.*

Tyler J.E. (1
68) *The Secchi disc.* Limnol.Oceanogr., *13,* 1-6, 1968.

Walker T.A. (1980) *A correction to the Poole and Atkins Secchi disc/light-attenuation formula.* J.Mar.Biol.Ass.UK., *60,* 769-771, 1980.

Walker T.A. (1982) *Use of a Secchi disc to measure attenuation of underwater light for photosynthesis.* J.Appl.Ecol., *19,* 539-544, 1982.

Weinberg S. (1976) *Submarine daylight and ecology.* Mar.Biol., *37,* 291-304, 1976.

Williams J. (1968) *The meaningful use of the Secchi disc.* Tech.report 45. Ref. 68-15, Chesapeake Bay Institute, 1968.

7. *Acknowledgement*

I acknowledge the cooperation of Dr. R. Uncles, Mr. A. Elliot and other colleagues at the Institute of Marine Environmental Research, Plymouth, in the collection of turbidity data presented in this paper.

Continental Shelf Research. Vol. 7. Nos 11/12. pp. 1425–1428. 1987.
Printed in Great Britain.

0278–4343/87 $3.00 + 0.00

Measurement and estimation of the extinction coefficient in turbid estuarine waters

D. A. PILGRIM*

(*Received* 5 *September* 1986; *in revised form* 20 *May* 1987; *accepted* 20 *June* 1987)

Abstract—Measurement of the depth-mean PAR (photosynthetically active radiation) extinction coefficient, $\langle {}^{\circ}Ko \rangle$, is important in the study of estuarine productivity. Measurements of $\langle {}^{\circ}Ko \rangle$, beam attenuation coefficient and Secchi disc depth are presented for the turbid waters of the Tamar Estuary. Equations are formulated which allow good estimates of $\langle {}^{\circ}Ko \rangle$ to be determined both from the beam attenuation coefficient (at 660 nm) and from the Secchi disc depth. For comparison, similar data are presented for the clearer waters of the northeast Atlantic.

INTRODUCTION

AN important control on estuarine plant productivity is exerted by downwelling light (MCLUSKY, 1981), specifically quantum scalar irradiance in the 400–700 nm (photosynthetically active radiation, PAR) band. The purpose of this paper is to present measurements of the PAR extinction coefficient, attenuation coefficient and Secchi disc depth for the Tamar Estuary. The data are used to formulate equations to predict the PAR extinction coefficient from both the beam attenuation coefficient and the Secchi disc depth, for a medium whose optical properties are dominated by suspended particles.

Because aquatic flora are generally able to absorb light arriving from any direction (4π scalar irradiance, Eo), their productivity must depend upon the magnitude of ${}^{\circ}Eo$, where the superscript signifies measurements of quanta in the 400–700 nm PAR band. The vertical propagation of monochromatic irradiance, $E(\lambda)$, in an homogeneous medium is described by Beer-Lambert's law:

$$E(\lambda,z) = E(\lambda,0).\exp[-K(\lambda).z]. \quad (1)$$

The extinction coefficient, $K(\lambda)$, is an apparent propery of the water: $K(\lambda) = a_d(\lambda) + b_d(\lambda) - b_u(\lambda).R(\lambda)$ (PREISENDORFER, 1961), where $R(\lambda) = Eu(\lambda)/Ed(\lambda)$ is the irradiance reflectance, a_d is the diffuse absorption coefficient for downwelling photons, and b_d, b_u are the back-scattering coefficients for downwelling and upwelling photons. From equation (1): $K(\lambda) = -d(\ln[E(z)])/dz$.

Equation (1) may not adequately describe the depth profile of a broad-band irradiance such as ${}^{\circ}Eo(z)$. For example, $\ln[{}^{\circ}Eo(z)]$ profiles from the northeast Atlantic, and in exceptionally clear-water conditions in the Tamar, tend to have higher values of ${}^{\circ}Ko$ near the surface due to selective absorption of longer wavelengths (e.g. KIRK, 1977, 1983). In turbid water, this effect tends to be balanced by the increase in extinction with depth,

* Department of Marine Science, Plymouth Polytechnic, Plymouth PL4 8AA, U.K.

resulting from the downward flux becoming more diffuse due to scattering (KIRK, 1983). Therefore, in estuaries, $\ln[^\circ Eo(z)]$ is usually linear with z, so that a water column can be described at any time by a single, depth-mean value of the PAR extinction coefficient, $\langle ^\circ Ko\rangle$:

$$\langle ^\circ Ko\rangle = -\mathrm{d}(\ln[^\circ Eo(z)])/\mathrm{d}z. \quad (2)$$

METHODS

Direct measurement of ⟨°Ko⟩

Irradiances were measured with a Biospherical Instruments Inc. quantum scalar irradiance meter, incorporating a 4π underwater sensor, and an upward-looking 2π skylight sensor. $\langle ^\circ Ko\rangle$ was obtained from vertical profiles of $-\ln[^\circ Eo(z)/^\circ Eod(\mathrm{ref})]$, where $^\circ Eod(\mathrm{ref})$ is the downwelling ambient (sky) irradiance measured on the boat; this eliminated the considerable effect of rapidly varying skylight.

A biologically important parameter is the euphotic depth, *Zeu*, at which $^\circ Eo(z)$ is reduced to 1% of its surface intensity. *Zeu* is often used as an approximation of the compensation depth, *Zc*, at which the rate of photosynthesis is equal to the rate of respiration. From equation (2):

$$Zeu = \ln[0.01]/\langle ^\circ Ko\rangle = 4.6/\langle ^\circ Ko\rangle. \quad (3)$$

Estimation of ⟨°Ko⟩ *from the beam attenuation coefficient*, c(λ)

The measurement of an irradiance profile is a time-consuming procedure. Moreover, irradiance profiles cannot be obtained at night nor in very dull conditions. Where a continuum of observations is required, or where data are obtainable only at night, then good estimates of $\langle ^\circ Ko\rangle$ can be made from the easily measured beam attenuation coefficient, $c(\lambda)$. The ratio $c(\lambda)/K(\lambda)$ is about 2.7 in clear ocean water (TYLER, 1968), but increases in turbid waters; it must therefore be determined for the particular waters under investigation.

Values of $c(660\ \mathrm{nm})$ were obtained in the northeast Atlantic and Tamar using a 0.25 m path-length, Sea Tech. Inc. transmissometer. The attenuation of 660 nm light by gelbstoff is negligible compared with that due to the waters and their suspended particulate matter. Linear regressions of c/K data obtained by WILLIAMS *et al.* (1984) in the Patuxent River, Chesapeake Bay and Atlantic Ocean produced different slopes for the three cases. Our turbid (Tamar) and oceanic (northeast Atlantic) observations revealed a similar difference. Geometric regressions (PEDOE, 1970) of these data showed much closer agreement, however, and these equations are presented later.

Estimation of ⟨°Ko⟩ *from the Secchi depth*

The Secchi disc depth is a function of both attenuation and extinction: $Zs = \Gamma/(c+K)$. The parameter Γ, which varies with the reflectivity of the disc, the irradiance reflectance of the water, and the threshold visual contrast of the observer, lies between about 5.5 and 9.5 (PREISENDORFER, 1986). Traditionally, workers have estimated *Zeu*, which is a function of extinction only (equation 3), by assuming an empirical relationship of the form: $K.Zs = Js$, where Js is the diffuse optical depth of the Secchi depth (e.g. POOLE and ATKINS, 1929; DUNTLEY and PREISENDORFER, 1952; TYLER, 1968; WILLIAMS, 1968; HØJER-

SLEV, 1986). Generally, $1.3 < Js < 1.8$, depending on the local and temporal characteristics of the waters.

RESULTS AND DISCUSSION

$\langle °Ko \rangle$ and Secchi depth data from the northeast Atlantic and Tamar Estuary give

$$\langle °Ko \rangle = 1.591\ Zs^{-1} - 0.0625\ (r^2 = 0.946,\ n = 201);\ °Js = 1.53.$$

The value $°Js = 1.53$ is the gradient of the best straight line through the origin.

Secchi disc depth data were also partitioned for "oceanic" ($°Ko < 0.27$) and "turbid" ($°Ko \geqslant 0.27$) analyses. This separation is about midway between Jerlov's oceanic type III and coastal type I waters (see JERLOV, 1976; Table 27). The equations derived from these analyses are presented in Table 1.

The 153 "turbid" data-pairs were obtained in the same waters in which POOLE and ATKINS (1929) derived: $K.Zs = 1.7$ (based on 12 data points). Recalculation of their data (WALKER, 1980) gave a more accurate estimate: $K.Zs = 1.4$, a value closer to the 1.53 presented here. Unless the local value of $°Js$ has recently been derived from direct observations of $\langle °Ko \rangle$, then it is suggested that biologists adopt the working relationships (see equation 3):

$$°Js = \langle °Ko \rangle .Zs \simeq 1.5 \text{ and } Zeu \simeq 3\ Zs.$$

Regression analyses (see Table 1) show a small difference between turbid ($°Js = 1.527$) and oceanic ($°Js = 1.419$) waters, which is possibly a consequence of the fact that all of the turbid observations were made using a glass-bottomed bucket (to avoid the adverse effects of surface reflection and refraction), whereas the ocean observations were made from the deck of a research ship.

In conclusion, it has been shown that the optical measurement appropriate to the study of estuarine productivity is the mean coefficient of extinction of 4π quantum scalar irradiance in the 400–700 nm PAR band, $\langle °Ko \rangle$. Preferably, $\langle °Ko \rangle$ should be obtained from the slope of the $-\ln[°Eo(z)/°Eod(\text{ref})]$ profile, although it can be estimated from the beam attenuation coefficient, $c(\lambda)$, or the Secchi disc depth, Zs.

Table 1. Summary of regression equations. Beam attenuation coefficient, c, refers to c(660 nm) *values which have been corrected for forward scattering by the method given by* BARTZ et al. (1978) *for a hyperbolic particle size distribution with a slope of* 2.9, *and a refractive index of* 1.05

Equation	n	r^2
Oceanic ($°Ko < 0.27$); $0.0517 \leqslant °Ko \leqslant 0.2677$		
$\langle °Ko \rangle = 0.1270\ c^{1.575}$	14	0.955
$\langle °Ko \rangle = 0.511\ Zs^{-1} - 0.009;\ °Js = 1.419$	48	0.901
Turbid ($°Ko \geqslant 0.27$); $0.2902 \leqslant °Ko \leqslant 4.276$		
$\langle °Ko \rangle = 0.1066\ c^{1.314}$	23	0.927
$\langle °Ko \rangle = 1.652\ Zs^{-1} - 0.125;\ °Js = 1.527$	153	0.913
All obs; $0.0517 \leqslant °Ko \leqslant 4.276$		
$\langle °Ko \rangle = 0.1131\ c^{1.288}$	37	0.996
$\langle °Ko \rangle = 1.5912\ Zs^{-1} - 0.0625;\ °Js = 1.527$	201	0.946

REFERENCES

BARTZ R., J. R. V. ZANEVELD and H. PAK (1978) A transmissometer for profiling and moored observations in water. *Proceedings of the Society of Photo-Optical Instrumentation Engineers*, Vol. 160, *Ocean Optics*, **5**, 102–108.

DUNTLEY S. Q. and R. W. PREISENDORFER (1952) The visibility of submerged objects. Final report, Visibility Lab., MIT, 74 pp.

HØJERSLEV N. K. (1986) Visibility of the sea with special reference to the Secchi disc. *Proceedings of the Society of Photo-Optical Instrumentation Engineers*, Vol. 637, *Oceanic Optics*, **8**, 294–305.

JERLOV N. G. (1976) *Marine optics*. Elsevier, Amsterdam, 231 pp.

KIRK J. T. O. (1977) Use of a quanta meter to measure attenuation and underwater reflectance of photosynthetically active radiation in some inland and coastal SE Australian waters. *Australian Journal of Marine and Freshwater Research*, **28**, 9–21.

KIRK J. T. O. (1983) *Light and photosynthesis in aquatic ecosystems*. Cambridge University Press, 401 pp.

MCLUSKY D. S. (1981) *The estuarine ecosystem*. Blackie, Glasgow, 150 pp.

PEDOE J. (1970) *Advanced national certificate mathematics*, Vol. II, Hodder and Stoughton, London, 382 pp.

POOLE H. H. and W. R. G. ATKINS (1929) Photo-electric measurements of submarine illumination throughout the year. *Journal of the Marine Biological Association of the United Kingdom*, **16**, 297–324.

PREISENDORFER R. W. (1961) Application of radiative transfer theory to light measurements in the sea. *Union Géod. Géophys. Inst. Monogr.* **10**, 11–30.

PREISENDORFER R. W. (1986) Eyeball optics of natural waters: Secchi disk science. NOAA Tech. Memorandum, Environmental Research Laboratory RL PMEL-67, 90 pp.

TYLER J. E. (1968) The Secchi disc. *Limnology and Oceanography*, **13**, 1–6.

WALKER T. A. (1980) A correction to the Poole and Atkins Secchi disc — light attenuation formula. *Journal of the Marine Biological Association of the United Kingdom*, **60**, 769–771.

WILLIAMS J. (1968) The meaningful use of the Secchi disc, Tech report 45, Ref. 68–15, Chesapeake Bay Institute, 15 pp.

WILLIAMS J., F. SKOVE and J. FOERSTER (1984) The effect of suspensoids on optical parameters in a typical estuary. *Proceedings of the Society of Photo-Optical Instrumentation Engineers*, Vol. 489, *Ocean Optics*, **7**, 49–54.